The Interactions of Bacillithiol with Carbonyl-Containing Metabolites

Dominic Rodrigues

A thesis submitted for the degree of Doctor of Philosophy

School of Pharmacy

2017

Declaration

This thesis has been submitted to the University of East Anglia for the Degree of Doctor of Philosophy and is, to the best of my knowledge, original except where stated, referenced and acknowledged.

Dominic Rodrigues

Abstract

Bacillithiol (BSH) is a recently discovered low molecular weight (LMW) thiol found amongst several Gram-positive bacteria including *Bacillus anthracis, Staphylococcus aureus* and *Bacillus subtilis.* It plays a fundamental role in the redox processes within the cell, in addition to many other functions including the detoxification of electrophiles such as methylglyoxal (MG). MG is a reactive dicarbonyl produced as a by-product of glycolysis. It is found to be toxic to the cell as it is capable of modifying macromolecules such as proteins and DNA causing loss of biological activity. The previously established glutathione-dependent glyoxalase pathway comprises of the glyoxalase I and glyoxalase II enzyme, which are found to serve as a major mechanism for the detoxification of MG amongst eukaryotes. There is speculation that BSH follows through this same pathway.

Herein, the BSH-dependent glyoxalase pathway in *B. subtilis* is fully explored. The studies have shown a reaction between BSH and MG to occur spontaneously both *in vitro* and *in vivo*. Furthermore, these observations, have lead onto the discovery that, for the first time, BSH has shown to react with other metabolites in glycolysis. These include dihydroxyacetone phosphate, D-glyceraldehyde 3-phosphate and pyruvate. In each case they form a hemithioacetal (HTA). As a result, potentially significant concentrations of BSH may be sequestered in these 'unknown thiol reservoirs' which were not previously known to exist in the cell. Essentially, this raises questions regarding the true overall concentration of intracellular BSH.

Acknowledgements

First of all, I would like to thank my supervisor Chris, for all his advice and tutoring over the last few years. His enthusiasm for the subject and passion for research has been a real inspiration! I would also like to thank my second supervisor Nick, for his support and feedback.

In the earlier years of my PhD, I would like to thank Sunil and Miriam for all their guidance and getting me settled into the lab life. After they left, PhD life was a little quiet for some time until the hustle and bustle began with the arrival of a whole new group who brought around a great atmosphere in the lab. So I would like to thank Olly, Emma, Hazel, Andrew, Marco, Awais, Issa, James, Zoe, and Muayyad, with a particular mention to Ryan. He has spent hours on end teaching me which I very much appreciate!

A special thanks to Jesus, Serena and Francesc for their assistance in the whole cell NMR and also to Lionel Hill for his analysis of the mass spectrometric data.

Lastly, I would like to thank my parents and all my family for all their support!

Table of Contents

Figures

Schemes

Scheme 6.9. Effective quantification of glyceraldehyde 3-phosphate analysing the reduction of NAD+ to NADH catalysed by GA3PD.

Tables

Abbreviations

2,4-DNPH	2,4-Dinitrophenylhydrazine
5,5-DTNB	5,5- Dinitrothiobis-(2-nitrobenzoic acid)
AGEs	Advanced glycation end products
Bca	Bacillithiol *S*-conjugate amidase
BM	Belitsky minimal
BSH	Bacillithiol
BST	Bacillithiol *S*-transferase
BshA	Glycosyltransferase
BshB	*N*-acetylglucosamine malate deacetylase
BshC	Cysteine ligase
BSSB	Bacillithiol disulfide
CAT	Cysteinyl *S*-conjugate acetyltransferase
CoA	Coenzyme A
CoADR	CoA disulfide reductases
Cys	Cysteine
HCy	Homocysteine
CysNAc	*N*-acetyl cysteine
DHAP	Dihydroxyacetone phosphate
E^+	Electrophile

ESH	Ergothioneine
F1,6-BP	Fructose 1,6-bisphosphate
F6P	Fructose 6-phosphate
G3P	Glycerol 3-phosphate
G3PD	Glycerol 3-phosphate dehydrogenase
G6P	Glucose 6-phosphate
GA3P	Glyceraldehyde 3-phosphate
GA3PD	Glyceraldehyde 3-phosphate dehydrogenase
GASH	Glutathione amide
GlcNAc-Mal	*N*-acetylglucosamine malate
GlcN-Ins	Glucosamine-*myo*-inositol
GlxI	Glyoxalase I
GlxII	Glyoxalase II
GlxIII	Glyoxalase III
GSH	Glutathione
GST	Glutathione *S*-transferase
GshA	γ-glutamylcysteine ligase
GshB	glutathione synthetase
GSSG	GSH disulfide
HEPES	4-(2-Hydroxyethyl)-1-piperazineethanesulfonic acid

HMBC	Heteronuclear multi-bond correlation
HPLC	High performance liquid chromatography
HSQC	Heteronuclear single quantum coherence
HTA	Hemithioacetal
Hz	Hertz
IT-ToF	Ion-trap Time-of-flight
J	Coupling constant
K_{eq}	Equilibrium constant
k_1	First order rate constant
k_2	Second order rate constant
k_{-1}	Reverse rate constant
k_2/k_{-1}	Equilibrium constant
LB	Lysogeny broth
LC-MS	Liquid chromatography – Mass spectrometry
LMW	Low molecular weight
mBBr	Monobromobimane
mB-SR	Monobromobimane thiol conjugate
Mca	Mycothiol *S*-conjugate amidase
MG	Methylglyoxal
MgsA	MG synthase

MSH	Mycothiol
MST	Mycothiol *S*-transferase
NMR	Nuclear magnetic resonance
OD	Optical density
OVO	Ovothiol
PEP	Phosphoenolpyruvate
RDW	Residual dry weight
RPM	Revolutions per minute
RSH	Low molecular weight thiol
$T(SH)_2$	Trypanothione
TEA	Triethanolamine
TIMs	Triosephosphate isomerase
TNB^-	2-Nitro-5-thiobenzoate
UDP-GlcNAc	Uridine diphosphate-*N*-acetylglucosamine
UV-vis	Ultraviolet-visible
WT	Wild-type

1. Introduction

Bacteria have colonised every niche on this planet from the soils of this earth – *Bacillus subtilis* to the intestines of mammals – *Escherichia coli*.[1] They have the ability to thrive in a diverse range of conditions and are able to adapt to constant fluctuations in their environment, which impose cell stress.

Cell stress is defined as 'any change in the genome, proteome, metabolome or environment that imposes either reduced growth or survival potential.[2] The causes include changes in temperature, pH, osmolarity and ionic content.[3] This is representative across all bacteria and without the appropriate survival mechanisms, will undoubtedly result in cell death. For this reason, bacteria have evolved various different stress response mechanisms in an attempt to restore cellular homeostasis and prevent further stress challenges, which often respond via regulation of cellular processes often involving a feedback loop.

Exposure to toxic compounds including reactive electrophiles is one significant example of cell stress. The presence of these electrophiles can result in changes to the redox status via the interaction with low molecular weight (LMW) thiols and they can alkylate and modify the functions of macromolecules such as DNA, RNA and proteins. A variety of mechanisms including export systems, repair systems and detoxification enzymes limit the damage to these nucleic acids and proteins.[2]

Bacteria are commonly exposed to a wide range of electrophiles, some of which are toxic to the cell. This project focuses on the involvement of LMW thiol cofactors such as glutathione (GSH), cysteine (Cys) and bacillithiol (BSH) and their interaction with metabolites including methylglyoxal (MG).

1.1 LMW molecular weight thiols

1.1.1. Overview

The majority of bacteria require an oxidising environment to live, but in excess, this can be problematic to the cell. Therefore, it is important they maintain a redox-regulated intracellular environment. This relies on the interaction with specialised molecules in the cell that are capable of reducing these oxidative species through various biochemical processes.[4]

These molecules are LMW thiol cofactors (figure 1.1), which play an important role in the maintenance and regulation of many cellular processes (scheme 1.1). For example, glutathione (GSH) is the most abundant LMW thiol found amongst eukaryotes and Gram-negative bacteria. However, not all organisms produce GSH and they rely on other LMW thiol cofactors to undertake these cellular functions, which include the dominant LMW thiol cofactors, mycothiol[5] (MSH), trypanothione[6] ($T(SH)_2$), glutathione amide[7] (GASH) and bacillithiol[8] (BSH). In addition to their major LMW thiol cofactor, many organisms possess additional thiol cofactors which include, cysteine[9] (Cys), homocysteine[10] (HCy), coenzyme A[11] (CoA), ergothioneine[12] (ESH), and ovothiol[13] (OTH).

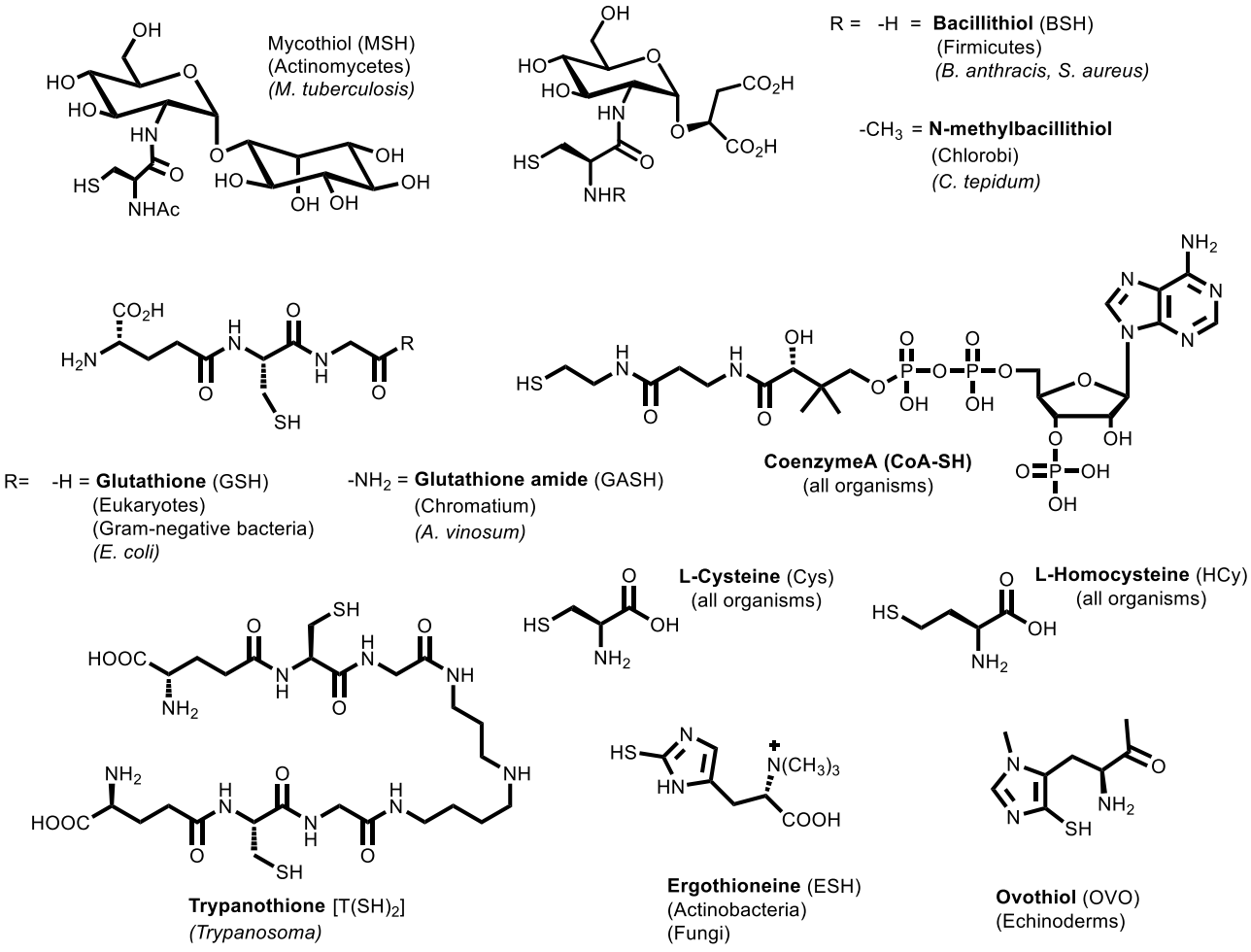

Figure 1.1. The LMW thiols present amongst different organisms

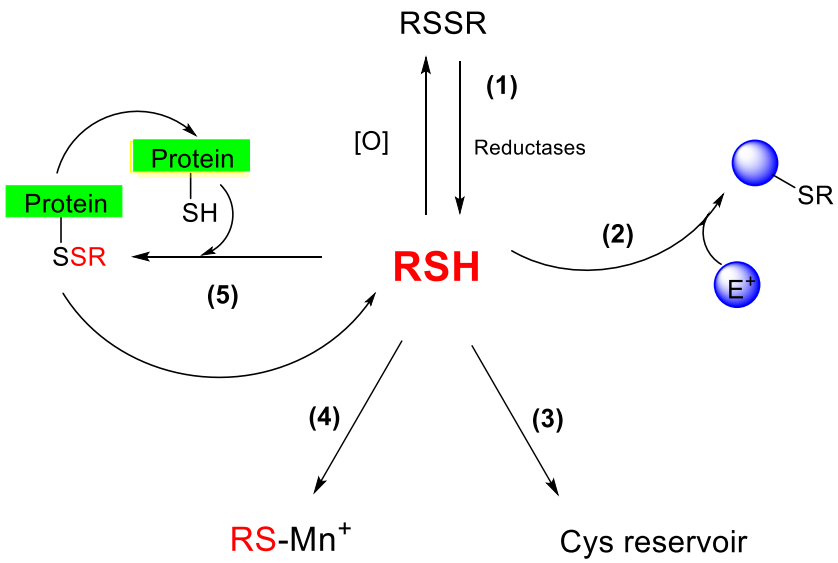

Scheme 1.1. The general cellular functions of the dominant LMW thiols; 1) as a redox buffer; 2) in electrophilic detoxification of xenobiotics and reactive carbonyl electrophiles; 3) as an intracellular Cys reservoir; 4) in metal ion homeostasis; 5) in redox regulation of proteins. All these roles exist amongst the dominant LMW thiol cofactors being, GSH, MSH, $T(SH)_2$ and BSH.

1.1.2. Glutathione

The majority of organisms including almost all eukaryotes and most Gram-negative bacteria utilise the dominant LMW thiol, glutathione (GSH).[14] GSH is a tripeptide containing glycine, cysteine and glutamate (figure 1.1). The biosynthetic pathway is a two-step enzyme catalysed process which involves an amide bond formation between Cys and glutamic acid catalysed by γ-glutamylcysteine ligase (GshA). This is followed by the addition of glycine onto the carboxylate of Cys, catalysed by the glutathione synthetase (GshB), forming GSH. The levels of GSH are regulated by feedback inhibition depending on the availability of Cys[15] where the intracellular concentrations of GSH are found to be present in the range of 3 – 7 mM in bacteria.[14]

As previously mentioned, all aerobic organisms are subjected to oxidative stress which is problematic to the cell causing protein and DNA damage. In the presence of these oxidative species such as H_2O_2 and NO, two GSH molecules can be oxidised to form the GSH disulfide (GSSG) by the enzyme glutathione peroxidase which in turn is reduced back to GSH by glutathione reductase. This protects against oxidative stress and therefore plays a major role in maintaining a physiological redox status in cells.[16, 17] GSH is also involved in other redox regulated processes including the post-translational modification for the redox regulation of proteins, by undergoing a process called glutathionylation, which is the formation of GS-*S*-protein mixed disulfides,[18] protecting cysteinyl residues on protein from oxidative stress. It also facilitates in metal ion homeostasis and is found to be involved in

the detoxification of toxic electrophiles (scheme 1.1). More recently, a derivative related to glutathione has been identified in prokaryotes, known as γ-L-glutamyl-L-cysteinylglycine amide (GASH) (figure 1.1). It exists in the cytoplasm of a purple anaerobe *Allochromatium vinosum* amongst the *Chromatium* species.[7] GASH is structurally very similar to GSH where an amide group replaces the carboxylate group of GSH.

1.1.3. Amino acids

Cysteine (figure 1.1) is an abundant LMW thiol present amongst all organisms and possesses a reactive thiol group.[19] The free thiol is present in all cells due to its importance as a main non-essential amino acid. It is present at low concentrations in the cell ranging from 0.03 - 0.2 mM depending on the stage of growth and organism.[20, 21] These low concentrations are a result of its involvement in protein synthesis.[22] Consequently, it is questionable to whether the levels of free Cys are sufficient to serve as a major thiol redox buffer. Similarly, homocysteine is another thiol-containing amino acid formed from the metabolism of methionine, which may play a role as a thiol redox buffer.[10]

1.1.4. Other LMW thiols

Most Gram-positive bacteria lack GSH, and Cys remains too low a concentration to serve as a major thiol redox buffer. [22] Therefore, the maintenance of a reduced environment relies on other LMW thiols. Mycothiol (MSH) is a major LMW thiol found amongst Actinobacteria including *Mycobacterium, Corynebacterium* and *Streptomyces*.[23, 24] It is composed of *N*-acetylcysteine (CysNAc) and a pseudo-disaccharide comprised of a glucosamine and *myo*-inositol (figure 1.1). It performs analogous functions to GSH (scheme 1.1),[14, 24] with the exception of one apparent difference being an additional pathway of xenobiotic detoxification. Herein, the mycothiol *S*-transferase (MST) first catalyses the conjugation of electrophile to mycothiol. The mycothiol-*S*-conjugate amidase (Mca) catalyses the mycothiol-*S*-conjugate producing mercapturic acid and glucosamine-*myo*-inositol (GlcN-Ins) which is exported from the cell. [25]

Trypanothione $T(SH)_2$ is another dominant LMW thiol cofactor, formed from two molecules of GSH joined via a spermidine linker (figure 1.1), present amongst the parasitic protozoa in the *Trypanosoma* and *Leishmania* species.[6] It possesses comparable cellular functions to the other dominant LMW thiols including protection against oxidative stress, certain heavy metals, and xenobiotics.[26]

Similar to Cys, there remain other LMW thiols which are found to only partially fulfil all the functions due to the involvement in other metabolic activity. One example includes coenzyme A (CoA) (figure 1.1), which is a LMW thiol cofactor present in all organisms and plays an essential role in metabolic processes such as lipid metabolism and the Krebs cycle.

In addition, the possession of the NAD(P)H-dependent CoA disulfide reductases (CoADR), have been isolated and characterised amongst, *B. anthracis*[27] and *S. aureus*[28], demonstrating CoAs involvement in redox regulation. However, a thiol pK_a of 9.83[29] would mean that CoA exists entirely in its unreactive form at physiological pH due to no availability of the thiolate anion required in thiol-disulfide exchange reactions.[4] Therefore, due to this high thiol pK_a and its involvement in other processes, it is questionable whether it serves as an efficient reducing buffer.

Ergothioneine (ESH) is an aromatic 2-thiolhistidine (figure 1.1), which is only biosynthesised in *Neurospora crassa*[30] in fungi and in *Mycobacterium smegmatis* [31] in the Actinomycetes,. However, it exists in other organisms from dietary sources.[26, 31] ESH exists in its reduced state at physiological conditions where it appears to serve as an effective antioxidant. However, no related enzymes have yet been discovered.

The ovothiols A-C (OVO) compromise of an *N*-methyl-4-mercaptohistidine group (figure 1.1), each with different degrees of *N*-methylation. They were first isolated from eggs and biological fluid of sea urchins and cephalopods amongst Echinoderms,[32] and are widely distributed amongst other organisms including *Dunaliella salina*, a halotolerant blue-green algae[33] and *Leishmania donovani,* a $T(SH)_2$ producing parasites.[32] ESH and OVO both show similarities in molecular structure and biosynthetic pathways[34] where they play an important role in resistance to oxidative stress amongst the specific organisms.

These LMW thiols are abundant amongst all organisms as they play a fundamental role in the redox processes within the cell. However, there remain many microorganisms with no identified LMW thiol. Only recently, the dominant LMW thiol, bacillithiol, emerged existing amongst the Firmicutes phylum in Gram-positive bacteria.

1.2. Bacillithiol

1.2.1. Overview

The dominant LMW thiol in low G+C Gram-positive bacteria, bacillithiol (BSH), an α-anomeric glycoside of L-cysteinyl-D-glucosamine with L-malic acid, is functionally analogous to related LMW thiols including MSH and plays a dominant role as a redox buffer.[14, 35] It is widely distributed in Gram-positive bacteria amongst the Firmicutes.[22] These include species amongst the *Bacillus* genus including *B. subtilis, B. anthracis, B. cereus, B. megatarium, B. pumilis* and are present in small amounts in *Geobacillus stereothermophilus* amongst the *Geobacilli*. It also exists amongst the *Staphylococcus* genus including *S. aureus* and *S. saphrophyticus* in addition to species in the S*treptococcus* and *Arthrobacter* genus (table 1.1), where is has been shown to exist in concentrations up to 5 mM in *B. subtilis* (table 1.2). Hence, it is found to be a widespread dominant thiol cofactor, emerging in many pathogenic strains of bacteria, highlighting its medical importance.[14]

More recently, this thiol cofactor has been indicated in other phyla outside the Firmicutes and possibly in Gram-negative bacteria. The presence of the three biosynthetic genes has been bioinformatically proven amongst *Chlorobium tepidum*. HPLC analysis on *Chlorobium tepdium* indicated a derivative of BSH, *N*-methyl-bacillithiol, a newly discovered LMW thiol in green sulfur bacteria within the chlorobi phylum *(Hiras, J unpublished 2017).*

Table 1.1. Intracellular concentrations of BSH µmol/g RDW[14]

Strain of bacteria	BSH concentration (µmol/g) RDW
Deinococcus radiodurans	0.6
Bacillus anthracis Sterne	0.2
Bacillus cereus	0.3
Bacillus megaterium	0.3
Bacillus pumilis	0.7
Bacillus subtilis 6051	0.3
Bacillus subtilis CU1065	0.6
Bacillus subtilis JH642	0.6
Geobacillus stearothermophilus	0.07
Staphylococcus aureus	0.7
Staphylococcus saprophyticus	0.2
Streptococcus agalactiae	0.2
Arthrobacter aurescens	0.09
Arthrobacter histodinolovorans	0.08

Table 1.2. Intracellular concentrations of thiols in *B. subtilis, E. coli* and human cells.

Concentrations of LMW thiol cofactors (at late phase exponential in bacteria)			
Cofactor	Organism	Concentration	Reference
Cys	*B. subtilis*	0.13 – 0.28 mM	(20)
	E. coli	0.02 mM	(24)
	Human plasma	8 – 10 µM	(36)
BSH	***B. subtilis***	**0.5 - 5 mM**	**(20)**
GSH	*E. coli*	> 10 mM	(37)
	Human plasma	< 5 mM	(36)

1.2.2. Biosynthetic pathway of BSH

BSH is biosynthesised in a three-step process (scheme 1.2). It is initiated by the enzyme glycosyltransferase (BshA)[38] which catalyses the glycosylation of L-malate and the substrate uridine diphosphate-*N*-acetylglucosamine (UDP-GlcNAc) to form the first intermediate *N*-acetylglucosamine malate (GlcNAc-Mal). An deacetylase (BshB)[39] then hydrolyses the acetyl group to form glucosamine malate (GlcN-Mal). The addition of Cys, catalysed by a cysteine ligase (BshC), produces the final product BSH (Cys-GlcN-Mal).[40, 41]

BshA is essential for the biosynthesis of BSH,[42] whereas, BshB is shown not to be necessary resulting in only a slight reduction of BSH in the mutant strain.[41] This is because it shares its deacetylase properties with BSH-*S*-conjugate amidase (Bca), which is also known to play a role in the drug detoxification of electrophiles.[22] There remains no evidence demonstrating the activity of BshC.[41] However, in *bshC* mutant strains, there is no production of BSH.

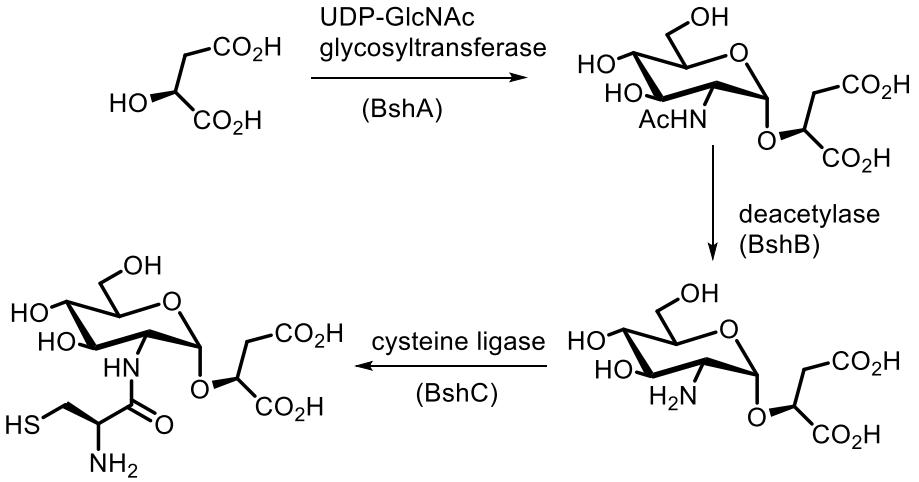

Scheme 1.2. Biosynthesis of bacillithiol.

1.2.3. Roles of BSH within the cell

The primary role of BSH is as a redox buffer, analogous to GSH and MSH. It maintains a reduced intracellular environment via the reduction of oxidants to produce bacillithiol disulfide (BSSB) through thiol-disulfide exchange mechanisms (scheme 1.3). The thiolate attacks the sulfur atom of the disulfide in a nucleophilic substitution to form a transition state complex, before the thiol is liberated as a leaving group.[43] The thiolate representing the ionised form is dependent on the pK_a of the thiol group which determines the rate of the reaction. These reactions are kept in a reduced form by NADPH-dependent flavoenzymes, known as the LMW thiol reductases, within the cell.

In addition to playing a role as a dominant redox buffer, BSH is found to be involved in many other functions (scheme 1.4). It plays a critical role in the post-translational modification of proteins and prevents exposed Cys residues from irreversible damage during oxidative stress.[44] Reactive oxidative species interact with BSH forming the mixed disulfide with the Cys residues of proteins. The process of *S*-bacillithiolation, is the formation of BS-*S*-Protein mixed disulfide, which functions as the main redox-regulatory mechanism in response to oxidative stress.[45] The de-bacillithiolation is then the reverse process, which involves the breaking of the disulfide bond forming the BSH moiety and the protein, catalysed by the bacilliredoxins, YphP and YqiW.[45]

BSH is also known to facilitate metal ion homeostasis. This is likely due to the close proximity of the amino and thiol group of the Cys moiety and carboxylate group of the malate moiety. It has been shown to chelate Zn^{2+} ions whilst maintaining the concentration of the free ion in the cytoplasm, acting as an effective buffer.[4] Therefore, it is anticipated that BSH functions as a reservoir of zinc and copper ions within the cell.[22] It is hypothesised to play a role in Fenton chemistry by reducing ferric ions and preventing oxidative stress caused by the reaction of metal ions and hydrogen peroxide generating hydroxide and hydroxyl radicals.[22]

Another key role of BSH, analogous to the related thiols GSH and MSH, is its involvement in the detoxification of xenobiotics and electrophiles in both enzyme-catalysed and chemical reactions.

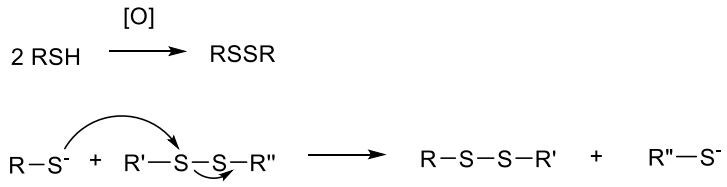

Scheme 1.3. Mechanism for thiol-disulfide exchange reactions. Reactive thiolate interacts with the disulfide in a nucleophilic substitution.

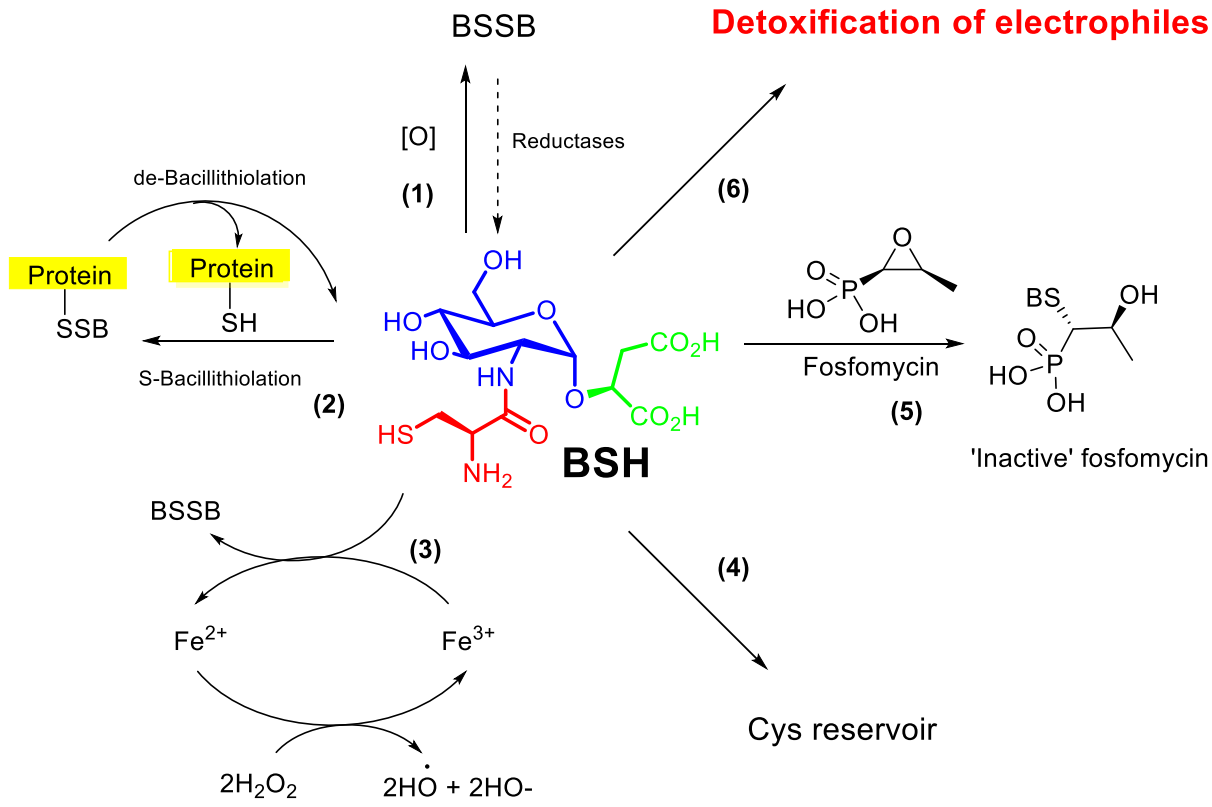

Scheme 1.4. The cellular functions of BSH: 1) redox buffers; 2) redox regulation of proteins; 3) metal ion homeostasis; 4) speculated intracellular cysteine reservoir 5) detoxification of xenobiotic fosfomycin 6) detoxification of electrophiles.

1.3. Detoxification processes of xenobiotics and electrophiles

The detoxification of electrophiles/xenobiotics occurs through interactions of thiols with the chemical species in either enzyme-catalysed reactions or a chemical reaction with highly reactive species.

1.3.1 Enzyme-catalysed reactivity of thiols

Thiols are known to react with many naturally occurring chemicals and xenobiotics. However, in some instances, the thiol is not a strong enough nucleophile to undergo these reactions. It therefore relies on the thiol-*S*-transferase enzymes, which lowers the thiol pK_a and increases their reactivity.[41] Currently, there are over 15 different enzyme classes in the glutathione *S*-transferase (GST) superfamily where there are four known GSTs which have been well studied.[46, 47] More recently, the bacillithiol *S*-transferases (BST) have emerged and shown to be responsible for some forms of antibiotic resistance. FosB is a BST which is known to be involved in the detoxification of the antibiotic, fosfomycin. This enzyme catalyses the BSH-dependent ring opening of the epoxide moiety of fosfomycin, rendering it inactive (scheme 1.4).[4, 42, 48, 49] In addition, FosA is an equivalent *S*-transferase found in some GSH-utilising bacteria.[50]

Another BST recently isolated in *B. subtilis*, has shown to be a member of the DinB superfamily. It contains the protein, YfiT, which catalyse xenobiotics in a BSH-dependent detoxification process.[51] YfiT has been shown to have *S*-transferase activity with monochlorobimane to form BSH-*S*-conjugates. Analogous to the MSH-dependent detoxification pathway present in mycobacteria,[52] an amidase, bacillithiol conjugate amidase (Bca), cleaves the amide bond to form GlcN-Mal and a Cys-*S*-conjugate. BshC catalyses the conversion of GlcN-Mal to reproduce BSH, whilst the Cys-*S*-conjugate is acetylated to form CysNAc-*S*-conjugates catalysed by cysteinyl *S*-conjugate acetyltransferase (CAT) where the conjugate is eventually exported from the cell (scheme 1.5).[53]

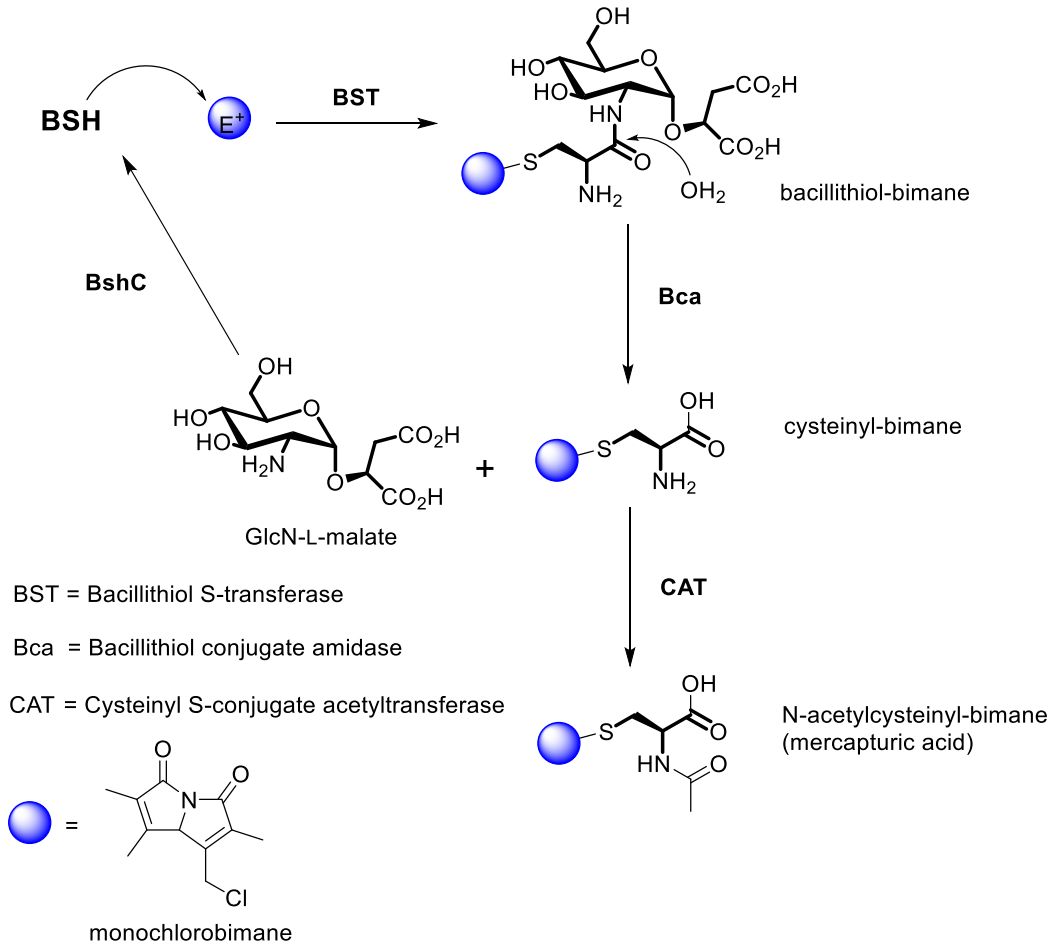

Scheme 1.5. Bacillithiol *S*-conjugate amidase (Bca) catalysed detoxification pathway of electrophilic xenobiotics/metabolites to produce mercapturic acid.

1.3.2. Chemical reactivity of thiols

Over 20 reactive carbonyl-containing species which have potential to interact with thiols in the cell have been identified, including formaldehyde, glyoxal, methylglyoxal, 3-deoxyglucosone and malondialdehyde.[54] In some instances, the carbonyl-containing species have proved to be good electrophiles, which interact with thiols non-enzymatically. For example, GSH has been shown to react with formaldehyde,[55, 56] a highly toxic metabolite produced as a by-product of methane and methanol metabolism. However, the most established reaction involves the highly reactive metabolite, methylglyoxal (MG), which was shown to react with GSH spontaneously, and follow through the thiol-dependent glyoxalase pathway.

1.4. Methylglyoxal

1.4.1. Overview

Methylglyoxal (MG) (scheme 1.6) is a toxic electrophile produced endogenously as a product of cellular metabolism, present in concentrations up to 1.5 mM in late exponential phase of *E.coli*.[57] It is composed of an aldehyde and ketone moiety, which co-exists as a monohydrate and dihydrate form in aqueous solution. As a strong electrophile found to be up to 20000-fold more reactive than glucose,[58] it is capable of non-enzymatically modifying macromolecules such as proteins, RNA and DNA causing a loss in biological activity (scheme 1.6).[59]

1.4.2. Toxicity of methylglyoxal

It was first identified that MG interferes with protein synthesis causing cell death in *E. coli* upon incubation of MG.[60] Studies have investigated the reactivity of amino acids with glyoxal derivatives, which were later confirmed to be involved in the formation of major advanced glycation end products (AGEs) in physiological systems.[61] Later on, it was shown that over 99% of methylglyoxal is reversibly bound to proteins.[62] *In vitro* experiments have shown that MG interacts with several protein amino acid side chains including arginine, lysine and cysteine.[63]

MG has also shown to modify nucleic acids suggesting another significant cause for its toxic effects. It was first reported that reactive aldehydes such as MG possess anti-viral activity due the interactions it has with DNA, therefore causing cell damage.[64] MG has also shown to crosslink DNA polymerase and the substrate DNA.[65] Subsequently, the significance of MG interaction with nucleic acids was confirmed by a numerous amount of studies highlighting its potent reaction and toxicity that it may cause to the cell.[65-67]

1.4.3. Formation of MG

There are several pathways of enzymatic and non-enzyme catalysed formation of MG (scheme 1.6). MG is formed from metabolic intermediates of carbohydrate, protein and lipid metabolism. The rate of formation of MG depends on the organism, tissue and cell metabolism and physiological conditions.[68] Acetoacetate is formed as a by-product of triglyceride metabolism. Acetone is then produced which is converted to acetol and then MG through a series of oxidation processes catalysed by the acetone and acetol monooxygenase, respectively. This pathway has only been known to exist in eukaryotes and has yet to be determined in bacteria.[69] Protein metabolism is another pathway of known MG formation. Herein, glycine and threonine can be degraded to form aminoacetone, which is then converted to MG, catalysed by amine oxidase.[70]

Glycolysis is found to be responsible for the majority of MG production. In glycolysis, glucose is metabolised in a 10-step pathway to form pyruvate. Fructose 1,6-bisphosphate produces one intermediate of each dihydroxyacetone phosphate (DHAP) and D-glyceraldehyde 3-phosphate (GA3P). They are isomers of each other, where their interconversion is catalysed by triose phosphate isomerase (TIMs). DHAP is problematic to the cell if allowed to accumulate as it contains a phosphate group which can therefore cause phosphate starvation within the cell. Therefore, the cell deals with high DHAP levels through the formation of MG, which occurs spontaneously[71] or via the catalysis of MG synthase (MgsA).[72] When MG is formed from DHAP, an inorganic phosphate is given off which is used to replenish the concentration of needed inorganic phosphate.[73-75] However, this leads to the accumulation of MG.

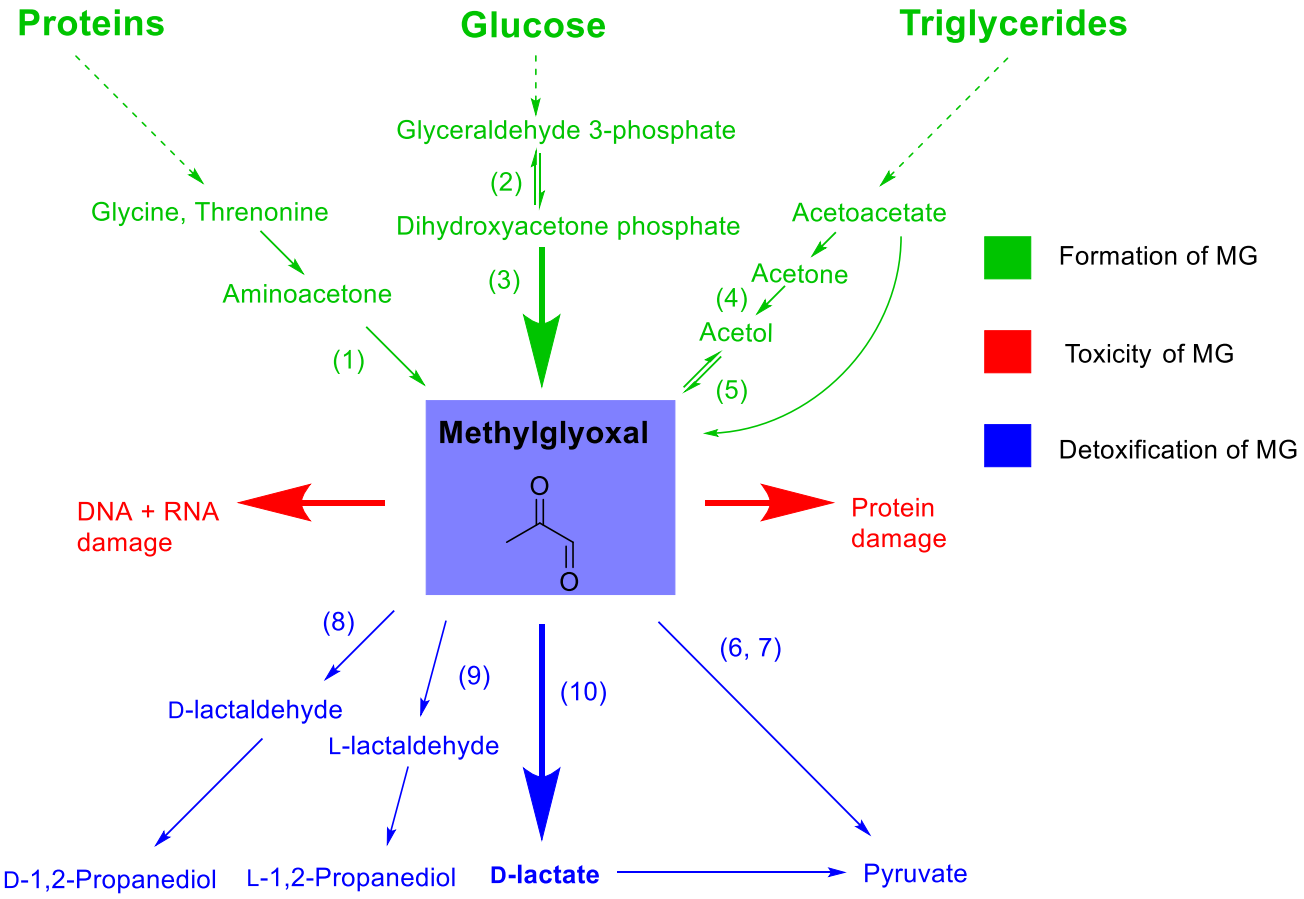

Scheme 1.6. The metabolism of methylglyoxal in eukaryotes. The enzymes are the following:- 1) amine oxidase 2) triose phosphate isomerase 3) methylglyoxal synthase 4) acetone monooxygenase 5) acetol monooxygenase 6) aldehyde dehydrogenase 7) 2-oxoaldehyde dehydrogenase 8) aldose reductase 9) methylglyoxal reductase 10) glyoxalase I/II.

1.4.4. Enzymes involved in the formation of MG

Triosephosphate isomerase (TIMs) catalyses the interconversion between GA3P and DHAP (scheme 1.7). This enzyme is a key component of glycolysis and is present in large concentrations to accommodate for the high levels of glucose undergoing metabolism. An enediolate intermediate is formed as an intermediate by TIMs formed from either DHAP or GA3P. With GA3P as a substrate, the K_m = 0.25 mM, k_{cat} = 6.2 x 10^3 s^{-1} and the catalytic efficiency is 2.5 x 10^4 mM^{-1} s^{-1}. With DHAP as a substrate, the K_m = 1.2 mM, k_{cat} = 1.1 x 10^3 s^{-1} and the catalytic efficiency is 903 mM^{-1} s^{-1}.[76] Therefore, there is a less efficient turnover for DHAP as a substrate relative to GA3P.[77]

MG synthase (MgsA) predominantly exists amongst bacteria but has recently been shown to exist in goat liver.[68] The enzyme is found to catalyse the conversion of DHAP with a K_m = 0.47 - 0.56 mM, k_{cat} = 325 s^{-1} and a catalytic efficiency of 613.2 mM^{-1} s^{-1}.[78, 79] Only the crystal structure of the bacterial enzyme has been determined.[80, 81] The specific reactivity of the enzyme is shown to be 25-fold greater than mutants strains, possessing an activity of 0.142 – 0.190 μM/min/mg protein amongst *E. coli*.[72] The absence of any known MgsA does not mean that MG does not exist amongst eukaryotes, as both DHAP and GA3P are found to be unstable at physiological cell conditions to form MG. The rate constant for DHAP and GA3P breakdown to MG in Kreb-Ringer phosphate buffer at 37 °C is 1.94 s^{-1} and 1.54 s^{-1}, respectively.[71, 82] Therefore, this is indicative that this degradation occurs amongst all eukaryotes.

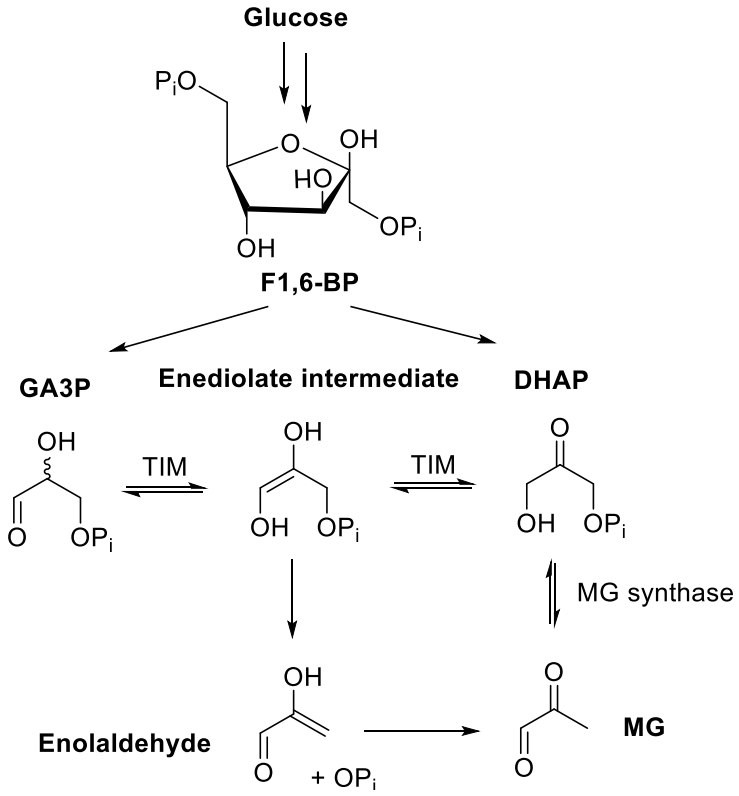

Scheme 1.7. The formation of MG via carbohydrate metabolism. GA3P and DHAP isomerises to form an enediolate intermediate.

1.5. Detoxification pathways of methylglyoxal

The toxic effects of MG makes it essential that the cell utilises the appropriate survival mechanisms. Currently, several MG detoxification pathways have been identified. Amongst bacteria, these include the thiol-dependent glyoxalase I-II pathway, the thiol-independent glyoxalase III pathway, and the MG reductase and dehydrogenase enzymes.

1.5.1. Thiol-independent detoxification pathways

The thiol-independent pathways of MG detoxification consist of several enzyme-catalysed reactions forming 1,2-propanediol, D-lactate and pyruvate, amongst bacteria. The two alpha-keto aldehyde dehydrogenase enzymes were the first thiol-independent MG detoxification enzymes to be discovered. They involve NAD and NADP-dependent oxidation of MG to pyruvic acid (scheme 1.6). [83, 84] Additionally, the aldose reductases, have shown to catalyse MG to form D-lactaldehyde and acetol, which then forms propanediol (scheme 1.6).[85-88] The YafB, YqhE, YeaE and YghZ proteins have been identified in *E.coli*.[86] In addition, *B. subtilis* has been shown to possess YhdN, the only known protein to be an aldose reductase amongst Gram-positive bacteria.[74] However, the most significant pathway of detoxification is thiol-dependent, which amongst eukaryotes is known as the GSH-dependent glyoxalase detoxification.

1.5.2. Thiol-dependent detoxification pathways

1.5.2.1 The glyoxalase pathway

The major MG detoxification pathway uses LMW thiol cofactors, which interact with MG and follow through a series of enzyme catalysed reactions known as the glyoxalase pathway.[89] Herein, MG non-enzymatically reacts with GSH to form a hemithioacetal (HTA) which in turn serves as a substrate for the glyoxalase I (GlxI)[90] enzyme (*S*-D-lactoyl-glutathione methylglyoxal-lyase), which isomerises the HTA to produce *S*-D-lactoyl-GSH. The glyoxalase II (GlxII)[91] enzyme, (*S*-2-hydroxyacylglutathione hydrolase), catalyses the hydrolysis of *S*-D-lactoyl-GSH to produce D-lactate while recycling the GSH (scheme 1.8). [92, 93]

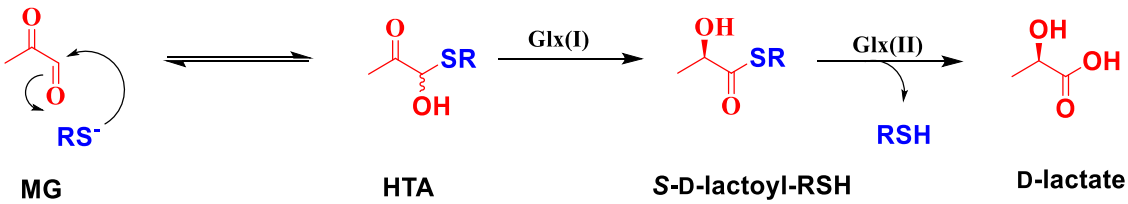

Scheme 1.8. The thiol dependent glyoxalase pathway.

1.5.2.2 The glyoxalase enzymes

GlxI is a member of the metalloglutathione transferase superfamily.[94] The enzyme has been characterised in humans, plants, yeast and a number of strains of bacteria including *E. coli, Yersinia pestis, Pseudomonas aeruginosa and Neisseria meningitidis.*[95-97] Recent data have emerged showing that there are different substrates for glyoxalase I including the GSH adducts with hydroxypyruvaldehyde, glyoxal and phenylglyoxal.[98] GlxII is shown to possess no similarities to GlxI. There is no characterised *glxII* amongst the prokaryotes. It is a member of a superfamily of hydrolases which includes the metallo-β-lactamases[99] and has a broad specificity for thioesters such as *S*-D-lactoyl-GSH.

Glyoxalase III (GlxIII) is an enzyme capable of catalysing the conversion of MG directly to D-lactate, with no need for GSH.[100] There is no current data of the class of enzymes of GlxIII. Research has emerged showing there are three enzymes which have been predicted to be homologues of glyoxalase III that convert MG to D-lactate, these being YdeA, YraA, YfkM, amongst *B. subtilis*.[74] However, this enzyme is found to have a minor contribution towards the overall degree of detoxification of MG.[101] The catalytic efficiency of GlxIII is found to be approximately 160-fold less efficient than GlxII and approximately 15000-fold less efficient than the GlxI (table 1.3). This large difference in catalytic efficiency confirms the overall significance of GlxI/II detoxification pathway over the thiol-independent glyoxalase III enzymes.

Table 1.3. The enzyme kinetics of the three glyoxalase enzymes of MG-SG substrate in *E. coli* strains

	Substrate	K_m (mM)	k_{cat} (s^{-1})	k_{cat} / K_m (mM^{-1} s^{-1}) catalytic efficiency	Organism
GlxI	MG-SG	0.027[102]	338-1120[102]	12,518-41,481	*E. coli*
GlxII	*S*-D-lactoyl-GSH	0.184[103]	53[103]	288	*E. coli*
GlxIII	MG	1.430[57]	2.615[57]	1.8	*E. coli*

1.5.2.3. KefB and KefC efflux system

The *S*-D-lactoyl-GSH intermediate also activates the KefB + KefC K^+ efflux system causing an efflux of potassium ions and H^+ influx, which protects against electrophiles by the lowering of the cellular pH.[104] A lower cellular pH results in a more protonated state and therefore less reactive form of the amino groups on DNA and proteins, and consequently, there is a reduced reactivity with electrophilic species in the cell such as MG (scheme 1.9).[74, 101]

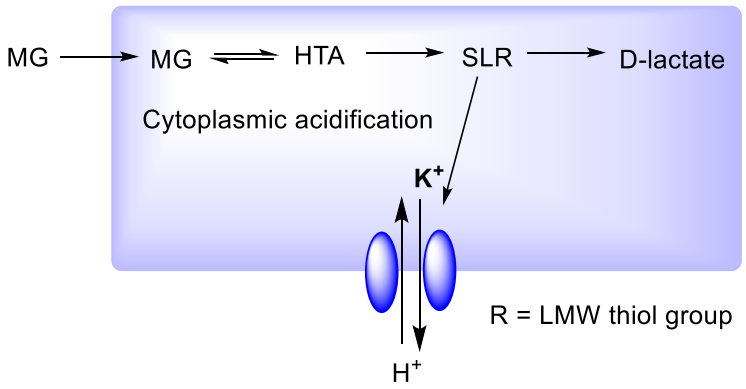

Scheme 1.9. *S*-D-lactoyl-RSH causes cytoplasmic acidification through the influx of H^+.

1.5.3. Does the BSH-dependent glyoxalase system occur in Gram-positive bacteria?

The pathway for GSH-dependent glyoxalase detoxification has been well established. It is found to be responsible for 70% of detoxification of MG in *E.coli* strains.[105] Considering the importance of this pathway amongst eukaryotes, the role of BSH amongst Gram-positive bacteria in the modification of MG has not been sufficiently investigated. The past research has reported that *B. subtilis* mutants lacking BSH are sensitive to MG, suggesting that, similar to GSH, BSH plays a role in the detoxification of MG.[53] It has also been reported that BSH confers protection against MG by converting MG to D-lactate where MG is responsible for rapidly depleting BSH in cells, providing some evidence that BSH follows through the glyoxalase pathway.[52] However, more research will be required to gain a full understanding of the involvement of BSH in the detoxification pathway.

1.6. Objectives of the research

The main objective of this research is to study the initial interaction of BSH with MG forming the HTA (scheme 1.10 ii/iii), which then proceeds through the glyoxalase pathway (scheme 1.10 vi). *In vitro* kinetics will focus on the initial step of chemical reactivity, i.e. the reaction between thiol and MG. This will include the determination of the relative rates of reactivity of MG with the different LMW thiols including BSH, Cys, GSH and CysNAc. In addition, the forwards and reverse rate constants of this reaction will produce a general idea of the most reactive thiols involved in this detoxification process.

For the *in vivo* studies, *B. subtilis* is used as the model organism. It is a soil dwelling Gram-positive bacteria, known to possess BSH as the dominant LMW thiol cofactor.[20] *B. subtilis* cells will be stressed with excess MG to determine the effects on the growth of the bacteria, as well as the intracellular thiol concentrations. In addition, the extracellular MG consumption will be investigated, to confirm the uptake and subsequent detoxification in the cell. In addition, there is relevance in determining the effects of MG on different levels of carbohydrate stress as MG is a by-product of glycolysis. Therefore the *in vivo* studies will, in general, potentially confirm the *in vitro* observations whilst also providing more evidence of the BSH involvement in the glyoxalase pathway.

Further studies will be carried out to confirm the formation of HTA. This will involve determination of the mass of HTA using mass spectrometry, in addition to NMR analysis of *in vitro* samples of HTA. This may potentially identify alternative products as a result of thiol reacting with MG. The evidence of these products will then be investigated using whole cell NMR analysis, providing direct *in vivo* evidence under physiological conditions that these HTAs are formed from the reaction between MG and BSH.

In summary, as BSH remains a newly discovered cofactor, there is much importance in unravelling its metabolic roles in the cell. Herein, this research focuses on investigating the nucleophilicity of BSH and its interaction with various electrophiles such as MG to form a possible HTA or a thiazolidine derivative. This will give us a greater understanding of the cellular functions of BSH amongst Gram-positive bacteria. Furthermore, it introduces the possibility of further interactions of LMW thiols with carbonyl-containing metabolites, which have the potential to exist amongst other organisms including eukaryotes and therefore of potential relevance in health-related conditions.

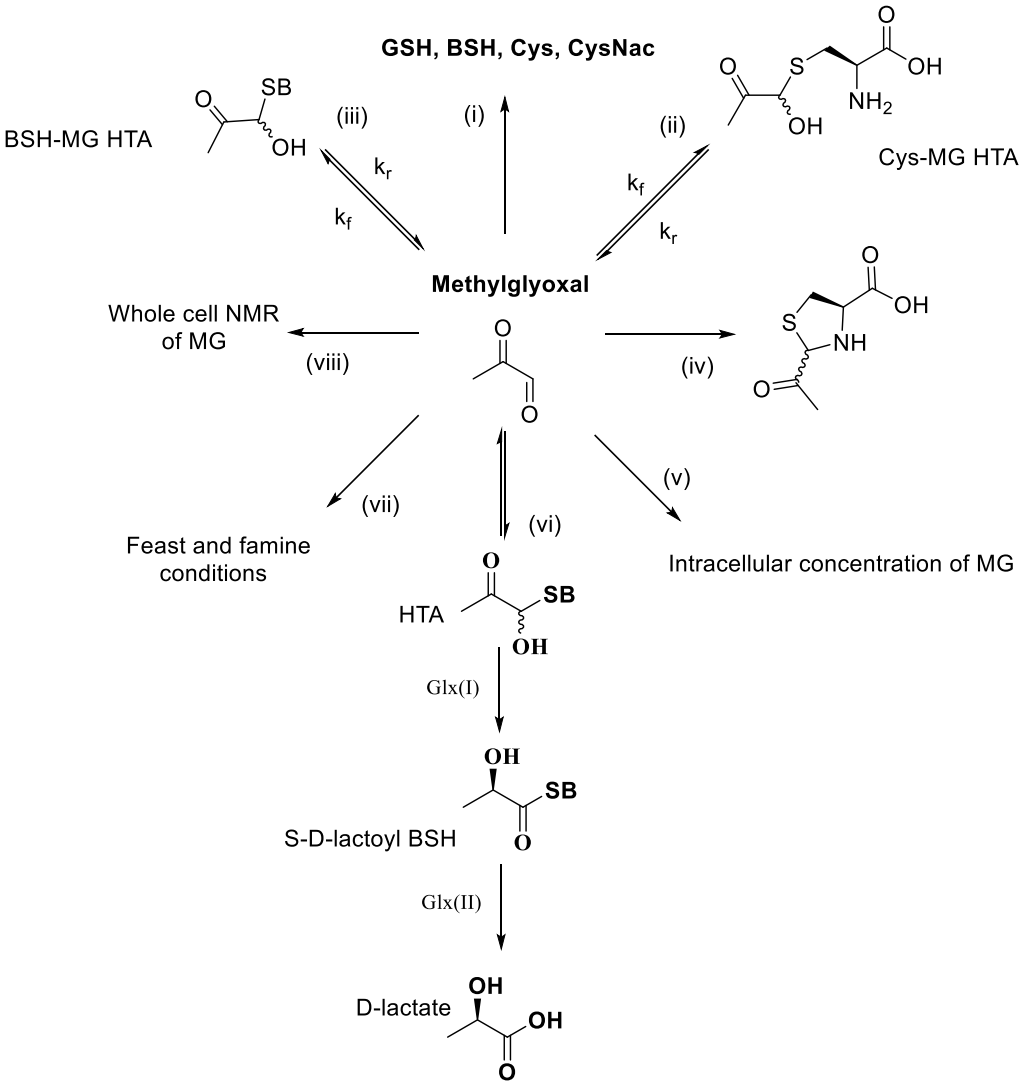

Scheme 1.10. Main objectives of this research project. i) Explore the relative reactivity of the four LMW thiol cofactors ii) Determination of rate constants for forwards and reverse reaction of Cys-MG HTA iii) Determination of rate constants for forwards and reverse reaction of BS-MG HTA iv) Determination of alternative detoxification pathways including the possible formation of a thiazolidine derivative v) Intracellular concentrations of MG vi) Exploration of the full involvement of thiol in the BSH-dependent glyoxalase pathway including thiol analysis and extracellular determination of MG concentration. vii) Analysis of the carbohydrate effects on growth, thiol levels and MG levels. viii) Whole cell NMR proving existence of BS-MG HTA.

2. Methylglyoxal and its interaction with low molecular weight thiols

2.1. Overview

The GSH-dependent glyoxalase detoxification pathway has been well established as the predominant detoxification pathway amongst GSH-utilising organisms.[89, 93, 98, 106] However, research remains limited into investigating the reactivity of other LMW thiols with MG. Although there is evidence that BSH reacts with MG and follows through the BSH-dependent glyoxalase pathway demonstrated in *B. subtilis*[74] (scheme 2.1), the focus of this chapter will involve investigating the roles of BSH as a chemical scavenger, primarily looking at the initial chemical reaction of BSH with MG in the formation of HTA (scheme 2.1A). Herein, the relative rates of reactivity, the rate constants, *in vitro* and *in vivo* studies of LMW thiols reacting with MG were determined, to produce an overall idea into the extent of involvement of each thiol in the detoxification process.

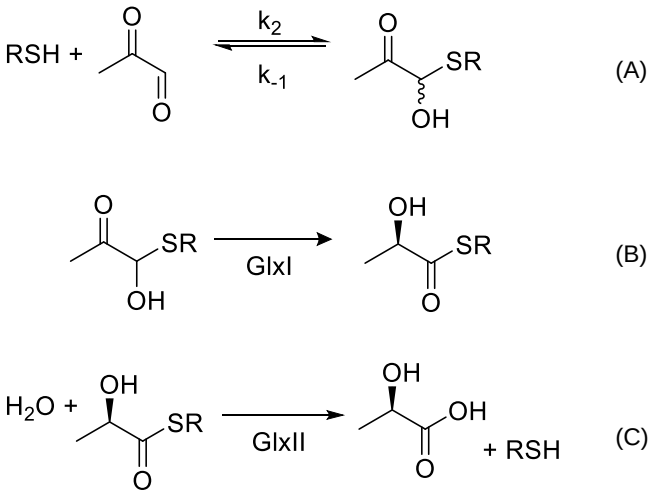

Scheme 2.1. The three reactions of the glyoxalase pathway.

2.2. *In vitro* chemical reactivity between LMW thiol cofactor and MG

2.2.1. Reactivity of LMW thiol cofactors

In the initial step, the thiol non-enzymatically reacts with MG to form an HTA, which follows second order reaction kinetics (scheme 2.1A). The thiol is a reactive nucleophile, which interacts with the aldehyde on the MG forming the HTA. It is also possible for the ketone on the MG to react, however this is a less likely reaction due to the steric effects and electron donating effects of the additional methyl group. Both Cys and BSH possess a zwitterionic nature as they also contain an amino group, which can potentially undergo reactions with electrophiles such as MG. However, previous research has shown that the thiol group is more likely to interact with the carbonyl group rather than the amino group, due to the thiol group being more nucleophilic.[107-109] In addition, it has previously been established that the presence of thiol has prevented the amino group to form hemiaminal.[110] In addition, the electrons in the outermost shell are more available to undergo a nucleophilic attack in sulfur relative to nitrogen due to the larger atom and lower electronegativity of the element. For these reasons, the research focuses predominantly on the reactivity of the thiol groups.

2.2.2. Influence of pK_a on the reactivity of LMW thiol cofactors

When investigating the reactivity of LMW thiols, an important aspect to consider is the pK_a of the thiol group. This reflects the proportion of thiol in its deprotonated form, known as the thiolate anion, which is the more reactive form representing a strong nucleophile. The lower the pK_a, the more deprotonated the thiol group and the higher the concentration of thiolate present at a specific pH. The zwitterionic nature of Cys and BSH have four ionisable forms, which represent the microscopic pK_a of the thiol cofactors (scheme 2.2, table 2.1).[20]The thiol pK_a of BSH is 7.97, which is found to be lower than Cys which has a thiol pK_a of 8.38. It is speculated that the protected cysteinyl carboxylate on the BSH with the uncharged amide group increases acidity of the thiol group by inductive effects.[20] In addition, the thiol pK_a of BSH is found to be significantly more acidic than GSH, which has a thiol pK_a of 8.93. This is possibly explained by the absence of a positively charged amino group on the Cys moiety which is responsible for stabilising the thiolate anion. As a result, the BSH is present in highest thiolate concentrations relative to Cys and GSH. At physiological pH in *B. subtilis*, pH 7.7, the percentage of thiolate for GSH, Cys and BSH are 6%, 15% and 22%, respectively (figure 2.1).[20] Therefore the thiol pK_a is likely to have a significant effect on the rate of reactivity of LMW thiols with potential electrophilic groups.

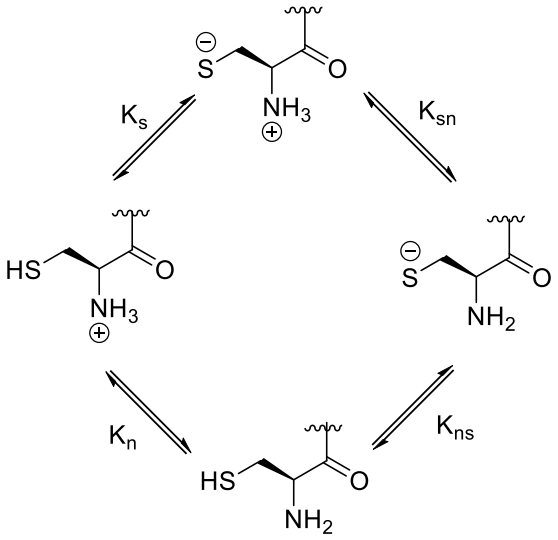

Scheme 2.2. The deprotonation pathways that represent the four microscopic pK_a of Cys and BSH.

Table 2.1. The microscopic pK_a of the LMW thiol cofactors, Cys, BSH and GSH.

Microscopic pK_a	Cys[20]	BSH[20]	GSH[111]
pK_s[a]	**8.38**	**7.97**	**8.93**
pK_n[a]	8.77	7.63	9.13
pK_{ns}[a]	9.94	9.55	9.08
pK_{sn}[a]	10.40	9.21	9.28

(a) The thiol pK_a abbreviations are indicated in scheme 2.2.

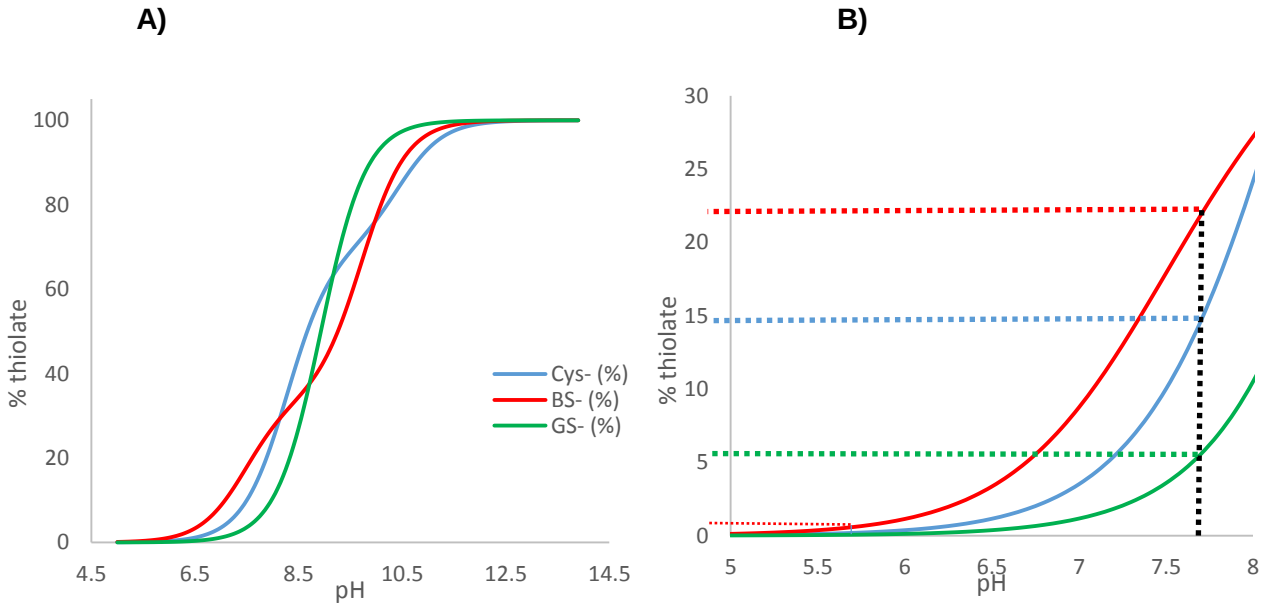

Figure 2.1. A) The pH-dependent proportions of total thiolate forms of Cys^-, BS^- and GS^-. B) The pH dependent proportions of thiolate forms of Cys^-, BS^- and GS^- at pH 5.6 and pH 7.7.[1]

2.2.3. Purification of MG

The majority of studies in this chapter use MG. Whilst MG is commercially available as a 40% aqueous solution, these solutions are contaminated with other molecules. Therefore to ensure that these studies are attributed definitely to MG, pure stocks were prepared from pyruvaldehyde dimethyl acetal (scheme 2.3).[112] Dowex-X8 resin (H^+-form, 2.5 g) was washed with water and treated with 1 M HCl. The resin was filtered and washed with water until reaching a neutral pH. A mixture of pyruvaldehyde dimethyl acetal, Dowex-X8 (H^+-form, 2.4 g) in MQ water was heated at 95 °C under a nitrogen atmosphere for 90 min and left overnight at room temperature. Water was added and the mixture was concentrated to a volume of ~120 mL under vacuum, and this was repeated five times. Finally, the Dowex resin was removed by filtration. The concentration of MG was determined by quantitative ^1H NMR (425 mM, >98% purity).

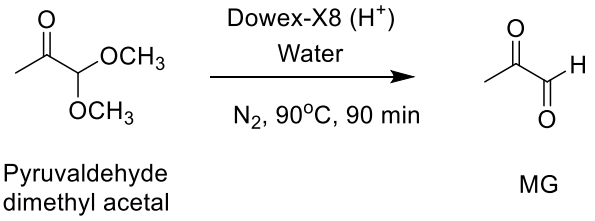

Pyruvaldehyde dimethyl acetal

MG

Scheme 2.3. Purification of MG.

2.2.4. Relative reactivity of Cys and BSH with MG

In vitro experiments were carried out to determine the rate of thiol consumption of BSH and Cys when reacted with MG. Herein, thiol (100 µM – 2000 µM) was reacted with excess MG (1500 µM) in a sodium phosphate buffer pH 5.6. Stopped assays were carried out where aliquots equating to 50 µM at t = 0, were removed at 10-second time points and quenched with Ellman's assay, to quantify the residual RSH (scheme 2.4).

The reaction between MG and thiol follows second order reaction kinetics. However, the reaction was carried out under pseudo-first order reaction conditions by using an excess of MG (1500 µM) relative to the thiolate concentration (0.15 – 4.6 µM). As a result, there is negligible consumption of MG over the course of the reaction, to produce a zero order reaction with respect to MG and a first order reaction with respect to thiolate. These conditions were used to produce a linear initial rate of thiol consumption and therefore allow an accurate comparison of both Cys and BSH reactivity with MG. As previously mentioned, physiological pH in the model organism, *B. subtilis*, is pH 7.7. However, the reactions could not be monitored at this pH because of the speed of the reaction, with a full consumption of Cys taking place within seconds. This was rectified by carrying out the reactions at pH 5.6, where only 0.46% of BSH and 0.15% of Cys is deprotonated. Therefore, there was a lower thiolate concentration resulting in a decreased rate of reactivity allowing the initial rate of thiol consumption to be determined.

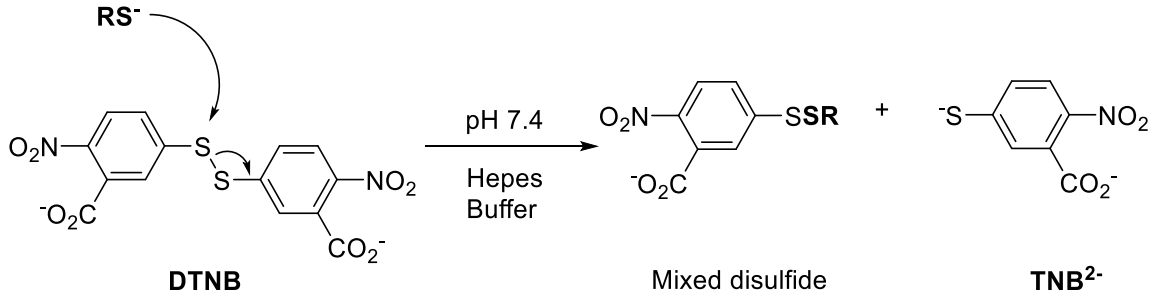

Scheme 2.4. Thiol quantification showing a thiol-disulfide exchange reaction between DTNB and reactive thiolate.

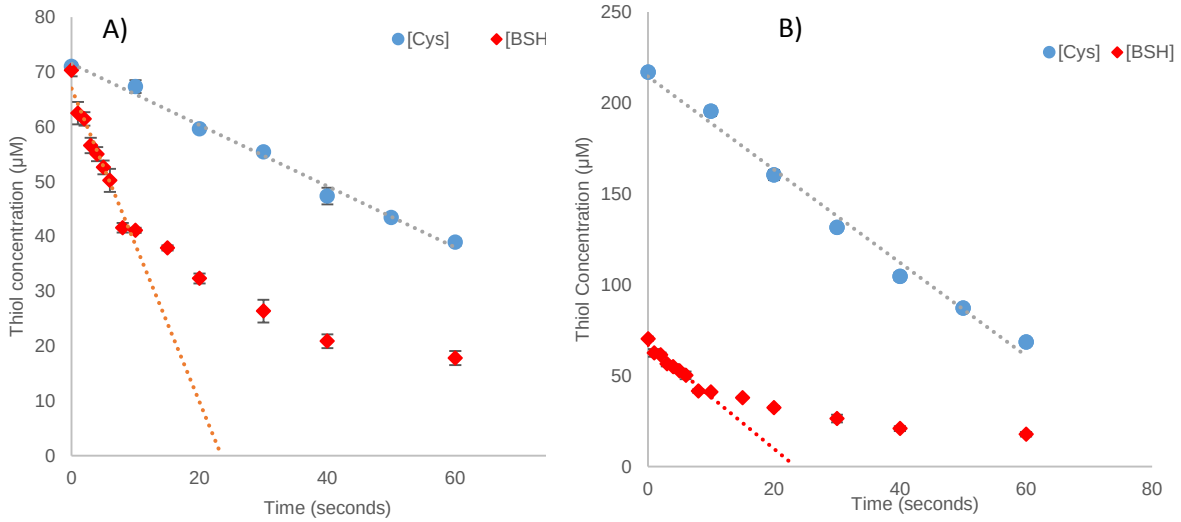

Figure 2.2. Reactivity of Cys/BSH (and thiolate anions) with MG (1500 µM) at; A) equivalent thiol concentrations at 70 mM; B) thiol concentration of Cys and BSH concentration at 218 µM and 70 µM, respectively, which correspond to the same thiolate concentration (0.29 µM) in sodium phosphate buffer, pH 5.6, 20 °C.

When comparing the relative rates of reactivity of BSH and Cys at pH 5.6, BSH is 5-fold more reactive than Cys at the same initial thiol concentration (figure 2.2A). This is represented by an initial rate of reaction of 2.9 µM/s for BSH as opposed to 0.56 µM/s for Cys. However, the rates are comparable when the same initial thiolate concentration of BSH and Cys are used (figure 2.2B). Cys consumption represents linearity for the first 60 seconds. However, the rate of consumption of BSH slows down after 10 seconds suggesting that it is attaining equilibrium.

The BSH and Cys thiolate represent equal reactivity; therefore, the predominant thiol species is based on the thiol pK_a and intracellular concentrations of the individual thiol. BSH has a lower thiol pK_a, and thus there is a higher portion of BS^- thiolate over the Cys thiolate at a specified pH (figure 2.1B). In addition, there is a higher intracellular concentration of BSH at approximately 3 mM at late-exponential phase of *B. subtilis* growth.[20] As a result, it can be concluded, that there is strong *in vitro* evidence to show that BSH reacts preferentially over Cys, identifying it as a main cofactor in MG detoxification.

2.2.5. The reactivity of other LMW thiols, GSH and CysNAc, with MG

The reactivity of other LMW thiols were then investigated. In view of GSH being the dominant thiol in eukaryotes, there is significant research that has investigated the reactivity of this thiol cofactor with MG and other carbonyl-containing molecules, dating back to 1934.[98, 106, 113, 114] Although there is extensive research, the assays of GSH and MG reactivity were carried out in a similar approach to Cys and BSH assays to allow an effective comparison. The thiol pK_a's of GSH and CysNAc, are 8.93 and 9.52, respectively.[115] There is approximately 10-fold less thiolate of GSH and 38-fold less thiolate of CysNAc at pH 5.6 relative to BSH. So, CysNAc (4200 µM) and GSH (2100 µM) were individually reacted with MG (5 mM) at pH 5.6, representing a comparable thiolate concentration to the Cys/BSH assays. As a result, both GSH and *N*-acetylcysteine (CysNAc) showed no reactivity with MG over a 3-hour period. The reaction was then investigated at a higher pH 7.7 with thiolate concentrations of approximately 200 times more concentrated relative to the Cys^- and BS^- thiolate concentrations at pH 5.6. The reactivity was analysed over a 20-minute period. GSH reacted with MG, producing a rate of reactivity of 9.53 nM/s (figure 2.3), showing a substantially decreased rate of reactivity when compared with BSH and MG. No reactivity of CysNAc was observed which is shown to differ in other research which demonstrates reactivity with MG to be approximately 3-4 times less reactive than Cys, regulated at 37 °C, pH 7.4, over a 6 hour time-period.[110]

Whilst the thiol pK_a has a large effect on the rate of reactivity of the thiol, the equally reactive BS^- and Cys^- at comparable thiolate concentration are shown to possess significantly faster rates of reactivity relative to GSH and CysNAc. Therefore, this suggests other aspects need to be taken into consideration. These include the chemical properties and steric effects of the individual thiol. Whilst BSH possesses the highest molecular weight, the thiol group on GSH is the most sterically hindered as it consists of an N-terminal glutamate on the Cys moiety. In addition, previous research has reported the availability of the amino group has been shown to affect the reactivity of a thiol group.[110]

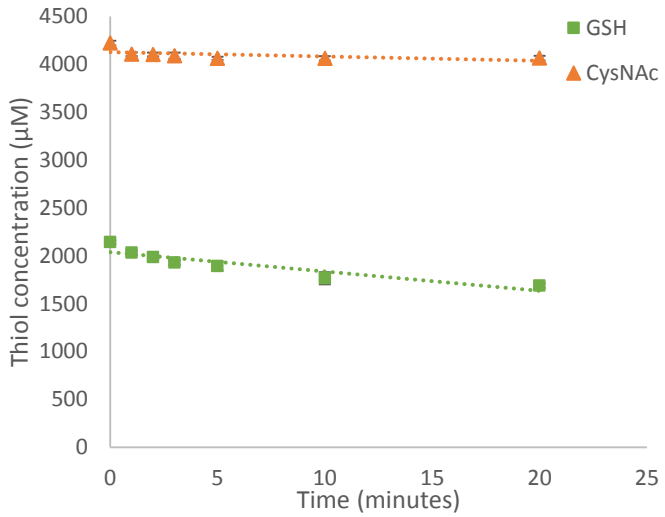

Figure 2.3. The rate of reactivity of GSH (2100 µM thiol, 61 µM thiolate) and CysNAc (4200 µM thiol, 61 µM thiolate) with MG (5000 µM) in HEPES pH 7.7, 20 °C, over a 20-minute time-period.

2.2.6. Long-term reactivity of thiol with MG

This research has predominantly investigated the initial rate of reactivity of thiols with MG determining the immediate kinetics. However, it remains unknown as to whether the thiol remains the predominant reactive group or the amino group may potentially be involved. This was investigated by monitoring the course of this reaction over a longer period.

The reactivity was monitored in a RSH:MG ratio of 1:1 and 1:5, at pH 7.4, at 20 °C, over a 4-hour period. For the 1:1 ratio, the majority of thiol had reacted within 2 minutes, with 80% reactivity of BSH and 60% reactivity of Cys. As the reaction proceeds, after reaching 80% reactivity of thiol groups for both BSH and Cys, the percentage of free thiol groups gradually decreases over the 4 hours (figure 2.4A). A similar reaction was observed in excess MG (figure 2.4B). As previously discussed, both Cys and BSH contain the nucleophilic thiol and amino group. It is known that there is an initial immediate reaction with the thiol group after the first 2 minutes representing the thiol group being involved in the fastest reaction process. Then the percentage of reacted thiol groups decreases which could represent a dissociation of the HTA and the formation of the hemiaminal from the amino group reacting with MG (scheme 2.5).[110]

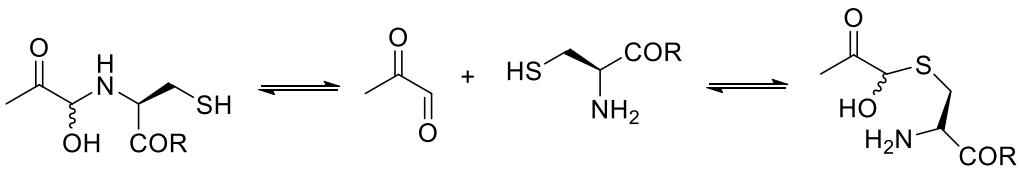

Scheme 2.5. Reaction of thiol and MG forming HTA and possibly hemiaminal

The reaction course curves differ significantly in other related LMW thiols including CysNAc and GSH.[110] Under the same conditions, it is reported that only 14% of thiol groups for GSH and 7% of thiol groups for CysNAc react within the first minute which gradually increases over the next 2 hours[110]. Therefore, suggesting that the reactivity of thiol groups of all LMW thiols with MG, decreased in order BSH > Cys > GSH > CysNAc.[110] This complies with the original kinetics investigating the relative rate of reactivity's of the different thiols (chapter 2.2.4, 2.2.5).

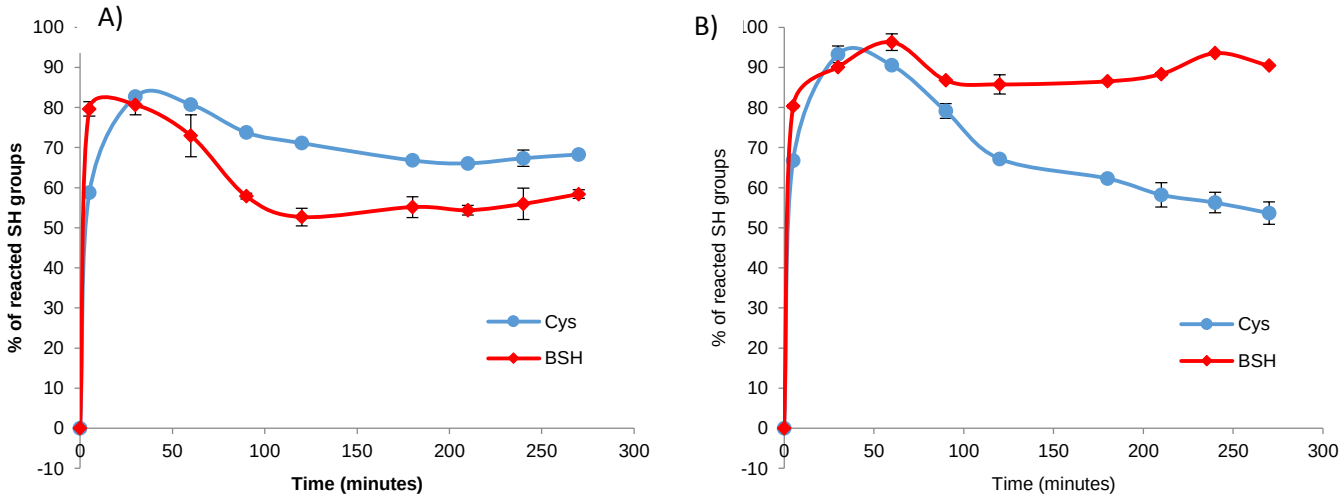

Figure 2.4. The time course of reaction of thiol groups with MG in reactant ratios of A) 1:1 2 mM RSH: 2 mM MG and B) 1:5 2 mM RSH: 10 mM MG at incubation in sodium phosphate buffer pH 7.4 at 20 °C.

2.2.7. Potential thiazolidine formation

Following HTA formation, in the case of both Cys-MG and BS-MG HTA, the presence of a thiol and amino group in close proximity, has the possibility of forming a thiazolidine derivative (scheme 2.6).[110, 116-118] It has shown to be more stable than the HTA and it is therefore plausible that there are higher concentrations of thiazolidine present in the cell,[119] representing another possible mechanism of detoxification for MG.

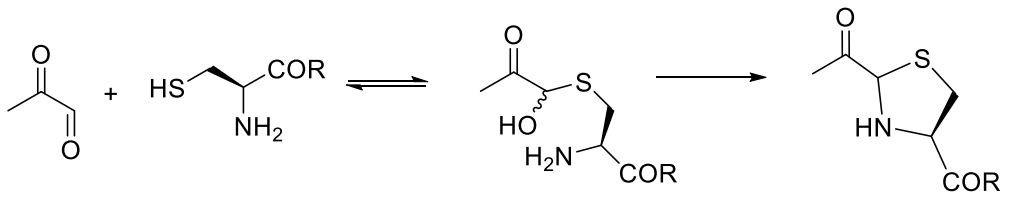

Scheme 2.6. Chemical scheme of thiol reactivity with MG to form HTA and then thiazolidine.

2.3. pH-dependent (pH 5.6) and pH-independent rate constants

2.3.1. Overview

Experimental analysis was required to determine the rate orders (chapter 6.5.4). This was carried out by investigating the fold-change of the rate of reaction when the concentration of a single species is changed. As a result, under excess MG concentration, a pseudo-first order reaction exists (Eq. 2.2). In addition, the dissociation of HTA also represents a first order reaction (Eq 2.3).

Rate of forwards reaction = k_2 [C=O][RSH] (Eq. 2.1)

Rate of forwards reaction = k_1 [RSH] (under pseudo-first order conditions) (Eq. 2.2)

Rate of reverse reaction = k_{-1} [HTA] (Eq. 2.3)

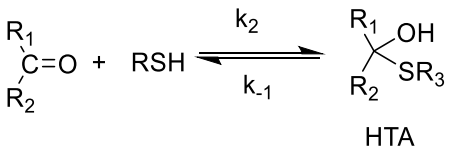

Scheme 2.7. Carbonyl-containing metabolite reacting with thiol to form HTA, representing k_2 and k_{-1}

2.3.2. Forwards rate constant (k_1) of thiol and MG reactivity

Under physiological conditions, many factors can alter the rate of reactivity of thiols reacting with MG. Other than the complexity of the cells with the many on-going cellular processes, the pH greatly affects the rate of reactivity of thiol with MG. Therefore, the data showing the relative rates of reactivity (chapter 2.2.4, 2.2.5) are limited because they represent only a specific concentration at specified pH of thiol reactivity. This was overcome by determining the pH-independent rate constants, which investigates the rate of reaction taking into account all the different thiolate concentrations.

The rate constants were determined for the reactivity of MG with Cys and BSH. The initial rate of reaction was first determined by investigating the consumption of thiol at different initial concentrations with excess MG (1500 μM). As a result, > 5 varied gradients representing a rate of reaction at different initial concentrations were produced (figure 2.5A/B). A plot of the initial rate of reaction against the initial thiol concentration produces a gradient which represents the rate constant (k_1) at pH 5.6. In addition, the plot which represents the thiolate concentration shows a gradient which represents the pH-independent rate constant (k_1) (figure 2.5D). The second order rate constant was then

determined by dividing the pseudo-first order rate constant by the MG concentration (table 2.2).

The pseudo-first order rate constants represented by the formation of HTA between MG with Cys and BSH were found to increase linearly up to 0.5 mM and 0.1 mM, respectively (figure 2.5C). However, above these concentrations, the rates of reaction levels off and becomes independent of MG concentration. This is shown by a hyperbolic curve representing a decreased rate of reaction at higher concentrations of Cys/BSH. The reason for this is possibly due to a higher concentration of MG in its hydrate form which is not detected in the Brady's reagent quantification of MG due to the different reaction conditions. As a result, there are lower concentrations of the keto- form of MG.

The reactivity of MG with BSH is found to have approximately 3-fold increase in rate of reactivity in comparison to MG with Cys (figure 2.5C), which reflects the relative rate of reactivity in preliminary investigation (figure 2.2A). However, the pH-independent rate constants which investigates the reactive species being the thiolate, were found to show approximately the same level of reactivity of each thiol with MG (figure 2.5D).

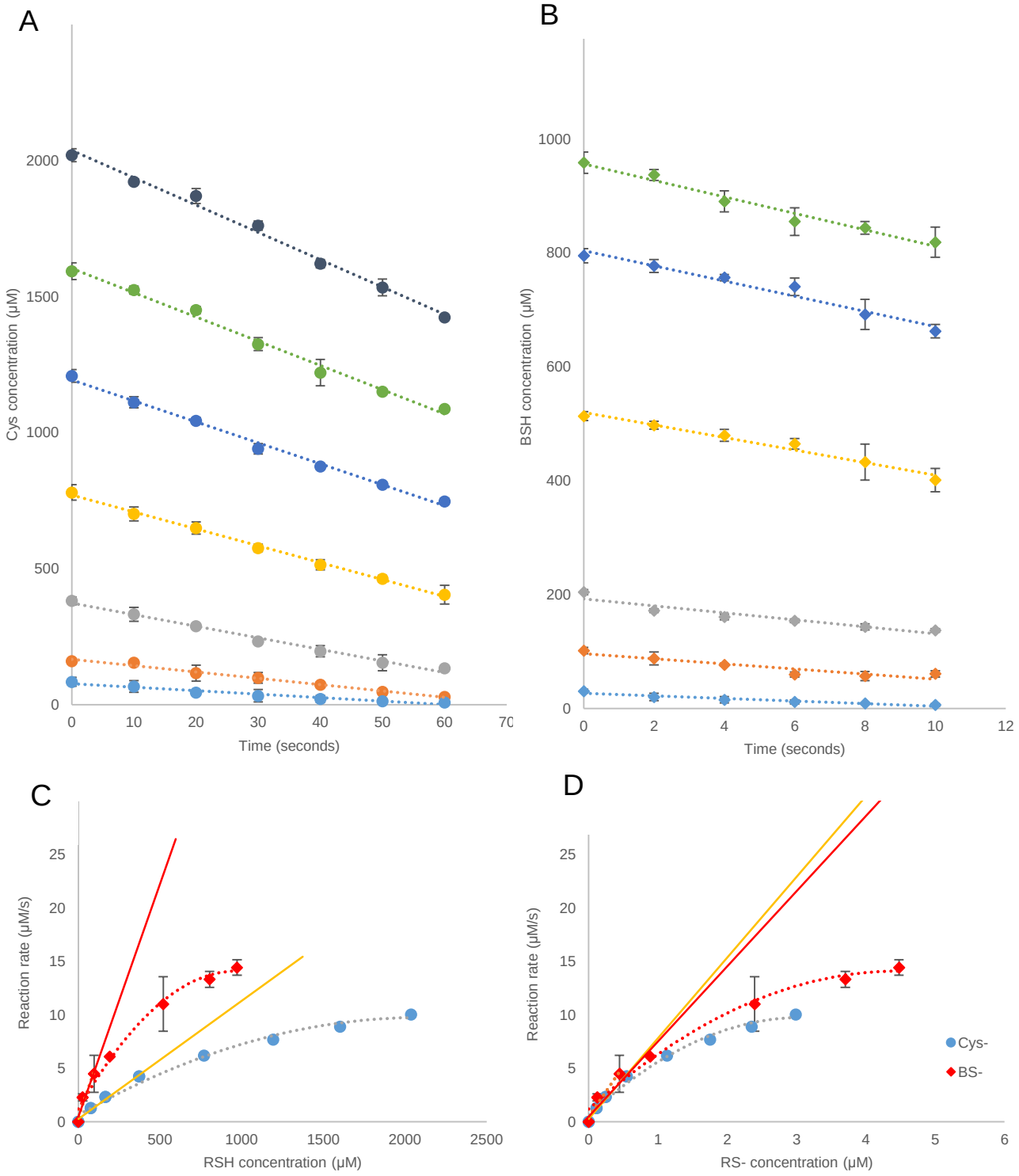

Figure 2.5. A) The consumption of Cys (100 μM – 2000 μM) with MG (1500 μM) in HEPES buffer (50mM), pH 5.6, 20 °C, representing pseudo first order reaction kinetics with each gradient representing the reaction rate. B) The consumption of BSH (100 μM – 1000 μM) with MG (1500 μM) in HEPES buffer (50mM), pH 5.6, 20 °C, representing pseudo first order reaction kinetics. C) The two rate constants of MG reactivity with Cys/BSH, at pH 5.6 D) The two pH independent rate constants of MG reactivity with Cys/BSH. Data was carried out in duplicate where error bars show ± SEM.

2.3.3. Reverse rate constant (k_{-1}) of HTA dissociation

The dissociation rate of HTA forming thiol and MG was determined. Thiol (5 mM) and MG (10 mM) was initially reacted in HEPES pH 7.7 until there was a full consumption of thiol, confirmed by Ellman's reagent, implying that the HTA has formed (scheme 2.4). Several dilutions of the newly formed HTA (125 - 750 µM) were then individually quenched with Ellman's reagent, pH 7.7. The Ellmans' reagent labels the residual thiol resulting in a shift in equilibrium allowing the dissociation of HTA to be determined (scheme 2.8). An increase in absorbance represents thiol being liberated as the HTA dissociates back to form thiol and MG (figure 2.6).

The gradient produced represents the dissociation rate constant (k_{-1}), which is observed in a linear range (figure 2.7A/B). It shows the dissociation of HTA to form BSH and MG to be faster than the dissociation of HTA from Cys and MG, by 5-fold (figure 2.7C). In each instance, the reverse rate is significantly slower than the forwards rate (table 2.2). Therefore, suggesting that the formation of HTA in the reaction of thiol and MG is favoured.

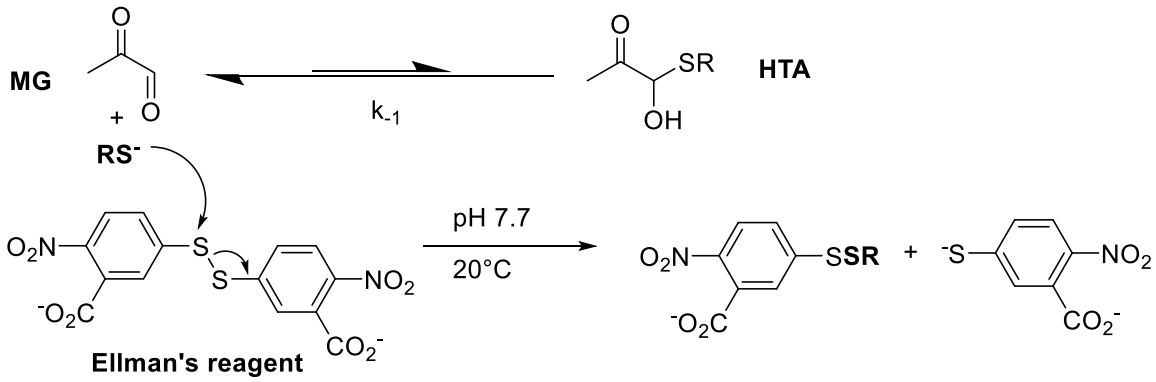

Scheme 2.8. DTNB reacting with residual thiolate therefore altering the equilibrium allowing determination of the off-rate of reaction.

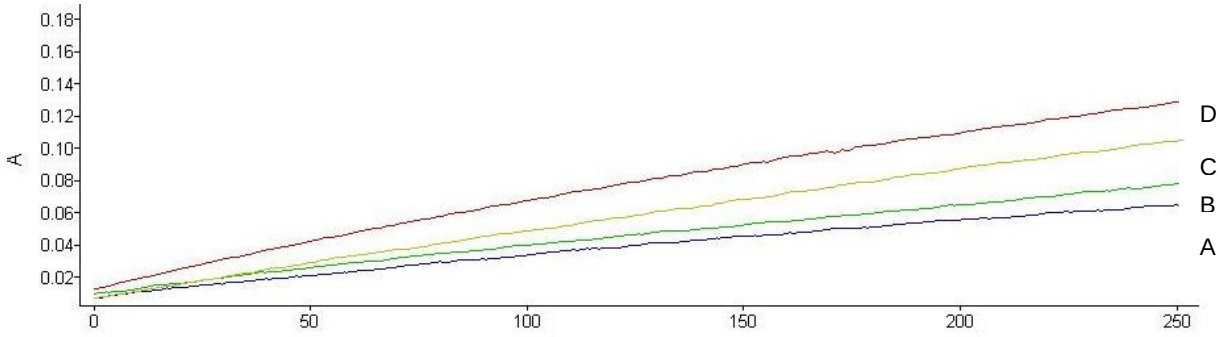

Figure 2.6. UV-vis spectrum showing the off rate of reactivity represented by the formation of thiol from HTA, which then further reacts to form the UV-active TNB^{2-}. Thiol (5 mM) and MG (10 mM) was reacted in HEPES pH 7.7 until equilibrium was reached. A range of different HTA concentrations A) 125 µM, B) 250 µM, C) 375 µM, D) 500 µM were prepared in Ellman's reagent, pH 7.7.

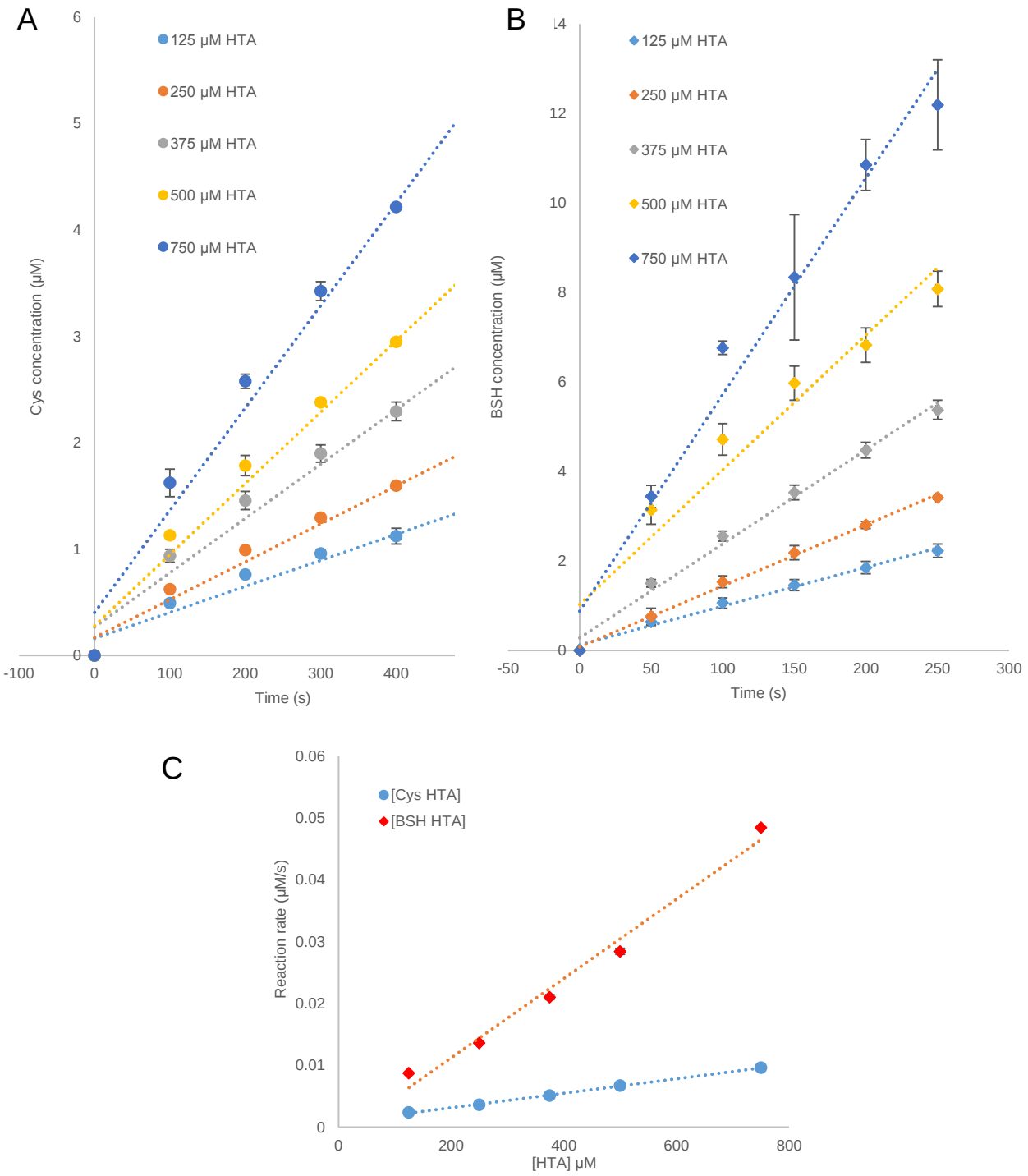

Figure 2.7 A) The dissociation of HTA (125 µM – 750 µM) using DTNB (2 mM) in HEPES buffer (50 mM) pH 7.7, 20 °C, over 500 seconds after carrying out an initial reaction of Cys (5 mM) with MG (10 mM) in HEPES buffer (50mM), pH 7.7, 20 °C, with each gradient representing the reaction rate. B) The dissociation of HTA (125 µM – 500 µM) using DTNB (2 mM) in HEPES buffer (50 mM) pH 7.7, 20 °C, over 250 seconds after carrying out an initial reaction of BSH (5 mM) with MG (10 mM) in HEPES buffer (50mM), pH 7.7, 20 °C, with each gradient representing the reaction rate. C) The two dissociation rate constants of HTA to form DHAP and Cys/BSH, at pH 7.7. Data was carried out in duplicate where error bars show ± SEM.

2.4. Thermodynamics – equilibrium constant (K_{eq}).

The pseudo-first order rate constant (k_1) was determined at pH 5.6, whereas the reverse rate constant (k_{-1}) was determined at pH 7.7. For the determination of the equilibrium constant, it is necessary the forwards and reverse reaction are at the same pH. Therefore, the predicted forward rate constants (k_1) were calculated at pH 7.7 to give a value of 1.13 s^{-1} and 2.08 s^{-1} for the reactivity of MG with Cys and BSH, respectively. Furthermore, the second order rate constants were then calculated to give a value of 753.5 $M^{-1}s^{-1}$ and 897.4 $M^{-1}s^{-1}$ for the reactivity of MG with Cys and BSH, respectively (table 2.2). The equilibrium constants were then determined (table 2.4) by incorporating the second order rate constant over the reverse rate constant (k_2/k_{-1}). As a result a large value (>10^5) is found suggesting that the forwards rate of reaction is favoured.

Table 2.2. Pseudo-first order rate constant (k_1), second order rate constant (k_2) and reverse rate (k_{-1}) constants for HTA formation from Cys and BSH reactivity with MG

	Rate constant pH 5.6 (±SEM)	Rate constant pH 7.7[a] (±SEM)	pH-independent rate constant (±SEM)
Pseudo-first order rate constant (k_1) with respect to thiol			
Cys-MG	1.39 x 10^{-2} s^{-1} (±5 x 10^{-5})	1.13 s^{-1} (±4.1 x 10^{-3})	9.46 s^{-1} (±2.2 x 10^{-2})
BS-MG	4.36 x 10^{-2} s^{-1} (±1.25 x 10^{-3})	2.08 s^{-1} (±6.0 x 10^{-2})	7.55 s^{-1} (±0.73)
Second order rate constant (k_2)			
Cys-MG	9.3 $M^{-1}s^{-1}$ (±3.3 x 10^{-2})	753.3 $M^{-1}s^{-1}$ (±2.7)	6306.6 $M^{-1}s^{-1}$ (±14.7)
BS-MG	29.1 $M^{-1}s^{-1}$ (±0.83)	897.4 $M^{-1}s^{-1}$ (±40)	5033 $M^{-1}s^{-1}$ (±486.7)
Reverse rate constant (k_{-1})			
Cys-MG	-	1.242 x 10^{-5} s^{-1} (±1.5 x 10^{-7})	-
BS-MG	-	6.262 x 10^{-5} s^{-1} (±5 x 10^{-7})	-

[a]Rate constant could not be determined at this pH because of the speed of the reaction and therefore the rate constant has been calculated based on the thiolate concentrations at pH 7.7 relative to pH 5.6.

Table 2.3. The half-life for the dissociation of HTA to form free thiol and MG.

	half-life ($t_{1/2}$)
Cys-MG	15 hours 30 minutes
BS-MG	3 hours and 6 minutes

Table 2.4 Determination of equilibrium constants from thiol and MG.

Equilibrium constant for Cys and MG	**Equilibrium constant for BSH and MG**
k_2 [C=O][Cys] = k_{-1} [HTA]	k_2 [C=O][BSH] = k_{-1} [HTA] (Eq. 2.4)
$\frac{k_2}{k_{-1}} = \frac{[HTA]}{[C=O][Cys]} = \mathbf{K}$	$\frac{k_2}{k_{-1}} = \frac{[HTA]}{[C=O][BSH]} = \mathbf{K}$ (Eq. 2.5)
$\frac{k_2}{k_{-1}} = \frac{753.3}{1.24 \times 10^{-5}} = \mathbf{1.5 \times 10^7}$	$\frac{k_2}{k_{-1}} = \frac{897.4}{6.26 \times 10^{-5}} = \mathbf{1.4 \times 10^7}$

2.5. *In vivo* analysis of the BSH-dependent glyoxalase pathway

This research has shown, the *in vitro* relative reactivity, rate constants and equilibrium constants of BSH and Cys reacting with MG. There is now relevance in understanding how these results compare with the observations made *in vivo*. To explore this, the next stage was to quantify the intracellular concentrations of Cys and BSH when exposed to excess MG, amongst *B. subtilis*.

2.5.1. Quantification of intracellular thiols

To quantify intracellular thiols, Ellman's reagent is not effective. A standard reagent for measuring the intracellular concentrations of thiol is known as monobromobimane (mBBr) reagent. It has been widely used for many decades to quantify the intracellular thiol concentrations when exposed to a variety of external environmental stresses. Once the cells have been stressed with a compound, at different time-points samples of cells can be treated with the cell permeable MBBr reagent. The compound selectively reacts with thiols in the cell to produce a highly fluorescent and stable thioester (mB-SR) (scheme 2.9).[120] However, in this case, it is important to be aware that the formation of HTA from thiol and MG, is also a reversible process. Therefore, it is important to determine whether the MBBr is detecting the remaining free thiol in the cell, or whether it is also labelling the reversibly conjugated BS-MG HTA.

To investigate this, excess MG (5 mM) was reacted with thiol (100 μM) until complete depletion of residual thiol confirmed by Ellman's assay. The mBBr derivatisation was then carried out on the HTA to confirm whether there is a shift in equilibrium detecting the newly formed free thiol (scheme 2.10). There was no detection of thiol therefore confirming that the mBBr derivatisation process is not detecting the reversibly conjugated BS-MG HTA (figure 2.8). This procedure was carried out with both BSH and Cys independently reacting with MG, and produced the same result. The importance of this observation, depending on the significance of HTA formation, is that these bimane-labelled methods may underestimate the true cellular thiol content by only detecting free thiol.

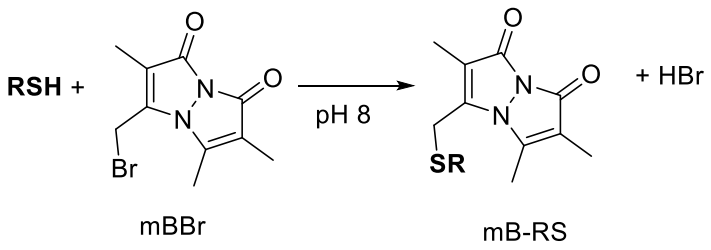

Scheme 2.9. Monobromobimane (mBBr) reacts with thiol to produce monobromobimane thioester which if fluorescently active and detected on HPLC.

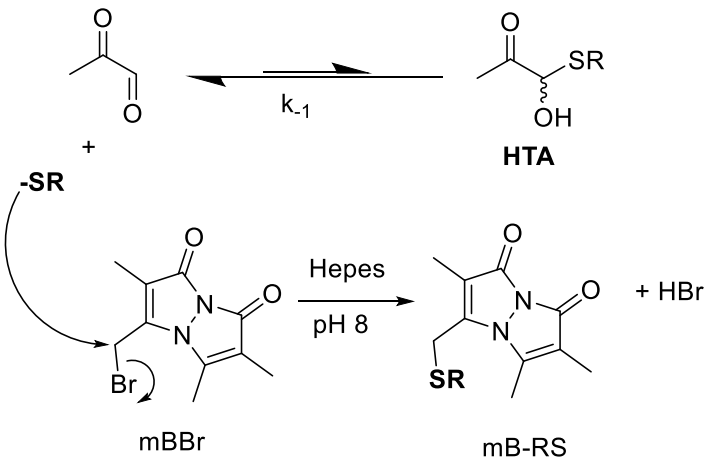

Scheme 2.10. The speculated dissociation of HTA taking place in the mBBr derivatisation process.

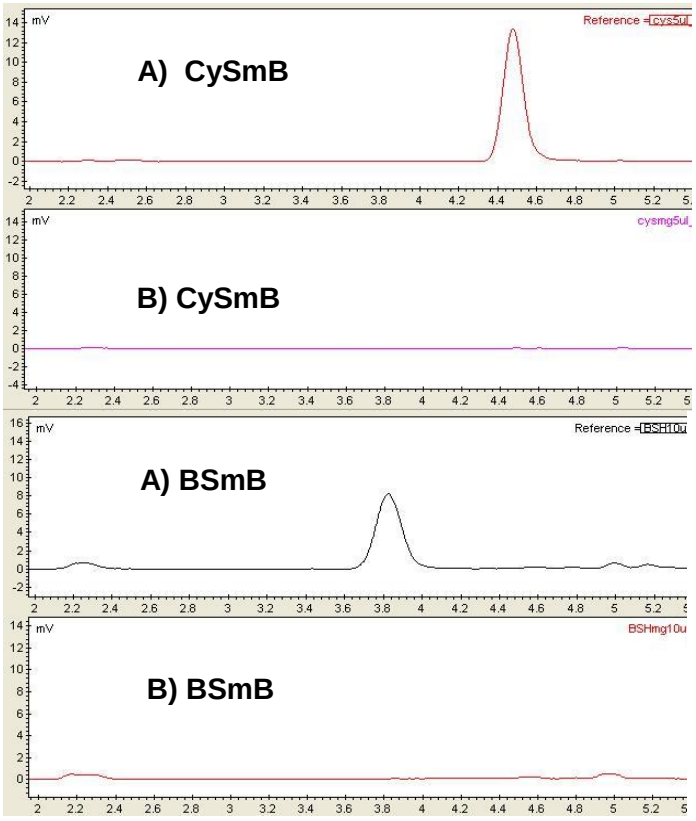

C)

Thiol/HTA	Time (min)	Ellman's titration (μM)	MBBr labelling (μM)
A)Cys	0	109	108
B)BSH	0	102	99
A)Cys-MG	30	< 3	< 3
B)BS-MG	30	< 3	< 3

Figure 2.8. HPLC analysis showing A) peak of RSmB B) no peak of RSmB suggesting that there is no shift in equilibrium from the mBBr derivatisation process therefore showing that HTA is not derivatised C) table of concentration of thiol detected on HPLC.

2.5.2. Extracellular consumption of methylglyoxal and thiol analysis in *B. subtilis* WT

Generally, the importance of the RSH-dependent glyoxalase I/II detoxification system is signified from the consumption of extracellular concentration of MG and its relation to intracellular thiol consumption. It is known that MG is detoxified through many different pathways with the RSH-dependent glyoxalase I/II system being the most dominant detoxification process.[101] In the WT strain, excess exposure of MG resulted in a stunted growth of *B. subtilis* by at least 3-fold (figure 2.9). The extracellular MG concentration was determined at 40-minute intervals using the derivatising agent, 2,4-dinitrophenylhydrazine[121, 122] (2,4-DNPH) (scheme 2.11). The WT strain had shown the fastest depletion of extracellular MG with a rate of 2.96 µM/min resulting in 50% consumption after 180 minutes of MG incubation (figure 2.9A). This result is representative of the extracellular MG being taken up in the cell and detoxified by the glyoxalase pathway and alternative pathways including the glyoxalase III, the aldose reductase and the aldehyde dehydrogenase enzymes.

In parallel, intracellular LMW thiols were quantified using mBBr [120] as previously discussed (scheme 2.9). The mBBr derivatisation process was used to determine the reactivity of MG with Cys and BSH, at 40-minute intervals. At mid-exponential phase, the BSH content is approximately 2.5 µmol/g in *B. subtilis* WT. As expected, the BSH levels rapidly deplete upon exposure to 1 mM MG, where the concentration of BSH decreases to 0.10 µmol/g of residual dry weight (RDW). The BSH levels then slowly begin to increase after 120 minutes (figure 2.9B). Cys levels were present in lower concentrations relative to BSH showing approximately 0.2 µmol/g at mid-exponential phase. Following MG treatment, Cys levels rise to 0.6 µmol/g (figure 2.9B). Previous research has shown electrophiles such as MG are responsible for an imbalance in thiol-redox homeostasis in *B. subtilis* because of depletion of LMW thiols. [123] This causes an upregulation of a cysteine metabolism repressor, *CymR,* and a global transcriptional regulator, *Spx*. They both function in the maintenance of thiol homeostasis under conditions of electrophile stress and therefore lead to synthesis of Cys.[123]

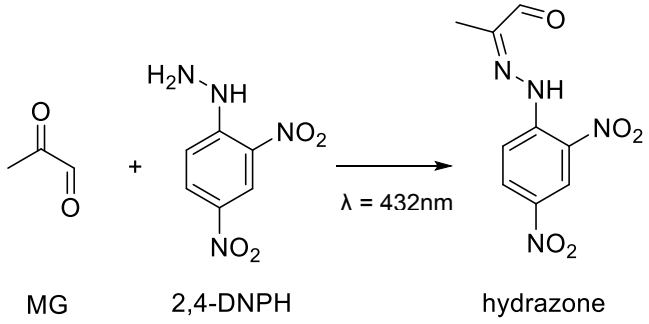

Scheme 2.11. 2,4-Dinitrophenylhydrazine (2,4-DNPH) reacts with MG to form 2,4-dinitrophenylhydrazone which is UV-active at 432 nm.

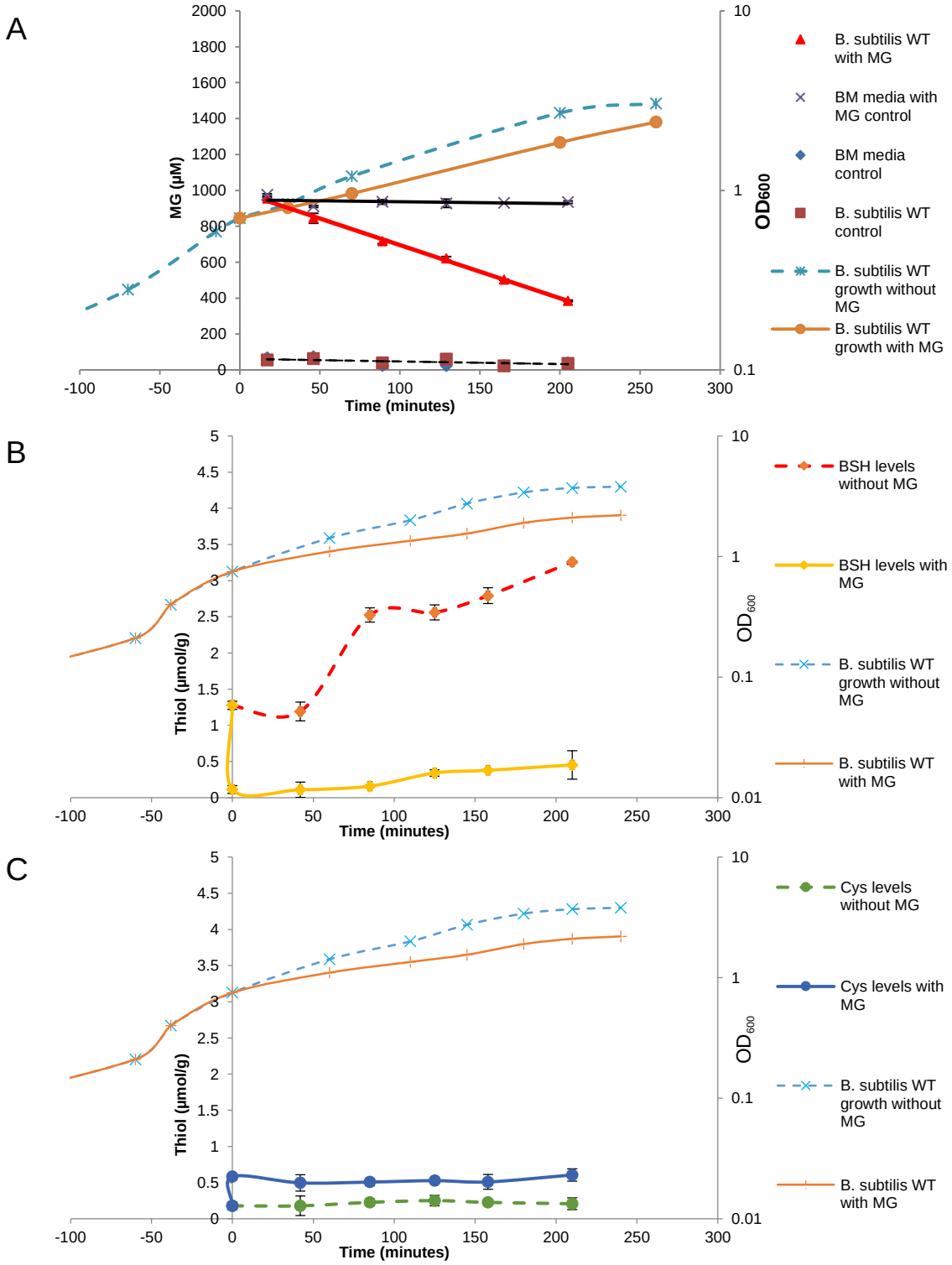

Figure 2.9. A) Extracellular consumption of MG after 1 mM incubation in *B. subtilis* WT (red triangles). Representative growth curves are shown for cells grown in absence (blue crosses) and presence (orange circles) of MG. B) Cellular BSH and C) Cellular Cys concentration after 1 mM MG incubation in *B. subtilis* WT. Cells are challenged with 1 mM MG (time 0) and harvested at approximately 40 minute time points. Cellular BSH levels in the absence (red diamonds) and presence (yellow diamonds) of MG and cellular Cys levels in the absence (green circles) and presence (blue circles) of MG which were quantified by HPLC after derivatisation with monobromobimane.

2.5.3. Immediate *in vivo* kinetics of thiol reactivity with MG in *B. subtilis* WT

After the cells are exposed to MG, there is approximately a 15-minute experimental delay for harvesting the cell pellets before the intracellular thiol is labelled with the mBBr reagent. This in turn allows ample opportunity for MG and thiol to react before the thiol concentration is determined and as a result, the initial reactivity could not be observed, *in vivo*. So, this initial reactivity was observed by streamlining the experimental process, allowing a more frequent quenching of mBBr with cell pellets. The *in vitro* kinetics show a full consumption of BSH in a matter of seconds when treated with excess MG. The *in vivo* kinetics, however, show the full consumption of BSH is not immediate, which is possibly explained by the time-lag for the MG to present intracellularly. This is indicated by the time-point at 6 minutes after MG exposure which shows the intracellular concentration has decreased from 3.8 µmol/g to 0.6 µmol/g. However, it further decreases to a lower concentration of approximately 0.2 µmol/g, at 22 minutes (figure 2.10A). The levels begin to gradually increase showing that the BSH is being recycled through the glyoxalase pathway (figure 2.10B).

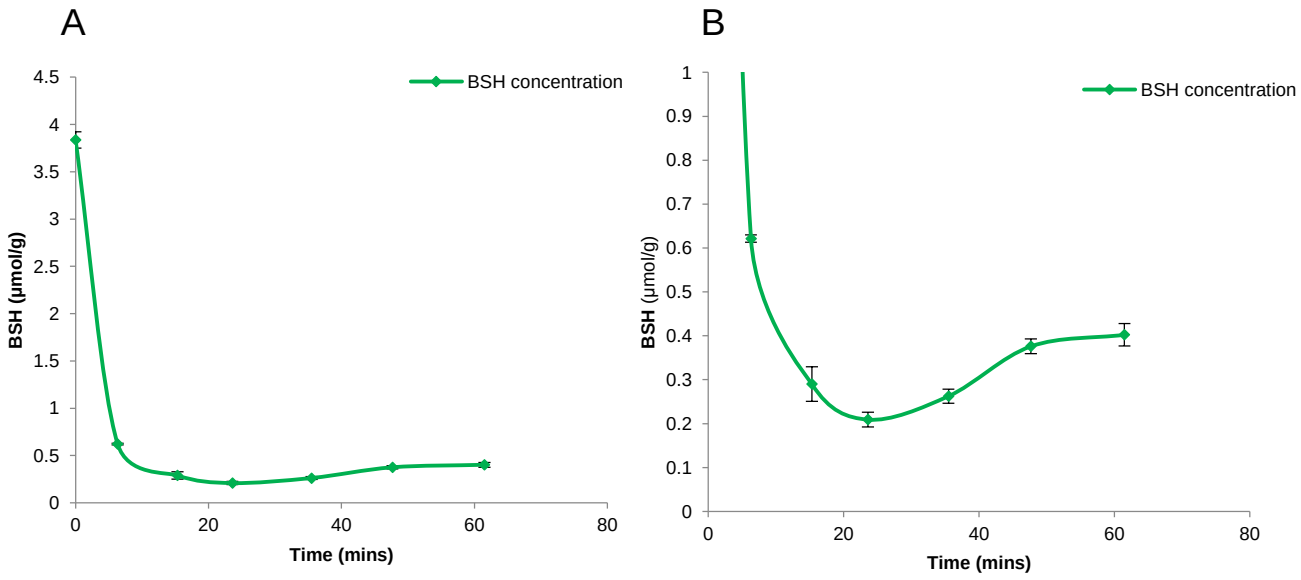

Figure 2.10. The immediate effect of the addition of 1 mM MG on BSH concentration. A) Full graph. B) Recovery of BSH.

2.5.4. Extracellular consumption of methylglyoxal and thiol analysis in *B. subtilis glxI* mutant

One potentially effective way of determining the efficiency of the glyoxalase system in the cells of *B. subtilis* was to analyse and compare the extracellular consumption of the WT to the mutant strains including *glxI, glxII* and BSH-null mutants.

The GlxI catalyses the isomerisation of HTA to *S*-D-lactoyl-BSH in the first step of the detoxification (scheme 2.12). It has previously been reported that the *glxI* mutant shows an increased sensitivity to MG, which correlates with the persistence of the MG in the growth medium.[101] Extracellular consumption of MG took place at a rate of 0.96 μM/min (figure 2.11A). There is a clear reduction in extracellular consumption of MG shown by the decreased rate of uptake into the cell relative to the WT strain. In relation to the thiol levels, the BSH levels are rapidly consumed (95% depletion) over the first 15 minutes (figure 2.11B). However, after 100 minutes of MG incubation there is shown to be a recovery of BSH. This confirms the equilibrium between MG and HTA where the dissociation of HTA is taking place forming the free BSH. There is no effect on Cys levels suggesting BSH is the predominant thiol involved in this first step of detoxification (figure 2.11C).

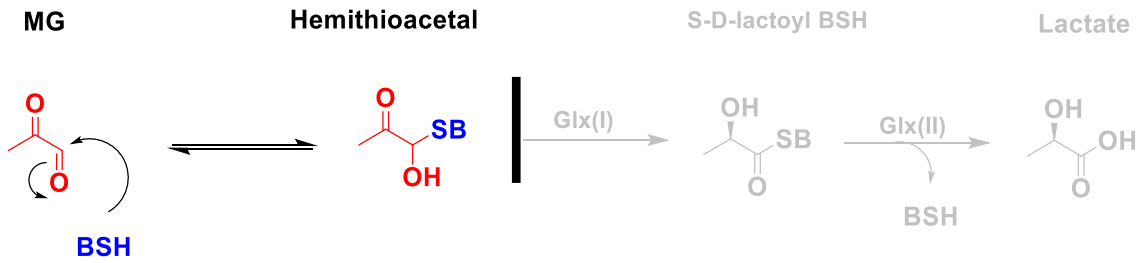

Scheme 2.12 Chemical scheme of the *glxI* mutant glyoxalase pathway.

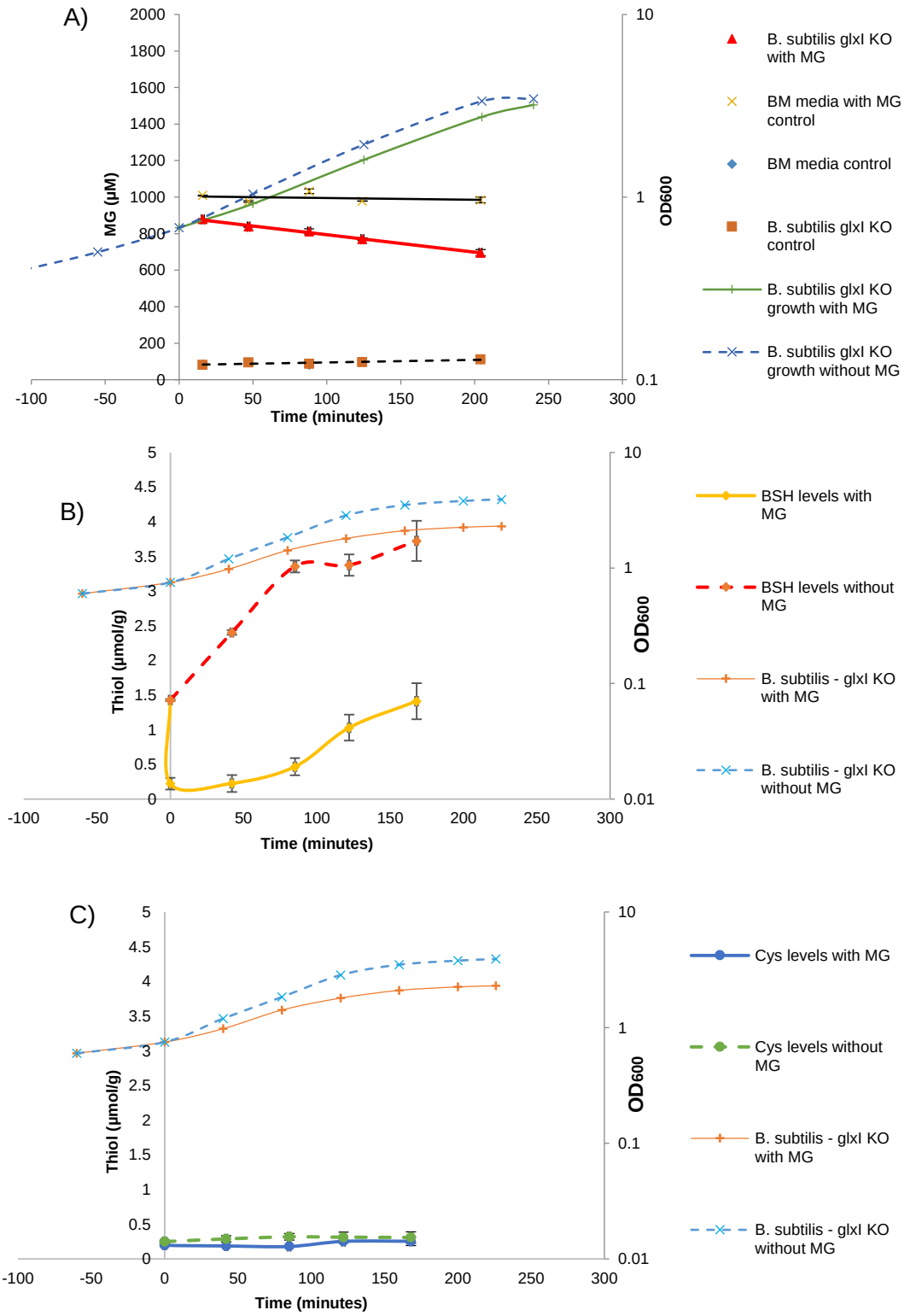

Figure 2.11 A) Extracellular consumption of MG after 1 mM incubation in *B. subtilis glxI* mutant (red triangles). Representative growth curves are shown for cells grown in absence (blue crosses) and presence (orange circles) of MG. B) Cellular BSH and C) cellular Cys concentration after 1 mM MG incubation in *B. subtilis glxI* mutant. Cells are challenged with 1 mM MG (time 0) and harvested at approximately 40-minute time points. Cellular BSH levels in the absence (red diamonds) and presence (yellow diamonds) of MG and cellular Cys levels in the absence (green circles) and presence (blue circles) of MG.

2.5.5. Extracellular consumption of methylglyoxal and thiol analysis in *B. subtilis glxII* mutant

The GlxII is responsible for converting the *S*-D-lactoyl BSH to D-lactate and the BSH is recycled (scheme 2.13). The extracellular detoxification of MG was shown to be faster than the *glxI* mutant with a rate of consumption of 1.72 µM/min (figure 2.12A). It was speculated that the extracellular MG would be consumed at a faster rate as the HTA is no longer in equilibrium with MG and free thiol. Thiol quantification shows BSH levels to be rapidly consumed which then persist at a low concentration (figure 2.12B). This confirms that the GlxI catalysed isomerisation is irreversible, hence, the BSH is trapped as *S*-D-lactoyl-BSH. It also proves that the GlxII enzyme is responsible for the recycling of BSH. The Cys levels were found to slightly reduce upon treatment with MG to 0.2 µmol/g (figure 2.12C). It is possible that the Cys is now reacting with MG due to the full depletion of the unrecoverable BSH.

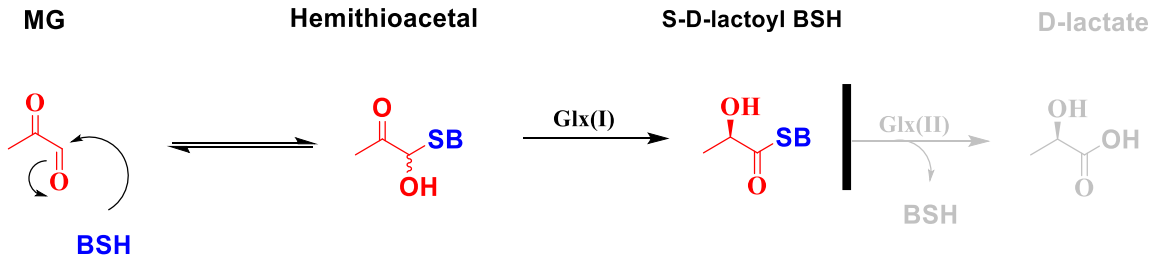

Scheme 2.13. Chemical scheme of the *glxII* mutant glyoxalase pathway.

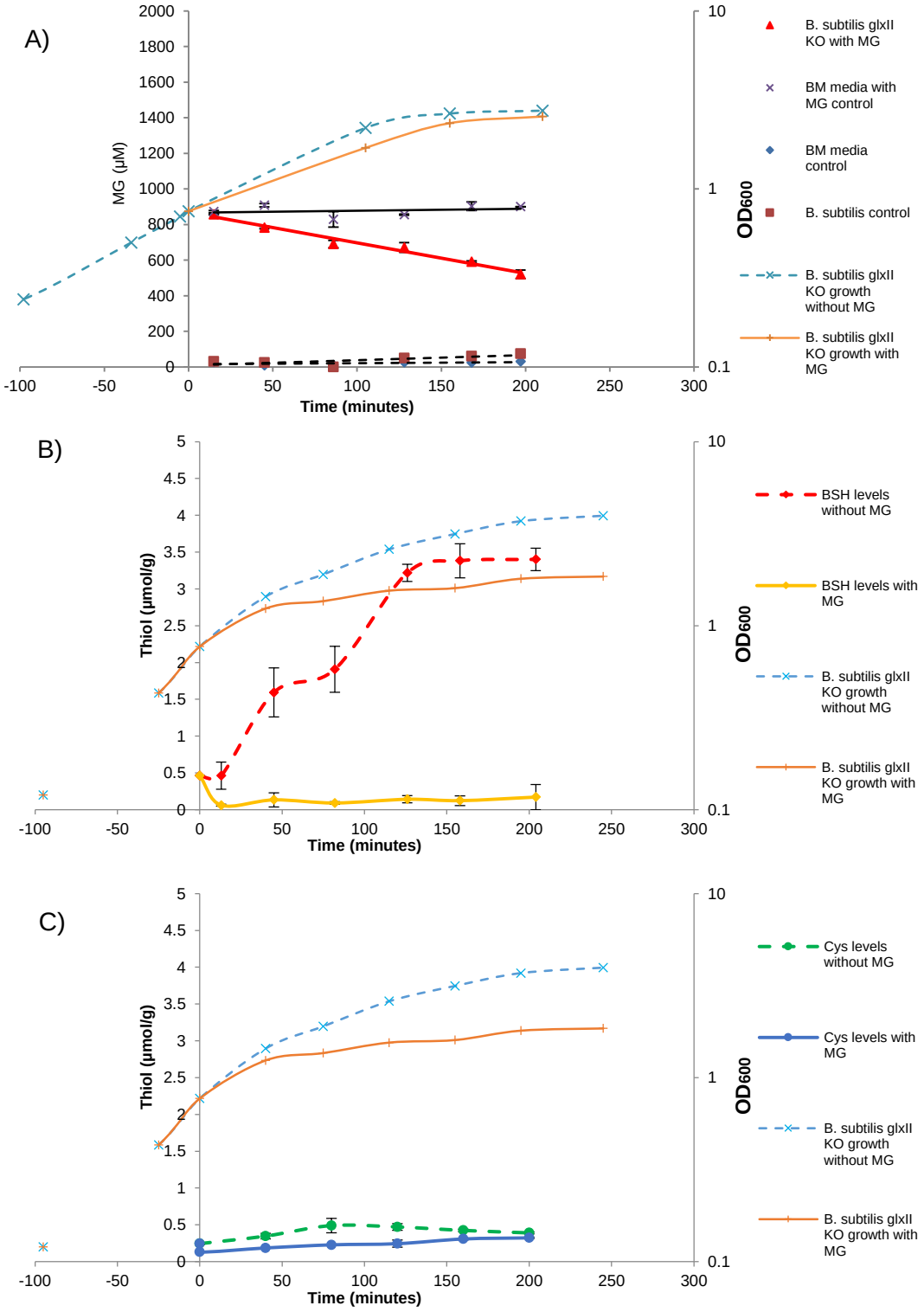

Figure 2.12. A) Extracellular consumption of MG after 1 mM incubation in *B. subtilis glxII* mutant (red triangles). Representative growth curves are shown for cells grown in absence (blue crosses) and presence (orange circles) of MG. B) Cellular BSH and C) cellular Cys concentration after 1 mM MG incubation in *B. subtilis glxII* mutant. Cells are challenged with 1 mM MG (time 0) and harvested at approximately 40-minute time points. Cellular BSH levels in the absence (red diamonds) and presence (yellow diamonds) of MG and cellular Cys levels in the absence (green circles) and presence (blue circles) of MG.

2.5.6. Extracellular consumption of methylglyoxal and thiol analysis in *B. subtilis glxI/II* mutant

As anticipated, the *glxI/II* mutant essential shows the same results as the *glxI* mutant with the extracellular MG consumption taking place at a slightly slower rate than *glxI* mutant at 0.81 µM/min (figure 2.13A). The absence of the GlxII enzymes becomes irrelevant when the GlxI enzymes are not present to continue the process of detoxification. Similarly to *glxI* mutant, there is shown to be a recovery of BSH, again confirming that an equilibrium is formed between the MG and the HTA (figure 2.13B).

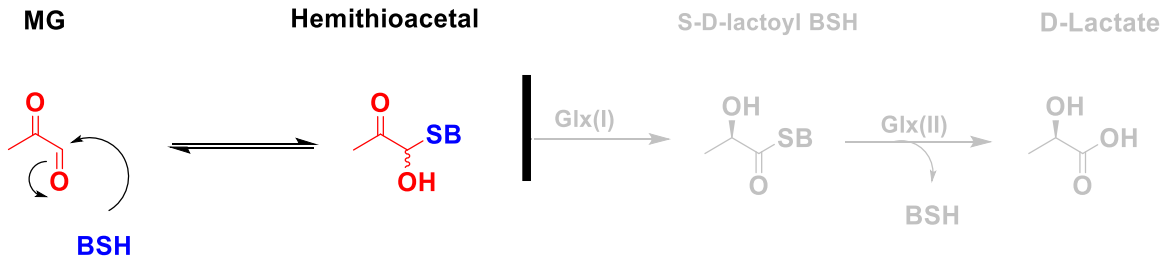

Scheme 2.14. Chemical scheme of the *glxI/II* mutant glyoxalase pathway.

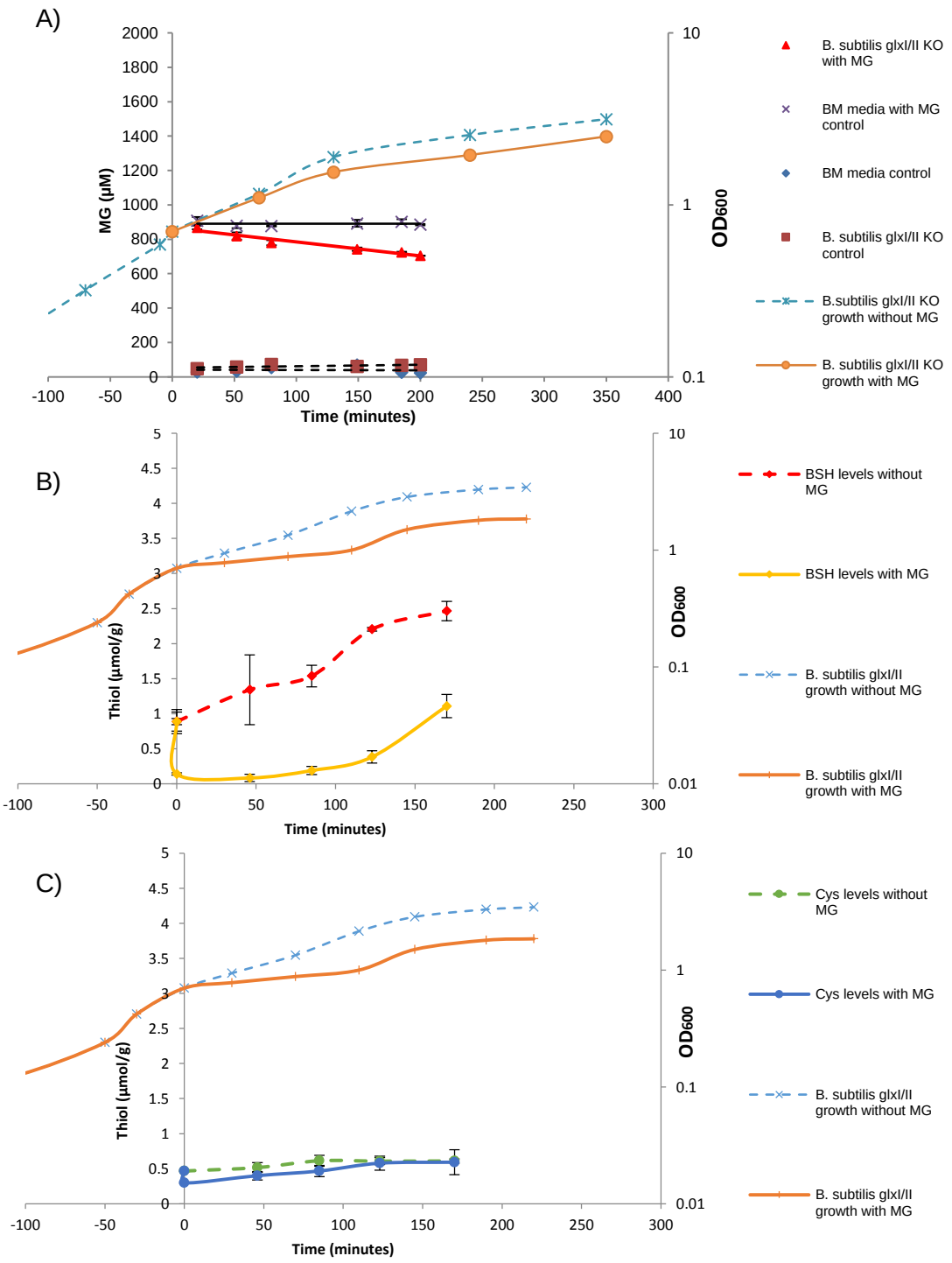

Figure 2.13. A) Extracellular consumption of MG after 1 mM incubation in *B. subtilis glxI/II* mutant (red triangles). Representative growth curves are shown for cells grown in absence (blue crosses) and presence (orange circles) of MG. B) Cellular BSH and C) cellular Cys concentration after 1 mM MG incubation in *B. subtilis glxI/II* mutant. Cells are challenged with 1 mM MG (time 0) and harvested at approximately 40-minute time points. Cellular BSH levels in the absence (red diamonds) and presence (yellow diamonds) of MG and cellular Cys levels in the absence (green circles) and presence (blue circles) of MG.

2.5.7. Extracellular consumption of methylglyoxal and thiol analysis in *B. subtilis bshC* mutant

A BSH-null mutant was achieved by the knock-out of the third biosynthetic gene, *bshC*, necessary for the biosynthesis of BSH. Regarding the *bshC* mutant, the metabolite cannot be detoxified through the glyoxalase pathway (scheme 2.15). As expected, there was found to be no BSH in the thiol analysis (figure 2.14B). As a result, the Cys concentration remained constant and did not deplete even in the absence of BSH (figure 2.14C). This suggests that Cys has no involvement in the detoxification of MG in the cell, despite the fact the *in vitro* kinetics represent reactivity. It is also suggestive that the extracellular consumption, at a slower rate of 0.77 μM/min, relative to all other mutant strains, is a result of thiol-independent detoxification pathways including the MG reductase and dehydrogenase enzymes (figure 2.14A). Therefore, this data shows the thiol-dependent glyoxalase pathway is not essential for the survival of the cell.

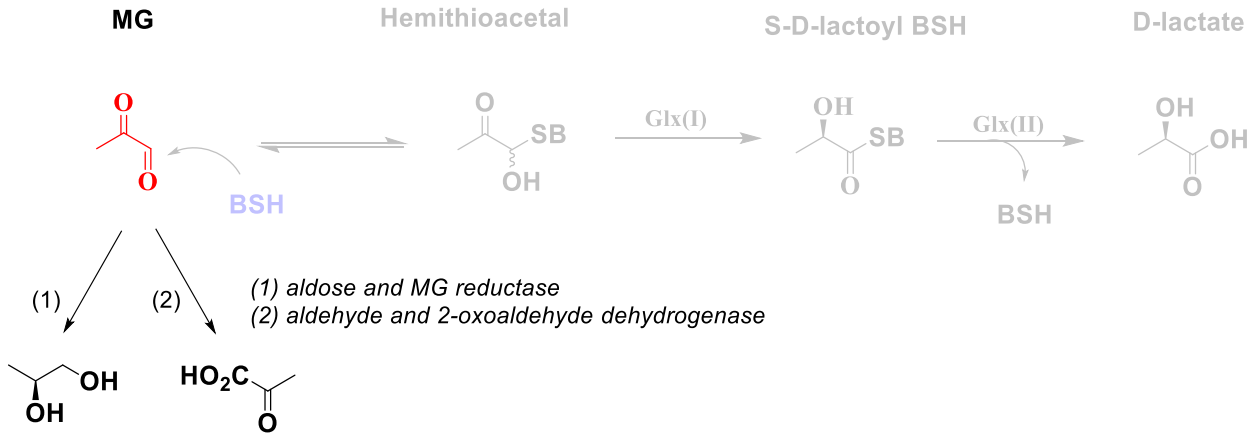

Scheme 2.15. Chemical scheme of BSH-null mutant and alternative detoxification pathways.

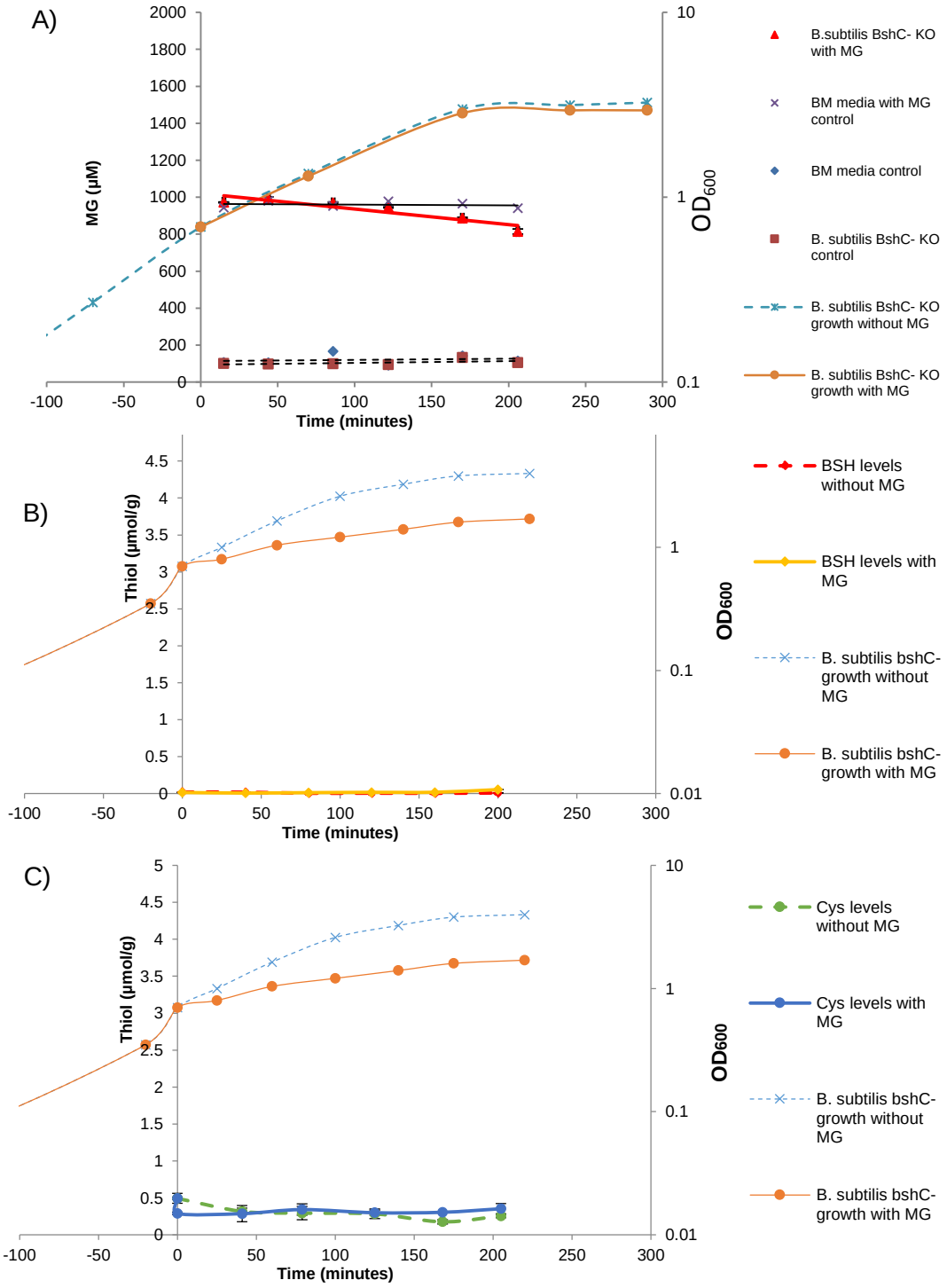

Figure 2.14 A) Extracellular consumption of MG after 1 mM incubation in *B. subtilis bshC* mutant (red triangles). Representative growth curves are shown for cells grown in absence (blue crosses) and presence (orange circles) of MG. B) Cellular BSH and C) Cys concentration after 1 mM MG incubation in *B. subtilis bshC* mutant. Cells are challenged with 1 mM MG (time 0) and harvested at approximately 40-minute time points. Cellular BSH levels in the absence (red diamonds) and presence (yellow diamonds) of MG and cellular Cys levels in the absence (green circles) and presence (blue circles) of MG.

B. subtilis KO	*Rate of extracellular consumption of MG (μM/min)*
WT	2.96 ± 0.054
glxI	0.96 ± 0.013
glxII	1.72 ± 0.053
glxI/II	0.81 ± 0.056
bshC	0.77 ± 0.021

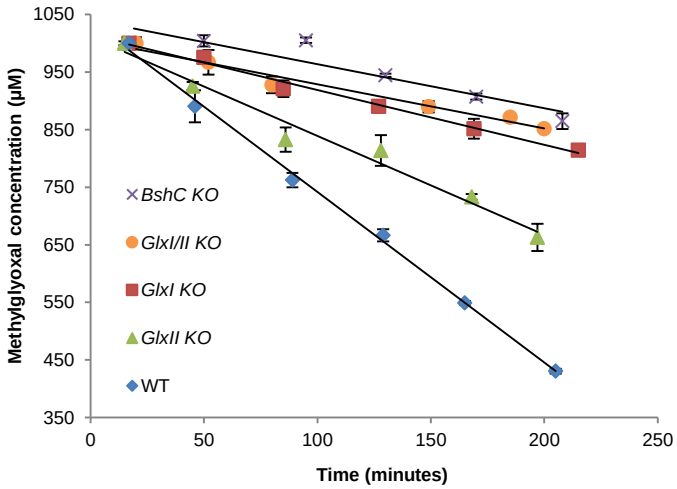

Figure 2.15. The rate of extracellular consumption of MG upon 1mM incubation in *B. subtilis* WT and KO.

2.5.8. *B. subtilis* WT, *glxI, glxII, bshC* mutant growth curves in LB media and minimal media

The growth curves in LB media are represented for all *B. subtilis* strains (figure 2.16). In the absence of MG, the mutant strains show similar growth to the WT. At an OD_{600} of 0.7, cells were incubated with 1 mM MG, all six strains show susceptibility to MG represented by a stunted growth. However, there is continued growth in all strains including the BSH-null mutant, which highlights that BSH is not essential for cell growth in both physiological conditions and when incubated with excess MG. The growth of all the strains were found to significantly differ when grown in Belitsky minimal (BM) media, with late-exponential phase reaching an approximate OD_{600} of 3 (figure 2.17).

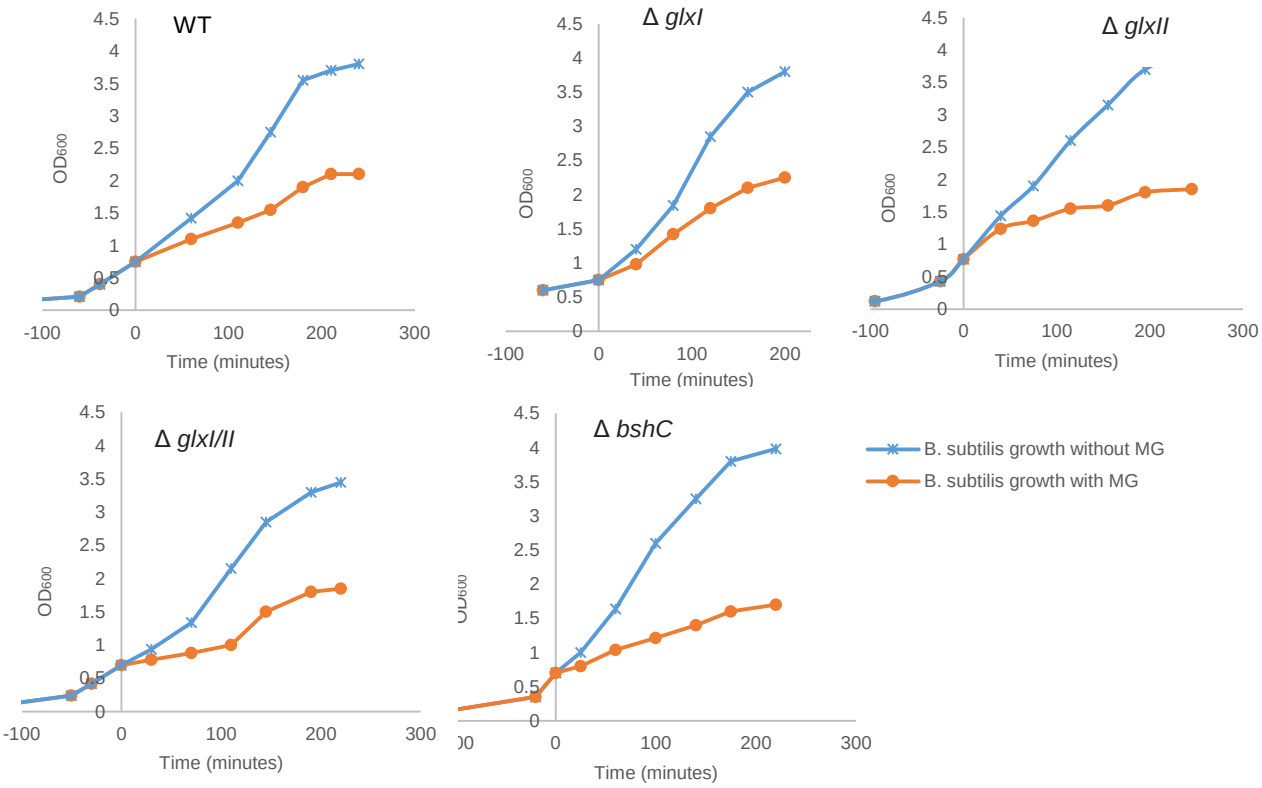

Figure 2.16. *B. subtilis* growth in the presence and absence of 1 mM MG in LB media.

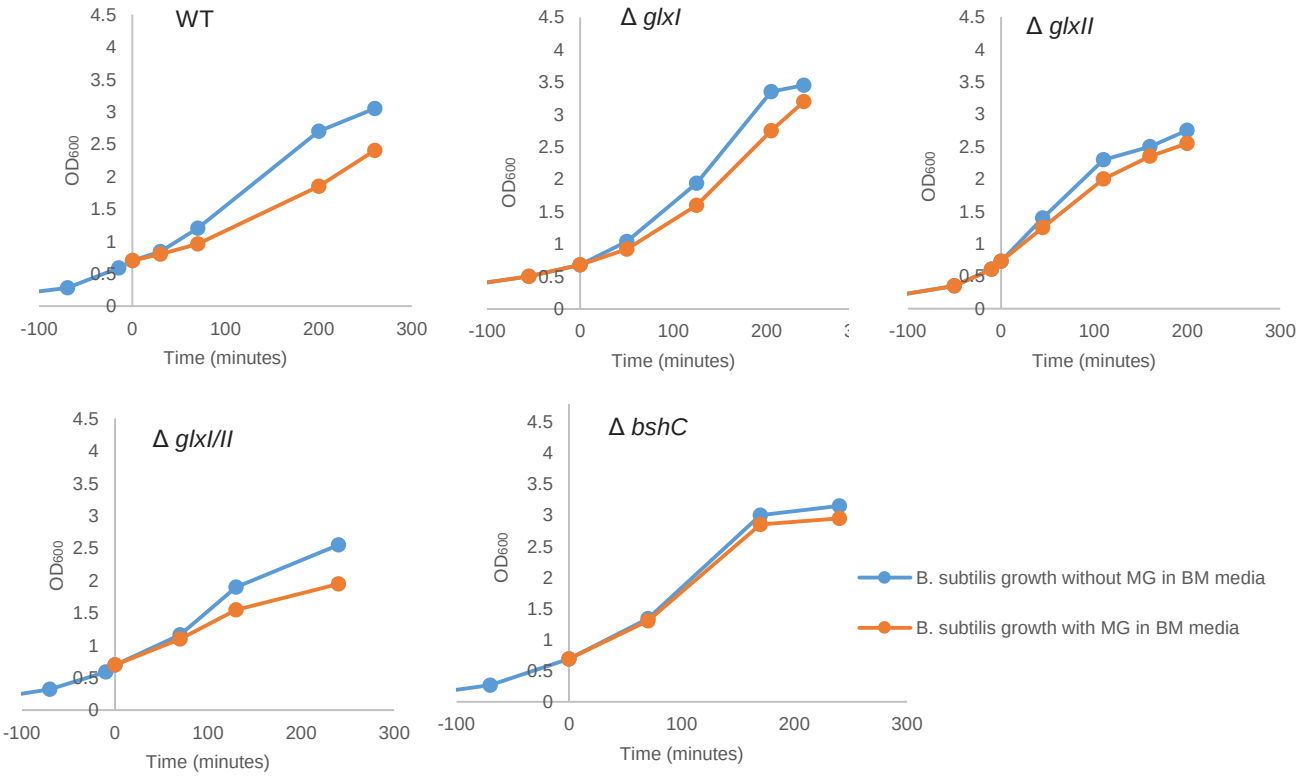

Figure 2.17. *B. subtilis* growth in the presence and absence of 1 mM MG in Belitsky minimal (BM) media.

2.5.9. Effect of different MG stress on growth of *B. subtilis* WT and bshC mutant

As previously discussed, 1 mM MG was shown to stunt growth of *B. subtilis,* however, the cells continue to grow. To further this investigation, the potency of MG in both *B. subtilis* WT and *bshC* mutant was determined by monitoring the growth using various different concentrations of MG (figure 2.18).

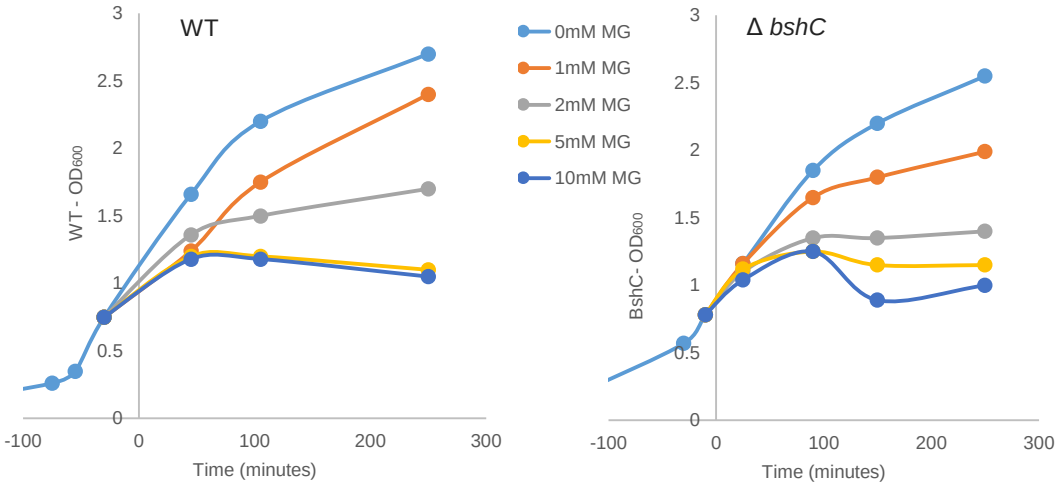

Figure 2.18: Different inoculation of MG concentration on A) *B. subtilis* WT and B) *bshC* mutant.

The growth of the WT and *bshC* mutant are found to be similar. Upon incubation of MG, an increasing MG concentration results in a reduced growth of *B. subtilis.* 1 mM MG incubation results in a higher growth rate in the WT than the BSH mutant. This is also observed with 2 mM MG incubation. However, when incubated with concentrations above 2 mM MG, there was no further growth of bacteria resulting in the death phase (figure 2.18). Research has previously shown that lethal levels of MG are known to be approximately 0.6 mM over 6 hours in *E. coli*.[104] However, this was not observed in the 4-hour period of growth of the mutant strains. A possible reason for this is the different strains of bacteria being analysed.

It was speculated that the BSH mutant would show more susceptibility to MG as there is no possible MG detoxification through the BSH-dependent glyoxalase pathway. However, both strains showed a similar response to the specified amount of MG inoculation, which demonstrates the non-essential nature of this pathway for MG detoxification.

2.5.10. Carbohydrate stress on *B. subtilis* WT and *bshC* mutant strain

In general, bacteria are diverse in nature and have the ability to thrive under different environmental conditions. There is particular interest on carbohydrate-rich condition, as it is speculated that under these conditions, glycolysis metabolism increases resulting in a higher production of MG, as a by-product. Therefore, there is relevance in confirming this accumulation of MG amongst *B. subtilis*.

The *B. subtilis* WT growth significantly increases in media supplemented glucose 0.5%/ arabinose 0.5%, reaching an OD_{600} of above 6 at late-exponential phase. *B. subtilis* cells readily utilise the glucose reaching an OD_{600} of 4 at 600 minutes. This is followed by the stationary phase suggesting a full consumption of glucose. The growth then resumes after 1400 minutes, which is possibly explained by the cells now using the arabinose as the main source of energy. With a further growth to approximately an OD_{600} of 6, there is a significant increase in MG levels. The WT released 90 µM of potential MG in the medium in comparison to 20 µM MG in the absence of the carbohydrate (figure 2.19A). It is clear that a direct stress of carbohydrate results in an increased workload for glycolysis resulting in a higher production of MG. This suggests that the growth of *B. subtilis* WT is limited by the lack of carbohydrate sources. These data therefore suggest that MG has potential to exist in moderately high concentrations in the cell which explains the importance of the detoxification routes of this metabolite.

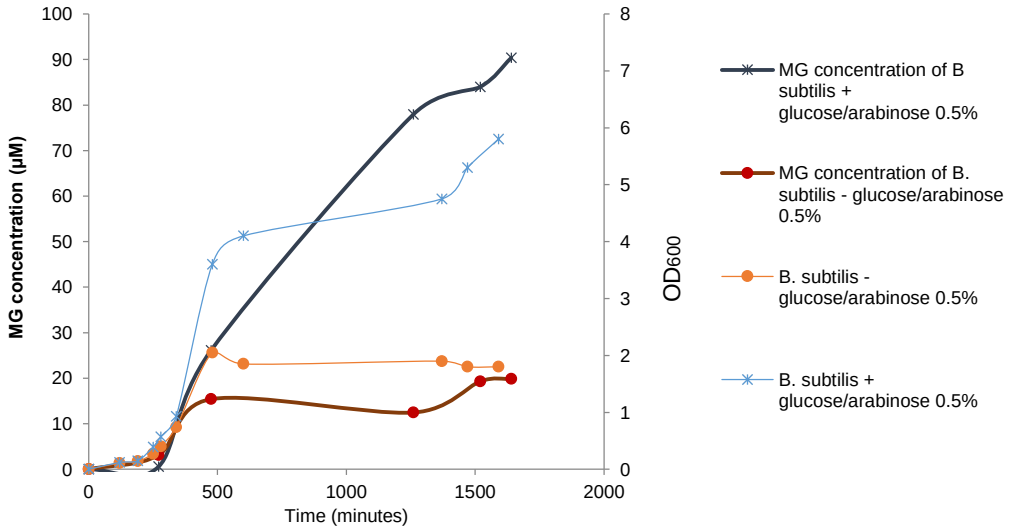

Figure 2.19: Effect of carbohydrate stress upon the levels of MG for *B. subtilis* WT. Representative growth curves are shown in the absence (blue) and presence (orange) of glucose 0.5%/arabinose 0.5% stress. The extracellular MG concentration in the absence (dark blue crosses) and presence (dark red circles) of glucose 0.5%/arabinose 0.5% stress which were derivatised with 2, 4-dinitrophenylhydrazine.

2.6. Summary

Cys and BSH have been shown to possess a similar reactivity with MG when comparing their thiolate. However, the thiol pK_a of BSH is lower than Cys and therefore more deprotonated at physiological conditions. As a result, there is more BSH thiolate resulting in a faster reactivity relative to Cys, both of which are > 100-fold more reactive than GSH and CysNAc. Using the rate constants of the reaction between BSH and MG, the predicted equilibrium constant was found to favour the forwards reaction highlighting that the HTA may be present in high intracellular concentrations relative to the reactants.

The *in vivo* studies provided more evidence of BSH involvement in the detoxification of MG. *B. subtilis* WT upon incubation with 1 mM MG, resulted in an extracellular consumption of MG, in parallel to a full depletion of intracellular BSH. All mutant strains showed extracellular consumption of MG including the BSH-null mutant strain at a slower rate, indicating the thiol-independent detoxification pathways are taking place. In addition, as anticipated, the *glxI* mutant showed recovery of BSH whilst the *glxII* mutant showed no recovery of BSH. All this data is suggestive that the role of BSH in *B. subtilis* is analogous to the role of GSH in the thiol-dependent glyoxalase pathway amongst eukaryotes. To further this investigation, the extracellular MG was analysed under carbohydrate rich and famine conditions, where MG was produced approximately 5-fold higher in a carbohydrate rich environment.

MG remains a prominent toxic metabolite formed as a by-product of glycolysis, in intracellular concentrations up to 1.5 mM.[57] The studies show strong evidence that BSH is the dominant LMW thiol in the detoxification of MG amongst *B. subtilis*. In addition, the reaction kinetics show BSH to be a strong nucleophile, present in high intracellular concentrations. This therefore questions the possibility of BSH reactivity with other carbonyl-containing metabolites present in the cell. Past research has investigated the reactivity of Cys with other carbonyl-containing molecules including acetone, acetaldehyde and formaldehyde.[124] Current literature has shown that the equilibrium constant for thiol with acetone is 100-fold smaller than acetaldehyde which is 20-fold smaller than formaldehyde.[124] Therefore, there is now considerable interest in investigating the interaction of BSH with other electrophilic chemical species, in particularly, the glycolytic metabolites.

3. The glycolytic metabolites and their interaction with low molecular weight thiols

3.1. Overview

The involvement of BSH and Cys in the reactivity with MG has been explored. There is now a clear progression to determine the reactivity of LMW thiols with other intracellularly carbonyl-containing species, with the main focus on the glycolytic metabolites.

3.2. Glycolysis

Glycolysis consists of 10 enzyme-catalysed reactions (figure 3.1), which can be broken down into two phases. The first phase encompasses the first five reactions. Glucose, the main carbohydrate source, is phosphorylated to form glucose 6-phosphate (G6P). G6P is then isomerised to produce fructose 6-phosphate (F6P) and subsequently phosphorylated to produce fructose 1,6-bisphosphate (F1,6-BP). F1,6-BP is then split into two 3-carbon sugars, dihydroxyacetone phosphate (DHAP) and D-glyceraldehyde 3-phosphate (GA3P).

The next five reactions comprise the second phase of glycolysis, which is called the 'payoff' phase because two high-energy phosphate bonds are produced herein. In this phase, GA3P loses two electrons and two protons reducing NAD^+ to NADH producing 1,3-bisphospho-D-glycerate (1,3-BPG). 1,3-BPG then donates a phosphate group to ADP producing 3-phospho-D-glycerate (3-PG) and ATP, which is then isomerised to 2-phospho-D-glycerate (2-PG). A dehydration step then produces phosphoenolpyruvate (PEP) which then loses a phosphate group to produce the final product, pyruvate (figure 3.1).

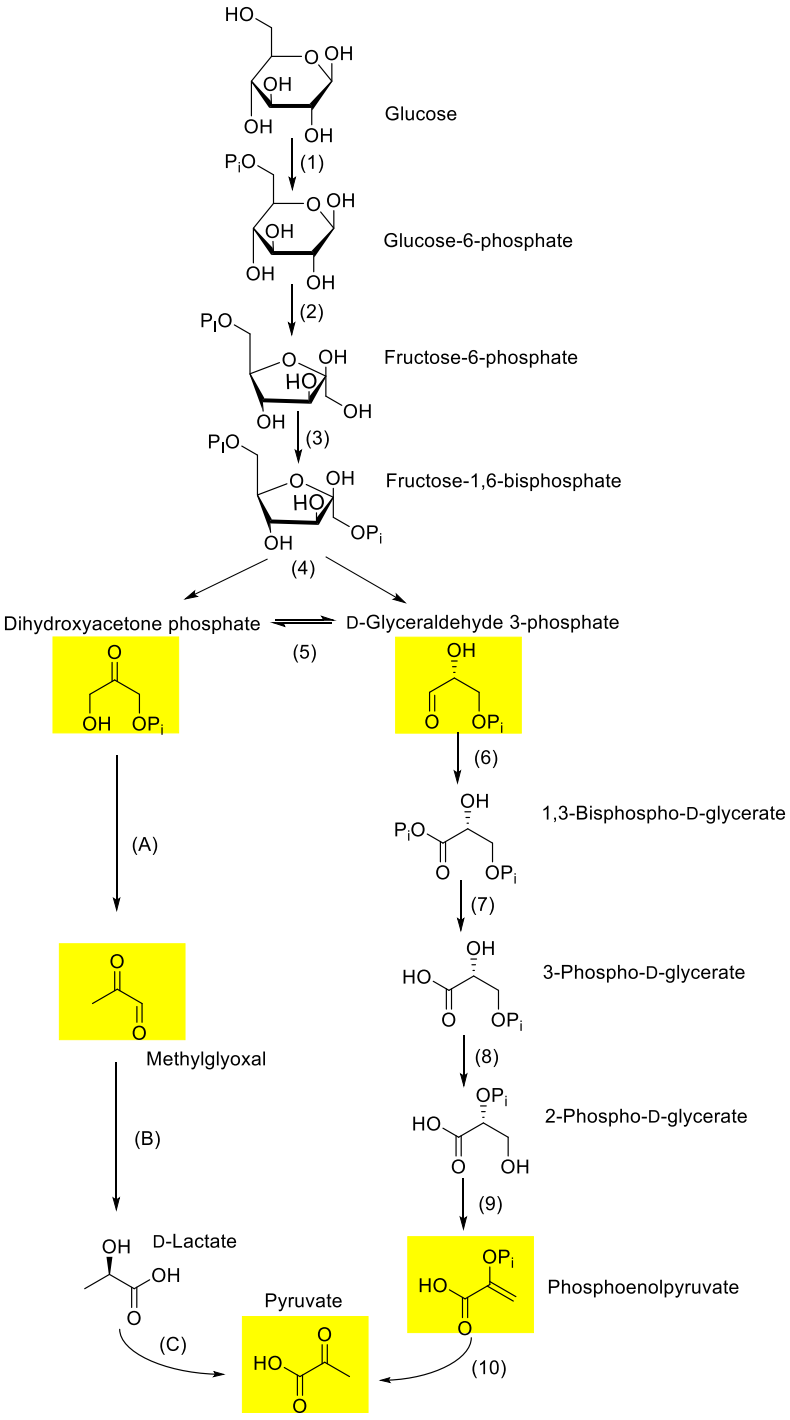

Scheme 3.1. The glycolytic pathway. 1) Hexokinase 2) phosphoglucoisomerase 3) phosphofructokinase 4) aldolase 5) triose phosphate isomerase 6) GA3P dehydrogenase 7) phosphoglycerokinase 8) phosphoglyceromutase 9) enolase 10) pyruvate kinase. In addition to the metabolism of DHAP to MG and glyoxalase pathway A) MG synthase B) glyoxalase I and II C) lactate dehydrogenase.

3.2.1. Potential reactivity of glycolytic metabolites

The metabolites of the first phase of glycolysis, consist of glucose, G6P, F6P and F1,6-BP, which all possess carbonyls in their open chain structure with approximately 0.004% in this form (scheme 3.2).[125] The majority of these sugars exist in their unreactive cyclic form. However, the open chain form and cyclic form are in equilibrium and therefore there is potential for reactivity of thiol to take place with the reactive carbonyl. However, the second phase metabolites of glycolysis possess electrophilic groups including aldehydes, ketones and Michael acceptors which are also less sterically hindered. They are more likely to undergo a nucleophilic attack from LMW thiols and therefore the focus will be on the second phase metabolites.

Past research has established that Cys and GSH react with various metabolites of glycolysis; Cys (10 mM) was shown to react with pyruvate (1 mM), pH 7.3, 20 °C, with 50% consumption after the first minute.[126] In addition, GSH (400 mM) was shown to react with GA3P (400 mM), pH 4-5, 25 °C, for 10 minutes, showing formation of HTA.[127] Therefore, evidence has shown previous reactivity of thiol and glycolytic metabolite, however, these high concentrations used do not represent physiological conditions.

The reactivity of BSH and Cys with carbonyl-containing metabolite were determined, focusing on the second phase metabolites. These include D-glyceraldehyde 3-phosphate (GA3P), dihydroxyacetone phosphate (DHAP), phosphoenolpyruvate (PEP), and pyruvate (scheme 3.1). The potential reactivity has scope to newly identify unknown reactions taking place in the cell whilst also exploring additional functions of BSH as a chemical scavenger.

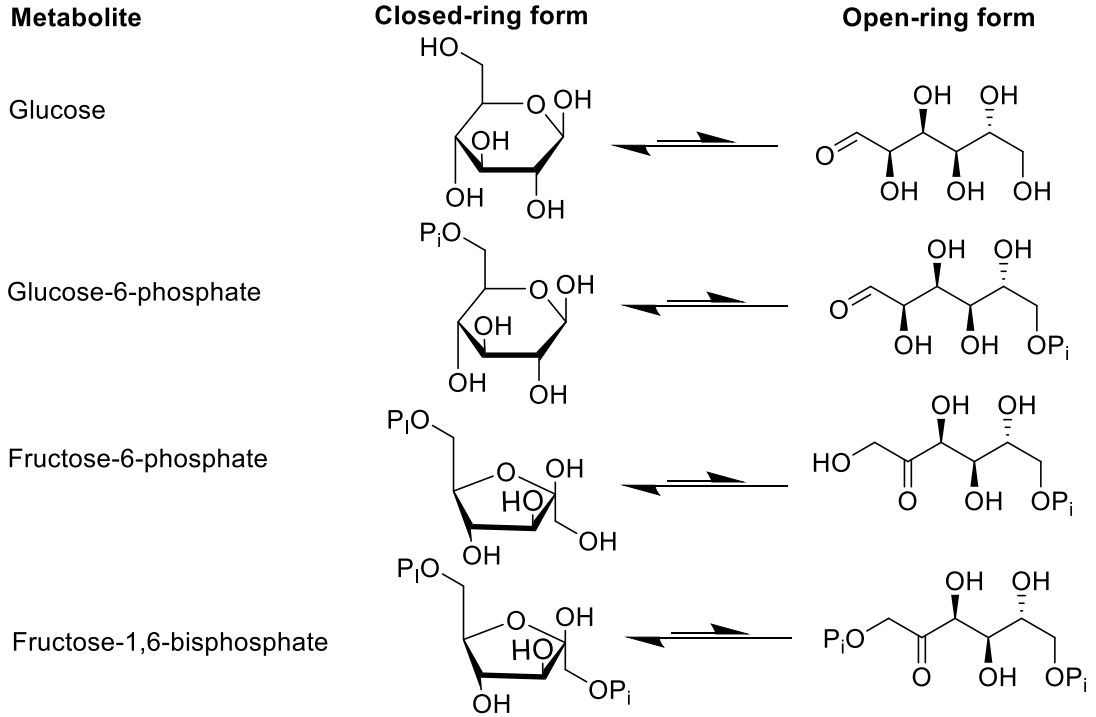

Scheme 3.2. First phase metabolites in their closed-ring and open-ring form.

3.2.2. Dihydroxyacetone phosphate and D-glyceraldehyde 3-phosphate

The second stage of glycolysis begins with the splitting of fructose 1,6-bisphosphate into the triose phosphates, DHAP and GA3P, catalysed by fructose 1,6-bisphosphate aldolase (scheme 3.1). They are isomers of each other, where their interconversion is catalysed by triose phosphate isomerase (TIMs). This enzyme is a key component of glycolysis found to accelerate the isomerisation by a factor of 10^9 relative to non-enzyme catalysis.[128] The triose phosphates are problematic to the cell if allowed to accumulate as they contain a phosphate group, which can therefore cause phosphate starvation within the cell. The phosphate can be liberated, either non-enzymatically[77] or enzymatically catalysed by MG synthase, to form MG.[73-75] Alternatively, GA3P is metabolised through glycolysis to eventually produce pyruvate (scheme 3.3).

Both DHAP and GA3P are found to be unstable under physiological conditions due to the chemical breakdown of the triose phosphate to MG.[71, 82] Control assays have shown the degradation of DHAP and GA3P to be 0.8 µmol/min and 2.7 µmol/min, respectively (figure 3.1). After 300 minutes, the DHAP concentration decreases from 3.8 mM to 3.6 mM representing at 5% decrease whilst the GA3P concentration decreases from 3.5 mM to 2.6 mM, representing a 26% decrease. The assays investigating the initial reactivity were carried out in a 10-30 minute time-frame and therefore are unlikely be affected by the possibly degradation of DHAP/GA3P to MG. However, the assays determining the steady-state equilibria for determination of the equilibrium constants (chapter 3.5) were carried out over a longer time-frame.

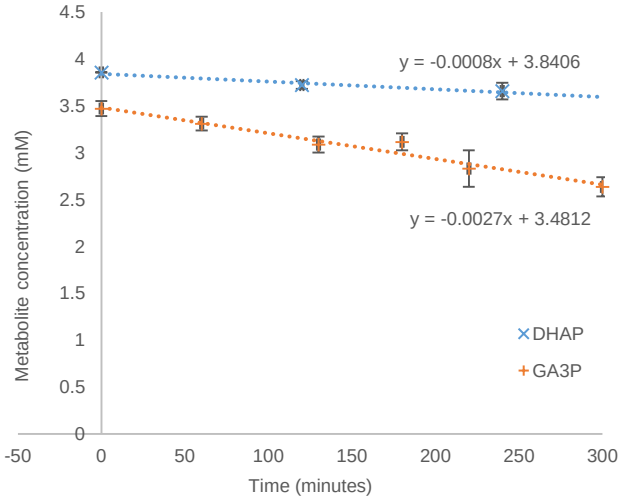

Figure 3.1. Controls of DHAP and GA3P stability in 50 mM HEPES buffer, pH 7.7, 20 °C.

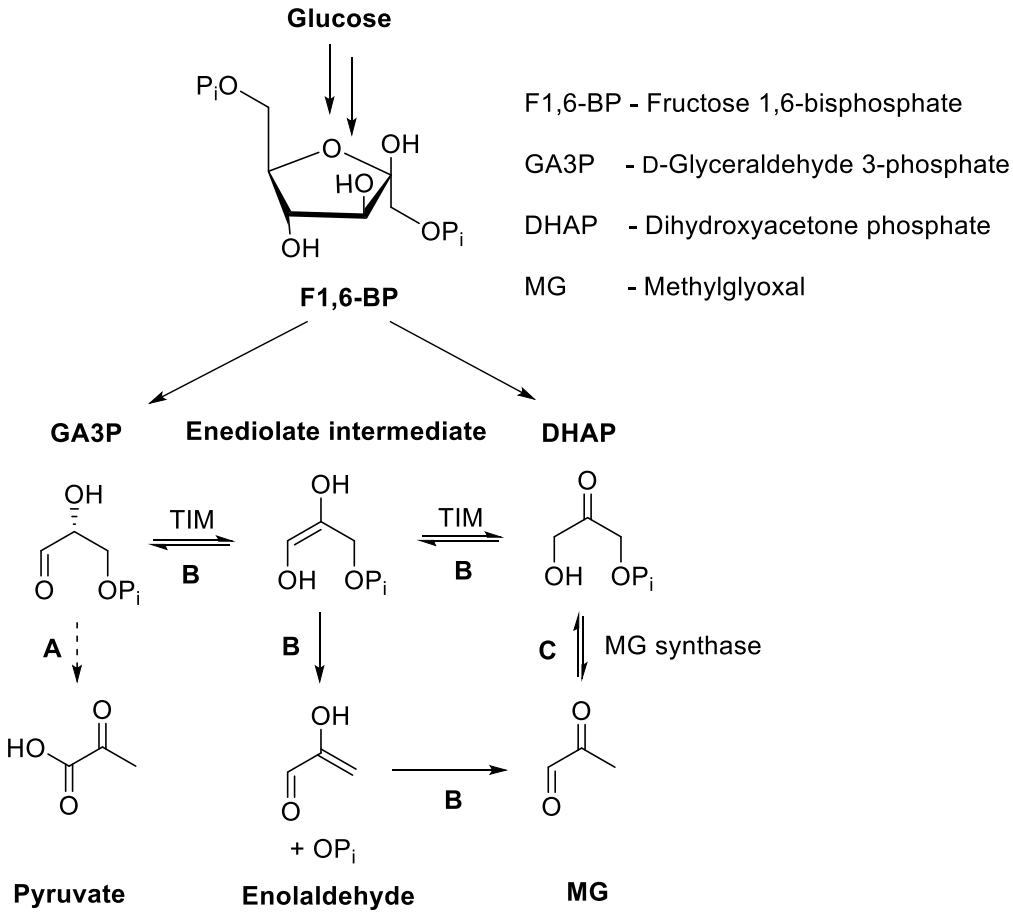

Scheme 3.3. The three ways of triose phosphate metabolism. A) GA3P forms 1,3-bisphosphoglycerate and proceeds through glycolysis to form pyruvate. B) The breakdown of the triose phosphate which non-enzymatically degrades to form an enediolate intermediate, and the MG. C) The enzymatically catalysed reaction of DHAP to form MG, via MG synthase.

3.3.3. Reactivity of glycolytic metabolites with LMW thiols

DHAP, GA3P, PEP and pyruvate (1500 µM) of the second phase of glycolysis (scheme 3.1) were reacted with thiol (3 mM Cys, 2 mM BSH, 8 mM GSH) for 30 mins at 20 °C, pH 7.7, to determine the possible reactivity at physiological conditions (table 3.1). The other remaining metabolites of the second phase of glycolysis, 1,3-bisphosphogylcerate, 3-phosphoglycerate, 2-phosphoglycerate, contain no reactive carbonyl groups and therefore no reactivity with LMW thiols will be observed.

Table 3.1. Initial screening reactivity of thiol cofactors and metabolites, pH 7.7, at 20 °C.			
Metabolite	**Cys (3 mM)**	**BSH (2 mM)**	**GSH (8 mM)**
DHAP (1500 µM) 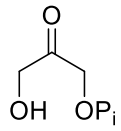	✓	✓	X
GA3P (1500 µM) 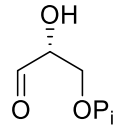	✓	✓	X
PEP (1500 µM) 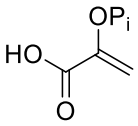	X	X	X
Pyruvate (1500 µM) 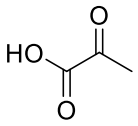	✓[1*]	✓[1*]	X
[1*]Initial reactivity was only determined in excess pyruvate (10 mM) and thiol (3 mM Cys, 2 mM BSH), pH 7.7, 20 °C			

Phosphoenolpyruvate (PEP) is an α, β-unsaturated carbonyl compound and can potentially undergo a Michael addition reaction with the thiol nucleophile being the Michael donor. There was, however, no reactivity observed between this metabolite and thiol. Similarly, there was no reactivity of thiol with pyruvate (1500 µM), but in excess pyruvate (10 mM), BSH and Cys were shown to react as discussed in chapter 3.4.

DHAP and GA3P were both found to react with Cys and BSH, in the preliminary investigation (table 3.1). Therefore, pseudo first order reaction conditions were implemented to compare reactivity. Metabolite (10 mM) was reacted with thiol (3 mM Cys, 2mM BSH) at 20 °C, pH 7.7. 3 mM Cys and 2 mM BSH both equate to 0.44 mM of thiolate. The relative reactivity of BSH to Cys was approximately the same, with both thiols reacting significantly faster with GA3P than DHAP, by approximately 3-fold (figure 3.2). Both Cys and BSH reacting with DHAP showed 40% reactivity after 30 minutes whilst the GA3P showed > 95 % reactivity (figure 3.2A/B). This reaction continued for 4 hours with DHAP until a full depletion of the thiols. The difference in reactivity is thought to arise because of the more reactive electrophilic aldehyde group that GA3P possesses as opposed to the ketone group on DHAP.

Whilst these preliminary experiments demonstrate comparable reactivity between Cys and BSH thiolates with DHAP and GA3P, they are not necessarily a true reflection of their potential significance in the intracellular setting. *In vivo*, DHAP and GA3P are constantly being consumed and produced. In addition, intracellular BSH is often more abundant than Cys in B. *subtilis*. So, the concentrations of metabolites and thiols as well as the intracellular pH vary under different cellular conditions. Therefore, determination of the pH-independent rate constants and equilibrium constants would provide a more informative set of values that could be used to assess the significance of these reactions in different physiologically relevant conditions.

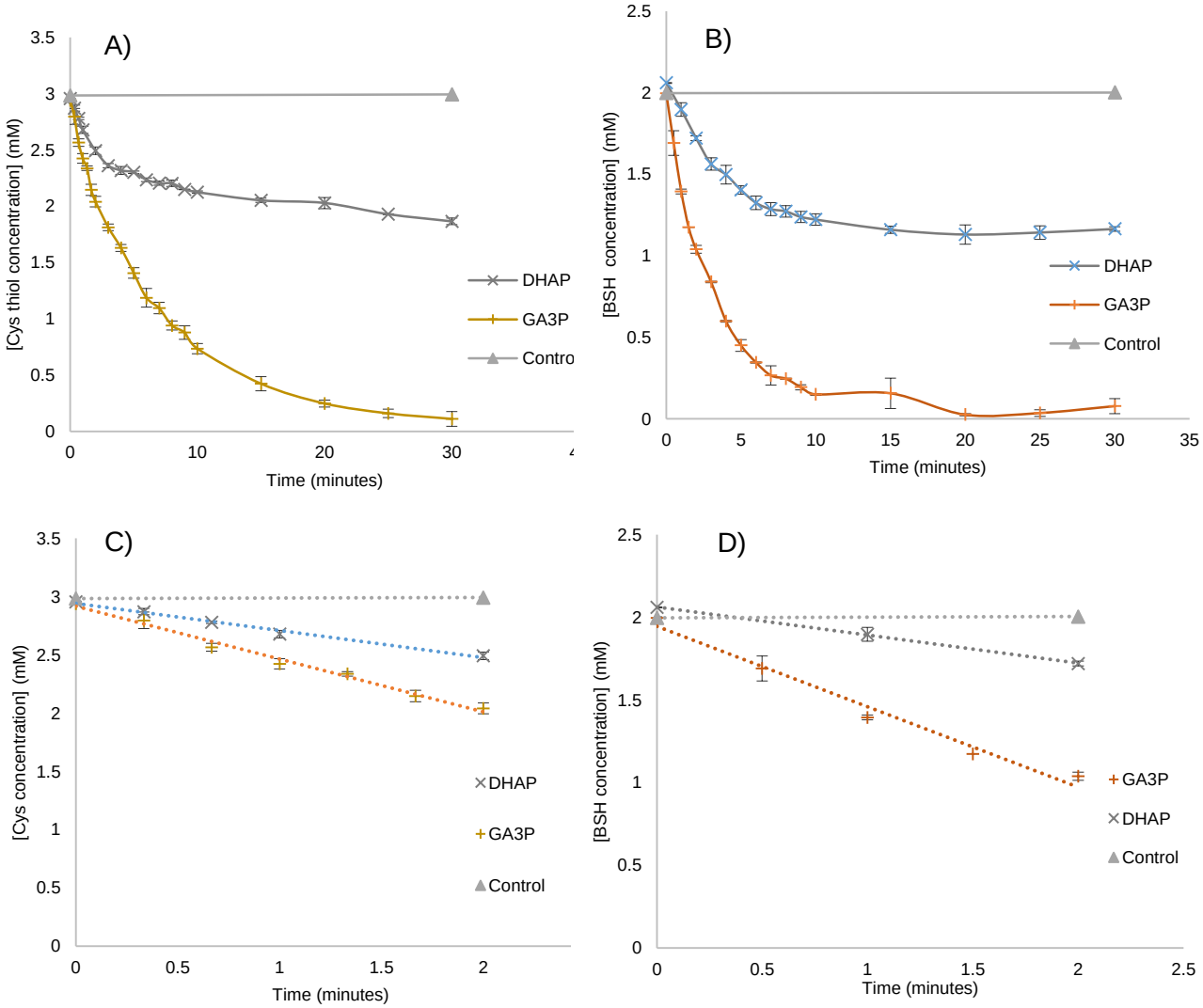

Figure 3.2. The relative reactivity of DHAP and GA3P (10 mM) with A) Cys (3 mM) for 30 mins B) BSH (2 mM) for 30 mins, C) Cys (3 mM) for 2 mins and D) BSH (2 mM) for 2 mins, at 20 °C, HEPES (50 mM) pH 7.7. Data was carried out in duplicate where error bars show ± SEM.

3.3. pH-dependent (pH 7.7) and pH-independent rate constants

3.3.1. Forwards and reverse rate constants for the reactivity of DHAP with thiols

The pH-independent pseudo-first order rate constants (k_1) were determined for the reactivity of DHAP and GA3P with both, Cys and BSH. The rate of HTA formation by reaction from the reaction between Cys and DHAP increased linearly up to 0.75 mM. The rate of reaction above this value was found to decrease relative to the concentration. This is possibly due to the first order reaction becoming a second order reaction or possibly because of experimental error shown by a large SEM in the last two data points, at thiol concentration 1200 µM and 1600 µM (figure 3.3C).[108] The rate constant was determined from the linear region of the graph where it appeared to be following pseudo-first order kinetics, which was found to be 6 x 10^{-4} s^{-1} at pH 7.7, whilst the pH-independent constant was found to be 4.4 x 10^{-3} s^{-1}.

The rate constant for HTA formation between BSH with DHAP was found to be 7 x 10^{-4} s^{-1} at pH 7.7, and therefore possesses a similar reactivity to Cys reacting with DHAP (figure 3.3C/D). However, due to the higher thiol pK_a of Cys, there is less Cys^- thiolate relative to BS^- thiolate at pH 7.7. As a result, the pH-independent rate constant for BS^- reacting with DHAP was 3.1 x 10^{-3} s^{-1}, which is found to be 1.4 times slower than the Cys and DHAP pH-independent rate constant. In addition, the second order rate constants were determined by dividing the pseudo-first order rate constant by the DHAP concentration (0.01 M) (table 2.2).

The reverse rate constants were determined following the same technique investigating the dissociation of the RS-MG HTA (chapter 2.2.3). The reverse rate constants were found to be approximately 100 times less than the forwards rate constant. The dissociation for both Cys-DHAP and BS-DHAP HTA took place in a similar manner (figure 3.4) Whilst both Cys and BSH have shown to possess similar rates of reaction with DHAP, BSH is found to be present at higher intracellular concentrations of approximately 3 mM as opposed to approximately 0.2 mM of Cys, at late exponential phase of *B. subtilis* growth. Therefore, the potential BS-DHAP HTA is more likely to be present in a higher concentration than the Cys-DHAP HTA.

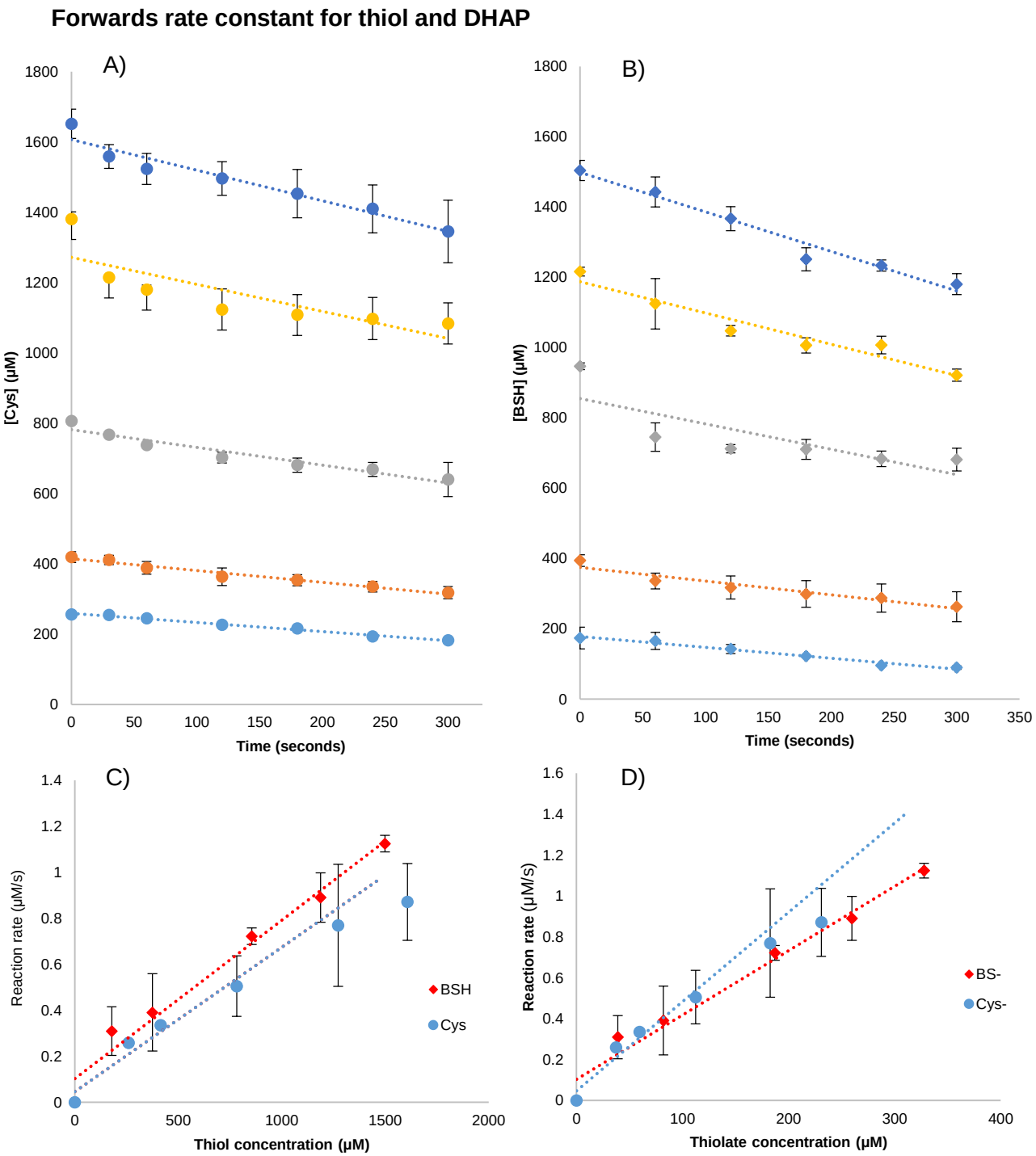

Figure 3.3. A) The consumption of Cys (200 μM – 1600 μM) with DHAP (10 mM) in HEPES (50 mM), pH 7.7, 20 °C, representing pseudo first order reaction kinetics with each gradient representing the rate of reaction. B) The consumption of BSH (200 μM – 1600 μM) with DHAP (10 mM) in HEPES buffer (50 mM), pH 7.7, 20 °C, representing pseudo first order reaction kinetics with each gradient representing the rate of reaction. C) The two rate constants of DHAP reactivity with Cys/BSH, at pH 7.7 D) The two pH independent rate constants of DHAP reactivity with Cys/BSH. Data was carried out in duplicate where error bars show ± SEM.

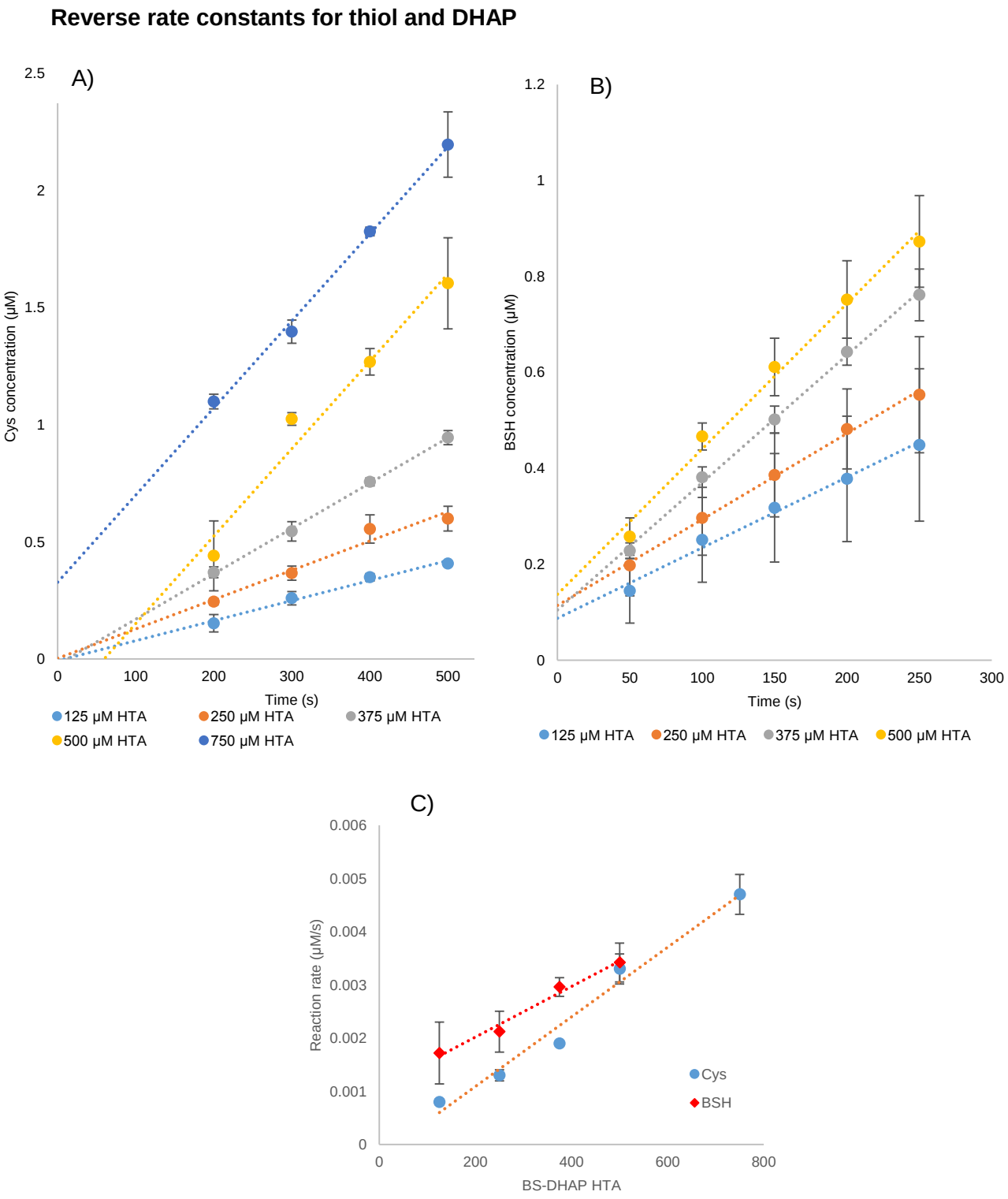

Figure 3.4. A) The dissociation of HTA (125 μM – 750 μM) using DTNB (2 mM) in HEPES buffer (50 mM) pH 7.7, 20 °C, over 500 seconds after carrying out an initial reaction of Cys (5 mM) with DHAP (10 mM) in HEPES buffer (50 mM), pH 7.7, 20 °C, with each gradient representing the rate of reaction. B) The dissociation of HTA (125 μM – 500 μM) using DTNB (2 mM) in HEPES buffer (50 mM) pH 7.7, 20 °C, over 250 seconds after carrying out an initial reaction of BSH (5 mM) with DHAP (10 mM) in HEPES buffer (50 mM), pH 7.7, 20 °C, with each gradient representing the rate of reaction. C) The two dissociation rate constants of HTA to form DHAP and Cys/BSH, at pH 7.7. Data was carried out in duplicate where error bars show ± SEM.

3.3.2. Forwards and reverse rate constants for the reactivity of GA3P and thiols

Rate constants for the interaction between thiol and GA3P were found to show a faster rate of reaction relative to DHAP by approximately 2-fold (table 3.2). The BSH was found to react 1.3 times faster than Cys with GA3P, at pH 7.7 (figure 3.5C). Yet, considering the higher thiol pK_a of Cys, the pH-independent rate constant was 1.1 times faster for the Cys^- relative to the BS^- (figure 3.5D). However, in general, there is only a slight difference in reactivity between the rates of Cys and BSH reacting with GA3P, which agrees with the initial relative rate of reactions observed (table 3.2).

The dissociation of HTA takes place in a similar rate for both DHAP-SR and GA3P-SR. However, the reverse rate constant for GA3P-SR (figure 3.6) was found to be approximately 200-times less than the forwards rate constant (figure 3.5). The half-life of each dissociation reaction were all greater than 24 hours suggesting that the forward reaction dominates (table 3.3).

Table 3.2: Pseudo first order rate constant (k_1), second order rate constant (k_2) and reverse rate (k_{-1}) constants for HTA formation from Cys and BSH reactivity with DHAP/GA3P

	Rate constant pH 7.7[a] (± SEM)	pH-independent rate constant (± SEM)
Pseudo-first order rate constant (k_1) with respect to thiol		
Cys-DHAP	$6 \times 10^{-4}\ s^{-1}$ ($\pm 1.5 \times 10^{-4}$)	$4.4 \times 10^{-3}\ s^{-1}$ ($\pm 1.1 \times 10^{-4}$)
BS-DHAP	$7 \times 10^{-4}\ s^{-1}$ ($\pm 1 \times 10^{-4}$)	$3.1 \times 10^{-3}\ s^{-1}$ ($\pm 4.5 \times 10^{-4}$)
Cys-GA3P	$1.1 \times 10^{-3}\ s^{-1}$ ($\pm 1 \times 10^{-4}$)	$7.3 \times 10^{-3}\ s^{-1}$ ($\pm 5 \times 10^{-4}$)
BS-GA3P	$1.4 \times 10^{-3}\ s^{-1}$ ($\pm 5 \times 10^{-5}$)	$6.6 \times 10^{-3}\ s^{-1}$ ($\pm 1.5 \times 10^{-4}$)
Second order rate constant (k_2)		
Cys-DHAP	$0.06\ M^{-1}s^{-1}$ (±0.015)	$0.44\ M^{-1}s^{-1}$ (±0.011)
BS-DHAP	$0.07\ M^{-1}s^{-1}$ (±0.01)	$0.31\ M^{-1}s^{-1}$ (±0.045)
Cys-GA3P	$0.11\ M^{-1}s^{-1}$ (±0.01)	$0.73\ M^{-1}s^{-1}$ (±0.05)
BS-GA3P	$0.14\ M^{-1}s^{-1}$ (±0.005)	$0.66\ M^{-1}s^{-1}$ (±0.015)
Reverse rate constant (k_{-1})		
Cys-DHAP	$7 \times 10^{-6}\ s^{-1}$ ($\pm 1.1 \times 10^{-6}$)	-
BS-DHAP	$5.6 \times 10^{-6}\ s^{-1}$ ($\pm 5 \times 10^{-7}$)	-
Cys-GA3P	$6 \times 10^{-6}\ s^{-1}$ ($\pm 7.5 \times 10^{-7}$)	-
BS-GA3P	$8 \times 10^{-6}\ s^{-1}$ ($\pm 5 \times 10^{-7}$)	-

[a]Rate constant could not be determined at this pH because of the speed of the reaction and therefore the rate constant has been calculated based on the thiolate concentrations at pH 7.7 relative to pH 5.6.

Table 3.3. The half-life for the dissociation of HTA to form free thiol and DHAP/GA3P.

	Half-life ($t_{1/2}$)
Cys-DHAP	27 hours 30 minutes
BS-DHAP	34 hours and 24 minutes
Cys-GA3P	32 hours and 6 minutes
BS-GA3P	24 hours and 6 minutes

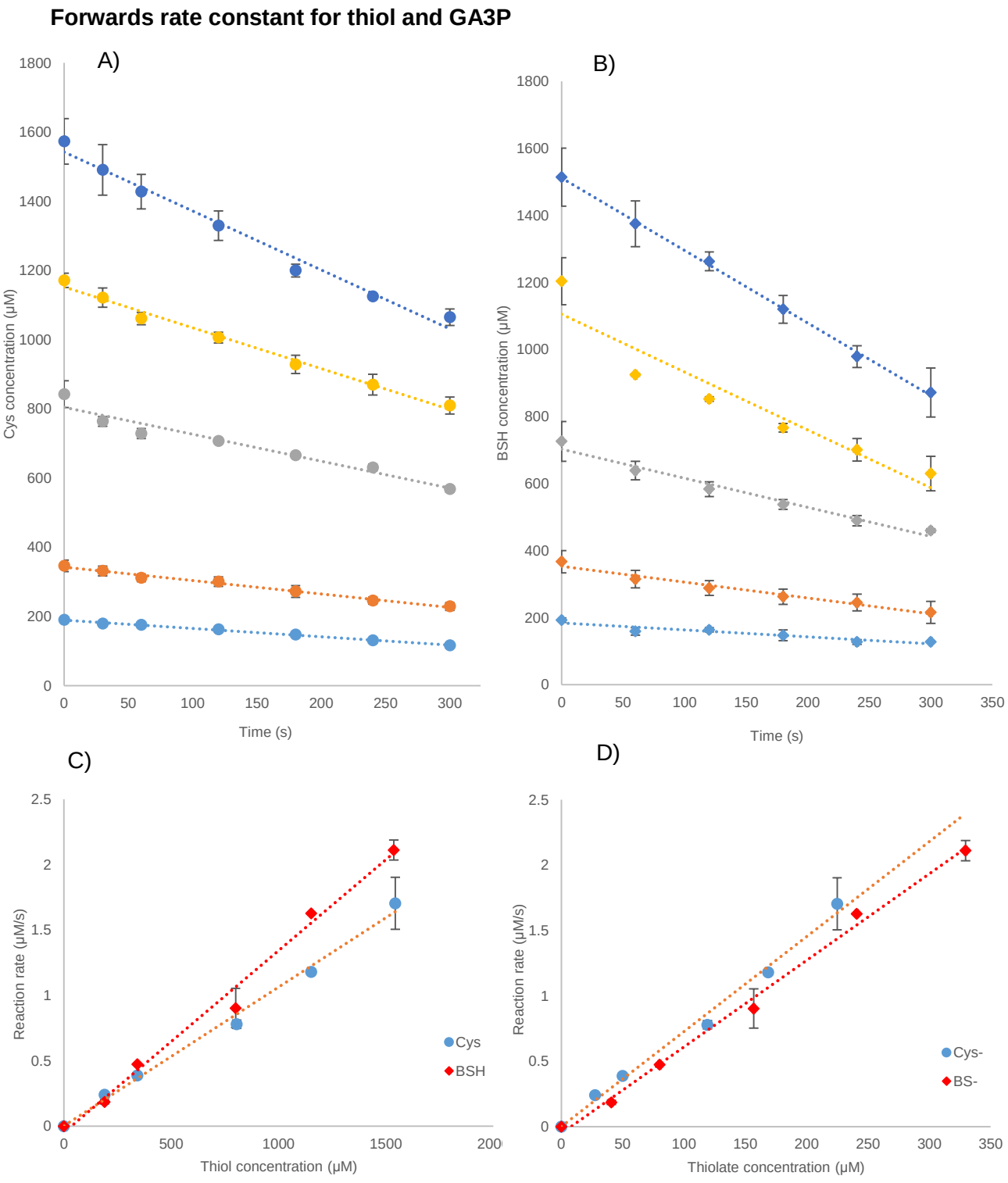

Figure 3.5. A) The consumption of Cys (200 μM – 1600 μM) with GA3P (10 mM) in HEPES buffer (50mM), pH 7.7, 20 °C, representing pseudo first order reaction kinetics with each gradient representing the rate of reaction. B) The consumption of BSH (200 μM – 1600 μM) with DHAP (10 mM) in HEPES buffer (50mM), pH 7.7, 20 °C, representing pseudo first order reaction kinetics with each gradient representing the rate of reaction. C) The two rate constants of GA3P reactivity with Cys/BSH, at pH 7.7 D) The two pH independent rate constants of GA3P reactivity with Cys/BSH. Data was carried out in duplicate where error bars show ± SEM.

Reverse rate constant for thiol and GA3P

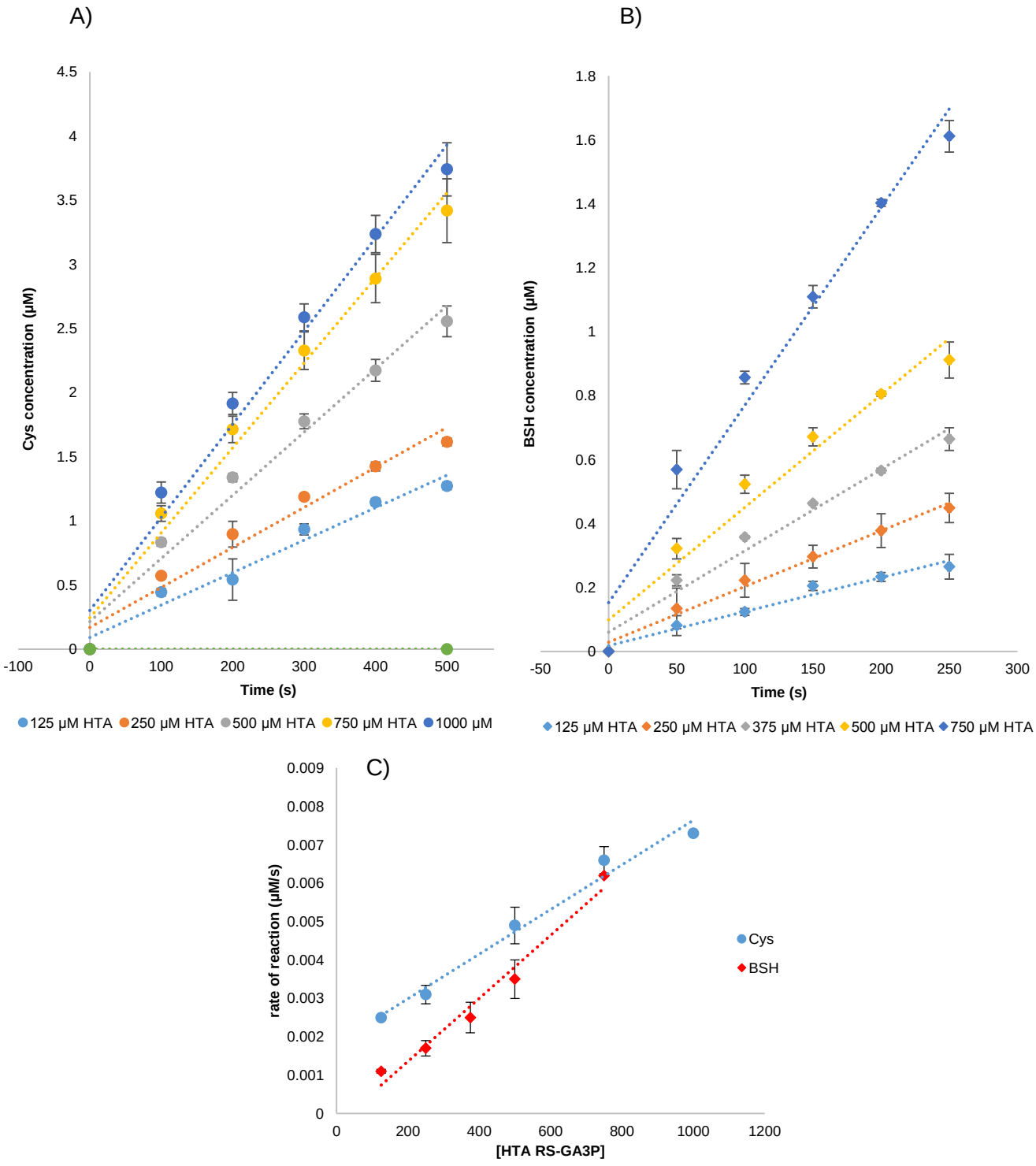

Figure 3.6. A) The dissociation of HTA (125 μM – 1000 μM) using DTNB (2 mM) in HEPES buffer (50 mM) pH 7.7, 20 °C, over 500 seconds after carrying out an initial reaction of Cys (5 mM) with GA3P (10 mM) in HEPES buffer (50mM), pH 7.7, 20 °C, with each gradient representing the rate of reaction. B) The dissociation of HTA (125 μM – 750 μM) using DTNB (2 mM) in HEPES buffer (50 mM) pH 7.7, 20 °C, over 250 seconds after carrying out an initial reaction of BSH (5 mM) with GA3P (10 mM) in HEPES buffer (50mM), pH 7.7, 20 °C, with each gradient representing the rate of reaction. C) The two dissociation rate constants of HTA to form GA3P and Cys/BSH, at pH 7.7. Data was carried out in duplicate where error bars show ± SEM.

3.4. Reactivity of thiol and pyruvate

It has been established that pyruvate is present in the cell at high concentrations (> 10 mM) in *B. subtilis* when in malate and glucose rich conditions.[129] Therefore, reactions were carried out implementing new assay conditions. This included the reactivity of thiol (2 mM Cys, 3 mM BSH, 8 mM GSH) with a higher concentration of pyruvate (10 mM) regulated at pH 7.7, 20 °C. As a result, reactivity was observed with both Cys and BSH (figure 3.7). The reactivity of pyruvate with Cys and BSH is found to be approximately 7-fold and 4-fold slower than with DHAP, respectively. Whilst the rates of reactivity are slower, pyruvate exists in up to a concentration of 145.01 mM[129] in the cell and therefore there is potential for the pyruvate-SB HTA to form in a significant concentration.

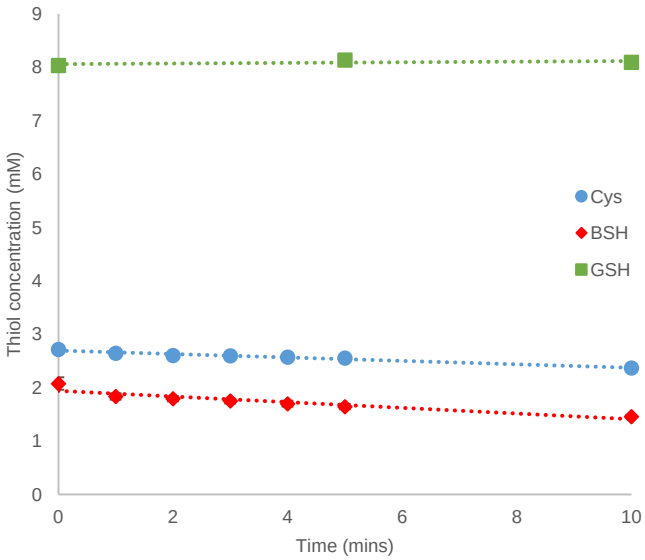

Figure 3.7. The reaction of 2 mM Cys, 3 mM BSH and 8 mM GSH with 10 mM Pyruvate in HEPES buffer, pH 7.7, 20 °C, representing the same thiolate concentration (0.44 mM).

3.5. Thermodynamics – equilibrium constant (K_{eq})

3.5.1. Overview

The forwards and reverse rate constants have now been determined and prove that an interaction takes place between the thiol and metabolite. However, the significance of these reactions is yet to be determined. This is dependent firstly on the concentrations that the cofactors and metabolites are present in the cell and secondly on the equilibrium constants (K_{eq}) of the reaction.

There are 2 distinctive methods for the determination of the equilibrium constant that have been implemented in this research. The first method uses the rate constants of the reaction between thiol and metabolite reactivity. k_{-1} and k_2 are both constants where the ratio (k_2/k_{-1}) represents the equilibrium constant (K_{eq}) (equation 3.5). The second method involves quantification of thiol, metabolite and HTA directly at equilibrium, and when represented in the form of equation 3.6, produces the $K_{eq.}$

Method 1: The rate constants of the forward reaction against the reverse reaction produces the equilibrium constant (K_{eq}):

$$K_{eq} = \frac{k_2}{k_{-1}} \qquad \text{Eq. 3.5}$$

Method 2: The reaction of metabolite and thiol in different ratios each produces a steady state. At steady state, the concentrations of HTA against the concentration of thiol and metabolite produces the equilibrium constant (K_{eq}):

$$K_{eq} = \frac{[HTA]}{[C=O][RSH]} \qquad \text{Eq. 3.6}$$

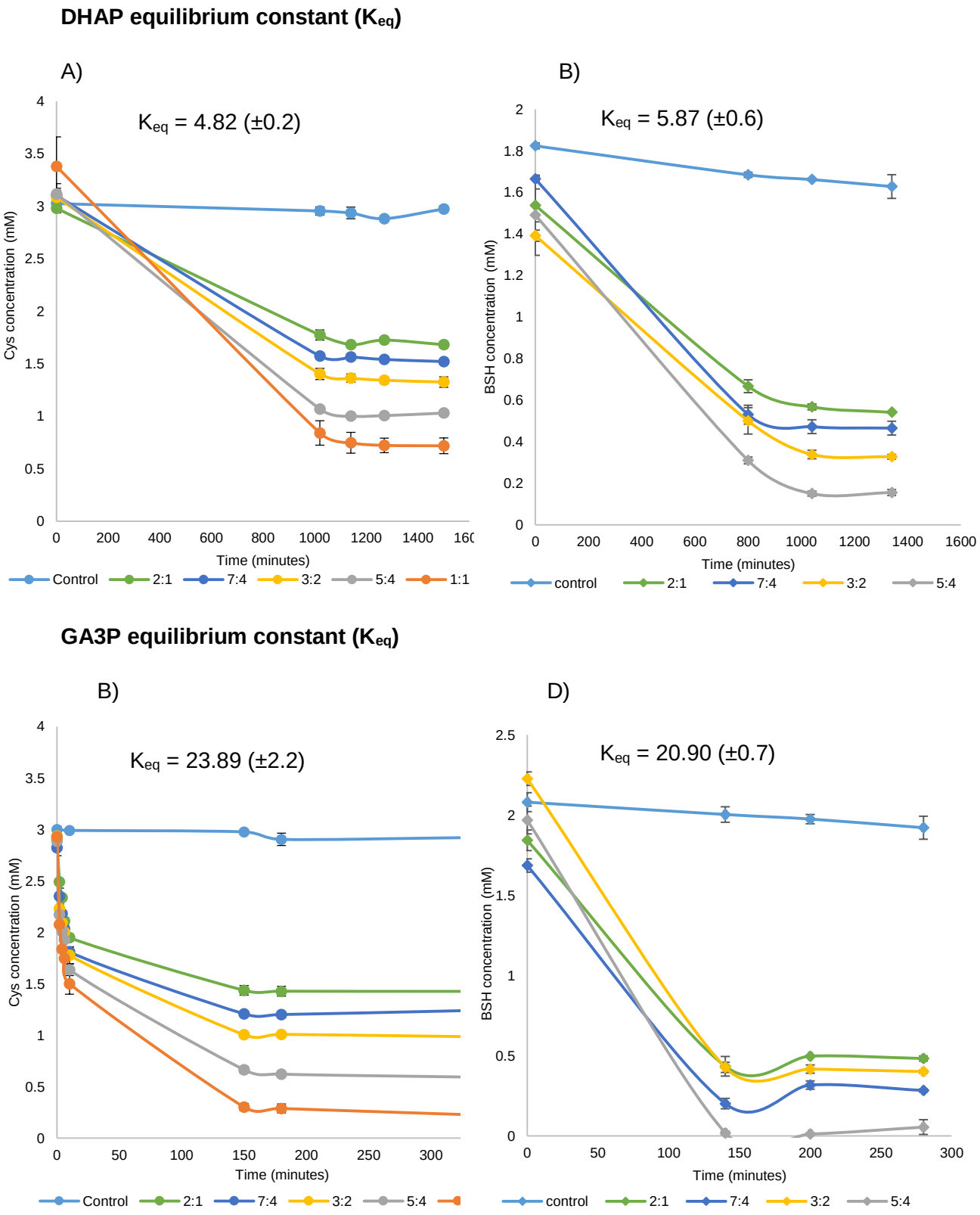

Figure 3.8. A) Reactivity of different ratios of thiol to metabolite (2:1 (3 mM: 1.5 mM), 7:4 (3 mM: 1.7 mM), 3:2 (3 mM: 2 mM), 5:4 (3 mM, 2.4 mM), 4:5 (3 mM, 3.75 mM), 1:1 (3 mM: 3 mM) in 50 mM HEPES pH 7.7, under nitrogen conditions) to determine state of equilibrium and equilibrium constant (K_{eq}) ± SEM in A) Cys and DHAP. B) BSH and DHAP. C) Cys and GA3P. D) BSH GA3P.

3.5.2. Method 2 - Calculation of equilibrium constant (K_{eq}) example

Table 3.4: The first set of K_{eq} found from the reaction between Cys and DHAP. The reaction of the 5:4 ratio of RSH:C=O is used as an example for the determination of K_{eq}.

Ratio RSH:C=O	[Cys_0] mM	[Cys_t] mM	[$DHAP_t$] mM	[HTA] mM	**K_{eq}**
5:4	3.08	0.72	0.65	2.36	**5.04**
3:2	3.12	1.03	0.51	2.09	**4.00**
7:4	3.09	1.33	0.26	1.76	**5.16**
2:1	3.10	1.52	0.22	1.58	**4.70**

Ellman's titration was carried out at t = 0 to quantify the starting concentration of thiol (RSH_0). Once equilibrium had been met, Ellman's titration was carried out again to quantify the concentration of thiol at equilibrium (RSH_t). In parallel to this, DHAP was quantified using the DHAP assay (chapter 6.5.2.1) when the equilibrium had been met to determine the concentration of residual concentration of DHAP ($DHAP_t$).

The following equation was then used to calculate the K_{eq}

$$K_{eq} = \frac{[HTA]}{[DHAP][RSH]} \quad \text{Eq. 3.7}$$

$$K_{eq} = \frac{[RSH_0 - RSH_t]}{[DHAP_t][RSH_t]} \quad \text{Eq. 3.8}$$

$$K_{eq} = \frac{[3.08 - 0.72]}{[0.65][0.72]}$$

$$K_{eq} = 5.04$$

This calculation was carried out for every data value which had been recorded at equilibrium (table 3.4). Then the mean of all these reactions were then calculated for each set of reactions, in this instance, the DHAP and Cys reaction. The K_{eq} achieved represents the mean value with ± SEM.

Table 3.5. Percentage of HTA at equilibrium for all 4 reactions of interest.

Thiol and metabolite reaction, in HEPES pH 7.7	K_{eq} - Method 1		K_{eq} - Method 2	
	K_{eq}	% (1:1 ratio)	K_{eq}	% (1:1 ratio)
Cys (1 M) + DHAP (1 M)	8571 (±3490)	98.9%	4.8 (±0.2)	64%
BSH (1 M) + DHAP (1 M)	12500 (±2900)	99.1%	5.9 (±0.6)	66%
Cys (1 M) + GA3P (1 M)	18333 (±3750)	99.3%	23.9 (±2.2)	82%
BSH (1 M) + GA3P (1 M)	17500 (±1720)	99.3%	20.9 (±0.7)	80%

A) Method 1 - k_2/k_{-1}

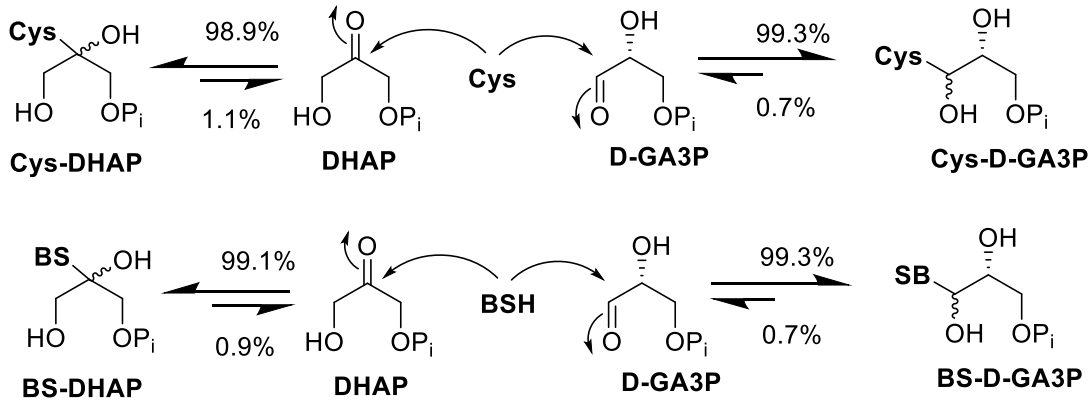

B) Method 2 - steady state equilibria

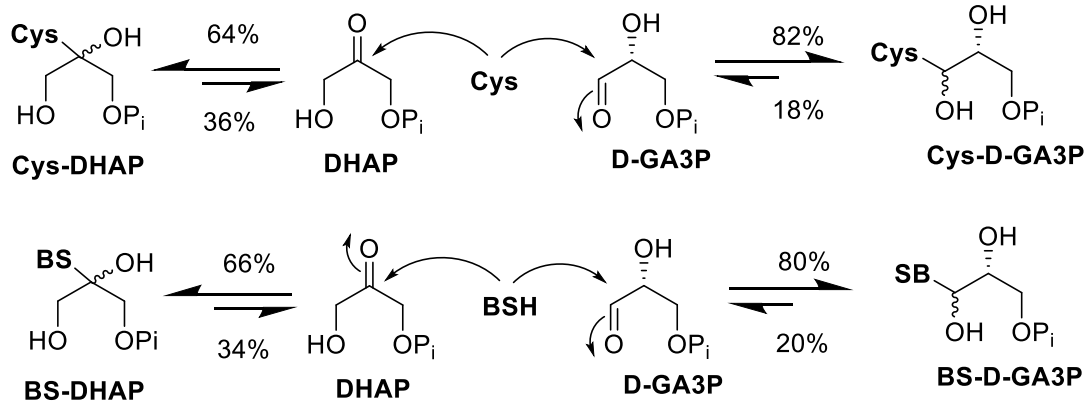

Scheme 3.4. 4 reactions of interest with each thiol reacting with DHAP and GA3P, representing the percentage of the equilibrium shift in the forwards and reverse reaction for both methods A) 1 – k_2/k_{-1} B) 2 – steady state equilibria.

3.5.3. Interpretation of thermodynamic equilibrium constant

The K_{eq} determined by the steady state equilibria (method 2) were found to be significantly different with a 500-2000-fold less than the K_{eq} determined from the ratio of k_2/k_{-1} (method 1) (table 3.5). To explain this difference, the experiments were left for approximately 140 minutes and 1050 minutes for thiol reacting with GA3P and DHAP, respectively, to allow equilibrium to be reached (figure 3.8, method 2). In this time frame, DHAP and GA3P are known to non-enzymatically degrade to MG, which may ultimately affect the position of the equilibrium. By the time the reaction has reached equilibrium, there is estimated to have been 10.8% degradation of GA3P whilst DHAP is estimated to have degraded by 20.8%. The K_{eq} determined from the ratio of k_2/k_{-1} (method 1) are based on the immediate kinetics from the rate constants and are therefore not subjected to this degradation.

The K_{eq} can be put into context using the quadratic equation to determine the percentage of reactant and product formation (chapter 6.5.2.6). With respect to method 2, the product formation is favoured with 64-66% and 80-82% formation of HTA for the reactivity of thiol with DHAP and GA3P, respectively. Whilst with respect to method 1, the product formation is more favoured with approximately 99% formation of HTA for the reactivity of thiol with DHAP and GA3P, respectively (scheme 3.4). Both Cys and BSH showed a similar relative reactivity suggesting an equal thermodynamic stability of the respective HTAs.

To conclude, all K_{eq} were found to be >1 and HTA formation is favoured >50% in all 4 reactions, implying a negative free energy change meaning the HTA is more stable than the free metabolite and thiol in solution. Therefore this may be of significance in a physiological setting. However, this is dependent on the intracellular concentrations of the metabolites of interest.

3.6. Physiologically relevant *in vivo*/ *in vitro* assays

3.6.1. Intracellular concentration of metabolites in *B. subtilis* WT

A second consideration for determining the importance of HTA formation is considering the intracellular concentration of metabolites. Table 3.6 represents the intracellular concentration of the glycolytic metabolites that have been measured in three different organisms, *E. coli* (Gram-negative bacteria), rat tissue (eukaryotes) and *B. subtilis* (BSH-utilising Gram-positive bacteria). The concentrations were found in a variety of sources and therefore there will be varied results depending on the sources and experimental conditions. For instance, the OD_{600} at which the metabolite concentration was determined ranges from 0.1-1.5. In addition, the level of carbohydrate significantly affects the concentration of glycolytic metabolites.[129] The metabolites which are shown to react with thiols, DHAP, GA3P and pyruvate are all found to range considerably in concentration from 0.07 mM[129] of GA3P to 145.01 mM[129] of pyruvate in *B. subtilis*. However, due to the slower reactivity of pyruvate the focus remains on DHAP reactivity with thiol.

All current *in vivo* data has been analysed using *B. subtilis* as the model organism grown in LB media. The intracellular concentration of GA3P was determined and there was no detectable GA3P in the cell, contrasting from the literature values which report a concentration of 0.07-0.12 µM[129]. The DHAP concentration, however, was found to exist in concentrations up to 528 µM at late-exponential phase (figure 3.9A). The literature value produced a similar result of 540 µM at exponential phase.[129] When comparing against all other literature values of glycolytic metabolites, with the exception of 3-PG and pyruvate, the DHAP is found to be present at the highest concentration. In addition, BSH is found in high concentrations of approximately 3 mM at late-exponential phase.[20] As a result, if thiol and DHAP are present at these concentrations and favourably equilibrate to form HTA, suggests that there may be significantly high intracellular pools of HTA in the cell.

Table 3.6. The literature values of the concentrations of glycolytic metabolites in three different organisms; *E. coli*, *Rattus* genus - liver tissue, and *B. subtilis*.

Metabolite	***E. coli*** + Glucose mM	***E. coli*** - Glucose mM	**Eukaryotes** + Glucose mM	**Eukaryotes** -Glucose mM	***B. subtilis*** + Glucose mM	***B. subtilis*** - Glucose mM
G-1P	1.85[b(130)]	0.09[c(131)]	4.15[(130)]		0.23[a(129)]	0.02[a(129)]
F-1,6-BP	6.6[b(130)]	0.1[c(131)]	1.85[(130)]		0.16[a(129)]	0.01[a(129)]
DHAP	0.37[(132)]	0.25[b(130)]	0.08[(130)]	0.16[(133)]	**0.93[a(129)]**	**0.54[a(129)]**
GA3P	0.049[(132)]		2.8[(130)]	0.08[(133)]	**0.12[a(129)]**	**0.07[a(129)]**
1,3-BPG				0.05[(133)]	0.1[a(129)]	0.07[a(129)]
3-PG	1.5[(132)]	0.34[c(131)]		0.2[(133)]	90.46[a(129)]	32.34[a(129)]
2-PG		0.33[c(131)]		0.02[(133)]		
PEP	0.18[(132)]	0.0356[(134)]	0.16[(130)]	0.065[(133)]	0.33[a(129)]	0.92[a(129)]
PYV	7.5[d(135)]	8.658[(134)]	0.5[(130)]		**8.9[a(129)]**	**145.01[a(129)]**

G-1P – glucose 1-phosphate, F-1,6-BP - Fructose 1,6-Bisphosphate

a - *B. subtilis* was grown in M9 minimal medium consisted of the following components (per litre): 8.5 g of $Na_2HPO_4.2H_20$, 3 g of KH_2PO_4, 1 g of NH_4Cl, 0.5 g of NaCl. The cells were grown to an OD_{600} of 0.1-1.5. Malate was used in absence of glucose.[(129)]

b - *E. coli* K12 was grown in minimal medium containing 30 g/L of glucose to a cell density of 10 g/L.[(130)]

c - *E. coli* was grown in media containing 4.7g/L KH_2PO_4, 13.5 g/L K_2HPO_4, 1 g/L K_2SO_4, 0.1 g/L $MgSO_4{\cdot}7H_2O$, and final concentrations of 10 mM NH4Cl, and 4g/L of glucose to an OD_{600} of approximately 0.1.[(131)]

d - *E.coli* was grown in LB media supplemented with 20 g/L glucose 10mg/L inositol.[(135)]

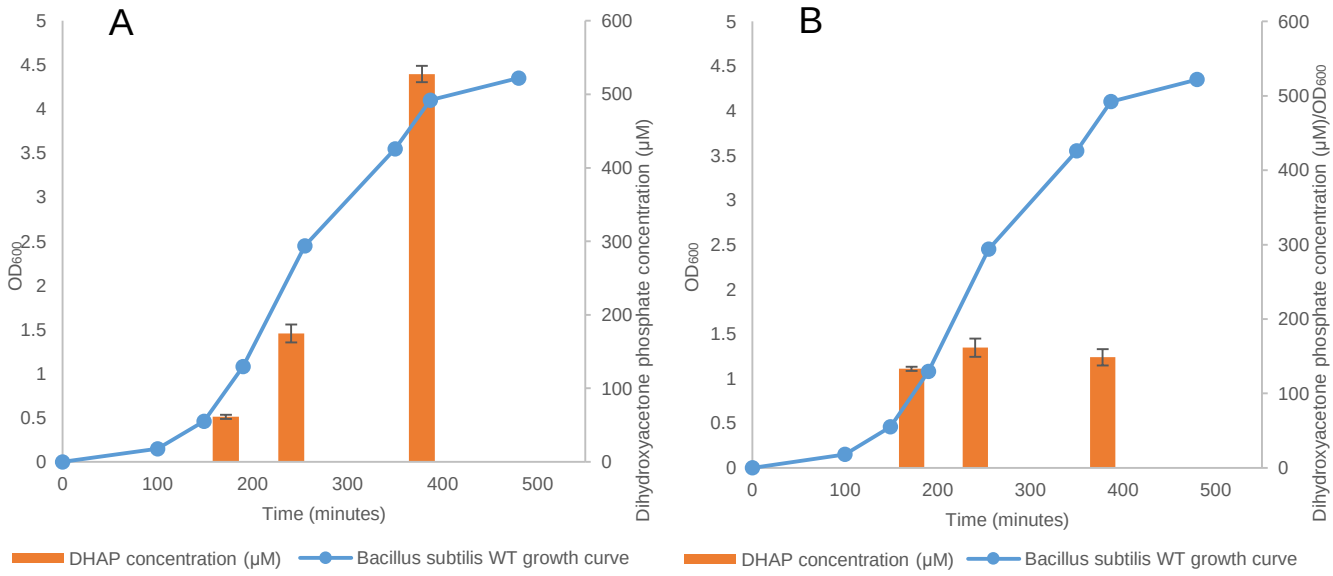

Figure 3.9. A) The growth curve of *B. subtilis* WT. The intracellular DHAP concentrations at early, mid and late-exponential phase of the growth. B) The intracellular DHAP concentrations at early, mid and late-exponential phase of the growth normalised to an OD_{600} of 1.

3.6.2. The *in vitro* reactivity of DHAP with Cys and BSH, under physiologically relevant conditions

The reaction between 0.5 mM DHAP with both 0.2 mM Cys and 2.5 mM BSH was analysed in parallel, replicating physiological cell conditions, at pH 7.7, 20 °C. Possessing an equal stoichiometry of BSH to DHAP, it was speculated that approximately 0.5 mM of BSH would be consumed over the 200 minutes. However, more consumption is shown to take place due to oxidation of BSH to BSSB. The amount of oxidation taking place can be accounted by comparison with the controls.

As a result, a full consumption of DHAP was found after 40 minutes of reaction with thiol, with approximately 0.5 mM BSH reacting (figure 3.10). BSH was 21-fold more reactive than Cys, with 0.04 mM of Cys reacting within 40 minutes. Approximately 0.4 mM of BSH is depleted within the first 10 minutes suggesting, within this period, a substantial concentration of DHAP could be sequestered as an HTA.

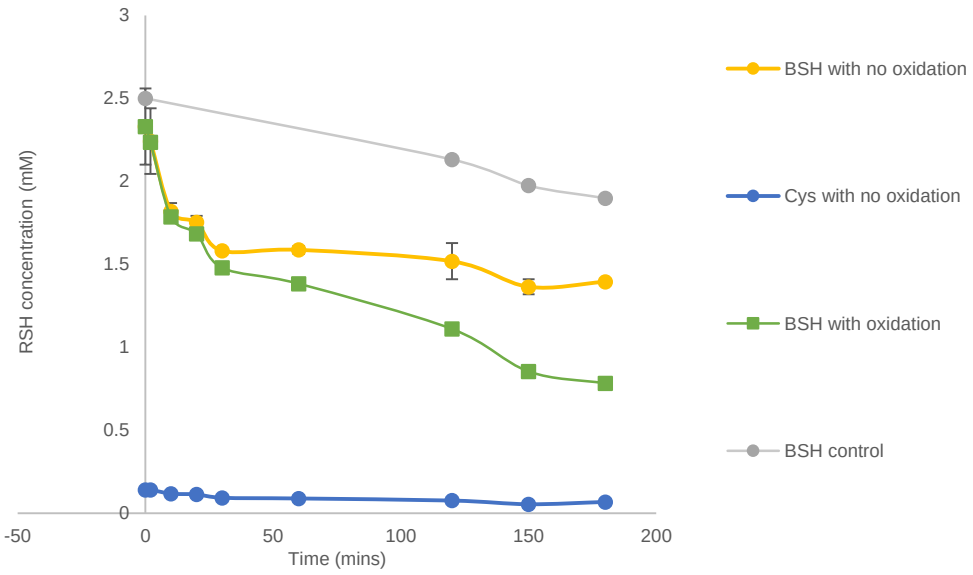

Figure 3.10. Physiological conditions of BSH (2.5 mM) and Cys (0.2 mM) reactivity with DHAP (0.5 mM) at pH 7.7, 20 °C.

3.6.3. Potential physiological observations in *B. subtilis*

Working on the assumption a cell could reach equilibrium between DHAP and BSH, it is possible to calculate the theoretical maximum HTA concentration (equation 3.9 - 3.10). As a result, the theoretical HTA concentration is shown to be in a large concentration, presenting at least twice the concentration of the free thiol/metabolite at late-exponential phase (figure 3.11). For example, at late-exponential phase of *B. subtilis* at an OD_{600} of 3.55, BSH is present in 3.2 mM and DHAP is present in 0.528 mM. If BSH and DHAP were in equilibrium, potentially 9.97 mM could be present as BS-DHAP HTA (figure 3.11B). However, in view of the complex nature of the cell with the constant production and metabolism of these metabolites, prevents the equilibrium of these reactions from being reached. This signifies that these theoretical HTA concentrations are unlikely but do represent the upper limits of HTA abundance.

Table 3.7. Concentrations of reactants and theoretical concentrations of HTA.

		Reactants			**Products**	
Phase	OD_{600}	BSH (mM)	Cys (mM)	DHAP (mM)	BS-DHAP (mM)	Cys-DHAP (mM)
Lag	0.46	0.7[20]	0.2[20]	0.061	0.25	0.06
Mid-exponential	1.08	1.2	0.5	0.175	1.24	0.42
Late-exponential	3.55	3.2	0.5	0.528	9.97	1.27
*Literature values were used for BSH and Cys concentration due to no reported data of thiol levels in the lag phase of growth in this research						

Table 3.8. Normalised data showing concentrations of reactants and theoretical concentrations of HTA relative to an OD_{600} of 1.

		Reactants			**Products**	
Phase	OD_{600}	BSH/OD_{600} (mM)	Cys/OD_{600} (mM)	DHAP/ OD_{600} (mM)	BS-DHAP /OD_{600} (mM)	Cys-DHAP /OD_{600} (mM)
Lag	0.46	1.52[20]	0.43[20]	0.13	1.17	0.29
Mid-exponential	1.08	1.11	0.46	0.16	1.05	0.35
Late-exponential	3.55	0.90	0.14	0.15	0.79	0.10
*Literature values were used for BSH and Cys concentration due to no reported data of thiol levels in the lag phase of growth in this research						

Calculation of theoretical DHAP-SB HTA concentration at late-exponential phase example:

$$K_{eq} = \frac{[HTA]}{[DHAP][BSH]} \quad \text{Eq. 3.9}$$

$$[HTA] = K_{eq}[DHAP][BSH] \quad \text{Eq. 3.10}$$

$$[HTA] = 5.9[0.528][3.2]$$

$$[HTA] = 9.97\ mM$$

A)

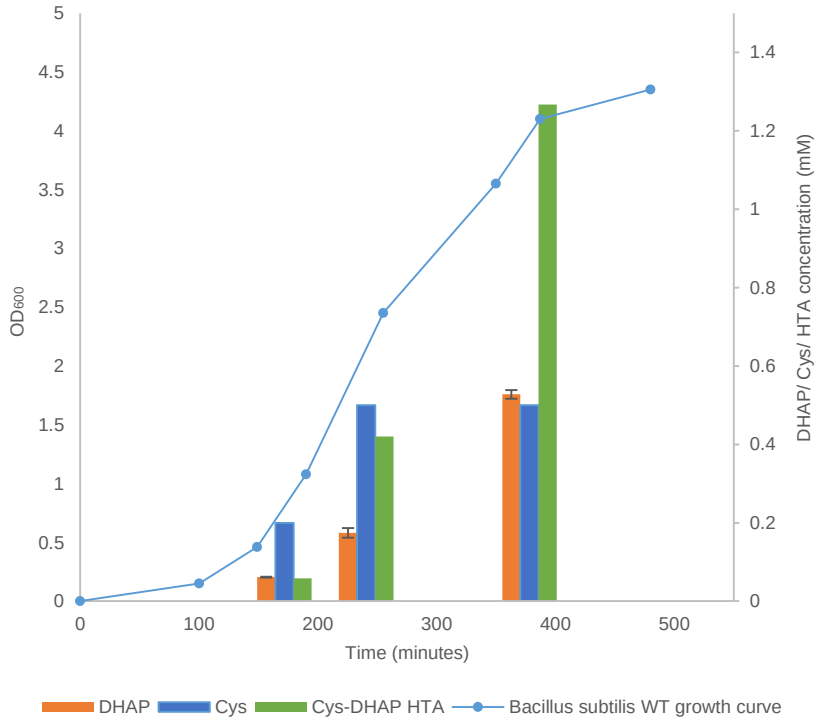

B)

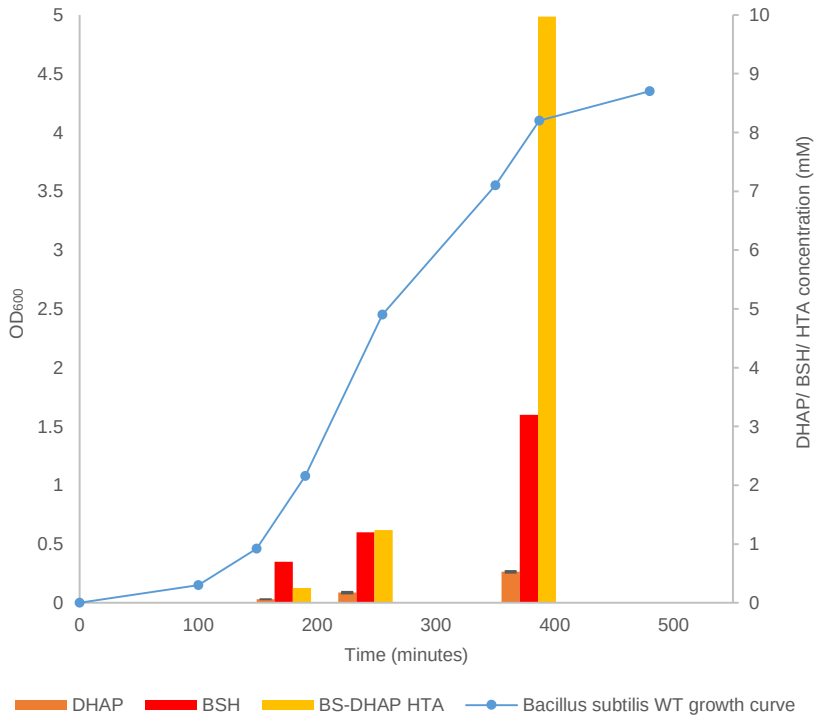

Figure 3.11. The growth curve of *B. subtilis* WT and metabolite/thiol/HTA concentration. A) The intracellular concentrations of DHAP, Cys and theoretical Cys-DHAP HTA concentration at lag, mid and late-exponential phase of the growth B) The intracellular concentrations of DHAP, BSH and theoretical BS-DHAP HTA concentration at lag, mid and late-exponential phase of the growth.

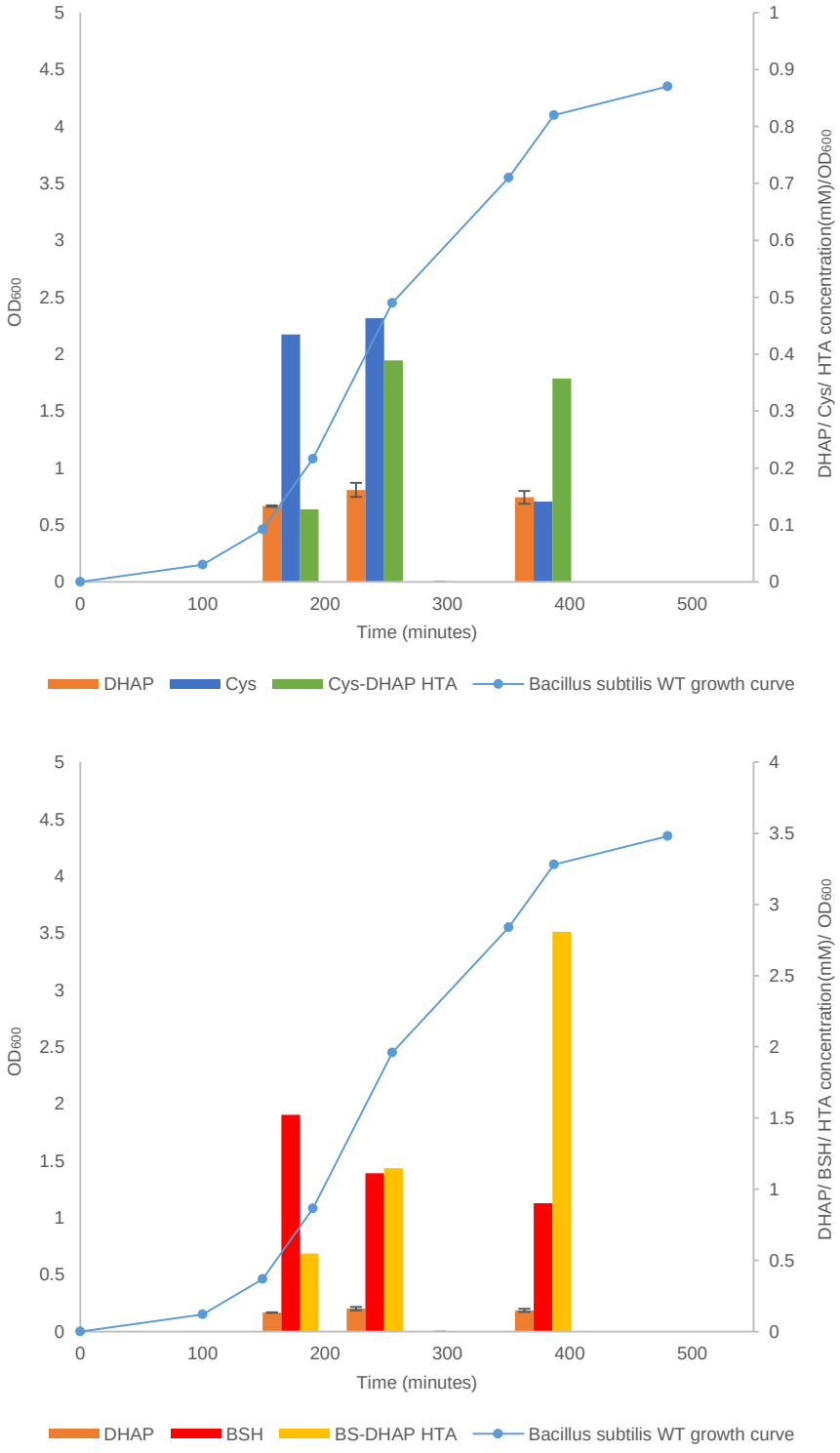

Figure 3.12. The growth curve of *B. subtilis* WT and metabolite/thiol/HTA concentration. A) The intracellular concentrations of DHAP, Cys and theoretical Cys-DHAP HTA concentration at lag, mid and late-exponential phase of the growth, normalised to an OD_{600} of 1 B) The intracellular concentrations of DHAP, BSH and theoretical BS-DHAP HTA concentration at lag, mid and late-exponential phase of the growth, normalised to an OD_{600} of 1.

3.7. Significance of research and potential impact in health-related conditions

There is speculation that these reactions may also exist amongst GSH-utilising eukaryotes. This may explain the thiol concentration changes upon high levels of glucose stress, which in the mammalian class of eukaryotes, is found to exist in a condition known as diabetes mellitus.

Diabetes mellitus, is a chronic medical condition characterised by the recurrent high blood glucose levels (hyperglycaemia) which arises from defects in insulin secretion. It is known that prolonged hyperglycaemia contributes to the development of many vascular complications of the condition including nephropathy, retinopathy, and neuropathy. These complications arise because of the increase in oxidative stress in the cells caused by the high concentrations of metabolites such as MG from the increased flux of glucose metabolism.[136-141] In relation to thiol concentrations, serum protein GSH levels show the opposite effect and deplete in the tissues of diabetics.[142-145] It has been shown that there is a decrease in thiol levels in diabetic patients possessing a serum thiol concentration of 605 μM relative to the control of 664 μM.[146] Whilst it is speculated that these decreased levels of thiol detected are partially due to the increase in oxidative stress, it becomes apparent that there may be a link between thiols and the carbonyl-containing metabolites.[147]

The research has showed that GA3P reacts with excess GSH (400 mM).[127] However, this research has shown no reaction of GSH with metabolite under physiological conditions in eukaryotic cells; GA3P (80 μM)[133], DHAP (160 μM)[133] reacting with GSH (5 mM), pH 7.4. However, Cys (200 μM)[21] is known to react with DHAP and GA3P at physiological conditions. This has much significance amongst eukaryotes due to Cys being a fundamental precursor in the biosynthesis of GSH. In hyperglycaemia, an increase in metabolites would result in a high concentration of Cys forming the thermodynamically favoured, HTA. The decrease in free Cys available will significantly reduce the concentrations of GSH due to the decrease in its biosynthesis. In addition, this decrease in thiol will result in an overburden of oxidative stress in the cell, suggesting that the formation of HTA is a potentially significant reaction in the pathogenesis of the complications of diabetes mellitus.

3.8. Reactivity of other metabolites with GSH

There is also a possibility that the LMW thiols are reacting with other reactive carbonyls to form HTAs. Diabetes mellitus is also known to cause an excess acetoacetic acid. It is the simplest beta-keto acid group and it is of biochemical importance in the breakdown of fatty acids into acetyl-CoA. However, *in vitro* analysis under physiological conditions in humans showed no reactivity of either Cys or GSH with acetoacetic acid. 3-Deoxyglucosone, malondialdehyde and 4-hydroxynonenal are all toxic dicarbonyl species which are found to be present in higher concentrations in diabetics. These are all toxic metabolites which have been known to react with the amino acid lysine causing amino acid disruption leading to vascular complications. There is importance in analysing the reactivity of these toxic carbonyl metabolites with Cys and GSH to determine whether this reaction takes place and the extent of the involvement of this possible reaction.

3.9. Summary

This research has shown that thiol cofactors including Cys and BSH chemically react with three glycolytic metabolites, in the order of reactivity of GA3P > DHAP > pyruvate. Both Cys and BSH have shown a similar rate of reactivity, with pH-independent rate constants of approximately 1600-fold slower reactivity than MG. Therefore, it is likely that BSH will react with MG preferentially over other metabolites in the cell. However, *in vivo* assays show that DHAP concentrations are shown to be in concentrations of 527.6 μM in the late-exponential phase. In addition, the equilibrium constants have shown that the reaction favours the formation of HTA when reacted with the thiol. Equal concentrations of DHAP/GA3P and thiol results in ~ 64 - 93% formation of HTA, with a theoretical maximum concentration of 9.9 mM and 1.24 mM of BS-DHAP and Cys-DHAP, respectively.

The context of these results can also relate to eukaryotes. While GSH has not shown to react with any metabolite under physiologically conditions, Cys does show reactivity. Cys forms a necessary biosynthetic intermediate of GSH. Therefore, in metabolic conditions such as diabetes mellitus, which is known to have increased concentration of GA3P, DHAP, pyruvate and MG, have unexplained reasons for low thiol levels upon hyperglycaemia. It is possible that the increased concentrations of metabolites are reacting with the Cys forming HTA. The current analytical techniques (Ellman's reagent and MBBr reagent) have only shown to detect free thiol and not HTA. This may therefore explain the lower levels of thiol experienced in hyperglycaemia, in addition to potentially unravelling many different hidden thiol pools that may exist in the cell. As such, further evidence to support the formation of HTA is vital in proving these reactions take place.

4. HTA/thiazolidine detection

4.1. Overview

Studies in the previous chapters of the reactions between thiol and carbonyl-containing metabolites only indirectly measured the formation of HTA. Herein, evidence to support HTA formation and the subsequent thiazolidine formation is presented using mass spectrometry and *in vitro* NMR analysis. Lastly, evidence of HTA existence in *B. subtilis* is obtained by whole cell NMR.

4.2. Mass spectrometry analysis

All six HTAs/thiazolidine derivatives were analysed on a Shimadzu ion-trap ToF mass spectrometer carried out by Lionel Hill (John Innes centre). The *in vitro* reactions of all samples were first carried out, allowing the potential HTAs to form. Approximately 5 mM thiol and 5 mM metabolite were reacted in MQ water to avoid excess levels of buffer salts suppressing the detection of HTA ions in the mass spectrometer. At various time points, the residual thiol was titrated using Ellman's reagent to confirm sufficient HTA formation (figure 4.1). After approximately 5 hours of reactivity between the thiol and metabolite, mass spectrometry analysis was carried out.

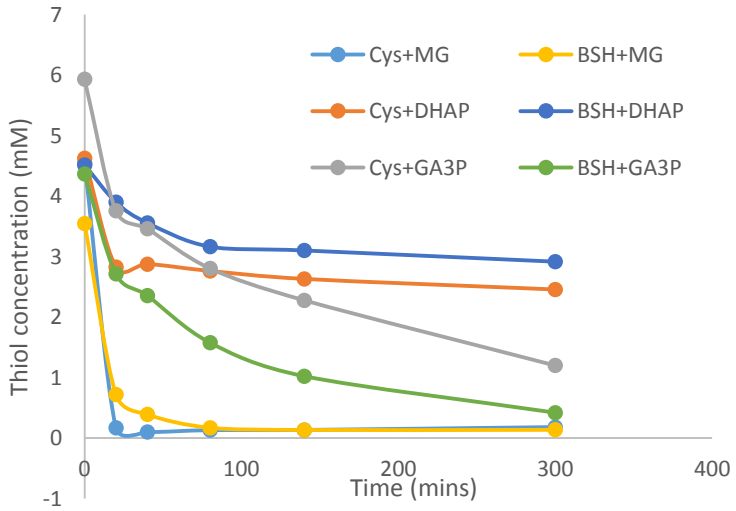

Figure 4.1 *In vitro* reactivity of three metabolites with BSH/Cys in MQ water.

4.2.1. MG and Cys

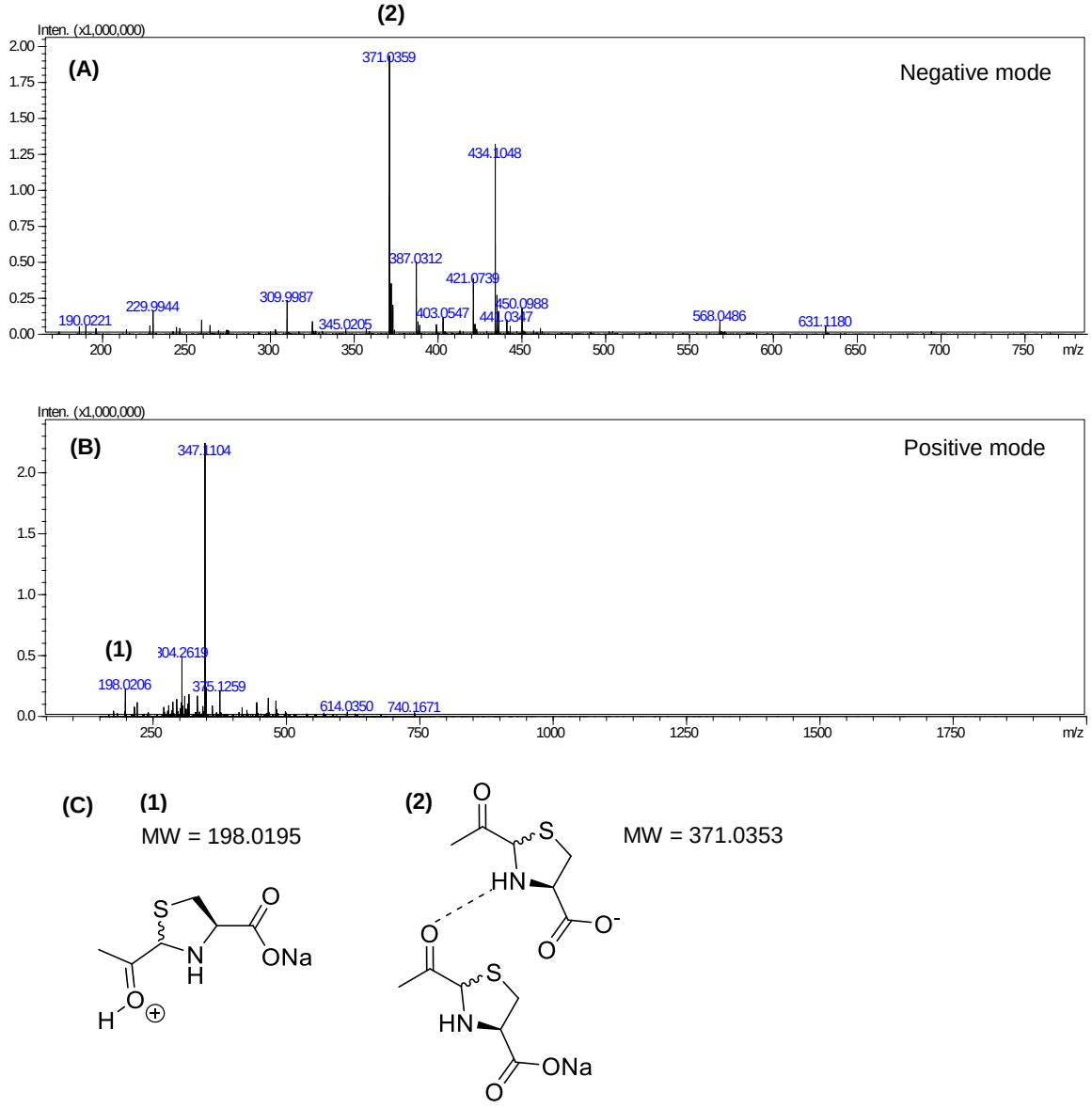

Figure 4.2. Spectrum of the reaction between MG and Cys, in A) region between 180-750 m/z in negative-mode after 13 hours B) full spectrum in positive-mode after 13 hours. C) Chemical structure of thiazolidine derivatives.

The mass of the Cys-MG HTA, M = $C_6H_{11}NO_4S$, is 193.0409. The base peak is appropriate for an in-source dimer of the thiazolidine associated with sodium (**2**) [2M-2H+Na] where the expected mass is 371.0353 and observed mass was 371.0359, when 2M = $C_{12}H_{18}N_2O_6S_2$. The identity of the other peaks remains unknown. In positive-mode, the thiazolidine monomer, associated with sodium (**1**), [M+Na] was detected, with an expected mass of 198.0195 and observed mass of 198.0206, when M = $C_6H_9NO_3S$ (figure 4.2).

4.2.2. MG and BSH

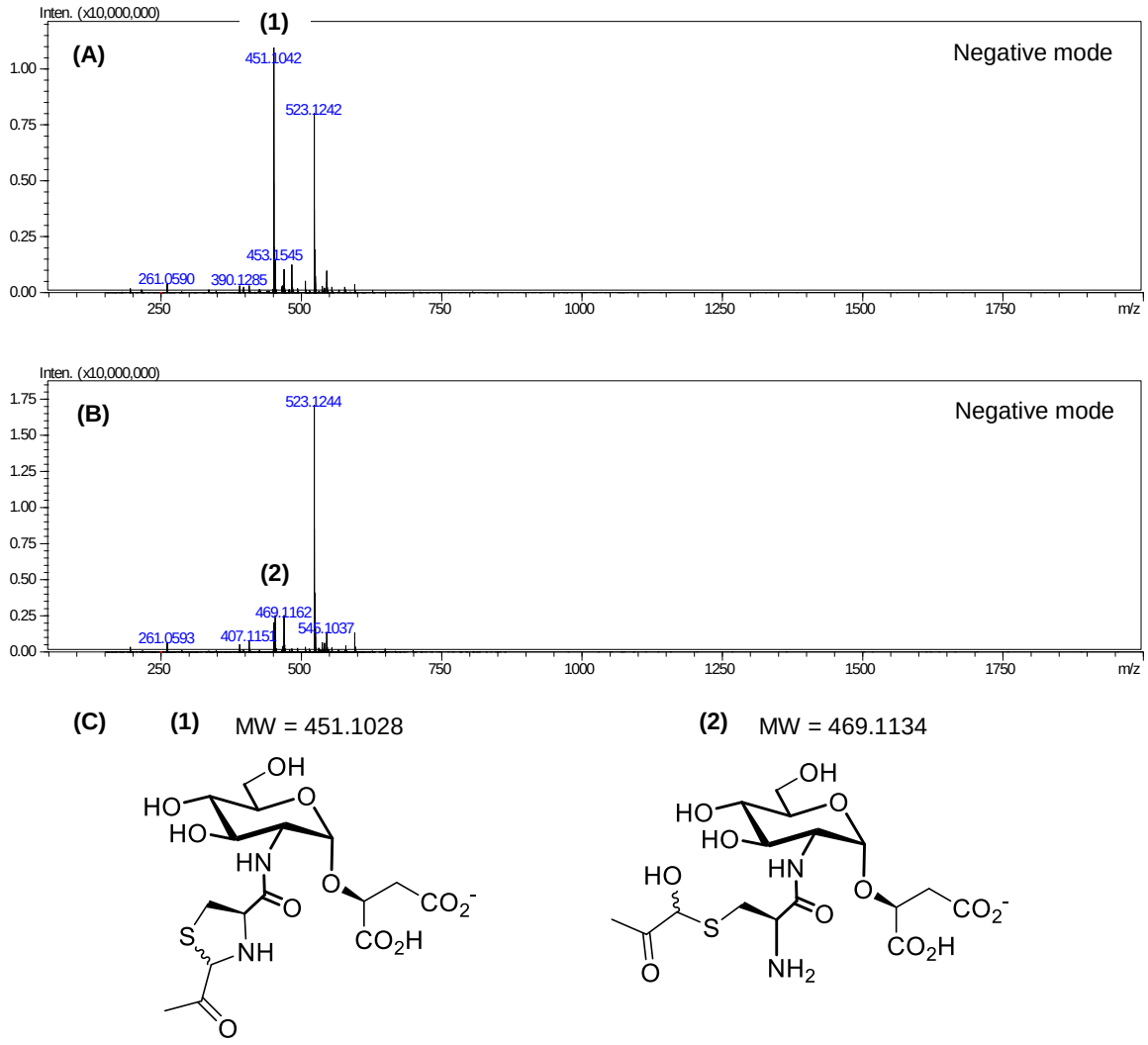

Figure 4.3. Full spectrum of the reaction between MG and BSH in A) negative-mode after 5 hours reaction time B) negative-mode after 13 hours reaction time C) Chemical structure of 1) thiazolidine derivative 2) HTA.

The mass of the BS-MG HTA, M=$C_{16}H_{26}N_2O_{12}S$, is 470.1206. The base peak observed in the spectrum after 5 hours is likely to be the negative ion of the thiazolidine derivative (**1**) [M-H] with an expected mass of 451.1028 and a observed mass of 451.1042, when M = $C_{16}H_{24}N_2O_{11}S$. After 13 hours, the mass of the BS-MG HTA adduct (**2**) was observed at 469.1162 m/z in negative mode [M-H] (figure 4.3). In the positive-mode spectrum, no mass for either HTA or thiazolidine was found.

4.2.3. DHAP and Cys

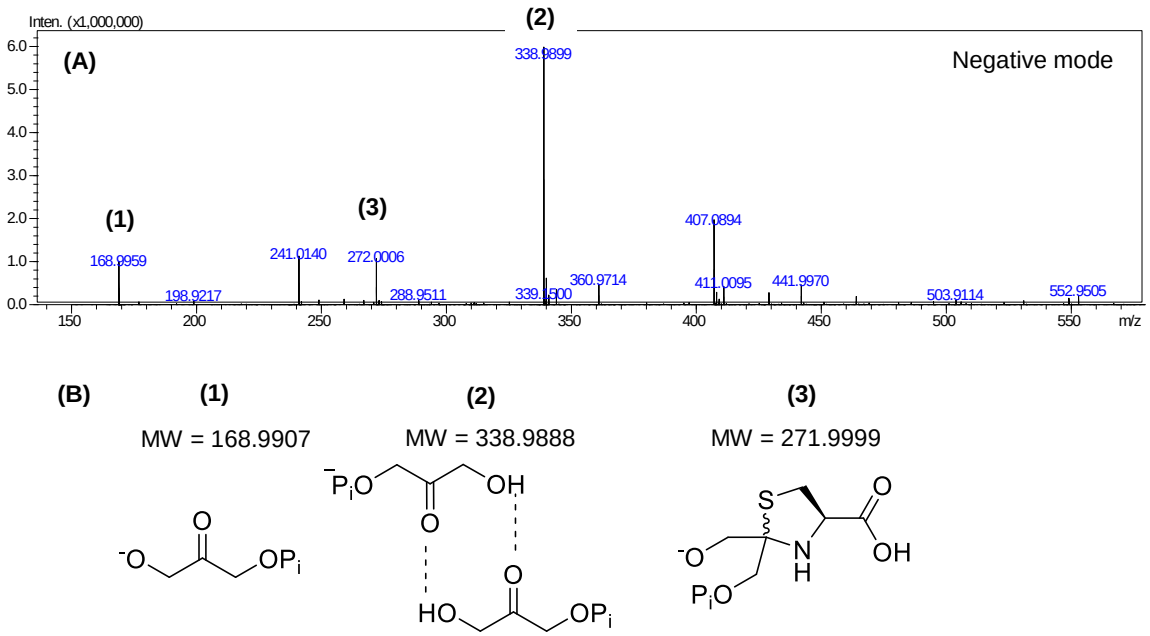

Figure 4.4. Spectrum in negative-mode of the reaction between DHAP and Cys, in A) region between 150-600 m/z. B) Chemical structure of DHAP where M= $C_3H_7O_6P$ is represented as, 1) [M-H] 2) [2M-H] and 3) thiazolidine derivative [M-H] where M = $C_6H_{12}NO_7PS$.

The mass of the Cys-DHAP HTA adduct, M=$C_6H_{14}NO_8PS$, is 291.0178. For DHAP (**1**) [M-H], the expected mass is 168.9907 and the found mass was 168.9959, when M= $C_3H_7O_6P$. The dimeric cluster ion for DHAP (**2**), [2M-H], was detected at 338.9899 m/z. The Cys-DHAP HTA adduct was not detected, however, a mass consistent with the thiazolidine derivative (**3**) was detected at 272.0006 m/z, when M = $C_6H_{12}NO_7PS$ and the theoretical mass is 271.9999 (figure 4.4). There was no indication of HTA/thiazolidine derivative in the positive-mode spectrum.

4.2.4. DHAP and BSH

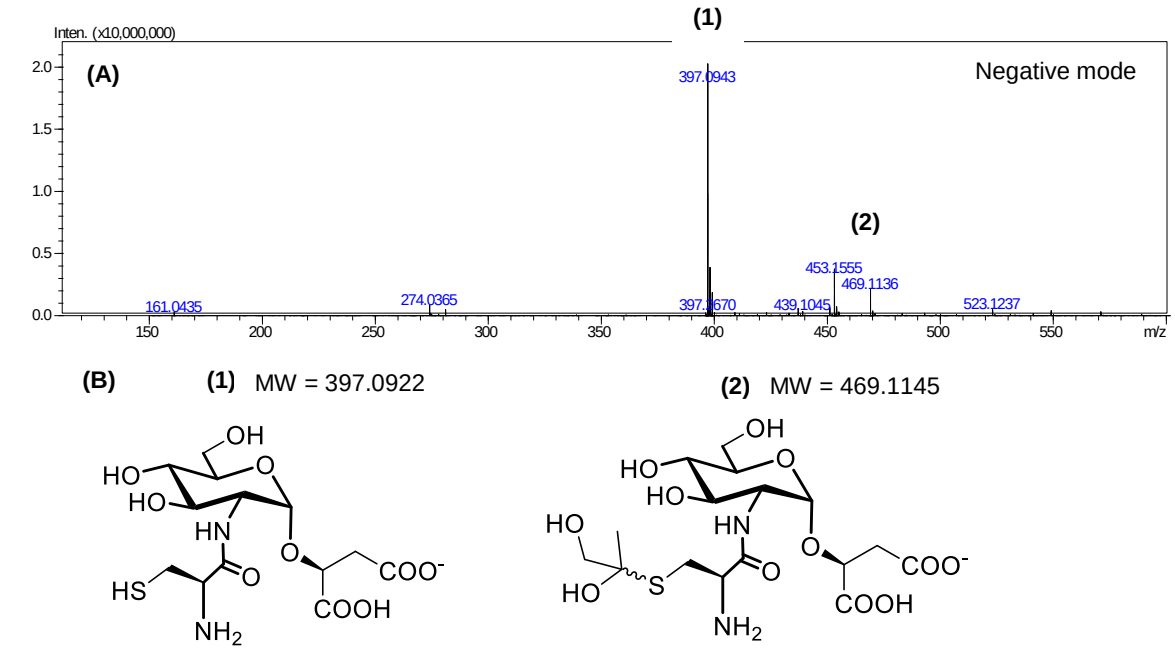

Figure 4.5. Spectrum in negative-mode of the reaction between DHAP and BSH, in A) region between 100-600 m/z. B) Chemical structure of 1) BSH [M-H] where M = $C_{13}H_{22}N_2O_{10}S$ 2) Dephosphorylated HTA [M-H] where M = $C_{16}H_{28}N_2O_{12}S$.

The mass of BS-DHAP HTA, M=$C_{16}H_{29}N_2O_{16}PS$, is 568.0975. The base peak on the negative-mode spectrum is BSH (**1**) [M-H], with an expected mass of 397.0922, which was detected at 397.0943 m/z, when M = $C_{13}H_{22}N_2O_{10}S$. Neither the HTA or the thiazolidine derivatives are detected. However, a dephosphorylated version of the HTA (**2**) [M-H] is shown indicated by a loss in H_3PO_4 which has an expected mass of 469.1145 and a mass of 469.1136 was detected, when M = $C_{16}H_{28}N_2O_{12}S$ (figure 4.5). The positive-mode spectrum only detected masses of the protonated BSH and its sodium adduct.

4.2.5. GA3P and Cys

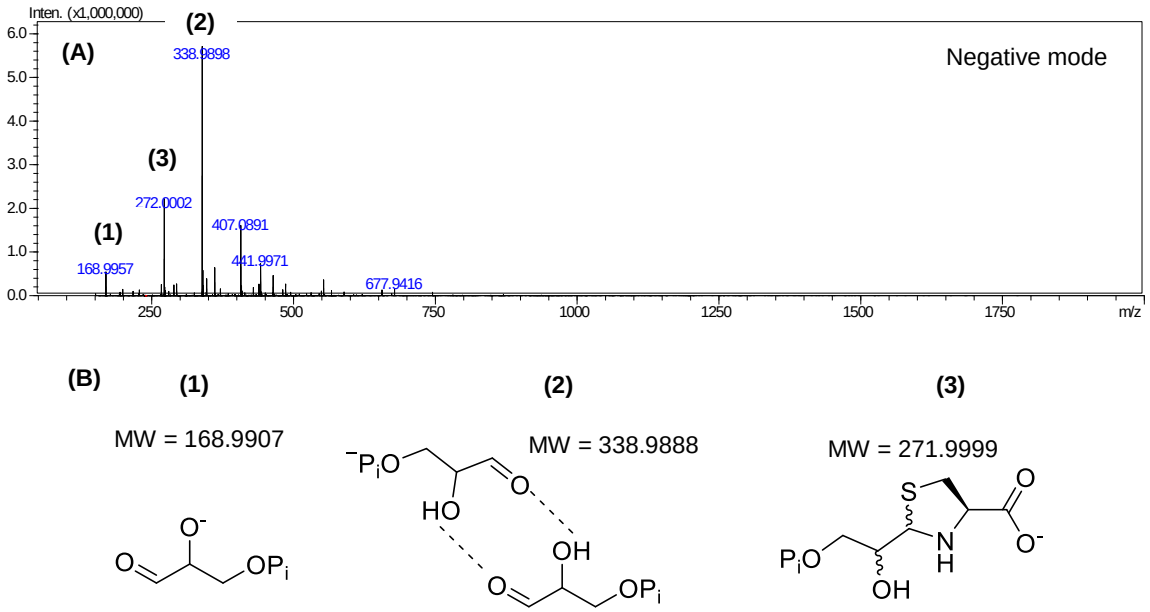

Figure 4.6. A) Spectrum in negative-mode of the reaction between GA3P and Cys after 13 hours. B) Chemical structure of 1) GA3P [M-H] where M=$C_3H_7O_6P$ 2) Cluster ion of GA3P [2M-H] 3) Thiazolidine derivative [M-H] where M= $C_6H_{12}NO_7PS$.

The exact mass of Cys-GA3P HTA, M=$C_6H_{14}NO_8PS$, is 291.0178. Since GA3P is an isomer of DHAP, similar peaks are observed for both. For GA3P (**1**) [M-H], the expected mass is 168.9907 and the mass detected was 168.9957, when M=$C_3H_7O_6P$. The base peak represents the cluster ion of GA3P (**2**) [2M-H] with an observed mass of 338.9898 . The HTA is not detected. However, the thiazolidine derivative (**3**) is detected [M-H] with a theoretical mass of 271.9999 and an observed mass of 272.0002, when M= $C_6H_{12}NO_7PS$ (figure 4.6). No masses of significance were shown on the positive-mode spectrum.

4.2.6. GA3P and BSH

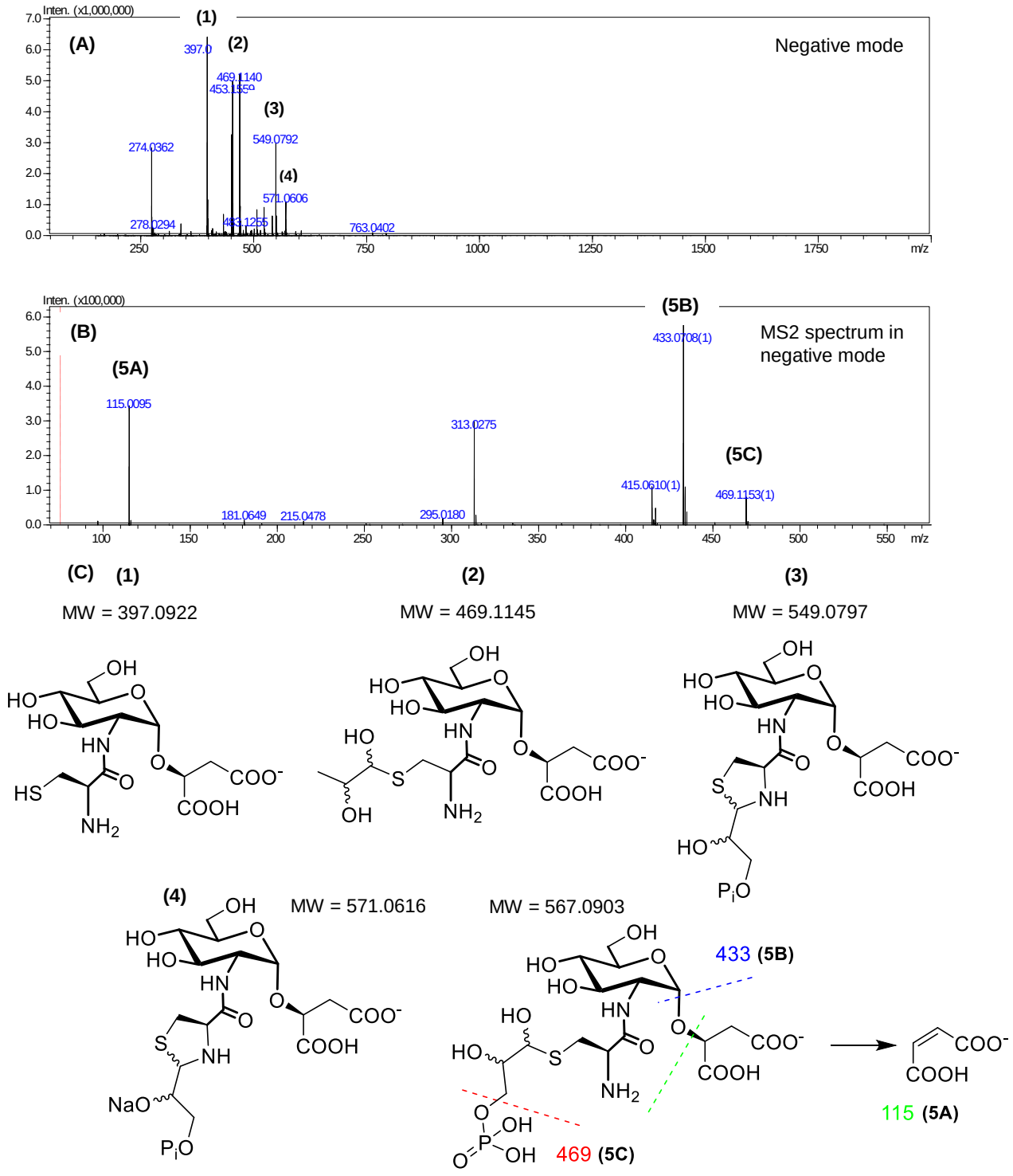

Figure 4.7. A) Spectrum in negative-mode of the reaction between GA3P and BSH after 13 hours B) MS2 spectrum. C) Chemical structure of 1) BSH [M-H] where M = $C_{13}H_{22}N_2O_{10}S$ 2) Dephosphorylated HTA [M-H] where M = $C_{16}H_{26}N_2O_{12}S$ 3) Thiazolidine derivative [M-H] where M = $C_{16}H_{27}N_2O_{15}PS$ 4) Thiazolidine derivative with associated sodium [M-2H+Na]. 5) Interpretation of the fragments found on the MS2 spectrum providing evidence of BS-GA3P HTA existence.

Analysis of the mass spectrum indicates a base peak for bacillithiol (**1**) [M-H] with an observed mass of 397.0941, when M = $C_{13}H_{22}N_2O_{10}S$. Similar to the BS-DHAP negative-mode spectrum, a dephosphorylated version of BS-GA3P (**2**) is found with an expected mass of 469.1145 and a found mass of 469.1140. The BS-GA3P thiazolidine derivative (**3**) [M-H] is observed with an expected mass of 549.0797 and a mass of 549.0792, when M = $C_{16}H_{27}N_2O_{15}PS$. Furthermore, a sodium adduct of the thiazolidine derivative (**4**) [M-2H+Na], is detected at 571.0606 m/z. A doubly charged ion of the thiazolidine derivative [M-2H] is also detected with an observed mass of 274.0362. The MS2 274 data shows more evidence of BS-GA3P HTA existence. It appears that fragments of the BS-GA3P HTA (**5**) are shown (figure 4.7), the fumarate which is formed from β-elimination of the malate group from the BSH scaffold is detected with a mass of 115.0095 (**5A**). The glucosamine, Cys and GA3P fragment (**5B**) was detected with a mass of 433.0706, and the dephosphorylated GA3P (**5C**) was detected with a mass of 469.1153.

4.2.7. *In vitro* mass spectrometric evidence of HTA or thiazolidine existence?

The mass spectrometry data has shown strong evidence for the formation of HTAs and thiazolidine derivatives forming from the reaction between thiol and glycolytic metabolites. In each instance, there was evidence for either the thiazolidine derivative or the HTA adducts, and in some cases, the sodium adduct was detected. However, HTAs involving Cys were not detected in addition to the BS-DHAP HTA, where only a dephosphorylated HTA was identified (table 4.1).

The masses mainly detected represent the thiazolidine derivative as opposed to the HTA. This favourability of thiazolidine detection may be possibly due to the formation *in situ* as an artefact of the mass spectrometer. In addition, the thiazolidines may fly better than the HTAs, allowing only trace amounts to be detected. It is also possible that the HTAs may not be detected due to poor stability and therefore degrading from the ionisation conditions of the spectrometer.

Table 4.1. Summary of HTA/thiazolidine determination in all 6 reactions of thiol with metabolite.

	Cys		**BSH**	
	HTA	thiazolidine	HTA	thiazolidine
MG	X	✓[1]	✓	✓
DHAP	X	✓	✓[2]	X
GA3P	X	✓	✓[3]	✓

[1]Associated sodium

[2]Dephosphorylated – loss of H_3PO_4

[3]MS2 data

4.3. Characterisation by Nuclear Magnetic Resonance (NMR) spectroscopy

MG has shown to be the strongest electrophile relative to all glycolytic metabolites studied in this research. In addition, the *in vivo* thiol analysis has shown a reaction between intracellular BSH consumption when incubated with 1 mM MG. Therefore, NMR analysis focused on the HTA formation and/or thiazolidine formation of MG-SR. The MG-SR exists as two diastereomers (table 4.2), which may form additional signals and complicate the NMR spectra. For this reason, preliminary investigation was first carried out on the HTA formation between acetone and Cys, which does not result in the formation of diastereomers.

Table 4.2. Two diastereomers formed from metabolite reacting with thiol.

	S,R-diastereomer	*R,R*-diastereomer
MG-SR	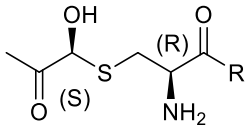	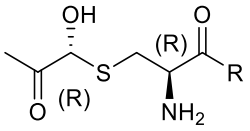

4.3.1. Acetone and Cys

A 2:1 ratio of acetone and Cys were incubated for 3 hours. As a result, the ^{13}C spectrum shows the emergence of three new peaks at δ 39.1, 66.4, 177.5, representing the CH_2 (**3'**), CH (**2'**) and C=O (**1'**) of the Cys moiety of the HTA, respectively (figure 4.8). The emergence of each peak is at a higher chemical shift relative to the free Cys, which is possibly due to electron withdrawing effects of the hydroxyl group on the HTA causing deshielding. The emergence of a peak at δ 75.1, confirmed by HMBC and DEPT experiment, was assigned to the quaternary carbon (**5'**) of the HTA.

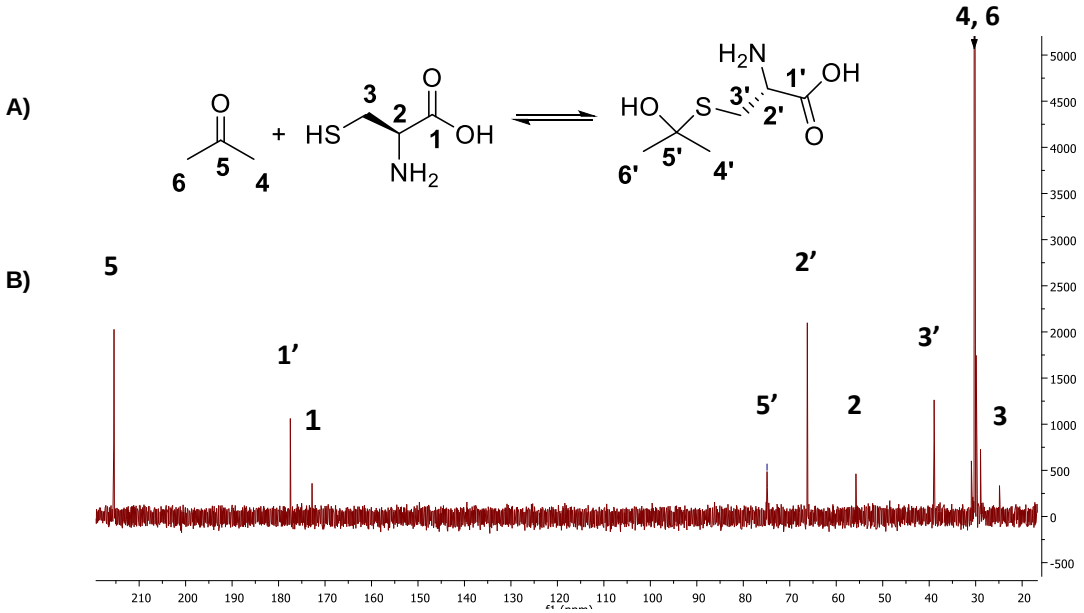

Figure 4.8. Acetone (200 mM) reacting with Cys (100 mM) in sodium phosphate buffer (200 mM, pD 8.1). A) Reaction scheme B) ^{13}C spectrum.

To differentiate between HTA or thiazolidine, periodic ^{1}H NMR analysis was carried out at 20-minute intervals after incubating acetone with Cys. Signals corresponding to HTA emerge after 20 minutes (figure 4.9 B2), with a 1:1 ratio of Cys to HTA forming after 80 minutes (figure 4.10). After 3 hours, two additional singlets form at δ 1.39 and δ 1.57 which correspond to faint carbon peaks at δ 30.6 and δ 28.5, respectively, in addition to a series of signals at δ 3.09-3.32 (figure 4.9 B4). These signals are speculated to be the formation of the thiazolidine derivative. Based on the integration, after 20 hours, the speculated thiazolidine was found in 1.3 mM whilst the HTA exist in 44.2 mM.

Furthermore, the HMBC shows coupling of the quaternary carbon (**5'**) to protons on the CH_3 (**4', 6'**) and CH_2 (**3'**) but not the CH (**2'**) (figure 4.11). In the thiazolidine derivative, the proton on the CH (**2''**) remains in close proximity within 3 bonds of the quaternary carbon whereas in the HTA, the proton is 4 bonds away from the quaternary carbon. Therefore, no coupling between the CH (**2'**) and the quaternary carbon is suggestive of HTA (figure 4.11).

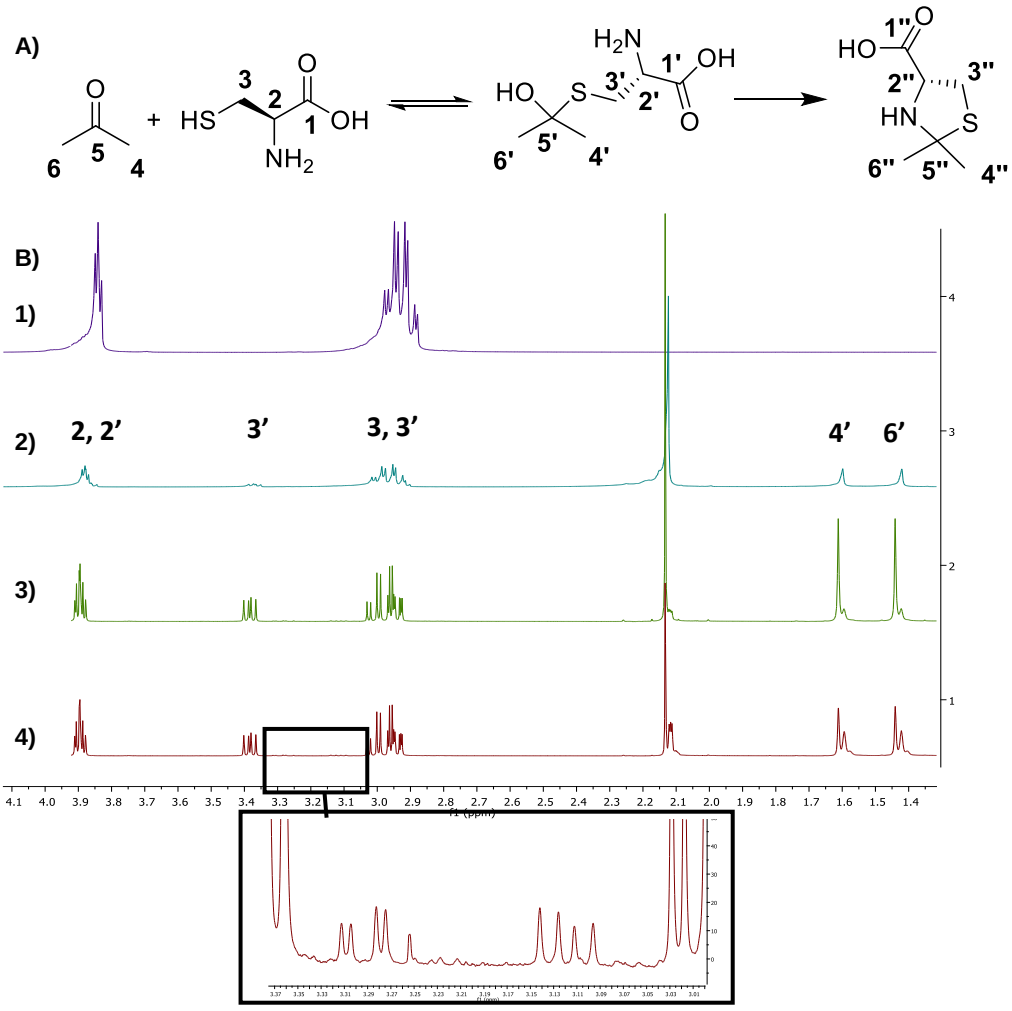

Figure 4.9. Acetone (200 mM) reacting with Cys (100 mM) in sodium phosphate buffer (200 mM, pD 8.1). A) Reaction scheme B) Periodic ^{1}H NMR spectra at 1) Cys control 2) 20 mins 3) 3 hours and 4) 20 hours.

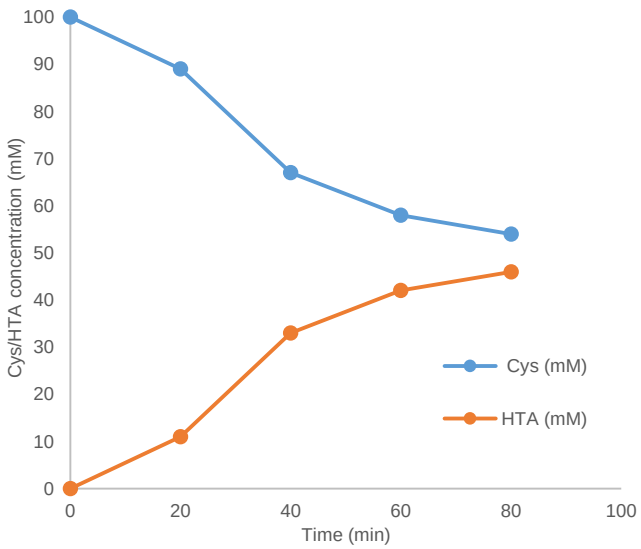

Figure 4.10 The consumption of Cys and the formation of HTA based on the relative ratio of Cys:HTA.

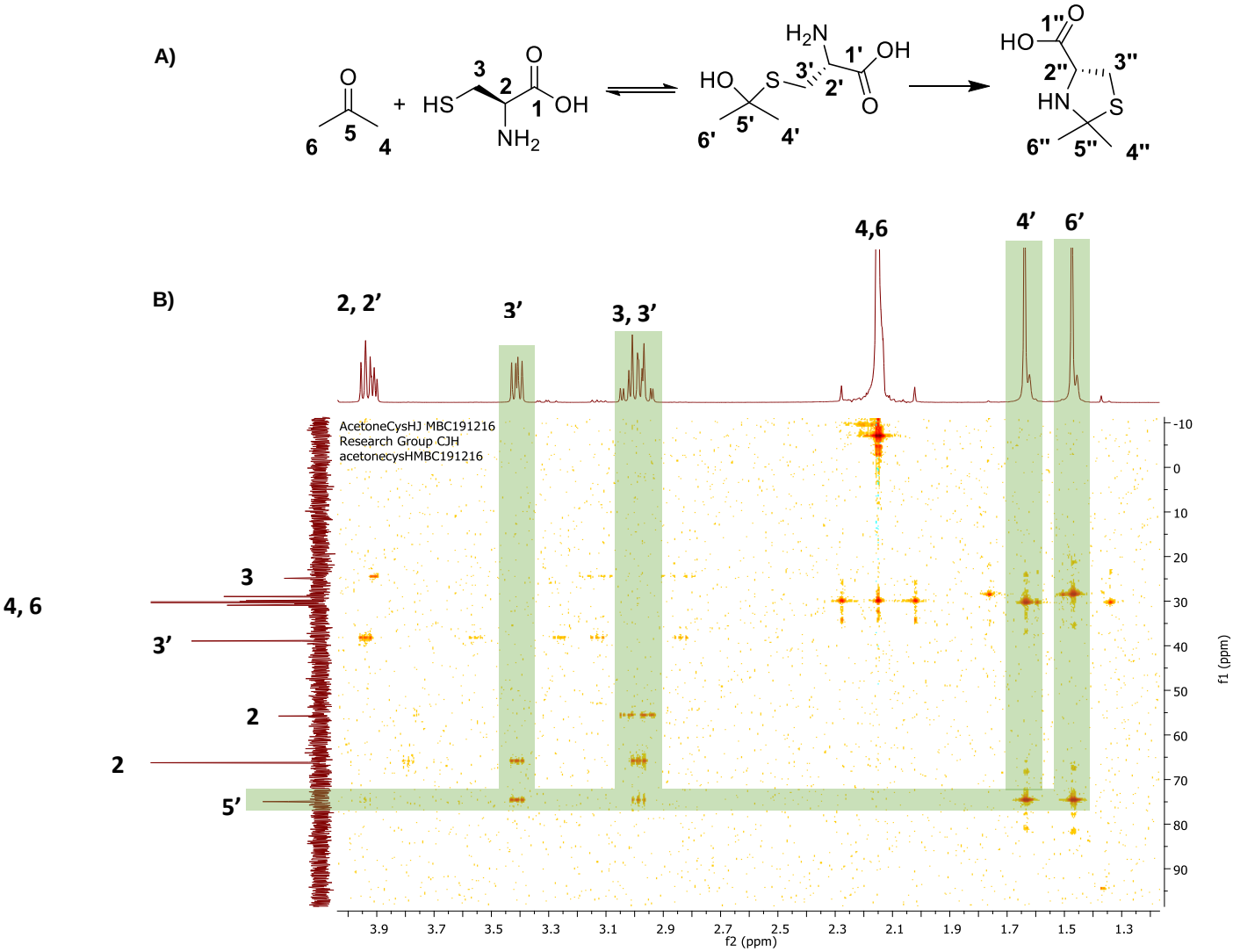

Figure 4.11. Acetone (200 mM) reacting with Cys (100 mM) in sodium phosphate buffer (200 mM, pD 8.1). A) Reaction scheme. B) HMBC spectrum after 3 hours.

4.3.2. MG and Cys

The formation of HTA from GSH and MG is a well-studied reaction as a result of the extensive research on the thiol-dependent glyoxalase detoxification pathway. NMR evidence of HTA formation has been proven in reactions between MG and GSH[148] [110], Cys[110] and CysNAc[110]. However, there has been no studies of the BS-MG HTA.

Initial studies focused on HTA formation between Cys and MG before determining the BS-MG HTA, carried out by Dr Sunil Sharma. The NMR spectra of an equimolar mixture of Cys and MG showed signals corresponding to free Cys and the two Cys-MG HTA diastereomers after 30 minutes. The CH_2 (**3**) for free Cys is found at δ 26.4 on the ^{13}C spectrum. In the HTA form, the CH_2 (**3'**) for both diastereomers are represented downfield at δ 37.0 and δ 37.3, representing a similar relative chemical shift to the CH_2 of the acetone-Cys HTA. The HSQC associates the CH_2 (**3'**) of the HTA with four different environments on the ^{1}H spectrum because of the two HTA diastereomers (figure 4.12). In relation to diastereomer (**A**), the proton signals at δ 2.62 and δ 3.23 represent the CH_2 (**3'**) which couple to a signal at δ 37.3 (figure 4.12). The associated protons for the CH (**2'**) are found at δ 3.70 (figure 4.13). Regarding diastereomer (**B**), the signals at δ 2.88 and δ 3.11 both couple to a carbon at δ 37.0, representing the CH_2 (**3'**) (figure 4.12). In addition, the associated protons are at δ 3.89 (figure 4.13).

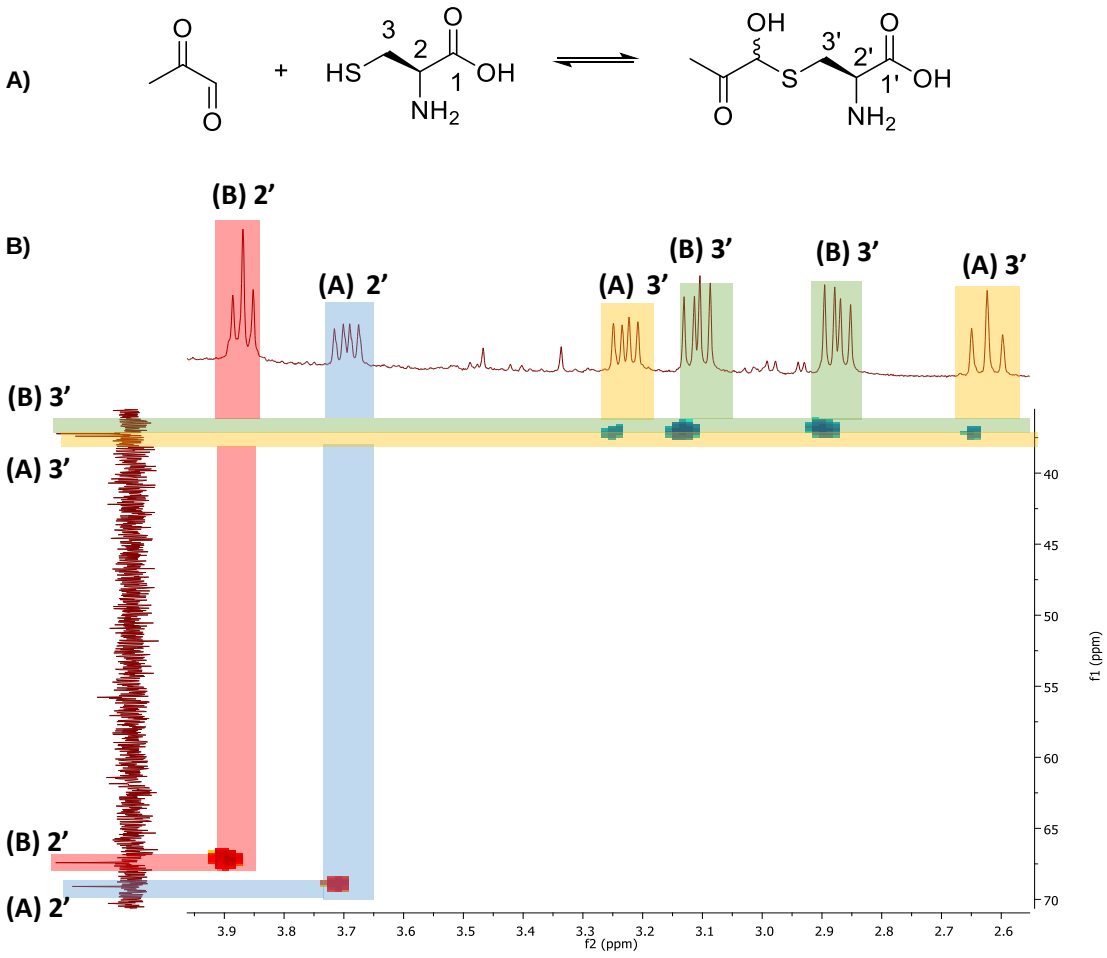

Figure 4.12. MG (10 mM) reacting with Cys (10 mM) in sodium phosphate buffer (50 mM, pD 8.1) A) Reaction scheme. B) HSQC spectrum showing the CH (2’) and CH_2 (3’) of the Cys moiety of the two diastereomers (A) and (B).

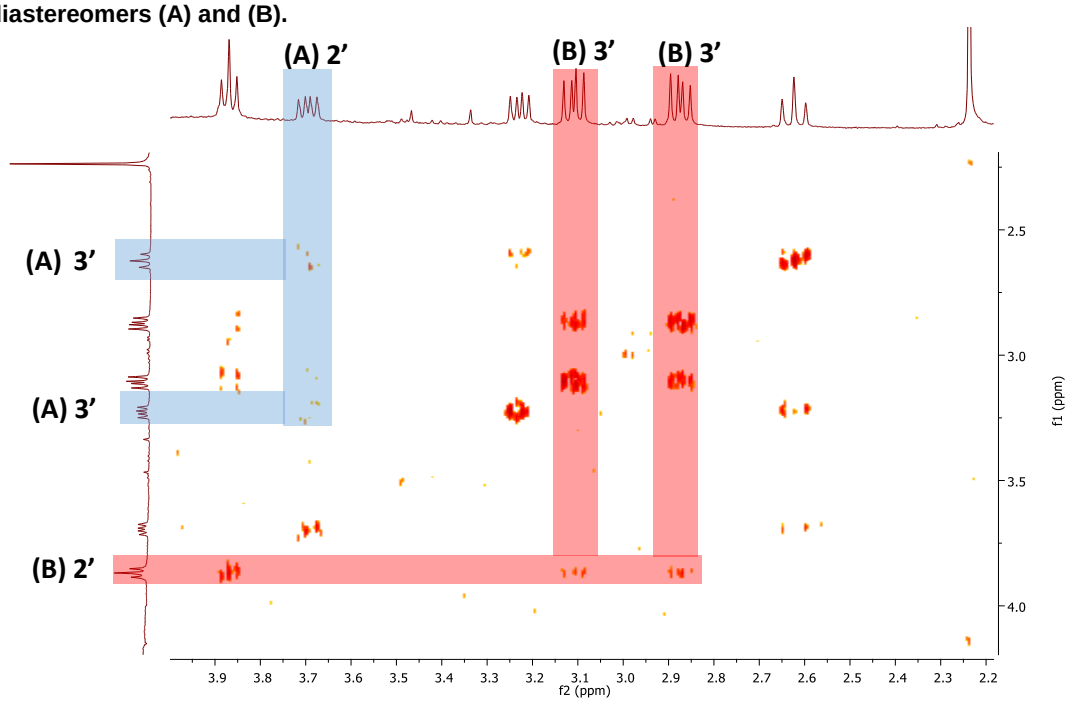

Figure 4.13. COSY spectrum of MG (10 mM) reacting with Cys (10 mM) in sodium phosphate buffer (50 mM, pD 8.1), representing coupling of CH_2 (3’) to CH (2’) of the Cys moiety of the two diastereomers (A) and (B).

4.3.3. MG and BSH

The literature values of free BSH were used to assign the CH_2 (**3**), the CH (**2**) and the C=O (**1**) of the Cys moiety.[8] After 30 minutes of BSH reacting with MG, the NMR spectra showed signals corresponding to free BSH and only one of the BS-MG HTA diastereomers. The signals at δ 37.6 and δ 61.4 in the ^{13}C spectrum are suggestive of the CH_2 (**3'**) and the CH (**2'**) for the HTA, respectively. These also resemble similar chemical shifts to the signals of the control adduct, Cys-MG HTA. The corresponding protons on the HSQC show CH_2 (**3'**) and the CH (**2'**) of the HTA at δ 2.69 and δ 4.06, respectively, (figure 4.14). However, resonances for the CH_2 (**3'**) of the HTA only shows one of the diastereomers. This does not parallel with Cys-MG HTA, where signals are observed in four chemical environments. This may be explained by the detection limits of the ^{13}C spectrum. Alternatively, the COSY spectrum couples the protons at δ 4.06 with δ 2.98 which may represent the CH_2 (**3'**) of the other diastereomer (figure 4.15).

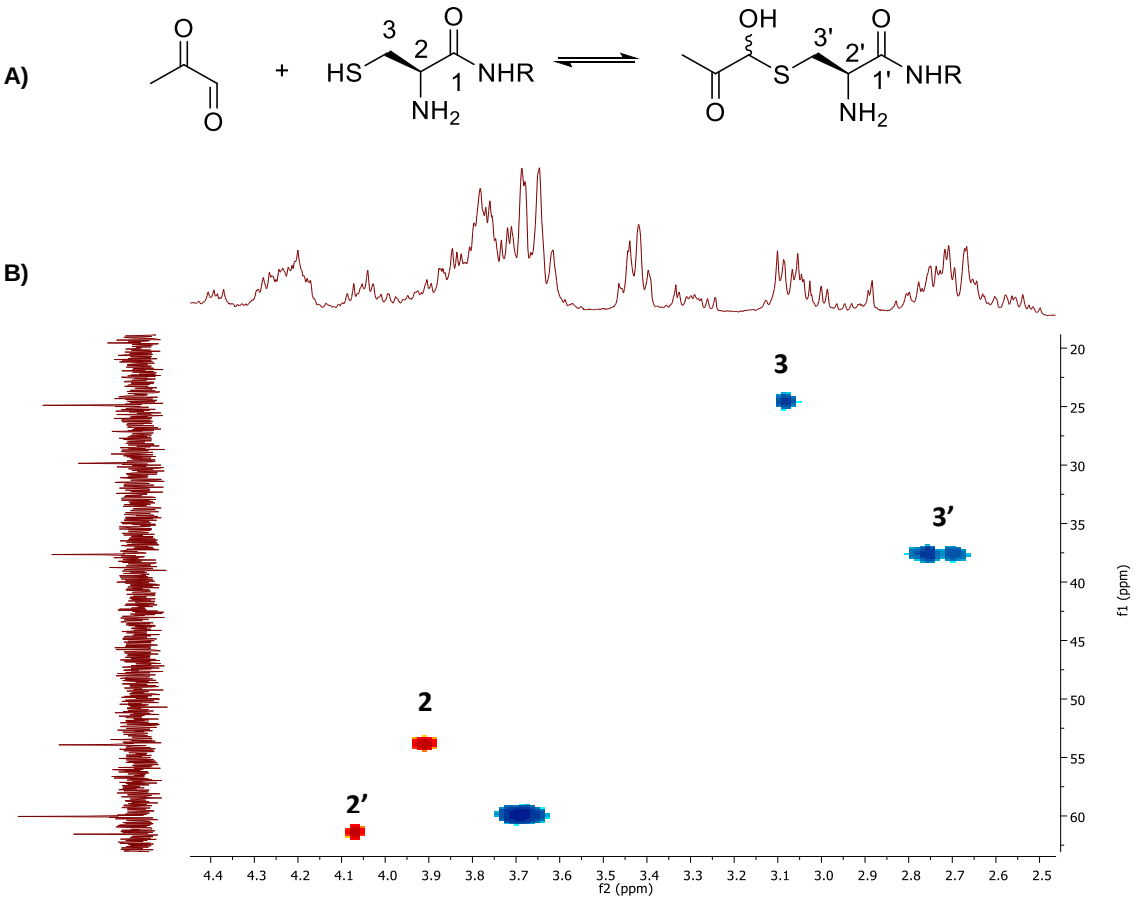

Figure 4.14. MG (10 mM) reacting with BSH (10 mM) in sodium phosphate buffer (50 mM, pD 8.1). A) Reaction scheme. B) The HSQC showing the CH_2 (3/3') and CH (2/2') of the Cys moiety on BSH and BS-MG HTA.

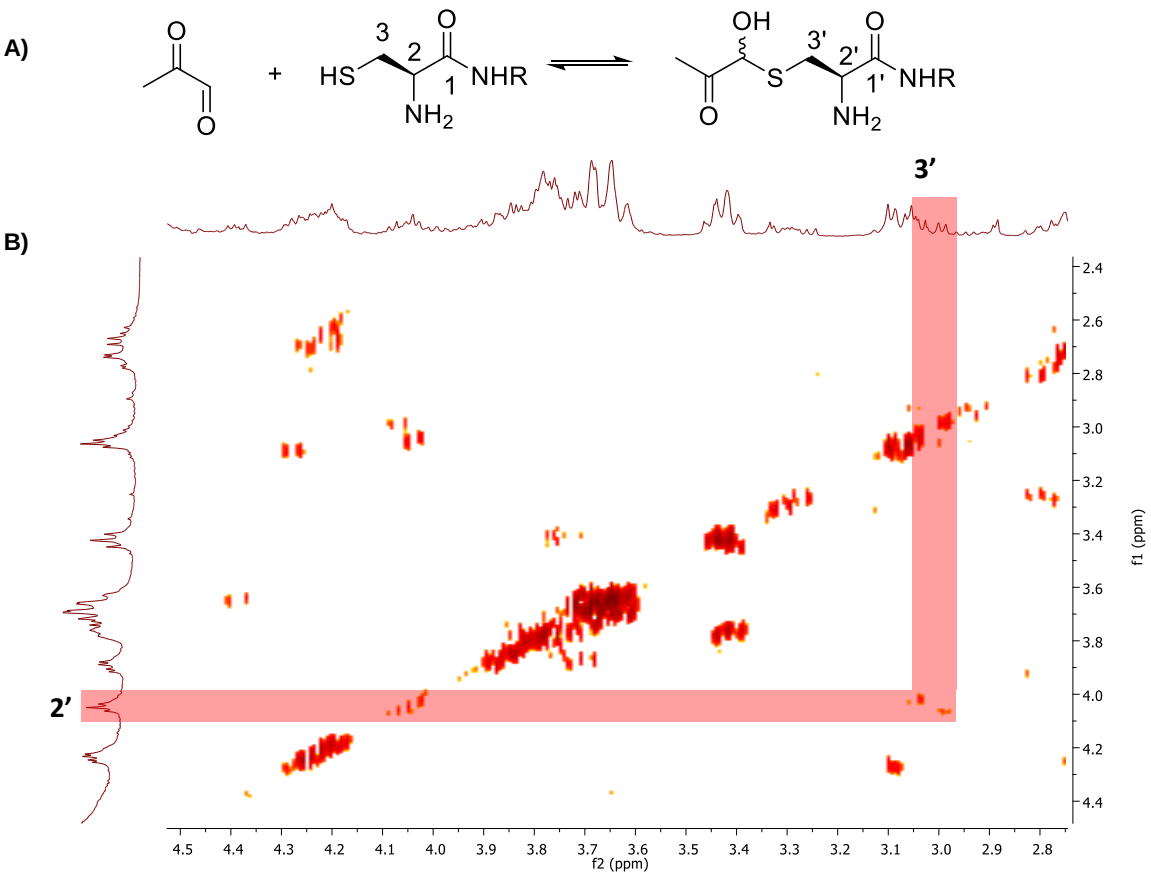

Figure 4.15. MG (10 mM) reacting with BSH (10 mM) in sodium phosphate buffer (50 mM, pD 8.1). A) Reaction scheme. B) COSY spectrum representing coupling of CH_2 (3') to CH (2') of the Cys moiety of only one diastereomer.

4.4. Whole cell NMR

Whole cell NMR was then carried out to provide direct evidence of BSH and HTA existing in the cell. This idea was prompted by recent studies of whole cell NMR which had been carried out on mammalian cells incubated with ^{13}C-labelled GSH (GSH-(glycine-$^{13}C_2$,^{15}N) to measure GSH and its disulfide in the cell.[149] On parallel lines, it was predicted that incubating *B. subtilis* with media supplemented with ^{13}C-Cys, would be taken up into the cell and biosynthesise into BSH. Cys, however, is not specific for the biosynthesis of BSH and there are other compounds, such as cystathionine, homocysteine, S-adenosylmethanione, CysNAc, CoA, acetyl-CoA, and L-methionine, which may be detected.[150] Nonetheless, BSH remains in high concentrations in late-exponential phase of *B. subtilis* and therefore it is anticipated that there will be detectable amounts of BSH and potential HTA in the cell.

4.4.1. *In vivo* formation of BSH

The experiments were carried out by Francesc Puig. *B. subtilis* WT and *glxI* mutant cell cultures were inoculated with ^{13}C-labelled Cys (1 mM) in the lag-phase. Cys rapidly oxidised to cystine in the culture,[151] which was confirmed by Ellmans titration after 2 hours, showing 50% oxidation at 37 °C, 200 RPM. However, this oxidation is favourable as *B. subtilis* cells can only uptake cystine.[151] At time-points of growth, the cultures were centrifuged and cell pellets were analysed under NMR. BSH was detected at ^{1}H = δ 3.03, 3.10 and ^{13}C = δ 28.2 (figure 4.16). The *in vitro* analysis confirms this, which shows BSH at ^{1}H = δ 3.05, ^{13}C = δ 28.1, representing the CH_2 (**3**) of BSH. There was no observable BSSB, which is explained by the low concentrations found in the cell relative to BSH, with a redox ratio ranging from 100:1 to 400:1, BSH:BSSB.[20] In addition, there is no observable Cys, which is possibly explained by being approximately 15-fold less concentrated than BSH at the late-exponential phase, and therefore below the detection limits of NMR.

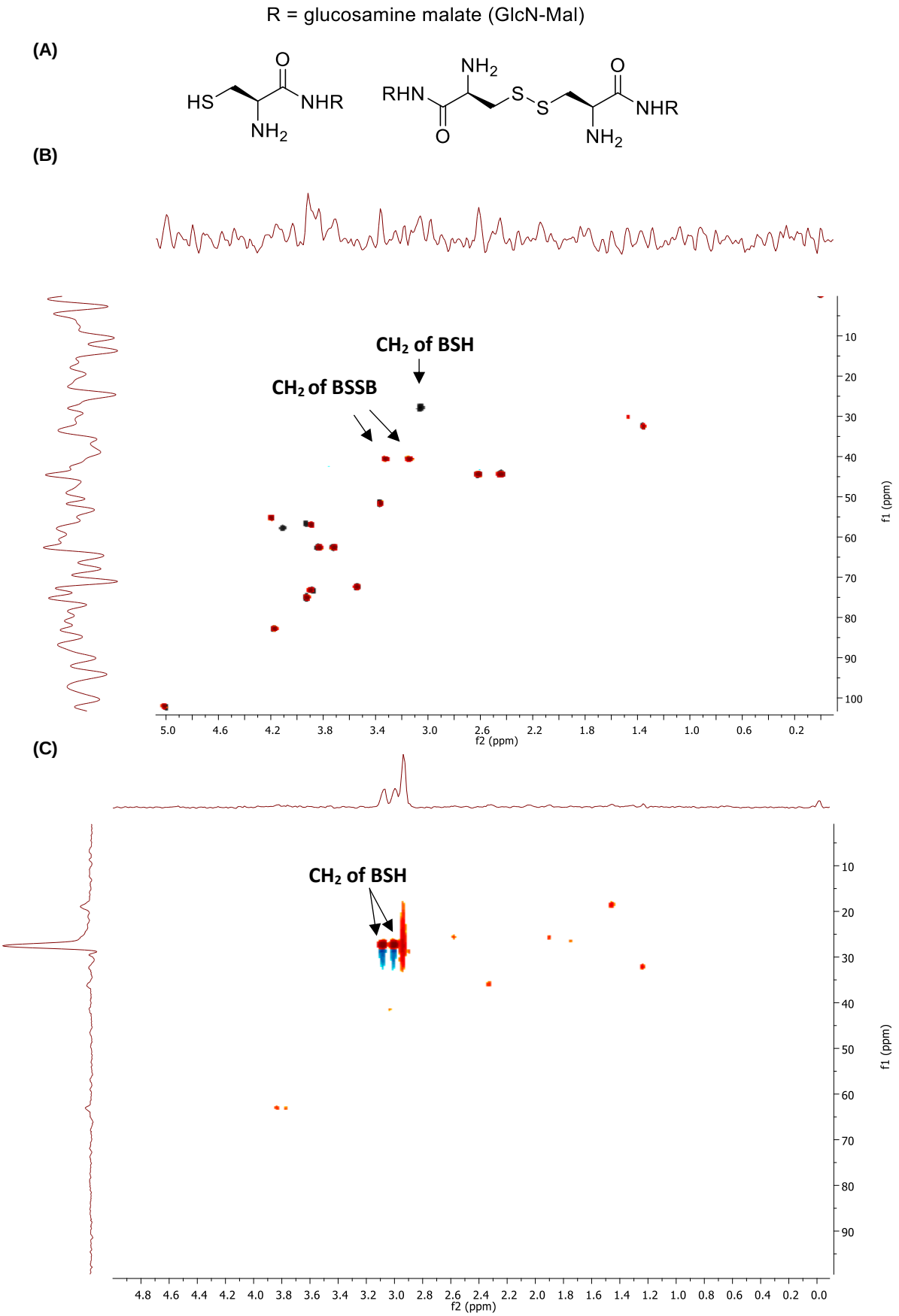

Figure 4.16. A) Chemical structures of BSH and BSSB. B) *In vitro* HSQC NMR, representing CH_2 (3) of BSH (black) and BSSB (red). C) *In vivo* HSQC NMR, representing the CH_2 of BSH.

4.4.2. *In vivo* formation of BS-MG HTA

In a separate experiment, the WT and *glxI* mutant cellular cultures were individually inoculated with 1 mM of MG for 30 minutes, the cell pellets were centrifuged and analysed under NMR. In relation to the WT strain, the signals representing the CH_2 (**3**) are at ^{1}H = δ 3.015, 3.095 and ^{13}C = δ 27.7, representing BSH. Upon addition of MG, the resonance remains, suggesting no reaction of BSH. This does not replicate the observations from the *in vivo* studies (chapter 2.5.2). A plausible reason for this is the time consuming nature of the NMR analysis allowed sufficient time for the BSH to react with MG to form HTA which then subsequently follow through the glyoxalase pathway and hence recover.

The *glxI* mutant prevents BSH from following through the glyoxalase pathway and therefore it is only in equilibrium with HTA. As a result, there was evidence of HTA formation. Firstly, the weak resonance of the CH_2 (**3**) of BSH indicates that it has reacted with MG (figure 4.17). In addition, four weak signals emerge, at ^{1}H = δ 2.72 and ^{13}C = δ 39.6, ^{1}H = δ 3.32 and ^{13}C = δ 40.0, ^{1}H = δ 3.21 and ^{13}C = δ 40.2 and ^{1}H = δ 2.96 and ^{13}C = δ 40.0. Whilst the *in vitro* NMR of BS-MG only identified one diastereomer, the signals emerging herein closely resemble the *in vitro* Cys-MG HTA (chapter 4.3.2 - figure 4.12). Since Cys is speculated to be below the detection limits of this analysis, it is plausible it could be BS-MG. However, further investigation would require a repeat of the *in vitro* BS-MG HTA NMR analysis to confirm these observations.

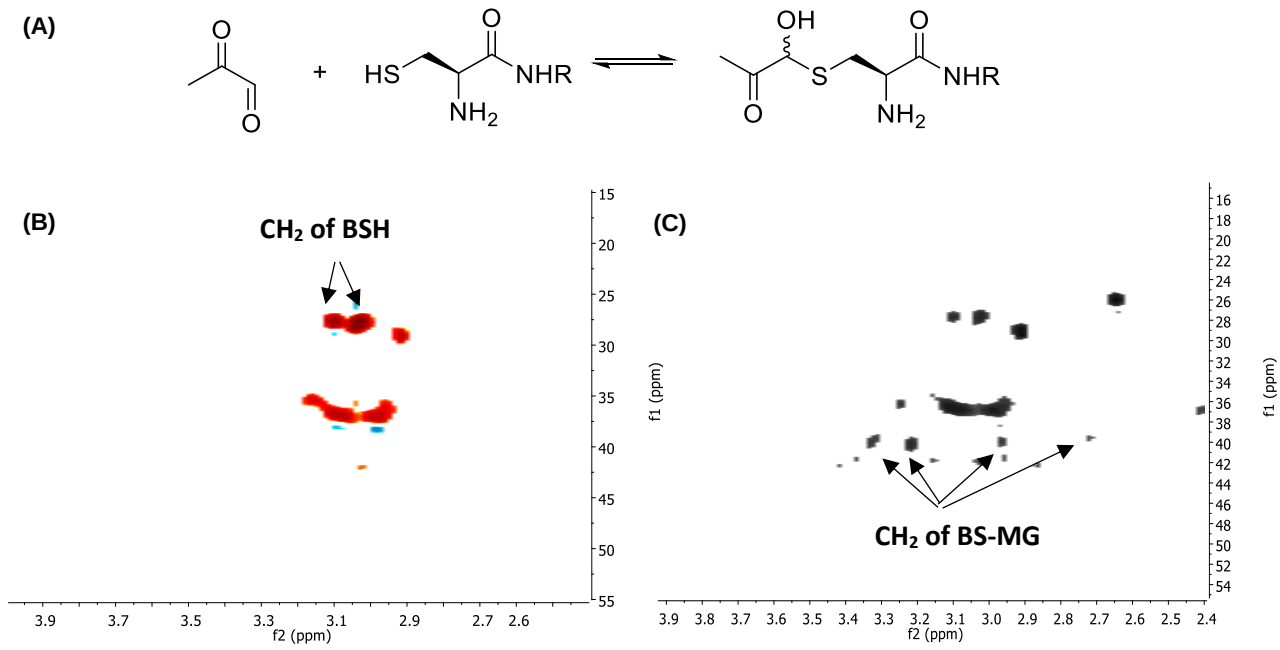

Figure 4.17. Whole cell HSQC NMR of ^{13}C-labelled Cys incubated *GlxI* mutant strain. A) Reaction scheme of MG and BSH reaction. B) The CH_2 of BSH with no addition of MG. C) Resonance of speculated CH_2 of BS-MG after the addition of 1 mM MG.

4.5. Summary

The mass spectrometry data analysis shows the favoured formation of thiazolidines as opposed to the HTA adduct. This contrasts from the *in vitro* NMR data which show HTA formation between acetone and Cys with only traces of thiazolidine being detectable. In addition, the similar relative chemical shifts of the CH and the CH_2 group of Cys-acetone, Cys-MG and BS-MG are suggestive that an HTA adduct is formed. The whole cell NMR provided *in vivo* evidence of HTA formation between BSH and MG. Whilst the WT strain showed no effect of BSH from MG, the *glxI* mutant strain showed some depletion of BSH and additional weak resonance, but the signals observed paralleled with the *in vitro* NMR spectra indicating possibly HTA formation.

The limitations of the NMR analysis were the weak signals observed for all the *in vitro* MG-SB spectra, only detecting one of the diastereomers. Therefore, future work should implement a higher BSH concentration which would produce a more accurate comparable measure for the whole cell NMR. There are many other metabolites that have shown to react with BSH, including DHAP which is shown to possess a high theoretical DHAP-SB concentration, however, due to time constraints were not investigated. Therefore, further investigation would involve determining the *in vivo* NMR existence of these glycolytic metabolites and BSH.

5. Conclusion

In summary, this research has shown clear evidence of the involvement of BSH in the thiol-dependent glyoxalase detoxification of MG. The *in vitro* kinetics have shown a similar rate of Cys and BSH thiolate reactivity with MG, producing comparable pH-independent rate constants of 9.46 and 7.55 s^{-1}, respectively. However, the thiol pK_a of BSH is lower than Cys which indicates that it is more deprotonated at physiological conditions, pH 7.7, in *B. subtilis,* resulting in a faster rate of reaction with MG. Moreover, the intracellular concentration of BSH is 15-fold higher than Cys at late-exponential phase*,* further suggesting the preferential reactivity with BSH.

One limitation of the *in vitro* kinetic studies was that they could not be determined at physiological cell conditions due to a full consumption of thiol occurring within seconds. Therefore, for further investigation, alternative techniques using stopped-flow assays for determination of the immediate kinetics could be implemented. This would provide a rate constant at pH 7.7 which is necessary for the determination of the equilibrium constant. In addition, another key aspect of the kinetic analysis is the potential reactivity of the amino group on Cys and BSH, which may react with MG to form a Schiff base. Therefore, further investigation using ninhydrin reagent[152] in determining the reactivity of the amino group is essential for the full analysis of BSH reactivity.

The *in vivo* studies, confirmed the kinetic observations which showed BSH levels to rapidly deplete upon exposure to 1 mM MG amongst *B. subtilis* cells. The BSH levels then gradually recover in the WT and *glxI* mutant, however BSH remains depleted in the *glxII* mutant. In parallel, there is extracellular consumption of MG in all strains which is indicative of the uptake of the metabolite into the cells and subsequent detoxification. Thus, providing strong evidence of chemical reactivity of BSH with MG, and its involvement in the glyoxalase system as a mechanism of MG detoxification, with BSH being the dominant thiol in the process.

In view of the strong nucleophilicity of BSH through its chemical reactivity with MG, there remained much interest in exploring the possible reactivity with other carbonyl-containing metabolites in glycolysis. DHAP, GA3P and pyruvate were all shown to react with Cys and BSH, with the most reactive being GA3P > DHAP > pyruvate. The rate constants were approximately 1600-fold slower than thiol reactivity with MG. However, the intracellular concentrations of DHAP were shown to exist in relatively high levels of approximately 0.5 mM at late-exponential phase of *B. subtilis* growth. Therefore, using the equilibrium

constants, a maximum theoretical HTA concentration was speculated to exist up to 1.27 and 9.97 mM of Cys-DHAP and BS-DHAP HTA, respectively. This is suggestive that the HTA has potential to form in vast concentrations in the cell.

Since these potentially high concentrations of HTA may form in the cell, it remained essential to provide direct evidence these molecules exist. Evidence suggesting RS-MG, RS-GA3P and RS-DHAP HTA formation were found using mass spectrometry. The masses predominantly detected were the thiazolidine as opposed to the HTA, which contrasted from the NMR data with the HTA being predominant in all the reactions. Furthermore, whole cell NMR provided indication of HTA formation of the MG-SR. It showed some depletion of BSH and potential HTA formation upon external MG incubation (table 5.1). However, further *in vitro* NMR analysis of BS-MG are required to confirm this data due to weak signals shown on the ^{13}C NMR spectrum.

In view of the time constraints of this research, further *in vivo* work to confirm the thermodynamic observations of HTA favourability from BSH reacting with DHAP, would be essential. Therefore, whole cell NMR analysis could be implemented. However, the BS-MG has shown to be on the threshold of the detection limits from the weak resonances observed. Thus, alternative techniques such as mass spectrometry on cell lysates, may prove effective for determining this intracellular reaction due to the higher sensitivity. However, this may be technically quite challenging.

Table 5.1 Mass spectrometry, in vitro NMR and whole cell NMR data confirmation of product formation from thiol and metabolite reactivity.

	Thiol	**MG**	**DHAP**	**GA3P**
Mass spectrometry	Cys	thiazolidine[1]	thiazolidine	thiazolidine
	BSH	HTA thiazolidine	HTA[2]	HTA[3] thiazolidine
In vitro NMR	Cys	HTA	Further investigation	-
	BSH	HTA	Further investigation	-
Whole cell NMR	Cys	No formation	Further investigation	-
	BSH	Possible HTA	Further investigation	

[1]Associated sodium

[2]Dephosphorylated – loss of H_3PO_4

[3]MS2 data

In general, this research relates to a wide range of different settings, from the growth of bacteria in carbohydrate-rich conditions, to yeast undergoing fermentation, or even the high blood sugar levels observed in diabetes. These are all examples of fluctuating levels of glycolytic metabolites in the cell and when present in high concentrations may result in a significant HTA concentration. This research therefore helps provide more of an insight into the functioning of cellular processes. For example, low concentrations of thiol are detected amongst hyperglycaemia in diabetics. [142-145] It has often just been assumed that this is due to an increase in oxidative stress resulting in a decrease in free thiol. However, this research has explored the idea of alternative observations, in that a glucose overload would result in more thiol sequestered as HTA. In addition, the fact that generic analytical techniques, such as mBBr do not detect HTA is suggestive that the true total thiol content in the cell exists in significantly higher concentration than previously thought.

In conclusion, the outcomes of this research have shown that potentially significant concentrations of thiol are being sequestered as HTA, which may be present when thiols react with the many reactive carbonyl-containing metabolites in the cell, all contributing to this 'unknown thiol reservoir.'

6. Materials and Methods

6.1. Materials and suppliers

Unless otherwise stated, all chemicals were obtained from Sigma-Aldrich, Fisher Scientific, VWR-BDH and Alfa-aesar. Glycolytic metabolites were purchased from Sigma-Aldrich at their highest purity. Methylglyoxal was obtained as a 40% solution and purified as described herein. All enzymes were purchased from Sigma-Aldrich.

6.2. Equipment specification

6.2.1. UV-vis spectrophotometer

Ultraviolet-visible (UV-vis) absorbance measurements were carried out on a PerkinElmer UV Lambda 25. Quartz cuvettes were used when measuring a full wavelength absorbance from 200 nm-800 nm whilst polystyrene cuvettes were used when measuring an absorbance above 340 nm. An Ultrospec 10 cell density meter was used for the determination of the Optical Density (OD_{600}) for the bacterial growth curves.

6.2.2. High Performance Liquid Chromatography

High Performance Liquid Chromatography (HPLC) analysis was carried out on Jasco HPLC system comprising of two Jasco PU 1580 pumps, a MX-2080-32 dynamic mixer, a DG-1580-53 3-line degasser, a JASCO AS-2055 auto-injector and a JASCO FP-2020 fluorescence detector. Milli-Q water and HPLC-grade solvents were used for all HPLC analysis.

Thiol-mB peaks were separated by HPLC on a Kinetex 2.6u C18 100A column measuring at 100 x 4.6 mm. Analysis was performed at 38 °C with 95% Solvent A (0.25% v/v acetic acid and 10% methanol, adjusted to pH 4 with NaOH) and 5% Solvent B (90% methanol). A gradient profile was carried out; 0 – 2 min; 5% solvent B, 2 – 8 min; 5 – 32 % solvent B, 8 – 10 min; 32 – 100% solvent B, 10 – 11 min; 100 – 5 % solvent B, 11 – 16 min; 5 % solvent B. Each pump was set to a flow rate of 1.5 mL/min. Detection was carried out using a Jasco fluorescence detector with excitation at 385 nm and emission at 460 nm, and a gain of 1x. Standard retentions times for BSmB and CysmB were 4.3 and 4.7 mins respectively.

6.2.3. Nuclear Magnetic Resonance spectrometer

^{1}H and ^{13}C Nuclear Magnetic Resonance (NMR) spectra were obtained on a Bruker 400 MHz and Bruker S500 MHz Spectrometer. Chemical shifts for ^{1}H and ^{13}C NMR are quoted in parts per million (δ) and coupling constants (J) are quoted in hertz (Hz). The abbreviations are used; s = singlet, d = doublet, t = triplet, dd = doublet of doublets, m = multiplet.

6.2.4. Mass spectrometer

Liquid chromatography - Mass spectrometry (LC-MS) analysis was carried out on a Shimadzu ion-trap Time-of-flight (IT-ToF) mass spectrometer using a Prominence/Nexera UHPLC system to introduce the samples.

6.2.5. pH meter

pH measurements were made on a SUNTEX microprocessor pH meter SP-2200. The pH probe was calibrated with standard buffers, pH 7 for basic measurements and pH 4 for acidic measurements.

6.2.6. Autoclave and laminar airflow cabinet

All growth media including Lysogeny Broth (LB), Belitsky minimal (BM) media, LB agar, equipment and apparatus unless otherwise stated were sterilised by autoclaving using Systec DB-100. All cell culture work was carried out in a sterile class II Laminar airflow safety cabinet.

6.3. Preparation of LMW thiols, MG and glycolytic metabolites

6.3.1. Preparation and storage of metabolites, cofactors and enzymes

All thiols, glycolytic metabolites and MG were stored at -30 °C. DHAP and GA3P were aliquoted into 1 M, 100 mM, 50 mM and 10 mM stocks. Purified MG was aliquoted into 425 mM, 100 mM, 50 mM and 10 mM. In each instance, a fresh stock was used on a daily basis due to poor stability.[71] Enzymes were aliquoted into eppendorf's containing 50 units each. Due to their susceptibility of denaturing, glycerol 3-phosphate dehydrogenase was prepared in 50 mM HEPES buffer, pH 7.7 and glyceraldehyde-3 phosphate dehydrogenase was prepared in 50 mM triethanolamine, pH 8. All thiols including Cys and GSH were commercially available apart from BSH, which was previously synthesised by Dr Sunil Sharma.[8]

6.3.2. Preparation of pure methylglyoxal

Commercially available MG (40% solution) presented in an impure form consisting of MG and pyruvaldehyde dimethyl acetal. Pure stocks of MG were therefore prepared, by Dr Sunil Sharma, from pyruvaldehyde dimethyl acetal as described below.[112]

Dowex-X8 resin (H^+-form, 2.5 g) was washed with water and treated with 1 M HCl for 2 hours. The resin was filtered and washed with water until reaching a neutral pH followed by methanol (30 mL) and DCM (30 mL). In a two neck round bottom flask fitted with a Vigurex condenser, a mixture of pyruvaldehyde dimethyl acetal (10 mL), Dowex-X8 (H^+-form, 2.4 g) in MQ water (150 mL) was heated at 95 °C under a nitrogen atmosphere for 90 min and left overnight at room temperature (scheme 6.1). An aliquot of 450 µL reaction mixture was mixed with 50 µL D_2O for NMR analysis to monitor the progress of the reaction and determine purity of the product. 50 mL water was added and the mixture was concentrated to a volume of ~120 mL under vacuum. This was repeated five times to remove remaining starting material and methanol. Finally, the Dowex resin was removed by filtration. The concentration of MG was determined by quantitative ^1H NMR (425 mM, >98% purity). The solution was stored at -30 °C.

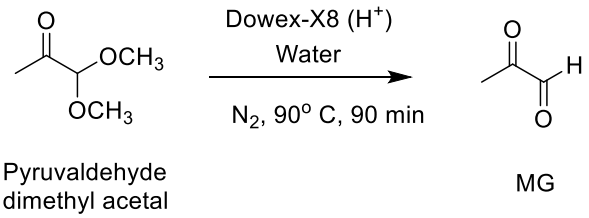

Scheme 6.1. The acid hydrolysis of pyruvaldehyde dimethyl acetal to purify MG solution (>98% purity).

6.4. Analytical methods

6.4.1. Thiol quantification by titration with Ellman's reagent – 5,5- dinitrothiobis-(2-nitrobenzoic acid) (DTNB)[153]

Thiol quantification was determined using Ellman's reagent – 5,5-dinitrothiobis-(2-nitrobenzoic acid) (DTNB). The thiol reacts with DTNB cleaving the disulfide bond in a nucleophilic substitution to produce 2-nitro-5-thiobenzoate (TNB^-) which ionises to the TNB^{2-} at pH 7.4 producing a yellow colour (scheme 6.2). A rapid reaction takes place which is stoichiometric, meaning the addition of one mole of thiol produces one mole of TNB^{2-}. The TNB^{2-} is measured at 412 nm on the UV spectrophotometer and quantified using the extinction coefficient of DTNB being 14150 $M^{-1}cm^{-1}$.[154] Using Beer-Lambert law, where A is absorbance, ε is the extinction coefficient (M^{-1} cm^{-1}), c is concentration (M) and l is path length (cm), the concentration of thiol was determined.

$$\varepsilon_{412} = 14150\ M^{-1}\ cm^{-1}$$

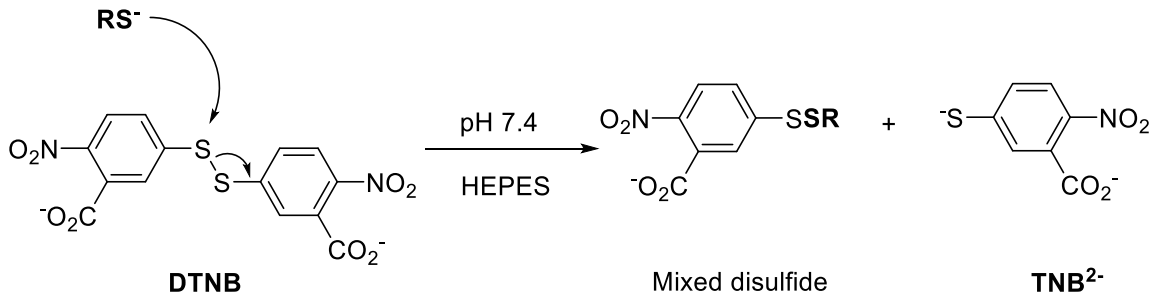

Scheme 6.2. Thiol quantification showing a thiol-disulfide exchange reaction between DTNB and reactive thiolate.

6.4.2. MG quantification by titration with Brady's reagent - 2,4-dinitrophenylhydrazine (2,4-DNPH)

MG concentration was measured using Brady's reagent. It is used qualitatively to detect carbonyl groups of ketone and aldehyde functional groups.[155] 2,4-DNPH reacts with MG to form a hydrazone (scheme 6.3).[121] [122] The hydrazone forms a yellow/orange colour which produces an absorbance at 432 nm on the UV spectrophotometer. Standardisation curves were produced ranging from 0 µM to 125 µM which were used as the comparable measure to determine the MG concentration.

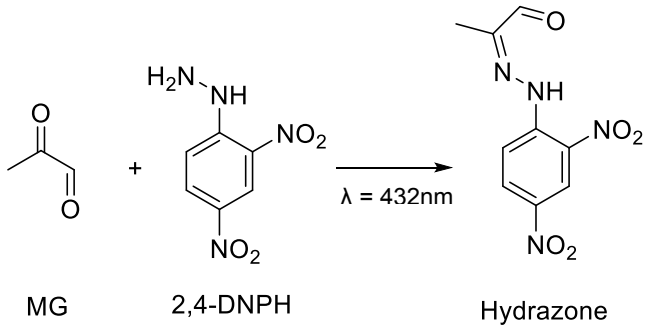

Scheme 6.3. 2,4-Dinitrophenylhydrazine (2,4-DNPH) reacts with MG to form 2,4-dinitrphenylhydrazone which is UV-active at 432 nm.

6.4.3. Thiol quantification using monobromobimane (mBBr)

Monobromobimane (mBBr) is a thiol labelling reagent used to quantify LMW thiols. The weakly fluorescent compound selectively reacts with thiols in a nucleophilic substitution reaction to produce a highly fluorescent and stable thioester (mB-SR) allowing detection on HPLC (scheme 6.4).[120] This technique can be used to detect all LMW thiols at picomolar concentrations for both *in vitro* and cellular samples. Cellular thiol concentration is expressed as µmol/g of residual dry weight (RDW).

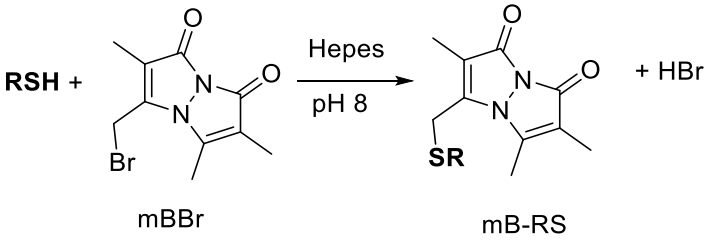

Scheme 6.4. Thiol quantification representing a reaction of the thiolate with mBBr to produce a fluorescent thioester which can be detected on HPLC.

6.4.4. DHAP quantification using the glycerol 3-phosphate dehydrogenase assay

The concentration of DHAP was determined by measuring the oxidation of NADH to NAD+ to produce glycerol 3-phosphate (G3P) (scheme 6.5). The reaction was catalysed by glycerol 3-phosphate dehydrogenase (G3PD) enzyme and monitored NADH consumption to NAD+ at 340nm on the UV-vis spectrophotometer. The extinction coefficient of NADH is found to be 6.22 × 10^3 M^{-1} cm^{-1} expressed in µmol of NADH produced per min per mg of protein.[156]

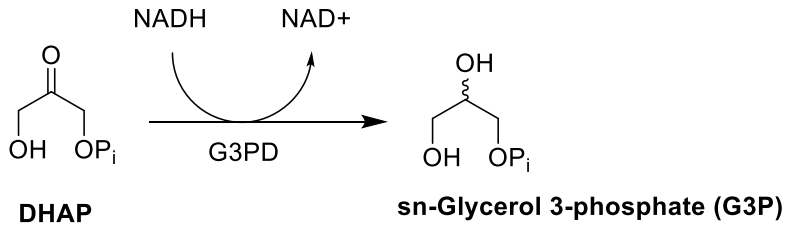

DHAP **sn-Glycerol 3-phosphate (G3P)**

Scheme 6.5. Quantification of DHAP analysing the reduction of DHAP to G3P, catalysed by G3PD.

6.4.5. GA3P quantification using the glyceraldehyde 3-phosphate dehydrogenase assay

The concentration of GA3P was determined by measuring the formation of NADH from NAD+ to form 3-phospho-D-glycerate catalysed by glyceraldehyde 3-phosphate dehydrogenase (GA3PD). The reaction was catalysed by the GA3PD enzyme and monitored at 340 nm on the UV-vis spectrophotometer. Free phosphate was required to form 1,3-bisphospho-D-glycerate however it was found that this reaction was reversible (scheme 6.6). Therefore, arsenate was used, irreversibly forming 3-phospho-D-glycerate (scheme 6.7). The extinction coefficient of NADH is found to be 6.22×10^3 M^{-1} cm^{-1}.[156]

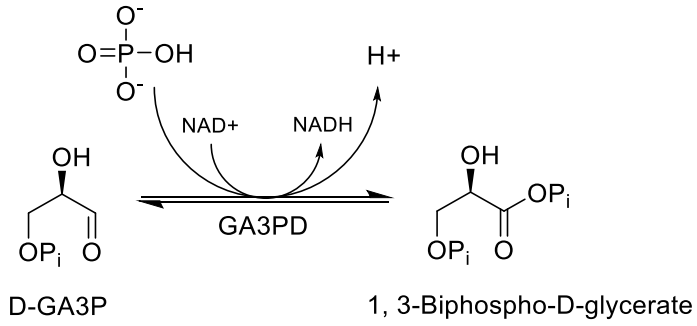

Scheme 6.6. Ineffective quantification of GA3P analysing the oxidation of D-GA3P to 1,3-BPG in sodium phosphate buffer catalysed by GA3PD.

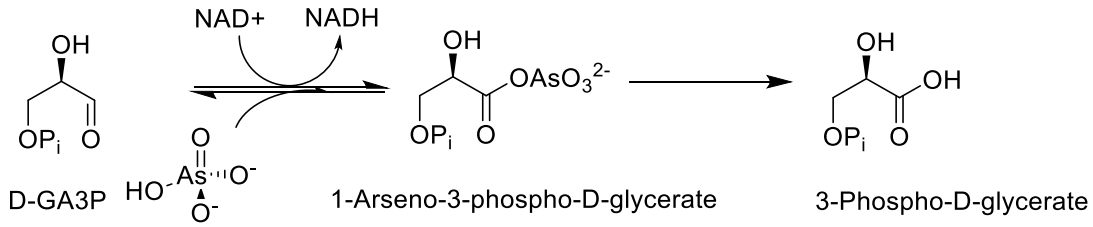

Scheme 6.7. Effective quantification of GA3P analysing the oxidation of D-GA3P to 1-arseno-3-phospho-D-glycerate. The use of arsenate forms the unstable 1-arseno-3-phospho-D-glycerate, which irreversibly breaks down to form 3-phospho-D-glycerate.

6.5 *In vitro* experiments

6.5.1. MG assays

6.5.1.1 Thiol quantification

Thiols were quantified by the absorbance measured (412 nm) on the UV-vis spectrometer upon reaction with 2 mM 5,5-dinitrothiobis (DTNB) in 50 mM HEPES (chapter 6.4.3). The extinction coefficient of DTNB is 14150 $M^{-1}cm^{-1}$.[153]

6.5.1.2. Relative rate of Cys/BSH reactivity with MG assay

MG (1500 µM) was reacted with Cys/BSH in sodium phosphate buffer pH 5.6 at 20 °C. Ellman's titration[153] (chapter 6.4.3) was carried out at 10-second and 1-second time points for Cys and BSH, respectively, under pseudo-first order reaction kinetics. Due to the higher concentrations of GSH/CysNAc required for reactivity, MG (5 mM) was reacted with GSH and CysNAc in a sodium phosphate buffer pH 7.7, 20 °C. Ellman's titration[153] was carried out at minute intervals over the first 5 minutes and then every 5 minutes, thereafter. Different initial concentrations of thiol were analysed to allow comparable thiolate reactivity (table 6.1). For example, at pH 5.6, 63 µM BSH and 200 µM Cys correspond to 0.2932 µM thiolate.

Table 6.1. Assay conditions for the reactivity of all 4 thiols with excess MG (1500 µM) in pseudo-first order conditions, allowing relative rate of reactivity at comparable thiolate concentrations.

Thiol cofactor	Thiol concentration (µM)	Thiolate concentration (µM)	MG concentration (µM)	pH	Time intervals (s)	Temp (°C)
Cys	70/200	0.1026/0.2932	1500	5.6	10	20
BSH	63	0.2932	1500	5.6	1	20
GSH	2100	61	5000	7.7	60	20
CysNAc	4200	61	5000	7.7	60	20

6.5.1.3. Determination of the forwards and reverse rate constants

For determination of the forwards rate constant, Ellman's titration was used to determine thiol consumptions over a range of initial thiol concentrations (100 µM – 2000 µM) when incubated with MG (1500 µM), in sodium phosphate buffer pH 5.6, 20 °C.

Likewise, Ellman's reagent was used for the determination of the reverse rate constant. Thiol (5 mM) and MG (10 mM) was initially reacted in HEPES pH 7.7 until there was a full consumption of thiol, confirmed by Ellman's reagent, implying that the HTA has formed (scheme 6.8A). Several dilutions of the newly formed HTA (125 - 750 µM) were then individually quenched with Ellman's reagent, pH 7.7. The Ellman's reagent labels the residual thiol resulting in a shift in equilibrium allowing the dissociation of HTA to be determined (scheme 6.8B). An increase in absorbance represents thiol being liberated as the HTA dissociates back to form thiol and MG

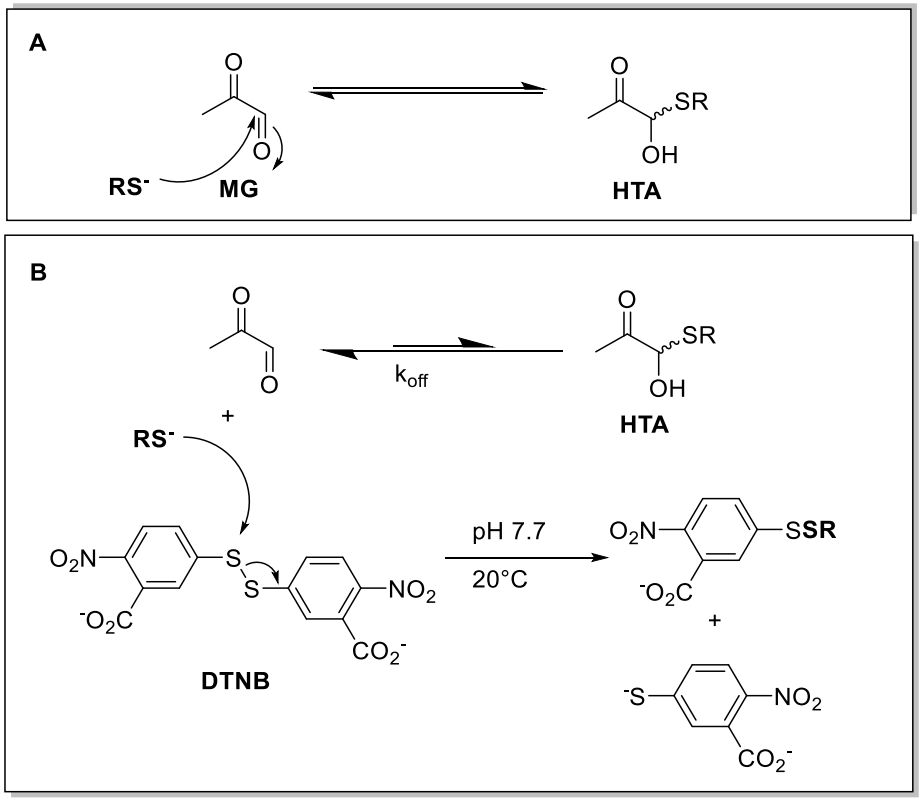

Scheme 6.8. A) The reaction of thiolate and MG to form HTA. B) DTNB reacting with residual thiolate therefore altering the equilibrium allowing determination of the off-rate of reaction.

6.5.1.4. Reactivity of thiol and MG >5 hours

Cys and BSH were incubated with different concentrations of MG at 37 °C where the reactivity was analysed over a longer period than previously investigated, (>6 hours). 2 mM Cys/BSH and 2 mM/10 mM MG were assayed in 1:1 and 1:5 ratio in sodium phosphate buffer, pH 7.4, for 6 hours.[110] The thiol groups were assayed at the appropriate time points using Ellman's reagent as previously described (chapter 6.4.3, 6.5.1.1).[153]

Due to the length of the reaction, a possible decrease in free thiol content could be the result of an oxidation process. Controls of thiol in sodium phosphate buffer were carried out where there was found to be 4% and 10% total thiol oxidation in Cys and BSH over the course of the experiment, respectively.

6.5.2. DHAP/GA3P assays

6.5.2.1. DHAP quantification using the G3P dehydrogenase assay

The concentration of DHAP was determined by measuring the conversion of NADH to NAD+ to produce glycerol 3-phosphate catalysed by glycerol 3-phosphate dehydrogenase. *B. subtilis* physiological cell conditions were adopted using HEPES buffer pH 7.7, 25 °C. The reaction mixture contained 134 mM HEPES and 0.1 mM DHAP. The addition of 0.13 mM NADH corresponded to ~ 0.7 A. The reaction was initiated by the addition of 1U of G3PD enzyme and NADH consumption to NAD+ was monitored at 340 nm for 5 minutes on the UV-vis spectrophotometer. Enzyme activity of 1 U is defined as the amount of enzyme producing 1 µmol product / min at 25 °C. [157] The extinction coefficient of NADH is found to be 6.22×10^3 M^{-1} cm^{-1} and using Beer-Lambert law, the concentration was found.[156]

6.5.2.2. Determining GA3P concentration using the GA3PD assay

The concentration of GA3P was determined by measuring the formation of NADH from NAD+ to form 3-phospho-D-glycerate catalysed by glyceraldehyde 3-phosphate dehydrogenase (GA3PD). This assay was carried out in a reaction mixture containing 100 mM triethanolamine (TEA),[158] pH 8, 1 mM NAD+, 10 mM sodium arsenate and 0.1 mM GA3P. The reaction was started by the addition of 1U of GA3PD enzyme and monitored at 340 nm for 15 minutes on the UV-vis spectrophotometer. The enzyme only catalyses the reaction of one of the enantiomers in the racemic mixture.

6.5.2.3. Triethanolamine/tris/phosphate buffer use in GA3PD assay

The literature has been shown to use many different types of buffer to regulate the pH of this assay.[159, 160] However, the use of different buffers results in a varied final absorbance. Originally, Tris[161] pH 8 was used as the buffer of choice, however it was found to produce an unexpectedly low absorbance after carrying out the assay. A plausible reason for this is due to the reactive nature of the primary amine in the Tris buffer which is possibly undergoing a nucleophilic substitution with the arsenate-containing metabolite. TEA contains a tertiary nitrogen making it less likely to react with carbonyl functional groups.

6.5.2.4. Importance of arsenate in the GA3PD assay

Originally phosphate buffer/tris buffer (supplemented with phosphate) was used with the idea that the free phosphate from the buffer would act as the source for the formation of 1,3-bisphospho-D-glycerate.[159] However, it was found that this reaction is reversible and therefore it doesn't quantify all the GA3P in solution. The use of arsenate resulted in a higher absorbance representing the higher expected concentration of GA3P. It was found that the addition of arsenate results in the production of arseno-3 phospho-D-glycerate which then irreversibly decomposes to form 3-phospho-D-glycerate (scheme 6.9).[157] Control assays show a quantification of 4.21 mM GA3P in the presence of arsenate as opposed to 3.70 mM GA3P in the absence showing a fairly significant difference in concentration (>10%).

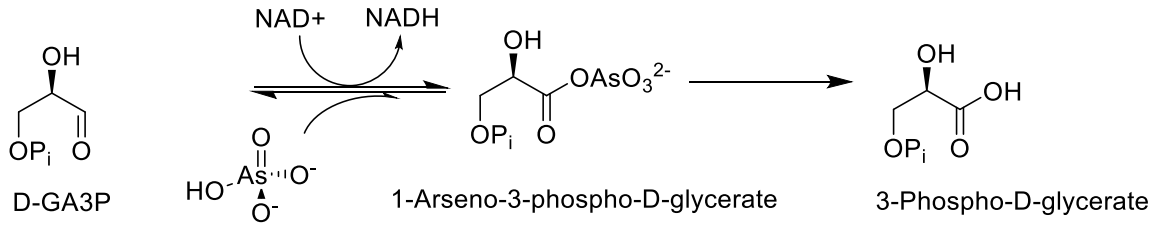

Scheme 6.9. Q132uantification of GA3P analysing the oxidation of D-GA3P to 1-arseno-3-phospho-D-glycerate. The use of arsenate forms the unstable 1-arseno-3-phospho-D-glycerate, which irreversibly breaks down to form 3-phospho-D-glycerate.

6.5.2.5. Determination of equilibrium constants (K_{eq})

Stock solutions of DHAP, GA3P and thiols were quantified using GPD assay, GA3PD assay and Ellman's titration, respectively. Assays were developed consisting of 5 different concentrations of thiol to metabolite ratios including 1:1, 5:4, 3:2, 7:4, 2:1, (RSH:C=O). The specific reaction was left to equilibrate in HEPES (50 mM) pH 7.7.

For determination of the equilibrium constant for DHAP and thiol, the thiol was first titrated using Ellman's reagent to determine the initial concentration of thiol before reacting with DHAP until equilibrium had been reached. The reaction was carried out in an inert atmosphere in a glove box to prevent any possible oxidation of the thiols. After 16 hours, the thiols were quantified and this was repeated on an hourly basis to confirm whether equilibrium had been reached. The residual DHAP concentration was then determined using the GPD assay.

For determination of the equilibrium constant for GA3P and thiol, similarly the thiol was titrated using Ellman's reagent to determine the initial concentration of thiol. However, it is known that the reaction between GA3P and thiol takes place at a faster rate than DHAP. After 3 hours, the thiols were quantified and this was repeated on 30-minute basis to confirm whether equilibrium had been reached. The residual GA3P concentration was then determined using the GA3PD assay. The equilibrium constant (K_{eq}) was calculated (Eq. 1 - chapter 6.5.2.6).

6.5.2.6. The use of the quadratic equation to determine HTA K_{eq} as a percentage

An alternative way of expressing the K_{eq} is representing the equilibrium as a percentage. This was achieved by using simultaneous equations (equation 6.2) and the quadratic equation (equation 6.7). 1 M DHAP/GA3P and 1 M BSH/Cys were used in the examples to determine the concentration dependent percentage of HTA formation at equilibrium (table 6.2).

Table 6.2. Calculations to determine algebraic equations to determine percentage of HTA at equilibrium.

	Thiol (M)	DHAP/GA3P (M)	HTA (M)
BSH/Cys and DHAP/GA3P reaction			
Initial concentration	1 M	1 M	0 M
Change in concentration	-x	-x	+x
Concentration at equilibrium	1 - x	1 - x	x

$$K_{eq} = \frac{[HTA]}{[C=O][RSH]} \quad \text{Eq. 6.1}$$

$$10 = \frac{[x]}{[(1-x)(1-x)]} \quad \text{Eq. 6.2}$$

$$K_{eq}[(1-x)(1-x)] = [x] \quad \text{Eq. 6.3}$$

$$10\,(x^2 - 2\,x + 1) = x \quad \text{Eq. 6.4}$$

$$10\,x^2 - 20\,x + 10 = x \quad \text{Eq. 6.5}$$

$$10\,x^2 - 21\,x + 10 = 0 \quad \text{Eq. 6.6}$$

$$x = \frac{-b \pm \sqrt{b^2 - 4ac}}{2a} \quad \text{Eq. 6.7}$$

$$x = \frac{21 \pm \sqrt{(^2 - 4 \text{ x } 10 \text{ x } 10}}{2 \text{ x } 10}$$

$$x = 0.73 = 73\ \%$$

6.5.2.7. Oxidation of thiols in the determination of equilibrium constants (K_{eq})

The assays carried out to determine the equilibrium constants (K_{eq}) were carried out over long period of time therefore the thiols are more susceptible to oxidation forming disulfide bonds. It was found that BSH oxidises more rapidly than Cys, with GSH being the most stable. Many different measures had been undertaken to prevent this oxidation including the maintenance of an anaerobic environment using nitrogen gas from the tap and nitrogen-infused balloons. However, the only proven technique that greatly reduces levels of oxidation was the use of nitrogen chamber where approximately 10% and 3% oxidation was determined in BSH and Cys after 12 hours, respectively.

6.5.2.8. Determination of the forwards and dissociation rate constants

For determination of the forwards constant, Ellman's titration was used to determine thiol consumptions over a range of initial thiol concentrations (>5) ranging from 200 µM – 1600 µM. The thiol was incubated with 10 mM DHAP/GA3P in 50 mM HEPES buffer, pH 7.7, 20 °C. Ellman's titration was carried out every 60 seconds to determine the concentration of residual thiol. In terms of the reverse rate constant, Ellman's reagent was used to quantify the formation of thiol from DHAP-SR HTA and GA3P-SR HTA The assay was carried out using the same method for the reverse rate constant for MG-SR HTA (chapter 6.5.1.3).

6.5.3 *In vitro* HPLC assays

6.5.3.1. *In vitro* kinetics of BSH and Cys reactivity with DHAP under physiological conditions

The reaction between DHAP with both BSH and Cys was assessed under physiological conditions. 3 mM BSH and 0.2 mM Cys were reacted with 0.528 mM DHAP in a sodium phosphate buffer, pH 7.7 at 20 °C. HPLC thiol analysis was required to quantify both thiols in parallel. MBBr derivatisation was carried out at time points = 0, 2, 5, 10, 20, 30, 60, 180 minutes. This process involved reacting 5 µL of bimane mix (50% acetonitrile containing 2 mM mBBr and 20 mM HEPES pH 8.0) with 5 µL sample. These samples were incubated at 60 °C for 10 min in the dark, and then cooled on ice. The samples were acidified by the addition of 5 M methanesulfonic acid, and a further 1 in 5 dilution in 10 mM methanesulfonic acid. HPLC was performed at 38 °C with 95% Solvent A (0.25% v/v acetic acid and 10% methanol, adjusted to pH 4 with NaOH) and 5% Solvent B (90% methanol). Samples were eluted with a gradient of Solvent B with a 1.5 mL/min as follows: 0 – 2 min; 5% solvent B, 2 – 8 min; 5 – 32 % solvent B, 8 – 10 min; 32 – 100% solvent B, 10 – 11 min; 100 – 5 % solvent B, 11 – 16 min; 5 % solvent B. Detection was carried out with a Jasco fluorescence detector with excitation at 385 nm and emission at 460 nm, and a gain of 1x. Standard retentions times for BSmB and CysmB are 4.3 and 4.7 mins respectively.

6.5.3.2. Assays to determine whether mBBr labelling methods detect HTA

Excess MG, DHAP and GA3P (10 mM) were reacted with the thiol (Cys, BSH, GSH) (2 mM) until complete depletion of residual thiol confirmed by Ellman's assay. The mBBr derivatisation was then carried out on the HTA to confirm whether this technique detects it. This process involved reacting 20 µL of bimane mix (50% acetonitrile containing 2 mM mBBr and 20 mM HEPES pH 8.0) with 20 µL sample. The procedure was then carried out as previously described (chapter 6.5.3.1).

6.5.3.3. Synthesis and preparation of thiol-mB standards for HPLC

Ellman's assay was used to determine the concentration of the thiol. 1 mM stock solutions of BSH/Cys were prepared from this which were reacted with mBBr to produce the fluorescent thiol-mB adducts as described previously (chapter 6.5.3.1). 20 nmol samples of BSH/Cys were then prepared from the stock solution of thiol-mB adducts. 200 µL dilutions of methanesulfonic acid (10 mM) were carried out to produce a 500 pmol peak from a 5 µL injection on the HPLC.

6.5.4. Determination of the reaction order for the forwards and reverse reaction

Experimental analysis was required to determine the rate orders (equation 6.8-6.10). The order of the reaction was determined by investigating the fold-change of the rate of reaction when the concentration of a single species is changed. With reference to the reaction between MG and Cys (table 6.3), the concentration increases by approximately a factor of 2. In addition, the initial rate increases by approximately a factor of 2. This therefore represents a first order reaction with respect to the Cys concentration (equation 6.11). Likewise, for determining the order of reaction with respect to BSH, the concentration increases by approximately a factor 3. In addition, the initial rate increases by approximately a factor of 3. Therefore, this represents a first order reaction with respect to BSH concentration (equation 6.12). With regards to the dissociation of HTA, the determination of the order of the reaction was carried out in a similar manner. The concentration increases by 2-fold. In addition, the initial rate increases by approximately 2-fold. Therefore, this represents a first order reaction (equation 6.13). This sample principle was applied to all reactions involved, including thiol reaction with DHAP and GA3P.

$$\text{Rate} = k\,[\text{Cys}]^{x} \qquad \text{Eq. 6.8}$$

$$\text{Rate} = k\,[\text{BSH}]^{y} \qquad \text{Eq. 6.9}$$

$$\text{Rate} = k\,[\text{HTA}]^{z} \qquad \text{Eq. 6.10}$$

$$\text{Rate} = k[\text{Cys}]^{1} \qquad \text{Eq. 6.11}$$

$$\text{Rate} = k[\text{BSH}]^{1} \qquad \text{Eq. 6.12}$$

$$\text{Rate} = k\,[\text{HTA}]^{1} \qquad \text{Eq. 6.13}$$

Table 6.3. Reaction order determination for Cys/BSH reaction with three metabolites, MG, DHAP and GA3P.

Experiment	[RSH] (μM)	[C=O] (μM)	Initial rate (μM/s)
Forwards reactions of Cys + MG – first order reaction			
1a. Cys + MG	166	1500	2.3
1b. Cys + MG	373	1500	4.3
Fold change	**2.2**	**1**	**1.9**
2a. BSH + MG	30	1500	1.8
2b. BSH + MG	96	1500	4.5
Fold change	**3.2**	**1**	**2.5**
Reverse reaction of the dissociation of HTA – first order reaction			
3a. HTA forming Cys and MG	250		0.0015
3b. HTA forming Cys and MG	500		0.0037
Fold change	**2**		**2.5**
4a. HTA forming BSH and MG	250		0.0018
4b. HTA forming BSH and MG	500		0.0030
Fold change	**2**		**1.7**
Forwards reaction of Cys and DHAP – first order reaction			
5a. Cys + DHAP	782	10000	0.51
5b. Cys + DHAP	1272	10000	0.77
Fold change	**1.6**	**1**	**1.5**
6a. BSH + DHAP	374	10000	0.39
6b. BSH + DHAP	855	10000	0.72
Fold change	**2.3**	**1**	**1.8**
Reverse reaction of the dissociation of HTA – first order reaction			
7a. HTA forming Cys and MG	250		0.0015
7b HTA forming Cys and MG	500		0.0037
Fold change	**2**		**2.5**
8a. HTA forming BSH and MG	250		0.0018
8b. HTA forming BSH and MG	500		0.0030
Fold change	**2**		**1.7**

Forwards reaction of Cys and GA3P			
9a. Cys + GA3P	342	10000	0.3883
9b. Cys + GA3P	804	10000	0.7792
Fold change	**2.4**	**1**	**2.0**
10a. BSH + GA3P	353	10000	0.47
11b. BSH + GA3P	703	10000	0.87
Fold change	**2.0**	**1**	**1.9**
Reverse reaction of the dissociation of HTA			
11a. HTA forming Cys and MG	250		0.0031
11b. HTA forming Cys and MG	500		0.0066
Fold change	**2**		**2.1**
12a. HTA forming BSH and MG	250		0.0017
12b. HTA forming BSH and MG	500		0.0035
Fold change	**2**		**2.1**

6.6 *In vivo* experiments

6.6.1. Media and buffers

6.6.1.1. *B. subtilis* strains

B. subtilis CU1065 WT, *B. subtilis* CU1065 *glxII*, *B. subtilis* CU1065 *glxI*, *B. subtilis* CU1065 *glxI/II*, *B. subtilis* and CU1065 *bshC* were received from Dr Pete Chandrangsu (Cornell University, USA).

6.6.1.2. Growth Media

B. subtilis was cultured in LB and BM media depending on the experimental choice in the appropriate antibiotic as stated in Table 6.4. LB media was made up from 1% bacto-tryptone, 0.5% yeast extract, 1% NaCl and 2% agar for solid material. BM media was made up from basal medium containing 15mM $(NH_4)_2SO_4$, 8 mM MgSO4, 27 mM KCl, 7 mM sodium citrate and 50 mM Tris HCl, pH 7.5. The basal medium was autoclaved before adding Tris HCl. Supplements (2 mM KH_2PO_4, 2 mM $CaCl_2$, 10 µM $FeSO_4$, 10 µM $MnSO_4$, 4.5 mM glutamic acid, 780 µM tryptophane, 0.2 % glucose) were sterile filtered using a 0.22 µM Millipore Extra PES membrane filter unit. The supplements were added to the basal medium before use. For specific experiments, glucose/arabinose 0.5% were added to the BM media which were sterile filtered using a 0.22 µM Millipore Extra PES membrane filter unit.

In the case of agar, after sterilisation it was cooled to temperatures below 50 °C before the addition of any specific antibiotics. The agar was poured into the plates and dried at room temperature before storage at 4 °C.

6.6.1.3. Bacterial strain and antibiotics

All antibiotic stock solutions were prepared 100x concentrated in the specified solvent and were filtered 0.22 µM Millipore Extra PES membrane filter unit. The antibiotic stock solutions were stored at 4 °C.

6.6.2. General maintenance, growth and culturing of bacterial strains

6.6.2.1. Storage of *B. subtilis*

Bacterial strains were grown on LB agar in the appropriate antibiotic(s) (table 6.4) at 37 °C overnight and then stored at 4 °C where they were kept for a maximum of 2 weeks. For long term storage bacteria strains were kept as glycerol stocks at -80 °C.

6.6.2.2. Growth and harvesting of bacterial culture

The appropriate media was inoculated with a single bacterial colony from the specified bacterial strain (table 6.5) grown on agar. The bacterial strains were cultured overnight in liquid media on the rotator at 37 °C whilst shaken at 200 revolutions per minute (RPM). The media was then re-inoculated with 1-1.5% (% v/v) of the overnight culture. The cultures were incubated at 37 °C on the rotator at 200 RPM. Growth was measured at regular time points by monitoring the optical density at 600 nm (OD_{600}) of 1 mL of cell culture.[74] Appropriate dilutions of 1:1 or higher were carried out at an OD_{600} above 0.9 in order to allow photometric measurements in a linear range. At the appropriate time points, the liquid culture was transferred to 50 mL falcon conical centrifuge tubes which were centrifuged for 5 minutes at 13500 RPM. The supernatant was discarded and the cells were re-suspended into pre-weighed eppendorfs. The cells were centrifuged for a further 3 minutes at 13500 RPM and frozen in liquid nitrogen. They were stored at -30 °C.

Table 6.4. The antibiotics used in LB agar to confirm the growth of the particular KO.

Antibiotic	**Final concentration (µg/mL)**	**Solvent for stock solution**
Chloramphenicol	5	EtOH
Kanamycin	10	Water
Spectinomycin	100	Water
Erythromycin	1	EtOH
Lincomycin	25	Water

Table 6.5: Details of the antibiotics and knockout type for each strain of *B. subtilis*.

Strain	Knock-out	Antibiotic
CU1065	WT	-
HB11069	CU1065 *glxII*::kan	Kanamycin
HB11079	CU1065 *bshC*::kan	Kanamycin
HB16505	CU1065 *glxI*::cm	Chloramphenicol
HB16545	CU1065 *glxI*::cm *glxII*::kan	Chloramphenicol, Kanamycin

6.6.3. *In vivo* experiments for the analysis of MG and LMW thiol content

6.6.3.1. Preparation, harvesting and thawing of *B. subtilis* cells

Overnight cultures were prepared by the inoculation of a single colony of bacterial cells from agar plates, incubated on the rotator at 37 °C shaken at 200 RPM. A 1 - 1.5% re-inoculation of the overnight culture was carried out. At the appropriate time point, depending on the OD_{600} of *B. subtilis* growth, the liquid culture corresponding to approximately 10 mg RDW was transferred into 50 mL falcon conical centrifuge tubes and centrifuged for 5 minutes at 13500 RPM. Supernatant was discarded and the cell pellet was re-suspended in media into pre-weighed 1.5 mL eppendorf microcentrifuge tubes. The samples were centrifuged again for 3 minutes at 13500 RPM. The cells were harvested and remaining supernatant was discarded. The samples were frozen under liquid nitrogen and stored at -30 °C. This process was carried out at 40-minute intervals covering all phases of the bacterial growth curve.

6.6.3.2. Calculated residual dry cell weights for thiol analysis

Cells were harvested at various different OD_{600} and therefore required different volumes of liquid culture to produce 10mg residual dry cell weight (RDW) required for mBBr thiol analysis and other techniques. A standardisation curve was produced; $y = 0.224 x + 0.089$, where the required volume of liquid culture was calculated to produce 10 mg RDW based on the specific OD_{600}. In *B. subtilis*, there is an equal ratio of RDW to intracellular water. Therefore, as an example, 0.2 µmol/g equates to 0.2 mM when the data is represented as a concentration.[20]

6.6.3.3. Growth comparisons of LB media and BM media

Bacillus subtilis WT CU1065 strain was used for growth, mBBr thiol analysis and the MG derivatization experiments. The bacterial strains were cultured overnight in LB media on the rotator at 37 °C. Two experiments were carried out in parallel containing LB media and BM media both inoculated with 1 – 1.5 % of the overnight culture. The cultures were incubated at 37 °C and put on the rotator at 200 RPM. OD_{600} readings were carried out at equal time intervals throughout the bacterial growth cycle to assess response and growth of *B. subtilis* to the different conditions.

6.6.3.4. Determination of thiol content using mBBr thiol analysis

MBBr derivatisation was carried out on all *B. subtilis* strains listed on table 6.5. This process was used to fluorescently label thiols to be detected via HPLC.[162] 20 µl of bimane mix (50% acetonitrile containing 2 mM mBBr and 20 mM HEPES, pH 8.0) were added per mg of estimated dry residual weight. The procedure was carried out as described previously (chapter 6.5.3.1).

6.6.3.5. Determination of extracellular MG levels using 2,4-dinitrophenyhydrazine (2,4-DNPH)

The extracellular MG concentration was determined in all *B. subtilis* strains listed on table 6.5. 2,4-Dinitrophenylhydrazine (2,4-DNPH) was used as the derivatising agent (chapter 6.4.2. scheme 6.3) used to qualitatively test for carbonyl groups. It reacts with the ketones and aldehyde of MG to produce 2,4-dinitrophenyhydrazone which can then be measured spectrophotometrically at 432 nm.

Initially cells were cultured in LB media, however 2,4-DNPH was found to react with LB media producing a negative gradient; y= -0.5404x. 2,4-DNPH was more stable in BM media, showing no reactivity and therefore the media of choice. BM media was inoculated with *B. subtilis* and grown as discussed previously. At an OD_{600} of 0.7, 1 mM of MG was added to the *B. subtilis* culture with the two additional controls; BM media with 1 mM MG, and *B. subtilis* alone.

A 2 mM stock solution of 2,4-DNPH was prepared in ethanol which was diluted 10-fold in 12 % HCl in ethanol.[155] At the appropriate 40-minute intervals, 0.2 mM 2,4-DNPH was reacted with the MG incubated *B. subtilis* culture for 45 minutes at 42 °C. Samples were then incubated at room temperature for 5 minutes. Spectrophotometer measurements were carried out at 432 nm. The concentrations were determined by comparison to a standardisation curve. This was prepared by reacting 0.2 mM 2,4-DNPH with 10 different MG concentrations ranging from 0 µM to 125 µM *in vitro*. A standardisation curve was prepared for every new supply of MG and 2,4-DNPH solution due to the varying concentrations in each stock.

6.6.3.6. Determination of extracellular MG in the presence of glucose/arabinose 0.5%

The extracellular MG concentration was determined in *B. subtilis* WT and *bshC* mutant strain in the presence and absence of glucose/arabinose 0.5%. BM media was supplemented with 0.5 % glucose/arabinose and the *B subtilis* KO were grown over 72 hours to achieve the full bacterial growth curve. At ~3 hour intervals, the cells were harvested and MG was quantified to determine the extracellular concentrations of MG as previously described.

6.6.3.7. Effect of *B. subtilis* WT and *bshC* mutant growth upon variable MG stress

B. subtilis WT and *bshC* mutant strain were re-inoculated from an overnight culture and grown on the rotator at 37 °C shaken at 200 RPM. At an OD_{600} of 0.7, variable concentrations of MG were added to the liquid culture including 0 mM, 1 mM, 2 mM, 5 mM and 10 mM. OD_{600} results were taken at hourly intervals over the first 3 hours to determine the effect that MG has on the growth of cells.

6.6.4. *In vivo* experiments for the analysis of glycolytic metabolites and LMW thiols content

6.6.4.1. Growth of *B. subtilis* in preparation for intracellular DHAP quantification

LB media was inoculated with a single bacterial colony from the specified bacterial strain grown on agar. The bacterial strains were cultured overnight in liquid media on the rotator at 37 °C whilst shaken at 200 RPM. 1000 mL LB media was then re-inoculated with 1-1.5% (% v/v) of the overnight culture. The cultures were incubated at 37 °C on the rotator at 200 RPM. At early-, mid- and late-exponential phase, the culture was transferred to falcon tubes and centrifuged as previously described. Due to the sensitivity limits of the DHAP assay, an estimated 50 mg RDW of *B. subtilis* cells was collected for each sample. The cells were immediately frozen in liquid nitrogen and stored at -30 °C.

6.6.4.2. Intracellular DHAP quantification

The intracellular DHAP concentration was determined at different stages of the *B. subtilis* growth. Many techniques were carried out to lyse the cells, which included acidification, freeze thawing and bead beating.[163, 164] Reported literature on lysing cells via acidification proved to be successful in some instances however regulating the pH proved to be difficult and therefore consistent results could not be reproduced in the experiments.[164]

Lysing the cell by bead beating with zirconium 0.1 mm beads proved the most successful. Samples containing an estimated 50 mg *B.subtilis* WT RDW were left at room temperature to thaw for 5 minutes. 300 µL of 50 mM HEPES buffer, pH 7.7, and 250 mg 0.1 mm zirconium beads (purchased from Sigma) were added to the cells. The samples were placed

on the disruptor genie for 1-minute intervals and then cooled on ice. This was repeated 5 times. The cells were then heated to 80 °C to denature enzymes and the cells were centrifuged for 10 minutes at 13000 RPM. The supernatant was then transferred to Amicon ultra-0.5 mL centrifugal filters and centrifuged for 30 minutes at 13000 RPM. The remaining dry cells were placed in the oven. 20 µl of 50 mM HEPES buffer, pH 7.7, was added to the supernatant and centrifuged for a further 10 minutes at 13000 RPM to ensure all molecules below 3000 MW had passed through the membrane. The DHAP assay as described earlier was carried out on the filtered supernatant (chapter 6.5.2.1). So, the concentration of intracellular DHAP was determined by measuring the depletion of NADH to NAD+ to produce G3P catalysed by G3PD. The assay was carried out in a reaction mixture containing 134 mM HEPES and filtered supernatant. The addition of 0.13 mM NADH corresponded to a ~ 0.7 A. Controls were carried out for background absorbance by monitoring absorbance change over 5 minutes prior to adding NADH and after adding NADH. The reaction was started by the addition of 1 U G3PD enzyme and monitored NADH consumptions to NAD+ at 340nm for 5 minutes on the UV-vis spectrophotometer.

6.7. Metabolomics studies

6.7.1. Mass spectrometric studies

Mass spectrometric samples, run on the Shimadzu ion-trap ToF mass spectrometer were run by Dr Lionel Hill (John Innes Centre, Norwich). The six potential HTAs including DHAP-Cys, GA3P-Cys, MG-Cys, DHAP-SB, GA3P-SB and MG-SB were analysed. The 5 mM concentration of the product was diluted 10-fold in 50% MeOH. The spectrometer was prepared and spectra were collected from m/z 200-2000 with a maximum ion accumulation time of 20 ms, and automatic sensitivity control set to a target of 70% optimal base peak intensity. For MG-Cys, the mass range was m/z 160-2000. The instrument also collected data-dependent MS2 of the most abundant precursor ions. MS2 was carried out at 50% collision energy, 50% collision gas, with an isolation window of 3Da, and an ion accumulation time fixed at 20 ms. Spectra were collected down to m/z 50. Spray chamber conditions were 250 °C curved desorption line, 300 °C heat-block, 1.5 $L.min^{-1}$ nebuliser gas, and drying gas “on”. The instrument was calibrated using sodium trifluoroacetate cluster ions.

6.7.2. *In vitro* NMR studies

6.7.2.1. Preparation of stock and buffer solutions

1 M stock solutions of Cys, DHAP, acetone and MG were prepared in D_2O. 2 M sodium phosphate buffer and 2 M HEPES buffer, pH 7.7, were prepared in water and pH calibrated.[165] The buffers were freeze-dried overnight and then prepared in D_2O ensuring no residual H_2O traces to produce 2 M sodium phosphate buffer and 2 M HEPES buffer, ~pD 8.1.

6.7.2.2. *In vitro* NMR assays

Acetone and MG were reacted with thiols in determination of HTA for NMR analysis:

1) A 2:1 ratio of acetone (200 mM) to Cys (100 mM) was prepared in sodium phosphate buffer (200 mM, pD 8.1) in D_2O.

2) A 1:1 ratio of MG (10 mM) to thiol (10 mM) was prepared in sodium phosphate buffer (50 mM, pD 8.1) in D_2O. The experimental process was carried out by Dr Sunil Sharma.

All NMR analysis consisted of ^{1}H NMR, ^{13}C NMR, heteronuclear single quantum coherence (HSQC) and heteronuclear multi-bond correlation (HMBC) analysis, which were performed on the Bruker 500 MHz spectrometer for acetone and the Bruker 400 MHz spectrometer for MG analysis.

6.7.3. Whole cell NMR analysis

6.7.3.1. Cell culturing

Whole cell NMR analysis was carried out by Francesc Puig. *B. subtilis* CU1065 (WT) strain and CU1065 (*glxI* mutant) strain was used for the whole cell NMR analysis. The bacterial strains were cultured overnight in LB media on the rotator at 37 °C at 200 RPM. A 2% inoculation of the overnight culture in 50 mL sulfur-free minimal media supplemented with each non-labelled and ^{13}C-labelled Cys (1 mM), which were grown to an OD_{600} of 0.4. 25 mL of the culture was incubated with MG (1 mM) for a further 30 minutes before the cells were harvested. The appropriate control of no MG was carried out in parallel. Cells were harvested by centrifuging at 5000 RPM for 3 min at 4ºC, which were washed with 200 µL of 25 mM deuterated phosphate buffer saline. Samples were frozen in liquid nitrogen and stored at -80ºC.

6.7.3.2. Media preparation

The sulfur-free minimal media was made up from basal medium containing 6 mM K_2HPO_4, 4.4 mM KH_2PO_4, 4 mM $MgCl_2$. 250 µM $CaCl_2$ and 10 µM $MnCl_2$. The basal medium was autoclaved before adding the supplements, 0.5 % D-glucose, 50 mM L-Tryptophan, 0.1% L-glutamine, 11 mM ferric ammonium citrate and 0.3 mM trisodium citrate. The supplements were sterile filtered using a 0.22 µM Millipore Extra PES membrane filter unit.

6.7.3.3. NMR analysis

Samples were thawed on ice and resuspended in 400 µL deuterated PBS. A coaxial insert containing 1 mM NMR standard DSS in D_2O. ^{1}H, ^{13}C and HSQC NMR analysis was carried out on the sample regulated at 5 °C.

Table 6.6. ^{1}H and ^{13}C NMR chemical shifts in acetone, Cys and Cys-acetone HTA.

Moiety		δ_H 500 MHz		δ_C 100 MHz	
		Free ligand	HTA	Free ligand	HTA
Free Cys 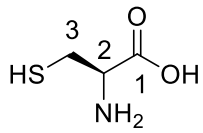	1	-	-	172.9	177.5
	2	3.89 1H, dd J=4 Hz	3.87 1H, dd J=4 Hz	55.8	66.4
HTA 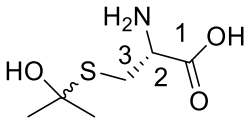	3	3.01, 2.95 2H, 2dd J=5.5, 4 Hz	2.93, 3.38 2H, 2dd J=9, 7 Hz	25.1	39.1
Acetone 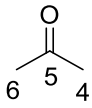	4	2.13 3H, s	1.61 3H, s	30.1	28.8
	5	-	-	215.4	74.8
HTA 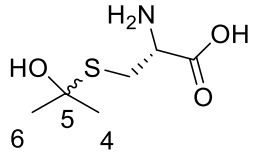	6	2.13 3H, s	1.43 3H, s	30.1	30.8

Table 6.7. ^{1}H and ^{13}C NMR chemical shifts of Cys, MG and Cys-MG HTA.

Moiety		δ_H 500 MHz			δ_C 100 MHz		
		Free ligand	HTA (**A**)	HTA (**B**)	Free ligand	HTA (**A**)	HTA (**B**)
Free Cys 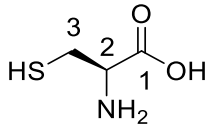	1	-	-		172.9[a]	177.6	176.6
	2	3.84 1H dd J=6.8 Hz	3.89 1H t J = 8.5 Hz	3.70, 1H dd J=6 Hz	55.8[a]	69.0	67.2
HTA 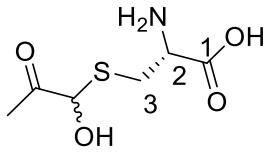	3	2.96, 2.90 2H, 2dd J= 5 Hz	2.62 t J= 10.4 Hz 3.23 dd J=6 2H	2.88 dd J=6.4, 6.8 Hz 3.11 dd J=6.8, 7.2 Hz	25.1[a]	37.3	37.0
Methylglyoxal 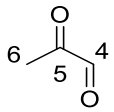	4	8.97[c], s	5.35, s,	5.10, s,	188.8[a]	57.30	64.2
	5	-	-	-	197.3[a]	-	
HTA 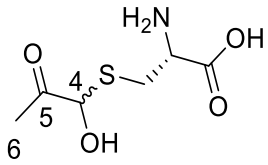	6	2.22[c], s	2.24, s, 3H	2.15, s, 3H	22.9[a]	27.1	25.7
a) No signals were determined in control experiments and therefore literature reactions are shown, in D_2O[(166)]							

Table 6.7.^{1}H and ^{13}C NMR chemical shifts in MG, BSH and BS-MG HTA.

Moiety		δ_H 500 MHz		δ_C 100 MHz	
		Free ligand	HTA[a]	Free ligand	HTA[a]
Free BSH 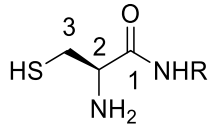	1	-	-	167.2	-
	2	3.9[b] m	4.06[b] m	53.9	61.4
HTA 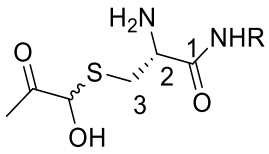	3	3.07[b] m	2.69[b] m	24.7	37.6
Methylglyoxal[d] 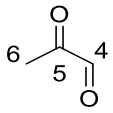	4	8.97[c] m		188.8[c]	174.5
	5	-	-	197.3[c]	-
HTA 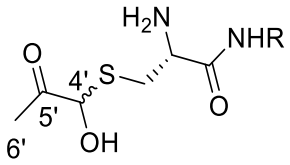	6	2.21[b] m	2.25[b] m	25.0[c]	27.1

a) The diastereomers of the HTA were not detected

b) Overlapping of peaks on ^{1}H NMR means the splitting is not interpretable

c) No signals were determined in control experiments and therefore literature reactions are shown in D_2O[(166)]

References

1. Marles-Wright J, Lewis RJ. Stress responses of bacteria. CURRENT OPINION IN STRUCTURAL BIOLOGY. 2007;17(6):755-60.
2. Booth IR. Stress and the single cell: Intrapopulation diversity is a mechanism to ensure survival upon exposure to stress. INTERNATIONAL JOURNAL OF FOOD MICROBIOLOGY. 2002;78(1–2):19-30.
3. Booth IR, Cash P, O'Byrne C. Sensing and adapting to acid stress. ANTONIE VAN LEEUWENHOEK. 2002;81(1):33-42.
4. Perera VR, Newton GL, Pogliano K. Bacillithiol: a key protective thiol in Staphylococcus aureus. EXPERT REVIEW OF ANTI-INFECTIVE THERAPY. 2015;13(9):1089-107.
5. Newton GL, Buchmeier N, Fahey RC. Biosynthesis and functions of mycothiol, the unique protective thiol of Actinobacteria. MICROBIOLOGY AND MOLECULAR BIOLOGY REVIEWS : MMBR. 2008;72(3):471-94.
6. Fairlamb AH, Cerami A. Metabolism and functions of trypanothione in the Kinetoplastida. ANNUAL REVIEW OF MICROBIOLOGY. 1992;46:695-729.
7. Bartsch RG, Newton GL, Sherrill C, Fahey RC. Glutathione amide and its perthiol in anaerobic sulfur bacteria. JOURNAL OF BACTERIOLOGY. 1996;178(15):4742-6.
8. Sharma SV, Jothivasan VK, Newton GL, Upton H, Wakabayashi JI, Kane MG, et al. Chemical and Chemoenzymatic syntheses of bacillithiol: a unique low-molecular-weight thiol amongst low G + C Gram-positive bacteria. ANGEWANDTE CHEMIE. 2011;50(31):7101-4.
9. Poole LB. The Basics of Thiols and Cysteines in Redox Biology and Chemistry. FREE RADICAL BIOLOGY & MEDICINE. 2015;0:148-57.
10. Zou CG, Banerjee R. Homocysteine and redox signaling. ANTIOXIDANTS & REDOX SIGNALING. 2005;7(5-6):547-59.
11. Begley TP, Kinsland C, Strauss E. The biosynthesis of coenzyme a in bacteria. Vitamins & Hormones. 61: Academic Press; 2001. p. 157-71.
12. Sheridan KJ, Lechner BE, Keeffe GO, Keller MA, Werner ER, Lindner H, et al. Ergothioneine Biosynthesis and Functionality in the Opportunistic Fungal Pathogen, Aspergillus fumigatus. SCIENTIFIC REPORTS. 2016;6:35306.
13. Turner E, Klevit R, Hopkins PB, Shapiro BM. Ovothiol: a novel thiohistidine compound from sea urchin eggs that confers NAD(P)H-O2 oxidoreductase activity on ovoperoxidase. THE JOURNAL OF BIOLOGICAL CHEMISTRY. 1986;261(28):13056-63.
14. Newton GL, Rawat M, La Clair JJ, Jothivasan VK, Budiarto T, Hamilton CJ, et al. Bacillithiol is an antioxidant thiol produced in Bacilli. NATURE CHEMICAL BIOLOGY. 2009;5(9):625-7.

15. Meister A. Glutathione metabolism and its selective modification. THE JOURNAL OF BIOLOGICAL CHEMISTRY. 1988;263(33):17205-8.
16. Yang MS, Chan HW, Yu LC. Glutathione peroxidase and glutathione reductase activities are partially responsible for determining the susceptibility of cells to oxidative stress. TOXICOLOGY. 2006;226(2–3):126-30.
17. Lu SC. REGULATION OF GLUTATHIONE SYNTHESIS. MOLECULAR ASPECTS OF MEDICINE. 2009;30(1-2):42-59.
18. Dalle-Donne I, Rossi R, Giustarini D, Colombo R, Milzani A. S-glutathionylation in protein redox regulation. FREE RADIC BIOL MED. 2007;43(6):883-98.
19. Fang Z, Dos Santos PC. Protective role of bacillithiol in superoxide stress and Fe–S metabolism in Bacillus subtilis. MICROBIOLOGYOPEN. 2015;4(4):616-31.
20. Sharma SV, Arbach M, Roberts AA, Macdonald CJ, Groom M, Hamilton CJ. Biophysical features of bacillithiol, the glutathione surrogate of Bacillus subtilis and other firmicutes. CHEMBIOCHEM : A EUROPEAN JOURNAL OF CHEMICAL BIOLOGY. 2013;14(16):2160-8.
21. Tian M, Guo F, Sun Y, Zhang W, Miao F, Liu Y, et al. A fluorescent probe for intracellular cysteine overcoming the interference by glutathione. ORGANIC & BIOMOLECULAR CHEMISTRY. 2014;12(32):6128-33.
22. Helmann JD. Bacillithiol, a new player in bacterial redox homeostasis. ANTIOXIDANTS & REDOX SIGNALING. 2011;15(1):123-33.
23. Fang Z, Roberts AA, Weidman K, Sharma SV, Claiborne A, Hamilton CJ, et al. Cross-functionalities of Bacillus deacetylases involved in bacillithiol biosynthesis and bacillithiol-S-conjugate detoxification pathways. THE BIOCHEMICAL JOURNAL. 2013;454(2):239-47.
24. Newton GL, Arnold K, Price MS, Sherrill C, Delcardayre SB, Aharonowitz Y, et al. Distribution of thiols in microorganisms: mycothiol is a major thiol in most actinomycetes. JOURNAL OF BACTERIOLOGY. 1996;178(7):1990-5.
25. Newton GL, Av-Gay Y, Fahey RC. A Novel Mycothiol-Dependent Detoxification Pathway in Mycobacteria Involving Mycothiol S-Conjugate Amidase. BIOCHEMISTRY. 2000;39(35):10739-46.
26. Van Laer K, Hamilton CJ, Messens J. Low-molecular-weight thiols in thiol-disulfide exchange. ANTIOXIDANTS & REDOX SIGNALING. 2013;18(13):1642-53.
27. Wallen JR, Paige C, Mallett TC, Karplus PA, Claiborne A. Pyridine Nucleotide Complexes with Bacillus anthracis Coenzyme A-Disulfide Reductase: A Structural Analysis of Dual NAD(P)H Specificity. BIOCHEMISTRY. 2008;47(18):5182-93.

28. Mallett TC, Wallen JR, Karplus PA, Sakai H, Tsukihara T, Claiborne A. Structure of coenzyme A-disulfide reductase from Staphylococcus aureus at 1.54 A resolution. BIOCHEMISTRY. 2006;45(38):11278-89.
29. Keire DA, Strauss E, Guo W, Noszal B, Rabenstein DL. Kinetics and equilibria of thiol/disulfide interchange reactions of selected biological thiols and related molecules with oxidized glutathione. THE JOURNAL OF ORGANIC CHEMISTRY. 1992;57(1):123-7.
30. Bello MH, Barrera-Perez V, Morin D, Epstein L. The Neurospora crassa mutant NcDeltaEgt-1 identifies an ergothioneine biosynthetic gene and demonstrates that ergothioneine enhances conidial survival and protects against peroxide toxicity during conidial germination. FUNGAL GENETICS AND BIOLOGY : FG & B. 2012;49(2):160-72.
31. Seebeck FP. In Vitro Reconstitution of Mycobacterial Ergothioneine Biosynthesis. JOURNAL OF THE AMERICAN CHEMICAL SOCIETY. 2010;132(19):6632-3.
32. Spies HS, Steenkamp DJ. Thiols of intracellular pathogens. Identification of ovothiol A in Leishmania donovani and structural analysis of a novel thiol from Mycobacterium bovis. EUROPEAN JOURNAL OF BIOCHEMISTRY. 1994;224(1):203-13.
33. Selman-Reimer S, Duhe RJ, Stockman BJ, Selman BR. L-1-N-methyl-4-mercaptohistidine disulfide, a potential endogenous regulator in the redox control of chloroplast coupling factor 1 in Dunaliella. JOURNAL OF BIOLOGICAL CHEMISTRY. 1991;266(1):182-8.
34. Braunshausen A, Seebeck FP. Identification and Characterization of the First Ovothiol Biosynthetic Enzyme. JOURNAL OF THE AMERICAN CHEMICAL SOCIETY. 2011;133(6):1757-9.
35. Newton GL, Rawat M, La Clair JJ, Jothivasan VK, Budiarto T, Hamilton CJ, et al. Bacillithiol is an antioxidant thiol produced in Bacilli. NATURE CHEMICAL BIOLOGY. 2009;5(9):625-7.
36. Banerjee R. Redox outside the Box: Linking Extracellular Redox Remodeling with Intracellular Redox Metabolism. JOURNAL OF BIOLOGICAL CHEMISTRY. 2012;287(7):4397-402.
37. Ferguson GP, Booth IR. Importance of Glutathione for Growth and Survival of Escherichia coli Cells: Detoxification of Methylglyoxal and Maintenance of Intracellular K+. JOURNAL OF BACTERIOLOGY. 1998;180(16):4314-8.
38. Upton H, Newton GL, Gushiken M, Lo K, Holden D, Fahey RC, et al. Characterization of BshA, bacillithiol glycosyltransferase from Staphylococcus aureus and Bacillus subtilis. FEBS LETTERS. 2012;586(7):1004-8.

39. Parsonage D, Newton GL, Holder RC, Wallace BD, Paige C, Hamilton CJ, et al. Characterization of the N-Acetyl-α-d-glucosaminyl l-Malate Synthase and Deacetylase Functions for Bacillithiol Biosynthesis in Bacillus anthracis. BIOCHEMISTRY. 2010;49(38):8398-414.
40. VanDuinen AJ, Winchell KR, Keithly ME, Cook PD. X-ray crystallographic structure of BshC, a unique enzyme involved in bacillithiol biosynthesis. BIOCHEMISTRY. 2015;54(2):100-3.
41. Gaballa A, Newton GL, Antelmann H, Parsonage D, Upton H, Rawat M, et al. Biosynthesis and functions of bacillithiol, a major low-molecular-weight thiol in Bacilli. PROCEEDINGS OF THE NATIONAL ACADEMY OF SCIENCES OF THE UNITED STATES OF AMERICA. 2010;107(14):6482-6.
42. Parsonage D, Newton GL, Holder RC, Wallace BD, Paige C, Hamilton CJ, et al. Characterization of the N-acetyl-alpha-D-glucosaminyl l-malate synthase and deacetylase functions for bacillithiol biosynthesis in Bacillus anthracis. BIOCHEMISTRY. 2010;49(38):8398-414.
43. Nagy P. Kinetics and Mechanisms of Thiol–Disulfide Exchange Covering Direct Substitution and Thiol Oxidation-Mediated Pathways. ANTIOXIDANTS & REDOX SIGNALING. 2013;18(13):1623-41.
44. Chi BK, Roberts AA, Huyen TT, Basell K, Becher D, Albrecht D, et al. S-bacillithiolation protects conserved and essential proteins against hypochlorite stress in firmicutes bacteria. ANTIOXIDANTS & REDOX SIGNALING. 2013;18(11):1273-95.
45. Gaballa A, Chi BK, Roberts AA, Becher D, Hamilton CJ, Antelmann H, et al. Redox regulation in Bacillus subtilis: The bacilliredoxins BrxA(YphP) and BrxB(YqiW) function in de-bacillithiolation of S-bacillithiolated OhrR and MetE. ANTIOXIDANTS & REDOX SIGNALING. 2014;21(3):357-67.
46. Jerina DM, Bend JR. Glutathione S-Transferases. In: Jollow DJ, Kocsis JJ, Snyder R, Vainio H, Saukkonen J, Witmer C, et al., editors. Biological Reactive Intermediates: Formation, Toxicity, and Inactivation. Boston, MA: Springer US; 1977. p. 207-36.
47. Habig WH, Pabst MJ, Jakoby WB. Glutathione S-Transferases: THE FIRST ENZYMATIC STEP IN MERCAPTURIC ACID FORMATION. JOURNAL OF BIOLOGICAL CHEMISTRY. 1974;249(22):7130-9.
48. Rajkarnikar A, Strankman A, Duran S, Vargas D, Roberts AA, Barretto K, et al. Analysis of mutants disrupted in bacillithiol metabolism in Staphylococcus aureus. BIOCHEMICAL AND BIOPHYSICAL RESEARCH COMMUNICATIONS. 2013;436(2):128-33.

49. Roberts AA, Sharma SV, Strankman AW, Duran SR, Rawat M, Hamilton CJ. Mechanistic studies of FosB: a divalent-metal-dependent bacillithiol-S-transferase that mediates fosfomycin resistance in Staphylococcus aureus. THE BIOCHEMICAL JOURNAL. 2013;451(1):69-79.
50. Beharry Z, Palzkill T. Functional analysis of active site residues of the fosfomycin resistance enzyme FosA from Pseudomonas aeruginosa. THE JOURNAL OF BIOLOGICAL CHEMISTRY. 2005;280(18):17786-91.
51. Newton GL, Leung SS, Wakabayashi JI, Rawat M, Fahey RC. The DinB superfamily includes novel mycothiol, bacillithiol, and glutathione S-transferases. BIOCHEMISTRY. 2011;50(49):10751-60.
52. Newton GL, Av-Gay Y, Fahey RC. A novel mycothiol-dependent detoxification pathway in mycobacteria involving mycothiol S-conjugate amidase. BIOCHEMISTRY. 2000;39(35):10739-46.
53. Newton GL, Fahey RC, Rawat M. Detoxification of toxins by bacillithiol in Staphylococcus aureus. MICROBIOLOGY. 2012;158(Pt 4):1117-26.
54. Kosmachevskaya OV, Shumaev KB, Topunov AF. Carbonyl Stress in Bacteria: Causes and Consequences. BIOCHEMISTRY BIOKHIMIIA. 2015;80(13):1655-71.
55. Chen NH, Djoko KY, Veyrier FJ, McEwan AG. Formaldehyde Stress Responses in Bacterial Pathogens. FRONTIERS IN MICROBIOLOGY. 2016;7:257.
56. Hopkinson RJ, Barlow PS, Schofield CJ, Claridge TD. Studies on the reaction of glutathione and formaldehyde using NMR. ORGANIC & BIOMOLECULAR CHEMISTRY. 2010;8(21):4915-20.
57. Subedi KP, Choi D, Kim I, Min B, Park C. Hsp31 of Escherichia coli K-12 is glyoxalase III. MOLECULAR MICROBIOLOGY. 2011;81(4):926-36.
58. Thornalley PJ. Dicarbonyl intermediates in the maillard reaction. ANNALS OF THE NEW YORK ACADEMY OF SCIENCES. 2005;1043:111-7.
59. Lee C, Kim I, Park C. Glyoxal detoxification in Escherichia coli K-12 by NADPH dependent aldo-keto reductases. JOURNAL OF MICROBIOLOGY (SEOUL, KOREA). 2013;51(4):527-30.
60. Együd LG, Szent-Györgyi A. On the regulation of cell division. PROCEEDINGS OF THE NATIONAL ACADEMY OF SCIENCES. 1966;56(1):203-7.
61. Takahashi K. The reactions of phenylglyoxal and related reagents with amino acids. JOURNAL OF BIOCHEMISTRY. 1977;81(2):395-402.
62. Lo TW, Westwood ME, McLellan AC, Selwood T, Thornalley PJ. Binding and modification of proteins by methylglyoxal under physiological conditions. A kinetic and mechanistic study with N alpha-acetylarginine, N alpha-acetylcysteine, and N

alpha-acetyllysine, and bovine serum albumin. THE JOURNAL OF BIOLOGICAL CHEMISTRY. 1994;269(51):32299-305.

63. Ferguson GP. Protective mechanisms against toxic electrophiles in Escherischia coli. TRENDS IN MICROBIOLOGY. 1999;7(6):242-7.

64. Tiffany BD, Wright JB, Moffett RB, Heinzelman RV, Strube RE, Aspergren BD, et al. Antiviral compounds. I. Aliphatic glyoxals, α-hydroxyaldehydes and related compounds. JOURNAL OF THE AMERICAN CHEMICAL SOCIETY. 1957;79(7):1682-7.

65. Murata-Kamiya N, Kamiya H. Methylglyoxal, an endogenous aldehyde, crosslinks DNA polymerase and the substrate DNA. NUCLEIC ACIDS RESEARCH. 2001;29(16):3433-8.

66. Krymkiewicz N. Reactions of methylglyoxal with nucleic acids. FEBS LETTERS. 1973;29(1):51-4.

67. Sartorelli AC, Iannotti AT, Booth BA, Schneider FH, Bertino JR, Johns DG. Complex formation with DNA and inhibition of nucleic acid synthesis by methylglyoxal bis(guanylhydrazone). BIOCHIMICA ET BIOPHYSICA ACTA (BBA) - NUCLEIC ACIDS AND PROTEIN SYNTHESIS. 1965;103(1):174-6.

68. Sousa Silva M, Gomes RA, Ferreira AE, Ponces Freire A, Cordeiro C. The glyoxalase pathway: the first hundred years... and beyond. THE BIOCHEMICAL JOURNAL. 2013;453(1):1-15.

69. Casazza JP, Felver M, Veech R. The metabolism of acetone in rat. JOURNAL OF BIOLOGICAL CHEMISTRY. 1984;259(1):231-6.

70. Elliott WH. Amino-Acetone: its Isolation and Role in Metabolism. NATURE. 1959;183(4667):1051-2.

71. Phillips SA, Thornalley PJ. The formation of methylglyoxal from triose phosphates. Investigation using a specific assay for methylglyoxal. EUROPEAN JOURNAL OF BIOCHEMISTRY. 1993;212(1):101-5.

72. Hopper DJ, Cooper RA. The regulation of Escherichia coli methylglyoxal synthase; a new control site in glycolysis? FEBS LETTERS. 1971;13(4):213-6.

73. Weber J, Kayser A, Rinas U. Metabolic flux analysis of Escherichia coli in glucose-limited continuous culture. II. Dynamic response to famine and feast, activation of the methylglyoxal pathway and oscillatory behaviour. MICROBIOLOGY. 2005;151(Pt 3):707-16.

74. Chandrangsu P, Dusi R, Hamilton CJ, Helmann JD. Methylglyoxal resistance in Bacillus subtilis: contributions of bacillithiol-dependent and independent pathways. MOLECULAR MICROBIOLOGY. 2014;91(4):706-15.

75. Hopper DJ, Cooper RA. The purification and properties of Escherichia coli methylglyoxal synthase. THE BIOCHEMICAL JOURNAL. 1972;128(2):321-9.

76. Lambeir AM, Opperdoes FR, Wierenga RK. Kinetic properties of triose-phosphate isomerase from Trypanosoma brucei brucei. A comparison with the rabbit muscle and yeast enzymes. EUROPEAN JOURNAL OF BIOCHEMISTRY. 1987;168(1):69-74.
77. Inoue Y, Kimura A. Methylglyoxal and regulation of its metabolism in microorganisms. ADVANCES IN MICROBIAL PHYSIOLOGY. 1995;37:177-227.
78. Pazhang M, Khajeh K, Asghari SM, Falahati H, Naderi-Manesh H. Cloning, Expression, and Characterization of a Novel Methylglyoxal Synthase from Thermus sp. Strain GH5. APPLIED BIOCHEMISTRY AND BIOTECHNOLOGY. 2010;162(6):1519-28.
79. Chakraborty S, Karmakar K, Chakravortty D. Cells producing their own nemesis: understanding methylglyoxal metabolism. IUBMB LIFE. 2014;66(10):667-78.
80. Saadat D, Harrison DHT. The crystal structure of methylglyoxal synthase from Escherichia coli. STRUCTURE. 1999;7(3):309-17.
81. Tsai PK, Gracy RW. Isolation and characterization of crystalline methylglyoxal synthetase from Proteus vulgaris. THE JOURNAL OF BIOLOGICAL CHEMISTRY. 1976;251(2):364-7.
82. Needham J, Lehmann H. Intermediary carbohydrate metabolism in embryonic life: Glyceraldehyde and glucolysis. BIOCHEMICAL JOURNAL. 1937;31(11):1913.
83. Ray S, Ray M. Purification and characterization of NAD and NADP-linked alpha-ketoaldehyde dehydrogenases involved in catalyzing the oxidation of methylglyoxal to pyruvate. JOURNAL OF BIOLOGICAL CHEMISTRY. 1982;257(18):10566-70.
84. Monder C. α-Keto Aldehyde Dehydrogenase, An Enzyme That Catalyzes the Enzymic Oxidation of Methylglyoxal to Pyruvate. JOURNAL OF BIOLOGICAL CHEMISTRY. 1967;242(20):4603-9.
85. JEZ JM, BENNETT MJ, SCHLEGEL BP, LEWIS M, PENNING TM. Comparative anatomy of the aldo–keto reductase superfamily. BIOCHEMICAL JOURNAL. 1997;326(3):625-36.
86. Ko J, Kim I, Yoo S, Min B, Kim K, Park C. Conversion of methylglyoxal to acetol by Escherichia coli aldo-keto reductases. JOURNAL OF BACTERIOLOGY. 2005;187(16):5782-9.
87. MURATA K, FUKUDA Y, SIMOSAKA M, WATANABE K, SAIKUSA T, KIMURA A. Metabolism of 2-oxoaldehyde in yeasts. EUROPEAN JOURNAL OF BIOCHEMISTRY. 1985;151(3):631-6.
88. Vander Jagt DL, Robinson B, Taylor KK, Hunsaker LA. Reduction of trioses by NADPH-dependent aldo-keto reductases. Aldose reductase, methylglyoxal, and diabetic complications. JOURNAL OF BIOLOGICAL CHEMISTRY. 1992;267(7):4364-9.
89. Dakin HD, Dudley HW. ON GLYOXALASE. JOURNAL OF BIOLOGICAL CHEMISTRY. 1913;14(4):423-31.

90. Thornalley PJ. Glyoxalase I – structure, function and a critical role in the enzymatic defence against glycation. BIOCHEMICAL SOCIETY TRANSACTIONS. 2003;31(6):1343-8.
91. Vander Jagt DL. Glyoxalase II: molecular characteristics, kinetics and mechanism. BIOCHEMICAL SOCIETY TRANSACTIONS. 1993;21(2):522-7.
92. Racker E. The mechanism of action of glyoxalase. THE JOURNAL OF BIOLOGICAL CHEMISTRY. 1951;190(2):685-96.
93. Thornalley PJ. The glyoxalase system: new developments towards functional characterization of a metabolic pathway fundamental to biological life. THE BIOCHEMICAL JOURNAL. 1990;269(1):1-11.
94. Creighton DJ, Hamilton DS. Brief history of glyoxalase I and what we have learned about metal ion-dependent, enzyme-catalyzed isomerizations. ARCHIVES OF BIOCHEMISTRY AND BIOPHYSICS. 2001;387(1):1-10.
95. Sukdeo N, Clugston SL, Daub E, Honek JF. Distinct classes of glyoxalase I: metal specificity of the Yersinia pestis, Pseudomonas aeruginosa and Neisseria meningitidis enzymes. THE BIOCHEMICAL JOURNAL. 2004;384(Pt 1):111-7.
96. He MM, Clugston SL, Honek JF, Matthews BW. Determination of the structure of Escherichia coli glyoxalase I suggests a structural basis for differential metal activation. BIOCHEMISTRY. 2000;39(30):8719-27.
97. Xue M, Rabbani N, Thornalley PJ. Glyoxalase in ageing. SEMINARS IN CELL & DEVELOPMENTAL BIOLOGY. 2011;22(3):293-301.
98. Vander Jagt DL, Han LP, Lehman CH. Kinetic evaluation of substrate specificity in the glyoxalase-I-catalyzed disproportionation of -ketoaldehydes. BIOCHEMISTRY. 1972;11(20):3735-40.
99. Cameron AD, Ridderström M, Olin B, Mannervik B. Crystal structure of human glyoxalase II and its complex with a glutathione thiolester substrate analogue. STRUCTURE. 1999;7(9):1067-78.
100. Misra K, Banerjee AB, Ray S, Ray M. Glyoxalase III from Escherichia coli: a single novel enzyme for the conversion of methylglyoxal into D-lactate without reduced glutathione. THE BIOCHEMICAL JOURNAL. 1995;305 (Pt 3):999-1003.
101. MacLean MJ, Ness LS, Ferguson GP, Booth IR. The role of glyoxalase I in the detoxification of methylglyoxal and in the activation of the KefB K+ efflux system in Escherichia coli. MOLECULAR MICROBIOLOGY. 1998;27(3):563-71.
102. Clugston SL, Barnard JFJ, Kinach R, Miedema D, Ruman R, Daub E, et al. Overproduction and Characterization of a Dimeric Non-Zinc Glyoxalase I from Escherichia coli: Evidence for Optimal Activation by Nickel Ions. BIOCHEMISTRY. 1998;37(24):8754-63.

103. O'Young J, Sukdeo N, Honek JF. Escherichia coli glyoxalase II is a binuclear zinc-dependent metalloenzyme. ARCHIVES OF BIOCHEMISTRY AND BIOPHYSICS. 2007;459(1):20-6.
104. Ozyamak E, Black SS, Walker CA, Maclean MJ, Bartlett W, Miller S, et al. The critical role of S-lactoylglutathione formation during methylglyoxal detoxification in Escherichia coli. MOLECULAR MICROBIOLOGY. 2010;78(6):1577-90.
105. Ferguson GP, Tötemeyer S, MacLean MJ, Booth IR. Methylglyoxal production in bacteria: suicide or survival? ARCHIVES OF MICROBIOLOGY. 1998;170(4):209-18.
106. Creighton DJ, Migliorini M, Pourmotabbed T, Guha MK. Optimization of efficiency in the glyoxalase pathway. BIOCHEMISTRY. 1988;27(19):7376-84.
107. Jencks WP, Gilchrist M. Nonlinear structure-reactivity correlations. The reactivity of nucleophilic reagents toward esters. JOURNAL OF THE AMERICAN CHEMICAL SOCIETY. 1968;90(10):2622-37.
108. Kallen RG, Jencks WP. The mechanism of the condensation of formaldehyde with tetrahydrofolic acid. THE JOURNAL OF BIOLOGICAL CHEMISTRY. 1966;241(24):5851-63.
109. Zeng J, Davies MJ. Evidence for the Formation of Adducts and S-(Carboxymethyl)cysteine on Reaction of α-Dicarbonyl Compounds with Thiol Groups on Amino Acids, Peptides, and Proteins. CHEMICAL RESEARCH IN TOXICOLOGY. 2005;18(8):1232-41.
110. Acimovic JM, Stanimirovic BD, Todorovic N, Jovanovic VB, Mandic LM. Influence of the microenvironment of thiol groups in low molecular mass thiols and serum albumin on the reaction with methylglyoxal. CHEMICO-BIOLOGICAL INTERACTIONS. 2010;188(1):21-30.
111. Rabenstein DL. Nuclear magnetic resonance studies of the acid-base chemistry of amino acids and peptides. I. Microscopic ionization constants of glutathione and methylmercury-complexed glutathione. JOURNAL OF THE AMERICAN CHEMICAL SOCIETY. 1973;95(9):2797-803.
112. Nemet I, Varga-Defterdarovic L, Turk Z. Preparation and quantification of methylglyoxal in human plasma using reverse-phase high-performance liquid chromatography. CLINICAL BIOCHEMISTRY. 2004;37(10):875-81.
113. Cliffe EE, Waley SG. The mechanism of the glyoxalase I reaction, and the effect of ophthalmic acid as an inhibitor. THE BIOCHEMICAL JOURNAL. 1961;79:475-82.
114. Platt M. The applicability of the manometric method to the study of glyoxalase THE JOURNAL OF BIOLOGICAL CHEMISTRY. 1934;104(281).

115. Podhradský D, Drobnica Ľ, Kristian P. Reactions of cysteine, its derivatives, glutathione, coenzyme A, and dihydrolipoic acid with isothiocyanates. EXPERIENTIA. 1979;35(2):154-5.
116. Ratner S, Clarke HT. The Action of Formaldehyde upon Cysteine. JOURNAL OF THE AMERICAN CHEMICAL SOCIETY. 1937;59(1):200-6.
117. Marchand S, de Revel G, Vercauteren J, Bertrand A. Possible Mechanism for Involvement of Cysteine in Aroma Production in Wine. JOURNAL OF AGRICULTURAL AND FOOD CHEMISTRY. 2002;50(21):6160-4.
118. Wondrak GT, Cervantes-Laurean D, Roberts MJ, Qasem JG, Kim M, Jacobson EL, et al. Identification of α-dicarbonyl scavengers for cellular protection against carbonyl stress. BIOCHEMICAL PHARMACOLOGY. 2002;63(3):361-73.
119. Kallen RG. The mechanism of reactions involving Schiff base intermediates. Thiazolidine formation from L-cysteine and formaldehyde. JOURNAL OF THE AMERICAN CHEMICAL SOCIETY. 1971;93(23):6236-48.
120. Fahey RC, Newton GL. Determination of low-molecular-weight thiols using monobromobimane fluorescent labeling and high-performance liquid chromatography. METHODS IN ENZYMOLOGY. 1987;143:85-96.
121. Barman BN. Accurate determination of aldehydes in amine catalysts or amines by 2,4-dinitrophenylhydrazine derivatization. JOURNAL OF CHROMATOGRAPHY A. 2014;1327:19-26.
122. Uchiyama S, Inaba Y, Kunugita N. Derivatization of carbonyl compounds with 2,4-dinitrophenylhydrazine and their subsequent determination by high-performance liquid chromatography. JOURNAL OF CHROMATOGRAPHY B, ANALYTICAL TECHNOLOGIES IN THE BIOMEDICAL AND LIFE SCIENCES. 2011;879(17-18):1282-9.
123. Nguyen TT, Eiamphungporn W, Mader U, Liebeke M, Lalk M, Hecker M, et al. Genome-wide responses to carbonyl electrophiles in Bacillus subtilis: control of the thiol-dependent formaldehyde dehydrogenase AdhA and cysteine proteinase YraA by the MerR-family regulator YraB (AdhR). MOLECULAR MICROBIOLOGY. 2009;71(4):876-94.
124. Lienhard GE, Jencks WP. Thiol addition to the carbonyl group. Equilibria and kinetics. JOURNAL OF THE AMERICAN CHEMICAL SOCIETY. 1966;88(17):3982-94.
125. Wang Y, Yu H, Shi X, Luo Z, Lin D, Huang M. Structural Mechanism of Ring-opening Reaction of Glucose by Human Serum Albumin. THE JOURNAL OF BIOLOGICAL CHEMISTRY. 2013;288(22):15980-7.
126. Wlodek L. The reaction of sulfhydryl groups with carbonyl compounds. ACTA BIOCHIMICA POLONICA. 1988;35(4):307-17.

127. Kanchuger MS, Byers LD. Acyl substituent effects on thiohemiacetal equilibriums. JOURNAL OF THE AMERICAN CHEMICAL SOCIETY. 1979;101(11):3005-10.
128. Davenport RC, Bash PA, Seaton BA, Karplus M, Petsko GA, Ringe D. Structure of the triosephosphate isomerase-phosphoglycolohydroxamate complex: an analog of the intermediate on the reaction pathway. BIOCHEMISTRY. 1991;30(24):5821-6.
129. Kleijn RJ, Buescher JM, Le Chat L, Jules M, Aymerich S, Sauer U. Metabolic Fluxes during Strong Carbon Catabolite Repression by Malate in Bacillus subtilis. JOURNAL OF BIOLOGICAL CHEMISTRY. 2010;285(3):1587-96.
130. Lowry OH, Carter J, Ward JB, Glaser L. The Effect of Carbon and Nitrogen Sources on the Level of Metabolic Intermediates in Escherichia coli. JOURNAL OF BIOLOGICAL CHEMISTRY. 1971;246(21):6511-21.
131. Buchholz A, Takors R, Wandrey C. Quantification of intracellular metabolites in Escherichia coli K12 using liquid chromatographic-electrospray ionization tandem mass spectrometric techniques. ANALYTICAL BIOCHEMISTRY. 2001;295(2):129-37.
132. Bennett BD, Kimball EH, Gao M, Osterhout R, Van Dien SJ, Rabinowitz JD. Absolute metabolite concentrations and implied enzyme active site occupancy in Escherichia coli. NATURE CHEMICAL BIOLOGY. 2009;5(8):593-9.
133. Bloch W, MacQuarrie RA, Bernhard SA. The Nucleotide and Acyl Group Content of Native Rabbit Muscle Glyceraldehyde 3-Phosphate Dehydrogenase. JOURNAL OF BIOLOGICAL CHEMISTRY. 1971;246(3):780-90.
134. Park C, Lee Y-j, Lee SY, Oh HB, Lee J. Determination of the intracellular concentrations of metabolites in Escherichia coli collected during the exponential and stationary growth phases using liquid chromatography-mass spectrometry. BULLETIN OF THE KOREAN CHEMICAL SOCIETY. 2011;32(2):524-30.
135. Yang Y-T, Bennett GN, San K-Y. The Effects of Feed and Intracellular Pyruvate Levels on the Redistribution of Metabolic Fluxes in Escherichia coli. METABOLIC ENGINEERING. 2001;3(2):115-23.
136. Rabbani N, Thornalley PJ. Glyoxalase in diabetes, obesity and related disorders. SEMINARS IN CELL & DEVELOPMENTAL BIOLOGY. 2011;22(3):309-17.
137. McLellan AC, Thornalley PJ, Benn J, Sonksen PH. Glyoxalase system in clinical diabetes mellitus and correlation with diabetic complications. CLINICAL SCIENCE (LONDON, ENGLAND : 1979). 1994;87(1):21-9.
138. Rabbani N, Thornalley PJ. The Critical Role of Methylglyoxal and Glyoxalase 1 in Diabetic Nephropathy. DIABETES. 2014;63(1):50-2.
139. Beisswenger PJ. Methylglyoxal in diabetes: link to treatment, glycaemic control and biomarkers of complications. BIOCHEMICAL SOCIETY TRANSACTIONS. 2014;42(2):450-6.

140. Maessen DE, Stehouwer CD, Schalkwijk CG. The role of methylglyoxal and the glyoxalase system in diabetes and other age-related diseases. CLINICAL SCIENCE (LONDON, ENGLAND : 1979). 2015;128(12):839-61.
141. Hsieh MS, Chan WH. Impact of methylglyoxal and high glucose co-treatment on human mononuclear cells. INTERNATIONAL JOURNAL OF MOLECULAR SCIENCES. 2009;10(4):1445-64.
142. Dhar A, Dhar I, Jiang B, Desai KM, Wu L. Chronic methylglyoxal infusion by minipump causes pancreatic beta-cell dysfunction and induces type 2 diabetes in Sprague-Dawley rats. DIABETES. 2011;60(3):899-908.
143. Mungli P, Shetty MS, Tilak P, Anwar N. Total thiols: biomedical importance and their alteration in various disorders. ONLINE JOURNAL OF HEALTH AND ALLIED SCIENCES. 2009;8(2).
144. Memisogullari R, Taysi S, Bakan E, Capoglu I. Antioxidant status and lipid peroxidation in type II diabetes mellitus. CELL BIOCHEMISTRY AND FUNCTION. 2003;21(3):291-6.
145. Vijayalingam S, Parthiban A, Shanmugasundaram KR, Mohan V. Abnormal antioxidant status in impaired glucose tolerance and non-insulin-dependent diabetes mellitus. DIABETIC MEDICINE : A JOURNAL OF THE BRITISH DIABETIC ASSOCIATION. 1996;13(8):715-9.
146. Pasaoglu H, Sancak B, Bukan N. Lipid peroxidation and resistance to oxidation in patients with type 2 diabetes mellitus. THE TOHOKU JOURNAL OF EXPERIMENTAL MEDICINE. 2004;203(3):211-8.
147. Beisswenger PJ, Howell SK, Touchette AD, Lal S, Szwergold BS. Metformin reduces systemic methylglyoxal levels in type 2 diabetes. DIABETES. 1999;48(1):198-202.
148. Rae C, Berners-Price SJ, Bulliman BT, Kuchel PW. Kinetic analysis of the human erythrocyte glyoxalase system using 1H NMR and a computer model. EUROPEAN JOURNAL OF BIOCHEMISTRY. 1990;193(1):83-90.
149. Rhieu SY, Urbas AA, Bearden DW, Marino JP, Lippa KA, Reipa V. Probing the intracellular glutathione redox potential by in-cell NMR spectroscopy. ANGEWANDTE CHEMIE. 2014;53(2):447-50.
150. Wu G. Amino acids: metabolism, functions, and nutrition. AMINO ACIDS. 2009;37(1):1-17.
151. Burguiere P, Auger S, Hullo MF, Danchin A, Martin-Verstraete I. Three different systems participate in L-cystine uptake in Bacillus subtilis. JOURNAL OF BACTERIOLOGY. 2004;186(15):4875-84.

152. Sun S-W, Lin Y-C, Weng Y-M, Chen M-J. Efficiency improvements on ninhydrin method for amino acid quantification. JOURNAL OF FOOD COMPOSITION AND ANALYSIS. 2006;19(2):112-7.
153. Riddles PW, Blakeley RL, Zerner B. [8] Reassessment of Ellman's reagent. Methods in enzymology. Volume 91: Academic Press; 1983. p. 49-60.
154. Aitken A, Learmonth M. Estimation of Disulfide Bonds Using Ellman's Reagent. In: Walker JM, editor. The Protein Protocols Handbook. Totowa, NJ: Humana Press; 1996. p. 487-8.
155. Wild R, Ooi L, Srikanth V, Munch G. A quick, convenient and economical method for the reliable determination of methylglyoxal in millimolar concentrations: the N-acetyl-L-cysteine assay. ANALYTICAL AND BIOANALYTICAL CHEMISTRY. 2012;403(9):2577-81.
156. Scheek RM, Slater EC. [53] Glyceraldehyde-3-phosphate dehydrogenase from rabbit muscle. Methods in enzymology. Volume 89: Academic Press; 1982. p. 305-9.
157. Oshima T, Fujita SC, Imahori K. [58] Glyceraldehyde-3-phosphate dehydrogenase from Thermus thermophilus. Methods in enzymology. Volume 89: Academic Press; 1982. p. 335-40.
158. Duggleby RG, Dennis DT. [56] Glyceraldehyde-3-phosphate dehydrogenase from pea seeds. Methods in enzymology. Volume 89: Academic Press; 1982. p. 319-25.
159. Russo AD, Rullo R, Masullo M, Ianniciello G, Arcari P, Bocchini V. Glyceraldehyde-3-phosphate dehydrogenase in the hyperthermophilic archaeon Sulfolobus solfataricus: characterization and significance in glucose metabolism. BIOCHEMISTRY AND MOLECULAR BIOLOGY INTERNATIONAL. 1995;36(1):123-35.
160. Aragon JJ, Sols A. Glyceraldehyde-3-phosphate dehydrogenase activity studied under physiological conditions with a linear assay. BIOCHEMICAL AND BIOPHYSICAL RESEARCH COMMUNICATIONS. 1978;82(4):1098-103.
161. Fahien LA. A Study of the Reaction of Glyceraldehyde with Glyceraldehyde 3-Phosphate Dehydrogenase. JOURNAL OF BIOLOGICAL CHEMISTRY. 1966;241(18):4115-23.
162. Newton GL, Dorian R, Fahey RC. Analysis of biological thiols: derivatization with monobromobimane and separation by reverse-phase high-performance liquid chromatography. ANALYTICAL BIOCHEMISTRY. 1981;114(2):383-7.
163. MOJSIN M, NIKCEVIC G, GRUJICIC NK, SAVIC T. Purification and functional analysis of the recombinant protein isolated from E. coli by employing three different methods of bacterial lysis. JOURNAL OF THE SERBIAN CHEMICAL SOCIETY. 2005.

164. Garrigues C, Loubiere P, Lindley ND, Cocaign-Bousquet M. Control of the shift from homolactic acid to mixed-acid fermentation in Lactococcus lactis: predominant role of the NADH/NAD+ ratio. JOURNAL OF BACTERIOLOGY. 1997;179(17):5282-7.
165. Krężel A, Bal W. A formula for correlating pKa values determined in D2O and H2O. JOURNAL OF INORGANIC BIOCHEMISTRY. 2004;98(1):161-6.
166. Nemet I, Vikic-Topic D, Varga-Defterdarovic L. Spectroscopic studies of methylglyoxal in water and dimethylsulfoxide. BIOORGANIC CHEMISTRY. 2004;32(6):560-70.